ANGLIA RUSKIN UNIVERSITY

Development, Validation and Application of a Biomechanical Model of Reclined Sitting Posture

DAVID WICKETT

A Thesis in partial fulfilment of the requirements of Anglia Ruskin University for the degree of PhD

Submitted: January 2013

Acknowledgements

I am heartily thankful to my supervisors, Dr. Rajshree Mootanah and Dr. Howard Hillstrom, whose encouragement, guidance and support from the initial to the final level enabled me to develop an understanding of the subject. I am grateful to Dr. Matthew Reed from the Michigan Transportation Research Institute for his advice on the state of the art in digital human modelling, and also Dr. Dan Gordon and his colleagues at the Human Energetics and Performance Centre, Anglia Ruskin University, for the use of laboratory space, electromyography equipment, research assistants and guidance on statistical analysis. I would like to thank Mark Lenhoff, Chief Engineer of the Motion Analysis Lab at the Hospital for Special Surgery (HSS), for writing the LabVIEW programme to filter the sEMG data. This thesis would not have been possible without the support and encouragement from my employer, Martin Battye, Chairman of the Kirton Healthcare Group Ltd. I would like to give thanks Professor Christine Haslegrave at the Institute for Occupational Ergonomics for the loan of the stadiometer, and to the subjects who kindly participated in the investigations. This research was sponsored by the Knowledge Transfer Partnership, Department of Trade and Industry.

ANGLIA RUSKIN UNIVERSITY

ABSTRACT

MEDICAL ENGINEERING RESEARCH GROUP

PHD

DEVELOPMENT, VALIDATION AND APPLICATION OF A BIOMECHANICAL MODEL OF RECLINED SITTING POSTURE

By DAVID WICKETT

January 2013

Empirical knowledge is lacking on reclined seating postures. To unify such data, a biomechanical model is needed that accurately predicts posture, the relative position of the pelvis, the point of load transfer to the seat, internal and external forces, and the motion paths of the support surfaces. The overall aim of this investigation was, therefore, to create and validate a biomechanical model of reclined seating postures, and to evaluate *in vivo* measured and predicted data.

A two-dimensional biomechanical model was developed, validated and applied. A comprehensive set of biomechanical data was collected from fifteen gender and age diverse subjects to examine the foundational principles for reclined seating ergonomics. The model agreed with 98.8% of measured data on posture across the seated test conditions. There was a significant relationship between modelled and measured force ($p < .001$, $r = .92$), which improved after normalisation ($p < .001$, $r = .97$) with an 8% full scale error. The model was robust across height and gender. Significant differences in interface pressure (peak pressure, average pressure and area), stature, back muscle activity and spinal curvature were found between all of the seated test postures. Significant relationships were found between the model predictions and all of the experimental data.

This research is unique in creating a framework around reclined seating postures which connects previously disparate areas of seating research. The biomechanical model, experimental results, and theories developed from this research have potential implications in research, and design, for applications including backcare chairs, seating for long-term care and patients with neuromotor deficits, wheelchairs and airline seating. Furthermore, this study exists at the interface of anthropometric and biomechanical modelling, and therefore may have cross over potential to digital humans, where their integration with biomechanical models is at the cutting edge of the field.

Key words: Reclined; Seating; Biomechanics; Ergonomics; Modelling; Posture

Table of Contents

List of Figures

List of Tables

Appendices

1 Introduction

A two-dimensional biomechanical model was developed, validated and applied to the evaluation of reclined sitting postures. A comprehensive set of biomechanical data was collected from subjects to develop a theoretical foundation for reclined seating ergonomics. This first chapter of the thesis presents the background of the study, states the problem, describes its significance, and presents the research aims and hypotheses. The chapter concludes by noting the delimitations of the study.

1.1 Background to the study

Sitting posture has been of scientific interest since as early as Åkerblom's monologue of 1948, around the time when the terms 'ergonomics' and 'human factors' became part of the modern lexicon (Meister, 1999). Although there has been a plethora of ergonomic research on seating and sitting posture since, contemporary seating ergonomic theory is based on a limited number of studies, many of which were carried out by orthopaedic surgeons (Harrison *et al*., 1999). Those medical professionals employed engineering principles which when applied to the musculoskeletal system, is commonly referred to as the field of biomechanics.

What these studies have shown is that the relative position of support surfaces in sitting determines posture, influences muscle activity, and affects the distribution of load within the body and at the body–support interface (Harrison *et al*., 1999). The distribution of load, particularly within the upper body, is an important factor in determining the extent to which spinal structures and innervated tissues are stressed (Adams *et al.*, 2006), and, in long-term sitting, this may affect comfort levels. The distribution of load at the body–support interface influences compressive forces acting on skin and muscle, and is, therefore, an important consideration in pressure ulcer management (Zacharkow, 1984; Sprigle & Sonenblum, 2011). Muscle activity is also an important factor in sitting, where reducing static muscle activity to a

minimum has long been a fundamental ergonomic principle (Åkerblom, 1948; Andersson *et al*., 1975). Studies on posture have tended to focus on the orientation of the pelvis and spinal curvature where arguments have centred on flexion versus extension (Pynt *et al.,* 2008).

Digital humans, such as Biodigital Human (www.Biodigitalhuman.com) and Jack (Blanchonette, 2010), are being developed as powerful tools to represent the three-dimensional (3D) surface geometry of human populations. Although anthropometrically accurate, digital humans do not have a biomechanical model (linkage-based static equilibrium, dynamic musculoskeletal or joint stress) as a foundation. The integration of biomechanical models and anthropometric 3D digital humans is emerging as the subject of current research (Paul & Lee, 2011).

1.2 Problem statement

Contemporary seating ergonomics is based on fragmented and sometimes conflicting research spanning over 60 years and lacks an accurate, validated, full body biomechanical model that predicts reclined sitting posture. There are no comprehensive quantitative studies on the effects of reclined seating and, in the absence of such research, the principles for upright, task orientated postures have been assumed (Pheasant & Haslegrave, 2006). Furthermore, without an accurate linkage-based biomechanical model of reclined sitting posture that accommodates pelvic rotation and its relative position to the support surfaces, it is not possible to predict the path of movement of support surfaces, nor the loading between the anatomical structures and the chair as the body flexes and extends. The path of movement and loading between the body and chair are postulated to be inter-related, which underlines the importance of understanding both these phenomena.

1.3 Significance of this study

This study contributes to a theoretical foundation for reclined seating ergonomics. Reclined seating is of particular importance when static upright seating fails to perform adequately. Examples include airline seating for long haul flights, recliner chairs for back pain alleviation, and specialist healthcare chairs for frail elderly and disabled people. Although healthy individuals were modelled and measured during this research, the theories developed may translate to future investigations of pathology. The development of the biomechanical model in this study may also advance digital human models for the analysis of seating by predicting posture, the orientation and relative position of the pelvis to the support surfaces, the ischial tuberosity (IT) contact, the point of load transfer to the seat, segment and reaction forces, and the motion paths of support surfaces.

1.4 Specific aims and hypotheses

The overall aim of this thesis is to biomechanically model reclined seating postures and compare *in vivo* measured and predicted data. The seated test postures in this study include: upright, standard recline, tilt-in-space 1, tilt-in-space 2, and tilt-in-space 3 which are defined precisely in Section (2.5). The specific aims and hypotheses are given below.

Specific Aim 1: To develop a two-dimensional (2D) biomechanical model of the seated test postures that simulates full body support and predicts forces (a) between adjacent body segments and (b) between a body segment and the adjacent seat support surface.

Hypothesis H1a: The model will agree with at least 95% of sitting height when simulating 50th percentile man in a car driver's posture and comparing to published anthropometric studies.

Hypothesis H1b: The model will accurately reproduce the force predictions of a previously published and validated biomechanical model, agreeing within 10% full scale error

Specific Aim 2: To validate the biomechanical model for the seated test postures. This will require the (a) design and development of a reclinable chair for *in vivo* biomechanical data collection, (b) verification of model geometry including the support surface motion paths, and (c) validation of interface loading at each seated test posture.

Hypothesis H2a: The model predictions of the position of anatomical landmarks (posterior head, scapula, ischial tuberosity) across the seated test postures will be accurate to at least 95%.

Hypothesis H2b: The model predictions of the support surface motion paths will agree with at least 95% of measured data across the seated test postures.

Hypothesis H2c: Model force predictions at the different body segments will agree within 10% full scale error of measured data across seated test postures.

Hypothesis H2d: There will be a significant relationship and strong correlation between predicted and measured force data ($p < .05$, $r > 0.7$) across seated test postures.

Specific Aim 3: To explore the relationship between model force predictions and measured interface pressure for seated test postures.

Hypothesis H3a: There will be a significant difference ($p < .05$) in peak pressure, average pressure and contact area between seated test postures, with increasing back pressure and contact area, and decreasing seat pressure and contact area, as the upper body approaches the horizontal.

Hypothesis H3b: There will be a significant relationship ($p < .05$) between model force predictions and peak pressure, average pressure and contact area for the seat and backrest across seated test postures.

Specific Aim 4: To explore the relationship between model force predictions and measured stature for seated test postures.

Hypothesis 4a: There will be a significant difference (p < .05) in stature change between the seated test postures, with stature gain greater for those postures where the upper body approaches the horizontal.

Hypothesis 4b: There will be a significant relationship (p < .05) between model force predictions for the upper body linkages and measured changes in stature resulting from a common fixed duration of sitting in each of the seated test postures.

Specific Aim 5: To explore the relationship between model force predictions and back surface electromyography (sEMG) for seated test postures.

Hypothesis 5a: There will be a significant difference (p < .05) in magnitude of back muscle EMG activity between the seated test postures, with less activity for those postures where the upper body approaches the horizontal.

Hypothesis 5b: There will be a significant relationship (p < .05) between model force predictions at specific regions of the upper body and measured changes in proximal back muscle EMG activity across the seated test postures.

Specific Aim 6: To explore the relationship between spinal curvature and seated test postures.

Hypothesis 6: There will be a significant difference (p < .05) in spinal curvature between the seated test postures.

1.5 Thesis structure

Figure 1 illustrates the content and structure of this thesis, and is an adaption of various models by Dunleavy (2003). In the context of British universities, this thesis departs from the traditional model by reporting less of the literature review in order to arrive at the core chapters sooner. Unlike the ‘paper model dissertation’ more common in America (Dunleavy, 2003), the core chapters hold different information that flow in sequence. Dunleavy describes this as the compromise model.

Chapter 2 begins with a historical perspective of seating and provides a terse discussion on the most influential research that underpins contemporary seating ergonomic theory. The second section discusses the two principle approaches to reclining chairs currently in use and a new concept design whilst connecting to previous research and literature. The third section gives a brief overview of biomechanical research methods including modelling and experimental data collection. The forth section describes the gap in knowledge this research seeks to address. The chapter concludes with a description of the test-rig and the seated test postures. The seated test postures are illustrated on the back page of this thesis which folds out to provide a permanent reference.

Chapter 3 describes the development of the biomechanical model, which is central to the philosophy of this thesis, and concludes with the model output parameters for later analysis (i.e. spine linkage forces, and seat, lumbar, thoracic and head total forces,).

Chapter 4 reports four laboratory tests to measure 1) interface pressure; 2) stature change; 3) back muscle activity; 4) spinal curvature and body/support displacement. The test-rig and configurations, described in Section 2.5, were consistent throughout, as were the heterogeneous group of 15 subjects.

An analysis of the model predictions and experimental data is given in Chapter 5 to test the hypotheses listed above. General findings from these results are then discussed in Chapter 6 which considers the research in the wider context of the literature. This includes a discussion on the effectiveness of the postures evaluated, including consideration of how the postures might apply to various applications, such as long haul flights, back care, long term care and wheeled mobility. The usefulness of the test-rig and test procedures, usefulness of the biomechanical model and future directions is also discussed, including consideration as to how the model might benefit digital human models.

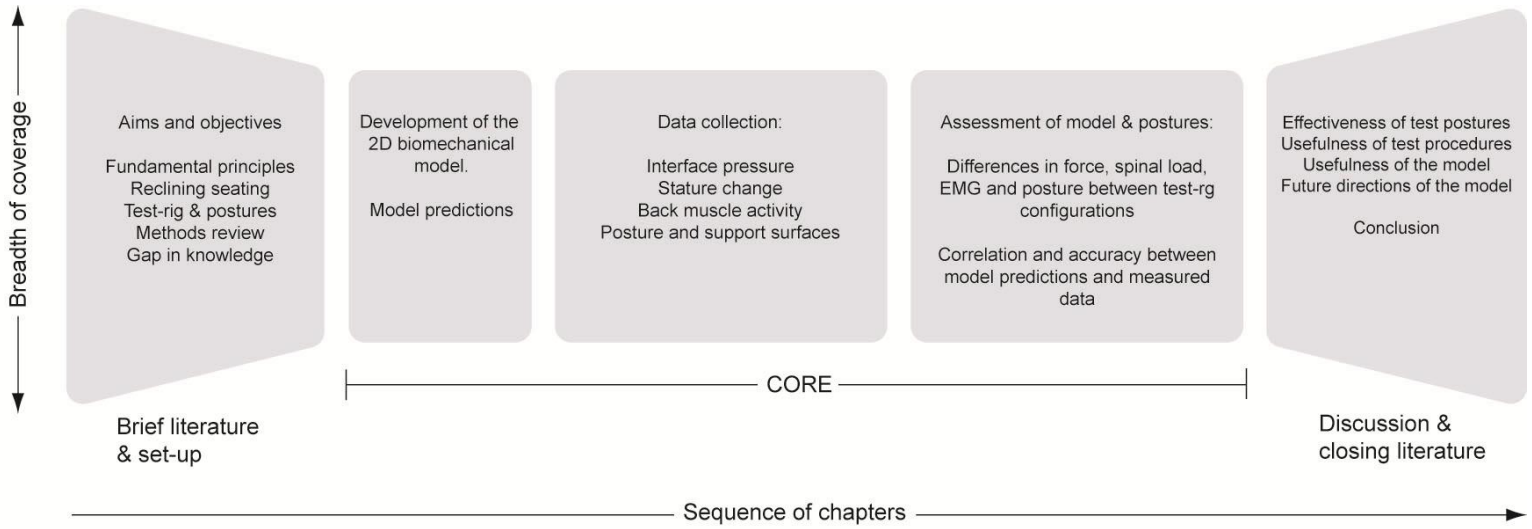

Figure 1 Thesis structure, adapted from Dunleavy (2003)

1.6 Delimitations

The boundaries of this study are listed below:

1. The biomechanical model is restricted to two dimensions. A multi-segment 2D mechanical model of reclined seating that includes accurate pelvic rotation and in vivo validation is not present in the peer-reviewed literature. A 3D model may be developed from the 2D model presented in this dissertation, but accurate 3D pelvic rotation data and in vivo validation will present a considerable challenge.

2. Only biomechanical data is collected from the laboratory experiments. Other physiological data, or subject self-assessments, such as comfort, are beyond the scope of this dissertation.

3. The seated test postures are evaluated only at the support surfaces. Note that the design of the seating interface is unchanged throughout (i.e. lumbar pad, pelvic pad, seat profiling, cushioning material type, covering materials).

4. Only static postures are evaluated.

5. Only healthy subjects participated in this study. The potential benefits of reclined seating for back pain and long term care are suggested for future research but no claims are made.

6. The experimental study is cross-sectional, describing only immediate effects of reclined seating. Therefore no long-term effect on benefits may be inferred.

7. Each measurement was made once (i.e. without replication) due to the total time required for this protocol.

2 An Overview of Seating Research

This chapter begins with a review the most influential research that underpins contemporary seating ergonomic theory. Following this, the two types of reclined seating systems currently in use are defined along with a new concept system that draws from the literature. A short review of previous research using biomechanical models, and methods for collecting biomechanical data, is provided. The gap in knowledge the present research seeks to address is derived from this review. Finally, the test-rig, that was specifically designed and built for this study, is described along with the chosen seating test postures.

2.1 Fundamental principles

For upright sitting, the primary goal is to encourage movement. This basic ergonomic principle has been known since Åkerblom published his monologue in 1948. In this he states that

> "followed to its logical conclusion, a good chair is one which permits of as many good postures as possible being adopted without interference with the work… the comfortable easy chairs which are to be seen nowadays, designed to follow the curves of the body, often suffer from the disadvantage that they only allow of the adoption of one position, which may be very comfortable in itself, but of which quickly tires".

This view has been held constant since. Nearly 60 years later, Adams, *et al*., (2006) explains that

> "there is no ideal sitting or standing posture, because no single posture can be comfortably maintained for a long period of time".

In 1951, an American orthopaedic surgeon presented a paper at the Meeting of the Clinical Orthopaedic Society, Omaha, Nebraska, which established the foundation for seating research (Keegan, 1953). The article was based on a study of over 3,000 people with low back complaints, 1,504 of whom had been operated on for herniation of a lower lumbar intervertebral disc, as well as on a special study of the alteration of the lumbar curve in various sitting and standing postures. Keegan hypothesised that sitting is an etiological factor for lower back pain. He explains that when sitting, the trunk to thigh angle reduces and the large posterior leg and gluteal muscles rotate the pelvis backwards. This posterior rotation of the pelvis forces the spine to flex which results in wedging of the disc. Keegan considered this to be a fundamental cause of lower back pain. He explains that, in middle aged people, some loss of elasticity occurs in the intervertebral disc and ligaments, and the reduction of the lumbar curve in sitting postures tends to force the degenerated and "somewhat separated central portion of the lower lumbar discs" posteriorly. Keegan theorised that this occurs in variable degrees in sitting, and causes painful stretching of the sensitive posterior longitudinal ligament of the disc, with pain in the mid-line of the lower back. Keegan went further to say that if the load was great enough, the disc could rupture and extrusion or herniation of the loose central fibrocartilage could cause pressure on the overlying nerve root within the spinal canal, resulting in radiating pain into the buttock and lower extremity (commonly referred to as sciatica). In Keegan's study into the alterations of the lumbar curve due to sitting postures, he found that all of the sitting postures flexed the spine. He noted that positions with and without back support in the low lumbar area showed the value of maintaining support at this level when sitting, but such a back support with the legs straight (as if on a footrest) cannot overcome the increased pull of the posterior thigh muscles which rotate the pelvis and flatten the back markedly.

Keegan recommends that the most important requirement of a chair is the provision of support to the lower lumbar region. Second to this, Keegan recommends that a chair should have a backrest that is at least 105° to the seat. Keegan also proposed that a 135° trunk-thigh angle and a 135° knee angle is the optimum or physiologically normal position, and that these angles result

in muscular balance of the thighs and lower legs. Although, at the time of writing, this research is 60 years old, the latest positional magnetic resonance imaging technology of the seated posture has only served to confirm Keegan's original findings (Bashir, *et al*., 2006).

An important study, but one that appears to have received little attention in the literature, was presented at the Symposium on Sitting Posture, Zurich 1968 (Schoberth, 1969). The publication was in German but was translated for the present study. Schoberth, a German orthopaedic surgeon, described the architecture of the human spine based on a study of 1035 school children. From his functional perspective, the human spine consists of one immobile middle part: the upper thoracic spine, and two mobile end pieces: the cervical spine on one side and the lumbar spine on the other side. The lumbar spine is connected to the sacrum which is rigidly connected to the pelvis. Schoberth goes on to say that the basis for the entire spinal architecture is the vertebral endplate of the sacrum. If this is tilted forwards the spine will move towards lordosis. If this is tilted backwards, the spine will move towards kyphosis. Schoberth carried out research into the interaction between the position of the pelvis and the form of the spine in sitting. He found that, if the endplate of the sacrum is greater than 16° anteriorly tilted with respect to the horizontal in the sagittal plane, the spine will always be in lordosis. If the endplate is more than 10° posteriorly tilted with respect to the horizontal in the sagittal plane, the spine will always be in kyphosis. He explains that these rules apply providing that the spine is free to move.

Schoberth proposes that when sitting, lumbar lordosis does not matter at all, and that it is easily compensated by rotating the pelvis (passively). He concludes to say that sitting in a total kyphosis is economically very favourable over a lordotic posture (based on electromyographical studies on muscle activity) and to be aimed at. Schoberth does explain however that sitting with a flexed spine can cause pain in the lumbar region which he attributes to prolonged flexing of the intervertebral discs. For this reason, he states that sitting with a totally rounded back without support of any kind is harmful and will lead to pain. Schoberth concludes to say that the position

of the pelvis determines the shape of the spine. The lumbar lordosis is of little importance in the sitting posture. In order to avoid fatigue, it is necessary to support the iliac crest and the sacrum. Support higher up on the backrest for resting positions should begin at the lower thoracic spine.

In the same decade as Schoberth's work, research was carried out by Nachemson and colleagues that resulted in a series of publications. In 1964, Nachemson and Morris published the results of an investigation that directly measured intervertebral disc pressure using a specially constructed needle with a pressure-sensitive membrane at its tip. The study established an approximate relationship between the disc pressures in sitting, standing, and lying positions, and showed that intradiscal pressures of subjects in the standing position were, on average, 30% less than those in the sitting position. The authors considered that mechanical forces might play a role in the production of pain since the outer anulus fibrosis had previous been shown to contain nerve endings of a type that is associated with pain or pressure perception (Hirsch, *et al*., 1963). A number of studies were published ten years later by the same research team which, among other seating parameters, evaluated the effects of lumbar support and backrest inclination on lumbar disc pressure. Andersson, *et al*. (1974) also found that lumbar disc pressure was considerably higher in unsupported sitting than in standing. In supported sitting, a decrease in pressure was obtained by an increase in backrest inclination and by an increase in lumbar support. These findings are discussed further in Chapter 6. What is important here is that the investigators state that in order to achieve low disc pressure, flexion of the lumbar spine should be avoided. They follow on by saying that this may be accomplished by a lumbar support or by fixation of the pelvis and simultaneously increase the backrest inclination. They advocate the use of a lumbar support explaining that when suitably placed it rotates the pelvis forward and at the same time moves the spine towards lordosis. They advise against supporting the pelvis based on their theory that shearing stresses in the lumbosacral region may develop (Andersson, *et al*., 1975).

In supported sitting, a decrease in disc pressure was obtained by an increase in backrest inclination and lumbar support. Of primary importance is that Andersson, *et al*., (1974) state that, in order to reduce disc pressure, flexion of the lumbar spine should be avoided. Furthermore, the authors state that this might be accomplished by a lumbar support or by simultaneous pelvic fixation and backrest inclination. They advocate the use of a lumbar support explaining that, when suitably placed, it rotates the pelvis forward and at the same time moves the spine towards lordosis. They advise against supporting the pelvis based on their theory that shearing stresses in the lumbosacral region may develop (Andersson, *et al*., 1975).

In the subsequent 20 years, research has shown that lordotic sitting postures may not be as beneficial as moderately flexed postures. Moderately flexed postures appear to be advantageous in terms of intervertebral disc nutrition, and unloading the zygapophysial joints (Adams & Hutton, 1980). Impaired metabolite transport is associated with disc degeneration (Nachemson, *et al*., 1970; Holm & Nachemson, 1982), and zygapophysial joint pain has been demonstrated in about 40% in an elderly population with chronic LBP (Schwarzer, *et al*., 1995). Studies have suggested that flexed postures can reduce spinal nerve root compression when compared to extended postures (Inufusa, *et al*., 1996) which could be beneficial for people with spinal stenosis (a condition where the spinal canal reduces and compresses the spinal cord and nerves). Many of the negative aspects of flexed postures have been discussed in the context of upright sitting. No studies have been found that consider how they might translate to reclined postures. These points are discussed further in Chapter 6.

2.2 Reclined seating

There are two approaches to the design of reclining chairs (Figure 2). The most common approach used in general reclining lounge chairs is to increase the seat to backrest angle and provide a footstool or extending leg rest. This is the approach that should be assumed if a chair

is referred to as a recliner. Another approach that is more prevalent in wheelchairs is known as tilt-in-space. Here, the seat to backrest angle does not change and the whole system tilts. Some tilt-in-space chairs also have an elevating leg rest. It must be noted that these two approaches are not mutually exclusive, and are often combined. However, for research purposes the distinction is useful.

Figure 2 The standard recline (left) and tilt-in-space (right) postures

The ergonomic principles developed by Schoberth (1969) for school seating, which has received little attention in the literature, could be extended to reclining systems. Schoberth describes the spinal architecture as consisting of two rigid parts, the pelvis and the thorax. These two structural girdles are connected by the spine, which is flexible between the pelvis and thorax, and flexible above the thorax. Schoberth recommends that it is the pelvis and thorax that should be supported and not the spine (as with a lumbar support), and that the shape of the spine is determined by the relative orientation of the pelvis and thorax. Based on this recommendation, it is possible to conceive of a backrest that independently supports the pelvis, thorax and head (Figure 3). These three supporting elements could then articulate as the chair reclines so that the posture of the spine changes as a function of seat tilt.

Tilt-in-space postures suffer from the disadvantage that the head is orientated back which is undesirable for general use such as holding conversation, watching television and reading. Efforts to remedy this problem with products currently on the market have been to introduce an adjustable headrest to bring the head forwards. A headrest that moves forward may not be desirable if it causes localised flexion at the area of C7/T1, which could become uncomfortable. By supporting the back as illustrated in Figure 3, the flexion that is required to maintain the head in a functional position would be shared across the entire spine by articulating the pelvis, thorax and head. In this instance, the upright posture would promote a neutral or lordotic spine and the reclined posture would promote a moderately flexed spine.

The benefits of lordotic and flexed sitting postures for upright seating continue to be debated (Adams, *et al*., 2006; Pynt, *et al*., 2008), and are discussed in Chapter 6. The interesting questions are how these arguments translate to recline postures with, presumably, different spinal mechanics, and how they translate to the various contexts of use that necessitate reclining seating when conventional upright postures fail.

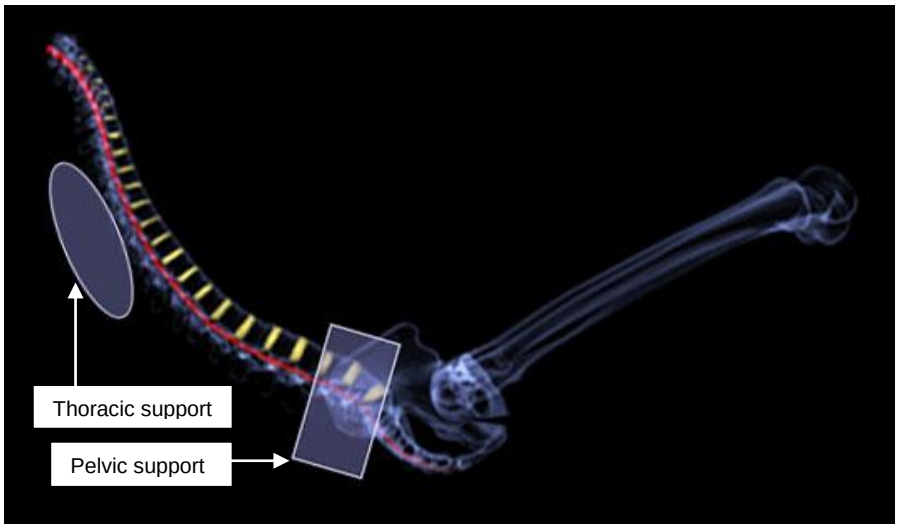

Figure 3 Articulating backrest concept

2.3 Overview of research methods

This section reviews some of the methods that have been used in seating research in the past. The review focuses on biomechanical models, interface pressure measurement, stadiometry (measurement of changes in stature to estimate spinal loading), surface electromyography of the back muscles, and measurement of posture and spinal curvature. Studies reporting subjective ratings of comfort and discomfort are not included.

2.3.1 Biomechanical models

The development of a biomechanical model is important to aid in the theoretical understanding of sitting posture. Furthermore, it is valuable for prediction of the loads likely to arise between specific body parts under various conditions as well as between a body part and the support surface of the seat (Eklund and Corlett, 1986; Duffy, 2008). A review of the literature on sitting biomechanics prior to 1998 is given by Harrison, *et al*., (1999) which evaluated early biomechanical models on sitting posture but reported only one where the head, spine and pelvis were included which was for pilot ejector seat simulations (Belytschko and Privitzer, 1978). Eklund and Corlett (1986) reported a simple model supported at the foot, the ischial tuberosities, a single location on the back just above L3, with an external force acting on the hands (resting or pushing on a table). Their model is capable of predicting compressive and shear loads in the horizontal plane at any chosen spinal level. It also permits the calculation of the moment induced load in the sagittal plane around any chosen disc and the shoulder joint. Dempster's data (1955) on the weight and location of the centre of mass for the body segments were used for the calculations in this model. Colombini, *et al*., (1986) modelled the loads at L3/L4 and C6/C7 based on the area of the L3/L4 disc. Both of these models are dependent on empirical data from lateral photographs and force plates.

A more complex two-dimensional biomechanical model of the sitting posture is provided by Goossens and Snidjers (1995). This is a full body model of recumbent sitting postures where all body segments are supported. The model is also based on Dempster's body segment parameters (1955) and predicts external vertical, normal, horizontal and parallel forces, and internal linkage forces. There are, however, several limitations. Model validation was attempted using a force plate in the seat and backrest which is only sensitive to force changes from gross body movements. Only the measurements of tangential forces, as measured by the strain gauges in the force plates, were used for model validation. The measured normal forces were not reported. Another limitation is the lack of anatomical detail. Dempster's body segment parameters represent the pelvis as a linkage connecting the hip joint to the L5/S1 joint. In Goossens and Snidjers' model this linkage extends to the ischial tuberosities where the model is grounded and the thigh linkage then attaches but is parallel to the seat. Goossens and Snidjers do not explain how they derived the position of the ITs. Figure 4a shows Goossens and Snidjers' model and Figure 4b shows how their model relates to support surfaces. It can be seen that there are some significant deficiencies with their model, as the thigh, knee and lower leg would be incorrectly positioned. Goossens and Snidjers also refer to a relationship between the inclination of the backrest (ρ in Figure 4) and pelvis (κ in Figure 4) from Stumbaum (1983), but this does not factor in the inclination of the thighs which have a significant influence over the orientation of the pelvis (Keegan, 1953; Schoberth, 1969).

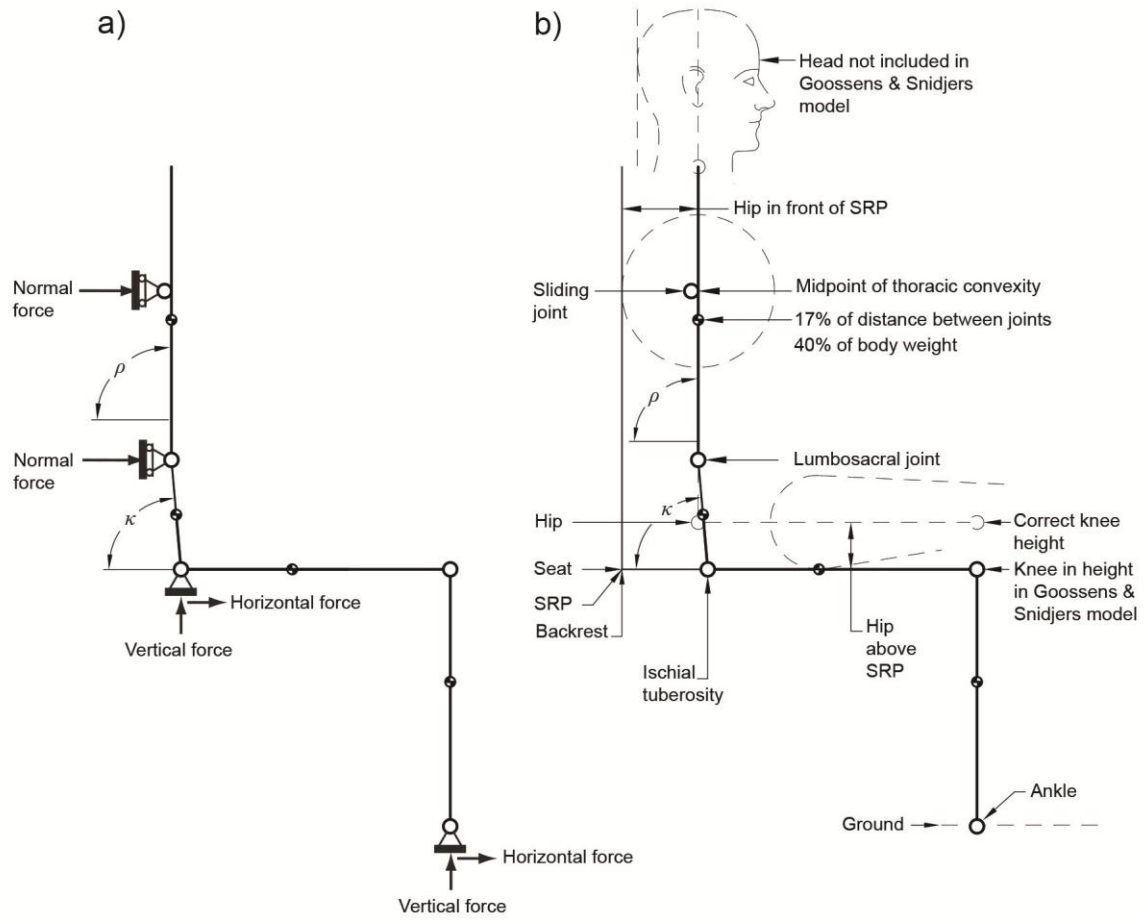

Figure 4 a) Goossens and Snidjers model; b) Goossens and Snidjers' model related to support surfaces as described by Goossens and Snidjers where the thigh linkage, that is parallel to the seat, connects to the ischial tuberosity

Current developments in biomechanical modelling are in the areas of transport design for crash test simulations (Golinski and Gentle, 2002; Keppler, 2003) and transfer of whole body vibration (Verver and Van Hoof, 2002), orthopaedic analysis (Lehner and Wallrapp, 1999), and sports science (King and Yeadon, 2006; Härtel, *et al*., 2006). Several commercially-available musculoskeletal modelling software packages include Santos (SantosHuman™ Inc.), AnyBody (AnyBody Technology A/S), LifeMod (LifeModeler Inc.), SIMM (Musculographics Inc.) and Madymo (TASS). To our knowledge, no publication demonstrates the application of these models for predicting and analysing sitting posture. 3D digital human surface models that integrate with computer aided design software exist which involve 3D anthropometry obtained from body scans and inverse kinematics for applications

in automotive and industrial ergonomics (Duffy, 2008). These anthropometric surface models, based on 3D anthropometric body scans, have evolved out of transportation research, as evident by the vast majority of publications in the digital human domain belonging to the Society of Automotive Engineers (SAE) literature (viewpoint from Dr Matthew Reed, University of Michigan Transportation Research Institute, email correspondence). A typical anthropometric digital human is the Jack (Blanchonette, 2010). Although anthropometrically accurate, Jack does not have a biomechanical model (linkage-base static equilibrium, dynamic musculoskeletal or joint stress) as a foundation. It cannot predict position, velocity or acceleration of movement or loads between body segments or at the body segment-seat interface. The integration of biomechanical models and anthropometric 3D digital humans is emerging as the subject of current research (Paul & Lee, 2011).

For the analysis of reclined sitting posture, an accurate, validated, two-dimensional biomechanical model is first needed that includes detail on pelvic dimensions, the ischial tuberosities and their contact with the seat for various postures and pelvic rotations, and the relationship between the model and the motion paths of support surfaces accounting for how the body flexes and extends. Such a model could have the potential to offer a theoretical foundation to experimental research into sitting where digital models have made no apparent impact, such as small to medium size organisation and the clinical context. An elegant two-dimensional biomechanical linkage model of the sitting posture could also be integrated with 3D digital human models and extend their utility beyond just geometrical and anatomical description.

2.3.2 Interface pressure measurement

The measurement of interface pressure in seating is frequently performed by researchers and clinicians. Although various early techniques for measuring interface pressure have been reported (Frisina & Lehneis, 1970; Linden, *et al*., 1965; Newell, *et al*., 1970; Mooney, *et al*., 1971; Fengusson-Pell, *et al*., 1976), multi-element array systems based on electrical resistance or capacitance have become the industry standard (Diesing, *et al*., 2002). Diesing, *et al*., evaluated three seat pressure sensing arrays and found good linearity for all systems although all underestimated the force applied on a small area. Pipkin and Sprigle (2008) demonstrated that one source of error is the presence of the mat in the body-support interface, which has been reported previously (Swain & Bader, 2002). Pipkin and Sprigle found that this perturbation error resulted in lower pressure readings when compared to baseline readings with no mat present.

A structured review was performed on tilted and reclined seated positions where interface pressure and/or force was an outcome. Eleven studies were found, nine of which involved spinal cord injured (SCI) subjects. The results from these investigations are summarised in Table 1. It is difficult to compare these studies because of the different subject types, pressure and force sensing systems, seating simulators or wheelchairs, varying cushions and amount of support, and varying isolated degrees of tilt-in-space, recline and combinational postures. For example, Shields and Cook (1988) investigated posture with subjects sitting on a hard surface and collecting data using a unique transducer called an ischiobarograph. Gilsdorf, *et al*., (1990) used a powered wheelchair to assess backrest recline and noted that a different recline system would yield different results. Hobson (1992) used a pneumatic pressure sensing array for measuring normal pressure and incorporated load cells into the seat base to measure tangential force. Henderson, *et al*., (1994) used a standard manual wheelchair with a backrest only supporting the lumbar region and a Tekscan pressure mapping system. To improve reliability, they reported peak pressures from an average of a 3 cm x 3 cm area. Spijkerman, *et al*., (1995) assessed individuals on air-filled cushions and reported peak pressures from a single pneumatic cell.

Pellow (1999) collected data from only two subjects, the participants in Vaisbuch, *et al*., (2000) study were children, and Aissaoui (2001) used able bodied-subjects.

Two recent studies have attempted to address the problems of comparing previous studies. Sprigle, *et al*., (2010) investigated the redistribution of load at the seat and backrest, during phases of tilt, recline, and stand assist. The investigators placed pressure mats beneath the cushions and converted the pressure data into force values before normalising to improve generalisation of their results. Their main finding was a linear relationship between angles of tilt, recline and stand assist for both seat and backrest forces. Giesbrecht, *et al*., (2011) focused on tilt only but with a similar objective to systematically measure the relative rate of reduction in interface pressure at the seat for SCI individuals. Although they differed in reporting regional pressures associated with the left IT, right IT and sacrum, in all cases the trend was non linear. Rather, these investigators found a quadratic relationship between tilt angle and change in interface pressure. They found that the rate of pressure reduction increased as the tilt angle increased. Giesbrecht, *et al*., reported greater reductions in pressure at larger angles of tilt than previous studies (Table 1). The investigators explain that this may be due to more up-to-date pressure mapping hardware and software.

Table 1 Interface pressures reported in previous studies for various recline, tilt-in-space and combination postures, expressed as percentage change from upright sitting (AB = able-bodied, SCI = spinal-cord injured). Positive values indicate an increase in pressure and negative values indicate a pressure reduction

		Recline							**Tilt-in-space**									**Combined recline + tilt-in-space**		
		110°	120°	150°	180	10°	15°	20°	25°	30°	35°	40°	45°	50°	55°	60°	65°	110° + 25°	120° + 30°	120° + 45°
Shields & Cook (1988)	AB					-10%														
Gilsdorf, *et al*., (1990)	AB			-28%																
Hobson (1992)																				
Maximum pressure	SCI	0	-12%			2%		-11%												
	AB	7%	13%			-1%		-14%												
Average pressure	SCI	15%	1%			-1%		-10%												
	AB	15%	11%			-3%		-10%												
Henderson, *et al*., (1994)																				
Maximum pressure	SCI										-27%						-47%			
Average pressure	SCI										-17%						-36%			
Spijkerman, *et al*., (1995)																				
Maximum pressure	SCI								-5%											
Burns & Betz (1999)																				
Maximum pressure	SCI												-33%							
Pellow (1999)																				
Average pressure	SCI			-44%							-26%		-33%							
Vaisbuch, *et al*., (2000)																				
Maximum pressure	SCI	-22%							-22%									-29%		
	AB	-9%							-13%									-36%		
Average pressure	SCI	24%							-8%									-9%		
	AB	11%							-11%									-15%		
Aissaoui (2001)																				
Maximum pressure	AB		-4%				-3%			-9%			-27%						-29%	-41%
Average pressure	AB		-6%				-5%			-10%			-24%						-25%	-37%
Sprigle, *et al*., (2010)																				
Load	SCI				-61%										-46%					
Giesbrecht, *et al*., (2011)						-4%		-6%		-23%		-44%		-65%						
Maximum pressure	SCI																			

Hobson (1992)
Zero shear

2.3.3 Stadiometry

An indirect approach to quantifying the compressive force on the spine is to measure the amount of stature change it causes over a specified period of time. It is well established that during the course of the day people lose approximately 15-25 mm of their stature (De Pukey, 1935; Tyrrell, *et al*., 1985; Krag, *et al*., 1990). This loss of stature is largely due to the intervertebral discs which lose approximately 20% of their height and volume, which is a result of sustained loading and creep (Botsford, *et al*., 1994; McMillan, *et al*., 1996). Creep of the intervertebral disc is primarily due to the expulsion of water (Adams & Hutton, 1983; Kraemer, *et al*., 1985; McMillian, *et al*., 1996), although 25% has been attributed to viscoelastic deformation of the anulus (Broberg, 1993). When people sleep at night, the spine is relatively unloaded which results in a swelling pressure in the discs. This swelling pressure imbibes water in from surrounding tissues, and the discs recover (Adams, *et al*., 2006). This circadian variation of the spine is modified by periods of hard work and rest (Tyrrell, *et al*., 1985).

The first reported investigation measuring changes in stature to evaluate spinal loading was by Eklund and Corlett (1984). A precision stadiometer was specifically developed for the investigation. The stadiometer controlled subject's standing posture to a degree where repeated measurements of stature varied no more than 1 mm. Experiments were carried out on subjects under different load conditions. After each loading condition, measurements of stature were made using the stadiometer. Several sitting postures were included in the experiments. The investigators found that the rate of shrinkage was highest for sitting on a stool, lowest for an easy chair and medium for an office chair. Sitting on a stool resulted in more shrinkage than standing which corresponds to intradiscal pressure measurements reported previously (Nachemson, 1964). The investigators also noted that an exponential function (Equation 1) could be used to model the rate of change in stature, given that the load on the spine was kept constant.

$$H(t) = A_1 + A_2 e^{-Kt} \tag{1}$$

Stadiometry went on to be used extensively in ergonomic research (Bonney, 1988; Sullivan & McGill,1990; Jafrey & Haslegrave, 1992; Althoff, *et al*., 1992; Burton & Tillotson, 1994; Michel & Helander, 1994; Magnusson & Hansson, 1994; Leivseth & Drerup, 1997; Hadley & Haslegrave, 2000; van Deursen, *et al*., 2000; Beynon & Reilly, 2001; van Dieën, *et al*., 2001; Bonney & Corlett 2002; Fryer, *et al*., 2010, Shan, *et al*., 2012). Several studies have also demonstrated good reliability with the technique (Kanlayanaphotporn, *et al*., 2003; Rodacki, *et al*., 2001; Healey, *et al*., 2005; Pennell, *et al*., 2012).

Althoff, *et al*. (1992) proposed an improved method for stature measurement. Because measurement of stature depends on the loading history of the spine, studies preceding Althoff, *et al*. (1992) had to be done at the same time of the day whilst controlling previously applied loads (i.e. sleep patterns and daily routine). In this way, the differences in the magnitude and rate of stature change observed in the experiments are attributed to the test interventions and not the loading history. Althoff, *et al*. proposed a pre-test period whereby the natural magnitude and rate of shrinkage could be ascertained. This rate of shrinkage was then estimated for the test period using the exponential function (Equation 1), at which time the subject participated in the experiment. The net difference between the prediction of the natural course of stature change and the actual height change during the test period was taken to define the height change as a result of the test intervention. This method eliminated the influence of the individual spinal loading history of the subjects. Using this method, the investigators found that identical spinal loads (whether applied in the morning or in the afternoon) caused the same net change of stature. The method proposed by Althoff, *et al*. was employed in several subsequent investigations (van Dieën, *et al*., 1994; Burton & Tillotson, 1994; Leivseth & Drerup, 1997; Beynon & Reilly, 2001).

Van Dieën and Toussaint (1993) published a review of the research using stadiometry which highlighted the inconsistent findings on age, showing that some studies reported a decreasing

shrinkage with age (Corlett & Eklund, 1986) whilst others reported the inverse (Magnusson, *et al*., 1990). Michel and Helander (1994) suggested that this could be due to a wide range of deflections that were associated with a moderate load. When the load on the spine is greater, the range of deflections is smaller and hence no correlation was observed. This is in approximate agreement with Van Dieën, *et al*. (1994) who suggested that a relationship between spinal shrinkage and age existed for the rate of shrinkage but that this relationship disappeared when the discs reached equilibrium deformation.

Lewis and Fowler (2010) studied the relationship between the length of the spine, measured with Magnetic Resonance Imaging (MRI), and total stature change, measured using stadiometry. They confirmed that a significant correlation existed between total lumbar length and stature (Lewis & Fowler, 2009), however, the investigators advised that stadiometry should not be used to quantify individual disc height (Lewis & Fowler, 2010).

2.3.4 Surface electromyography

Back muscle activity during sitting has been of scientific interest for over 60 years (Åkerblom, 1948; Morin & Portnoy, 1956; Steen, 1964; de Vries, 1965; Fountain, *et al*., 1966; Knutsson, et al., 1966; Nachemson, 1966). Apart from the study by Knutsson, *et al*. (1966), most of the early investigations reported on the assessment of only one or two sitting postures. Most of these early studies demonstrated rather than measured myoelectric activity and have generally been limited to a single region of the back. A series of studies were published in 1974 reporting more extensive use of electromyography to assess various sitting positions and seating types (Andersson, *et al*., 1974[a-f]).

The first of these studies used an experimental chair to investigate backrest inclination, lumbar support and thoracic support (Andersson & Örtengren, 1974[a]). Surface electrodes were placed on both sides of the spine at L3, L1, T8, T5, T1, C4 levels and at the trapezium. 20 subjects were included in the investigation. Full-wave rectified and averaged (FRA) myographic values were determined for each muscle. No statistical difference was found between the left and right side. No significant difference was found when comparing relaxed standing and unsupported sitting except for T5 (straight sitting) and T8 (all positions). Backrest inclination was found to be the most important sitting parameter with a reduction in recorded FRA values corresponding to an increase in inclination. The difference was significant between 80° or 90° and 130°. In general, changing the lumbar support only had a minor effect, however at 80° and 90° there was an increase in activity at L1 and a statistically significant increase at L3 level when the lumbar support increased towards lordosis (-2 to +4 cm). The thoracic support had almost no effect on myographic values for the different muscles.

Andersson and Örtengren noted that the amplitude of the myoelectric signal picked up by means of the surface electrode was affected by the thickness of the surrounding soft tissues. If the soft tissue layer was thin, larger values were recorded. The investigators explained that they still preferred surface electrodes because they were simple to handle, they picked up signals from a comparatively large volume of muscle, and they did not cause discomfort to the test subjects. The inter-individual differences that were observed were therefore partly attributed to the differences in the amount of soft tissue as well as differences in the distribution of muscle. In another study the investigators compared surface electrodes with wire electrodes which were inserted directly into the muscle. They found that wire electrodes were more sensitive to electrode location and therefore gave less precise estimates than surface electrodes (Andersson, *et al*., 1974[b]). This study was in agreement with the previous one showing that backrest inclination was the most important parameter for reducing myoelectric back muscle activity, and that lumbar support is of minor importance (Andersson & Örtengren, 1974[a]; Andersson, *et al*., 1974[b]).

In another study by Andersson, *et al*. (1974 [c]) simultaneous recordings of intradiscal pressure of the third lumbar disc and myoelectric activity of various back regions were investigated. The results were in agreement with the other studies (Andersson, *et al*., 1974 [a-b]), showing that there was little difference in myoelectric activity between standing and unsupported sitting, with backrest inclination being the most important variable. Backrest inclination also reduced disc pressure, however, disc pressure was found to be considerably higher in unsupported sitting, which is in agreement with earlier findings (Nachemson & Morris, 1964). The investigators calculated the correlation coefficients between disc pressure and myoelectric activity for all positions in which the back was supported. When calculated over all postures (including seat tilt, lumbar support, thoracic support and backrest inclination variables) the coefficients were too low to allow for accurate prediction of disc pressure by means of myoelectric activity at a single level. The investigators did consider that it might be possible to predict disc pressure by activity taken from several muscles, but did not demonstrate this in their publication. High positive correlation coefficients were found when isolating muscles at T10 and L3 levels on the left side and varying backrest inclination. The investigators noted that these levels provided the most systematic data. These high correlation coefficients were exhibited when varying backrest inclination for all lumbar support settings. Therefore, with knowledge of the posture of the back, the investigators demonstrated the possibility to predict disc pressure by means of myoelectric activity at T10 and L3 levels on the left side.

Andersson and colleagues went on to apply their research to three types of seating: an office chair (Andersson & Örtengren, 1974[d]), a wheelchair (Andersson & Örtengren, 1974[e]) and a car driver's seat (Andersson, *et al*., 1974[f]). As with their previous studies, the main factor influencing myoelectric activity was backrest inclination.

2.3.5 Posture measurement

Sitting posture refers to the position of spinal segments with respect to each other and with respect to gravity (Claus, *et al*., 2009). Sitting posture has been measured using radiographs (Åkerblom, 1948; Keegan, 1953; Schoberth, 1969; Andersson, *et al*., 1979, Columbini, *et al*., 1985, Dunk, *et al*., 2009; De Carvalho & Callanhan, 2012). Radiography is able to give accurate measurements of spinal posture but has an inherent health risk (Berrington de González & Darby, 2004). Recently, positional MRI has been used to assess sitting posture (Bashir, *et al*., 2006, Karadimas, *et al*., 2006; Hedberg, *et al*., 2012). Positional MRI has the advantage of providing accurate information on posture and disc volume without the health risk associated with radiology, however, at the time of writing, the method has limited accessibility. Those studies identified that reported use of positional MRI for sitting postures all used the same scanner in Aberdeen.

Various other techniques have been employed to carry out non-invasive measurements of spinal posture at the skin surface. Researchers have used inclinometers attached to the beams of anthropometers (Mølhave, 1958; Bendix and Biering-Sø, 1983; Bendix, *et al*., 1988), and electronic inclinometers attached either to contact belts (Wu, *et al*.,1998) or directly to the skin (Dolan, *et al*., 1988). Draughtsman's flexible curves capable of bending in one plane only and maintaining an adopted shape have been used for copying spinal profiles to paper (Israel, 1959; Anderson & Sweetman, 1975). The Flexicurve method was validated by Hart and Rose (1986) and by Burton (1986), however, these investigators differed in how they measured the curve. Burton measured the angle between tangents drawn to the curve at S2 and L4 for the lower lumbar curvature and L4 and T12 for upper lumbar curvature. Hart and Rose derived an angle from trigonometric measures. Two points on the curve, representing L1 and S2, were connected by a line (l). A perpendicular line (h) representing the height of the lumbar curve, bisected the line l. The length of each line was determined in millimetres, and the values were inserted into

Equation 2. Angles that were positive numbers were considered as lumbar extension, and angles that were negative numbers were referred to as lumbar flexion.

$$\theta = 4 \times \arctan(2h/l) \quad (2)$$

This trigonometric method for calculating lumbar curvature as described by Hart and Rose (1986) was used by other researchers (Frey & Tecklin, 1986; Link, *et al*., 1990; Reinecke, *et al*., 1994). Reinecke, *et al*., incorporated electronic strain gauges into the Flexicurve to overcome problems of measuring lumbar curvature when a person leaned against a backrest.

Optical motion capture systems have been used for measuring spinal posture (Pearcy, *et al*., 1987, Crawford, *et al*., 1999; Frigo, *et al*., 2003), however, not for sitting. This is due to the backrest obstructing the camera view of the retro-reflective markers on the back of the subjects. Articulating mechanical arms that digitise points in 3D space have been employed to analyse sitting postures (Bishu, *et al*., 1991; Matlais, *et al*., 1999). In these studies, vertical slots had to be cut out of backrests to allow access of the digital arm.

Electromagnetic motion capture systems provide an alternative to optical systems where the field of view is obscured. Early versions of these systems tracked single sensors (Pearcy & Hindle, 1989; Dolan and Adams, 1993), whereas newer systems tracked four (Swinkels & Dolan, 1998) and eight (Meskers, *et al*. 1998) sensors, with accuracies of 0.15° (Swinkels & Dolan, 1998) and 2.15° (Koerhuis, *et al*., 2003), respectively. To the author's knowledge, the use of an electromagnetic motion capture system to evaluate back profiles in seated postures where access to the upper body is limited by the backrest has not been reported.

2.4 Identification of the gap in knowledge

Contemporary ergonomic theory is based on fragmented research stretching back over 60 years, where previous studies have focused on upright, task orientated, seating (Pynt, *et al*., 2008). Posture, muscle activity, and creep loading in the discs have been described as important biomechanical principles for the effects of seating on the human spine. These three mechanisms are important because they determine the extent to which mechanical loading is distributed across spinal structures and innervated tissues (Adams, *et al*., 2006). No studies have been identified that evaluate how recline, tilt and combinational seating systems affect posture, muscle activity and creep loading.

Although digital human models are now commercially available, with some beginning to integrate biomechanical models, there have been no publications identified that demonstrate their application in the analysis of reclined sitting posture. Chaffin (2005) argued that the state of the art in digital humans using inverse kinematics and other robotic methods failed to accurately model posture, and that this was fundamental to an accurate biomechanical model. No evidence to date suggests that, in the context of reclined sitting where the body is fully supported, biomechanical digital models offer more sophistication over traditional methods of analysis, and that they have inherited rather than addressed the previous limitations. The vast majority of digital human models are elegant representations of a body 3D anthropometry. They do not include an associated static and dynamic model from which kinematics, kinetics and joint stresses (biomechanical variables) may be computed. Such developments of integrating digital human models with musculoskeletal static or dynamic biomechanical models are the subject of current and future research.

A gap in knowledge exists both for empirical data on reclined sitting posture and for a biomechanical model that accurately predicts posture, pelvic rotation and its relative position to

the support surfaces, ischial tuberosity contact and the point of load transfer to the seat, internal and external load distributions, and the relationship between the body and the support surface motion paths.

2.5 Test-rig design for seated test posture evaluation

A multi-adjustable test-rig (Figure 4) was designed and built specifically to collect biomechanical data for the purposes of this research. Figure 6 gives the dimensions for the test-rig support surfaces and illustrates their path of movement.

The test-rig has a tilt-in-space (TIS) function with elevating leg rest. The TIS angle is controlled by a mechanical locking mechanism and wired remote switch, and rotates about pivot 1 (Figure 6). Pivot 1 is in approximate alignment with the occupant's centre of mass. The leg rest elevation is synchronised with the tilt function and elevated about a virtual pivot (pivot 5 in Figure 6) which is approximately in line with the occupant's knee joint. Various seat lengths are available with the design to accommodate a population between 5th percentile woman and 95th percentile man (Pheasant and Haslegrave, 2006). The height and position of the leg rest are adjustable to maintain the same relationship with the different seat length options. The backrest to seat angle can be adjusted to any angle between 90° and 135° by a mechanical locking mechanism, and controlled with a remote wired switch. The location of the pivot for the backrest (pivot 2 in Figure 6) is in approximate alignment with the occupant's hip joint so that the backrest maintains a similar relationship with the subject's back for the different seating postures. Additional articulation for the backrest is provided by pivots at the approximate levels of LI/T12 and C7/T1 (5th%ile woman) and controlled by friction locks (Figures 5 and 6).

All adjustments can be measured by inspection of specially fitted protractors. The test-rig is built from aluminium and plywood with stainless steel fixtures. The test-rig is designed to collect biomechanical data including electromagnetic motion capture-based kinematics. Any mild steel parts would distort the electromagnetic data collection. The seat and backrest cushions are made of domestic grade 40kg density polyurethane foam upholstered in a 70% wool/ 30% viscose woven fabric. These interface materials were chosen because they were commonly used in domestic seating. In addition, the foam is relatively dense and does not have viscoelastic properties which are known to cause large amounts of creep. A pilot test was carried out with one investigator acting as the test subject to assess the creep characteristics of this foam type, and the amount of time required for stabilisation. The results are reported in Figure 27, Section 4.2.2.

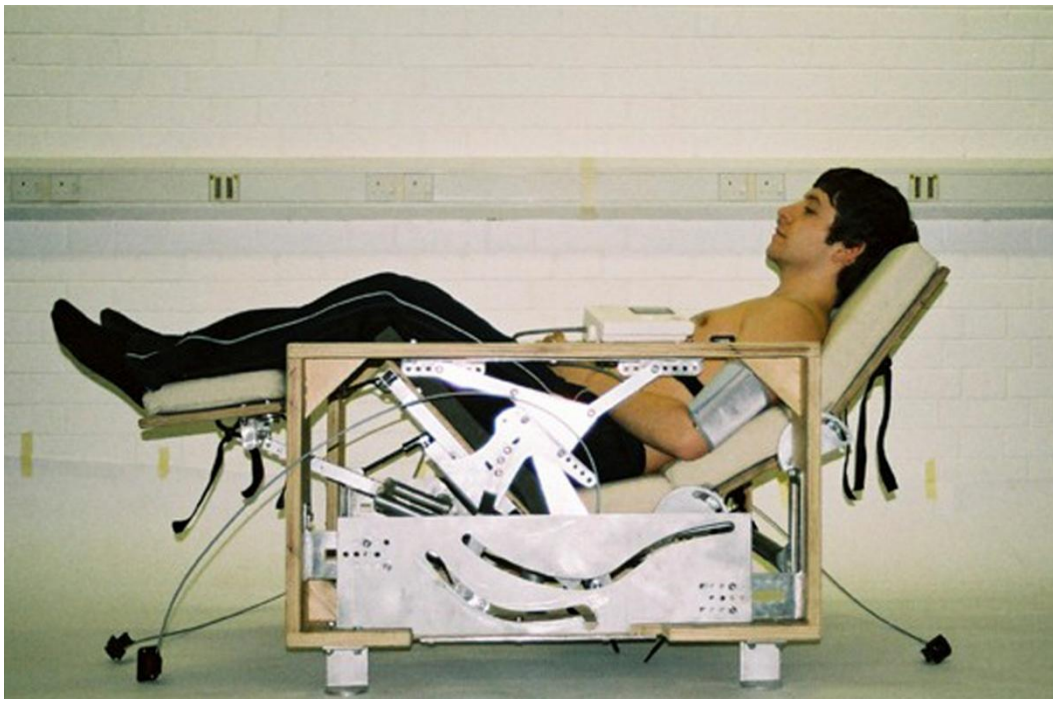

Figure 4 The multi-adjustable test-rig

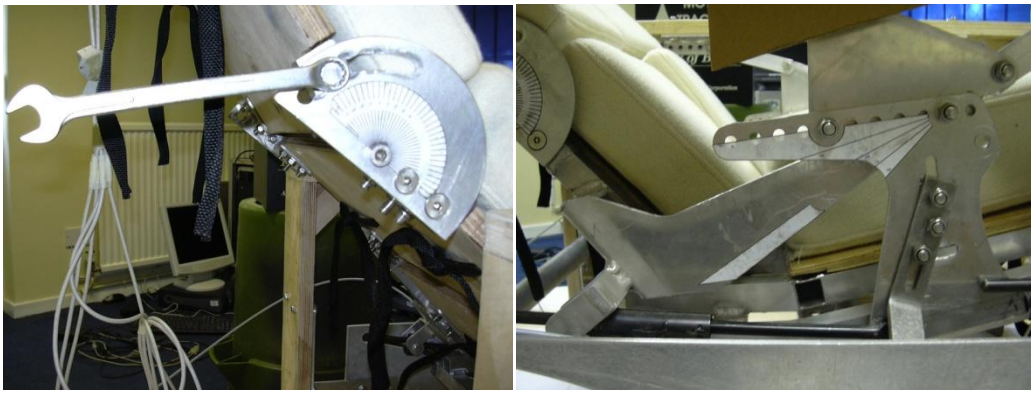

Figure 5 Test-rig parameter controls

Table 2 specifies the inclinations of the support surfaces for the five seated test postures, which are based on the coordinate system in Figure 6. The upright posture was established to serve as a baseline from which to compare the various recline and tilt-in-space postures. It was considered important that the upright posture reflected common static lounge chair postures, so that any effects observed for the reclined positions would represent a meaningful difference.

The standard recline posture was identified from market research where the average back recline was 125° with a seat tilt of 15°. These parameters fit well with Keegan's recommendation (1953) that a 135° trunk to thigh angle will promote muscular equilibrium and spinal lordosis.

Two versions of tilt-in-space (TIS) posture are included in the study, one full tilt-in-space with a seat angle of 60° (TIS 3) and one half tilt-in-space with a seat tilt of 35° (TIS 2). The backrest setting for the TIS postures is the same as for upright, with a seat to backrest angle of 105°. A tilt-in-space with articulating backrest (TIS 1) is included in the investigations whereby the backrest is articulated prior to the subject sitting in the test-rig.

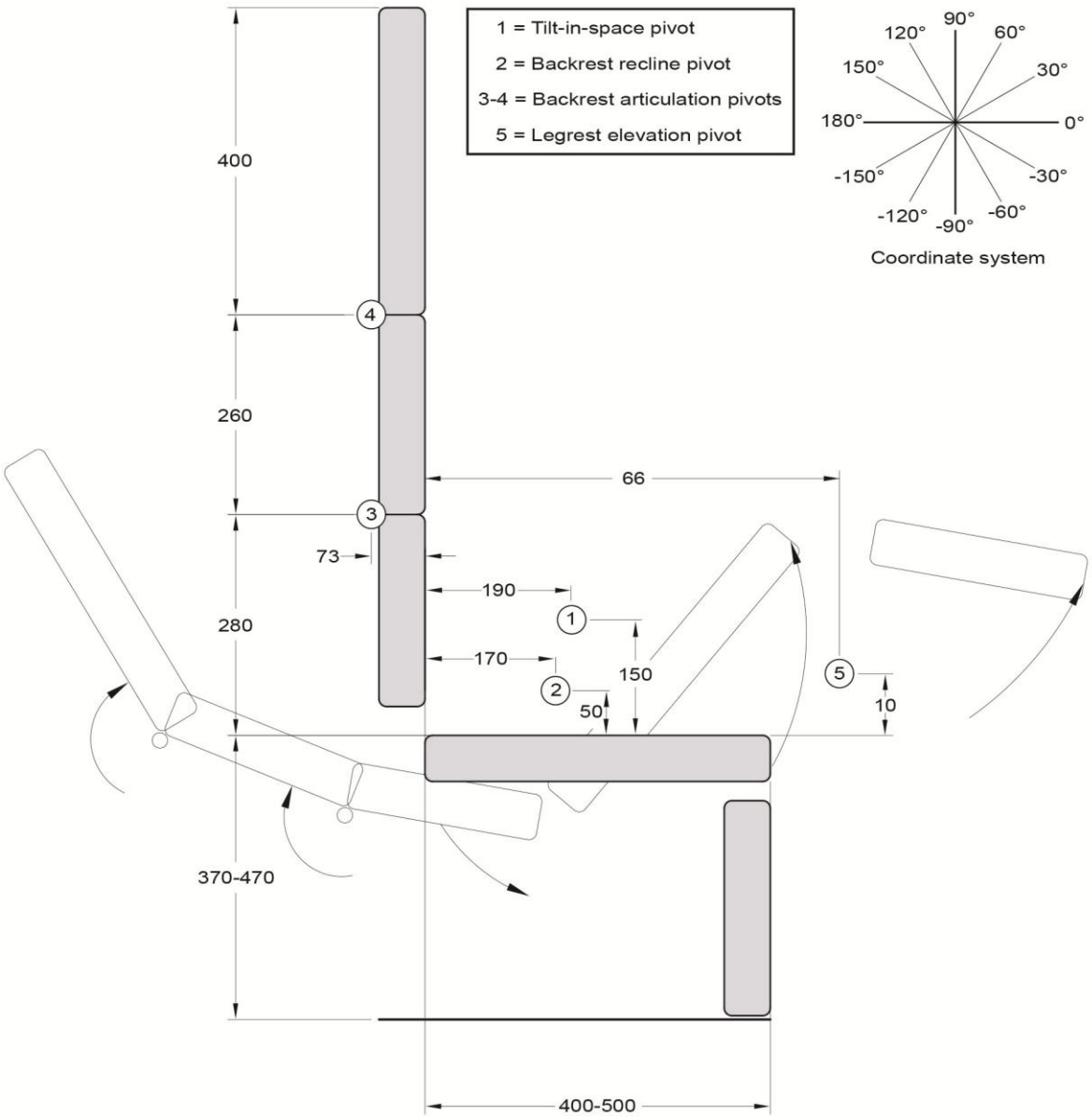

Figure 6 Diagram showing test-rig dimensions (mm) and illustrating motion. The centres of rotation of the support surfaces are denoted 1-5 and defined. The coordinate system that is used throughout this research is shown whereby positive angles are anticlockwise to the horizontal and negative angles are clockwise to the horizontal

Table 2 Inclinations of the test-rig supports for the seated test postures (°)

	Upright	Standard	TIS 1	TIS 2	TIS 3
Head	100	120	125	125	150
Thoracic	120	140	150	145	170
Lumbar	120	140	175	145	170
Seat	10	15	50	35	60
Lower leg	-70	-5	-10	-30	0

3 Development of a Two-Dimensional Biomechanical Model

This chapter describes the development of the biomechanical model, beginning with the body link diagram that describes the body segment parameters and sitting kinematics. The process for configuring the model to the test postures is given, along with various output parameters for model validation and interpretation of experimental data.

3.1 Model development

3.1.1 The pelvis

In standard seating ergonomics, pelvis motion is defined by a centre of rotation at the hip joint (Serber, 1994; Tilley, 2002). An analysis of pelvic motion given further into this chapter requires knowledge of the location of the ischial tuberosities (ITs). Standard anthropometric data and body segment parameters typically do not include the ITs position (Pheasant, 1986; Pheasant & Haslegrave, 2006). To address this deficiency, reference was made to Reynolds, *et al*., (1982) who obtained data from 80 male and 85 female skeletons. Reynolds, *et al*., published 3D coordinates detailing the small female, medium male and large male pelvises primarily for the design of automotive test mannequins. To determine the position of the inferior ITs in the present study, the medium male pelvis was recreated in 3D CAD software. The anatomical position was assumed to correspond to the pelvis in the standing posture and the medium sized male pelvis was assumed to correspond to 50th percentile man. Figure 7a gives the sagittal projection of the CAD model of the pelvis for standing and the position of the inferior IT, superimposed with a link model based on the body segment parameters from Pheasant (1986) in Table 3. The model joint for the IT includes a space for the soft tissues. This was derived when fitting the pelvis model to a link model in an anatomical position (Figure 16), where the vertical distance from the seat surface to the hip joint is known (Pheasant, 1986).

3.1.2 The torso and head

Standard body segment parameters represent the torso and head as two linkages, joined at C7 (Pheasant, 1986). To model the sitting posture for chair designs with shaped backrests or adjustable supports for the back and head, several linkages are needed to better represent the mobility of the upper body. Snyder, *et al*., (1972) studied motion of the torso in seated conditions and gave spatial data on almost all of the vertebrae. Based on their equations, Reynolds (1978) modelled the seated 50th% percentile man with spinal linkages connecting the interspaces of L5–S1, L2–L3, T12–L1, T8–T9, T4–T5, and C7–T1.

The additional torso segments, used in the body link diagram (Figure 7a), were derived from Reynold's interpretation of Snyder's, *et al*., data for the 50th percentile man. The same terminology is used in the body link diagram for torso segmentation; however, it is important to note that the model joints between L5–S1 and C7 are not spine joints. They are model joints described using spinal height levels but located on a straight line between L5–S1 and C7 (when a straight back is assumed). Two linkages for the lumbar spine connect L5–S1, the centre of the L3 vertebral body and T12–L1. No additional linkages were given for the thorax as this is generally immobile (Schoberth, 1969). The centre of the C7 vertebral body provided the location for the fourth joint. The lengths of the torso segments are given in Figure 7a and the percentages with respect to the total length of the trunk are described in Table 3. These proportions were used to estimate the mass of the spinal segments in Table 4 and for the lumbar segments the centres of mass were positioned at the linkage midpoints. Since the arms are unsupported, the mass of the arms was added to the thoracic segment.

Pheasant (1986) estimated various landmarks on the back and head that he considered important in the design of chairs. Pheasant's data includes the most posterior point on the back of the head for sitting erect and was used to determine the position of the sliding contact H in the

present model (Figure 7b). The location for the centre of mass of the head was taken from the standard body segment parameters (Table 4).

Table 3 Body segment lengths adapted from Pheasant (1986)

	Body Segment	Men	Women
d_1	Head	14.5% of stature	14.7% of stature
	Trunk	27.7% of stature	28.3% of stature
	d_2 Thorax	62% of trunk	62% of trunk
	d_3 Upper lumbar	19% of trunk	19% of trunk
	d_4 Lower lumbar	19% of trunk	19% of trunk
d_5	Pelvis	5.7% of stature	5.7% of stature
d_6	Thigh	24.3% of stature	24.2% of stature
d_7	Lower leg	23.6% of stature	23% of stature

Table 4 Body segment masses adapted from Pheasant (1986)

	Body Segment	*Mass*	*Location of Centre of Mass*
F_{g1}	Head	8.4% of body	57% of distance from J_1 to vertex (top of head)
	Trunk	36.6% of body	60% of distance from J_4 to Joint J_1
	F_{g2} Thorax	62% of trunk	35% of distance from J_2 to J_1
	F_{g3} Upper lumbar	19% of trunk	Midpoint of the upper lumbar segment
	F_{g4} Lower lumbar	19% of trunk	Midpoint of the lower lumbar segment
	F_{g5} Pelvis	13.4% of body	Approximately at the hip joint (midpoint of the line connecting IT and J_4)
F_{g6}	Thigh	10% of body	41% of distance from IT to J_6
F_{g7}	Lower leg	4.3% of body	44% of distance from J_6 to J_7
	Upper arm	2.8% of body	48% of distance from shoulder to elbow
	Forearm	1.7% of body	41% of distance from elbow to wrist joints
	Hand	0.6% of body	40% of hand length from wrist joint

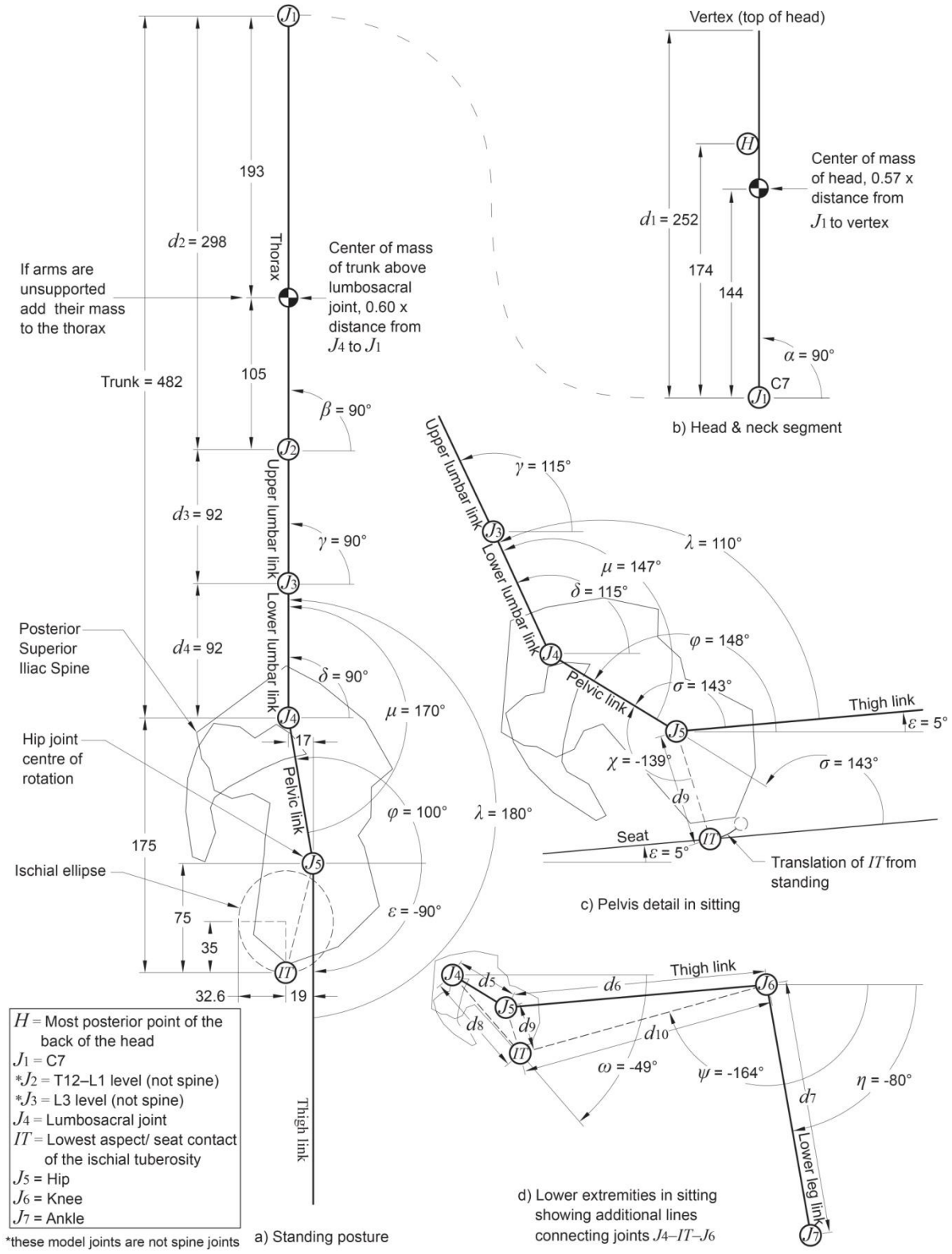

Figure 7 The body link diagram extended from Pheasant's body segment parameters (Pheasant 1986) (Tables 3 & 4). Modifications include pelvis detail from Reynolds, *et al*., (1982) (Section 3.1.1), additional torso linkages derived from Reynolds (1978) and the sliding head joint from Pheasant (1986) (Section 3.1.2), and the incorporation of data from Andersson, *et al.*, (1979) and Moes (2007) for sitting kinematics resulting in additional linkages to the IT and the ischial ellipse (Section 3.1.3). 7a) shows the sagittal projection of the 50th percentile male pelvis showing detail of the position of the inferior ischial tuberosity and its path of movement (ischial ellipse) overlaid with the model link system from thigh to C7; b) the model link system for the head; c) the sagittal projection of the 50th percentile male pelvis in a sitting posture showing the translation of the inferior IT overlaid with the model link system from thigh to upper lumbar; d) the lower extremities in a sitting posture showing detail of additional lines connecting joints J4–IT–J6. Note: The centres of mass for each segment are shown in Figure 10.

3.1.3 Sitting kinematics

The position of the pelvis when sitting is important as it determines the shape of the spine (Schoberth, 1969). Several early radiographic studies have identified changes in trunk–thigh angle as the primary source of motion of the pelvis (Keegan, 1953; Schoberth, 1969), which has been corroborated with positional MRI (Bashir, *et al*., 2006). This is mainly due to large passive forces that arise from the posterior thigh and gluteal muscles when the hip flexes, and the anterior trunk–thigh muscles when the hip extends (Keegan, 1953).

In unsupported sitting on a horizontal seat, the pelvis rotates posteriorly by approximately 30° from standing (Pheasant & Haslegrave, 2006). In this posture, passive forces arising predominantly from the posterior spinal ligaments are assumed to limit the rotation of the pelvis. There is little data available, however, to estimate the position of the pelvis for intermediate sitting postures. Andersson, *et al*., (1979) took radiographs of the pelvis and lumbar spine from 10 subjects during standing, sitting with backrest inclinations of 110° and 100°, and unsupported sitting. Various angles were then measured from these radiographs. Andersson, *et al*.'s, data for the pelvis angles (relative to the horizontal) are given in Figure 8, with the corresponding thigh–lumbar angles (λ) and pelvis–lumbar angles (μ) for those same postures. These data show, that for the posture with a 100° backrest inclination, the pelvis–lumbar angle reduced by approximately 30° (μ = 140°). When μ = 140°, L5–S1, L4–L5 and L3–L4 are assumed to be maximally flexed (passively) and the pelvis maximally rotated. Further reductions in thigh–lumbar angles below 100° (λ < 100°) are assumed to occur at the hip joint. The prediction of pelvis positions for postures with thigh–lumbar angles greater than 100° (λ > 100°) are based on Andersson *et al*.'s data on one intermediate posture (λ = 110°). The pelvis–lumbar angles, extrapolated from Andersson *et al*.'s data in Figure 8, are given in Table 5 with a polynomial interpolation of those values. These are the critical angles required by the model for predicting the orientation of the pelvis, since μ represents the orientation of the pelvis with respect to the spine, and is a function of λ (the thigh–lumbar angle). The polynomial interpolation in Table 5 was

calculated in Microsoft Excel after plotting the λ and μ values of in a scatter graph and fitting a polynomial trendline.

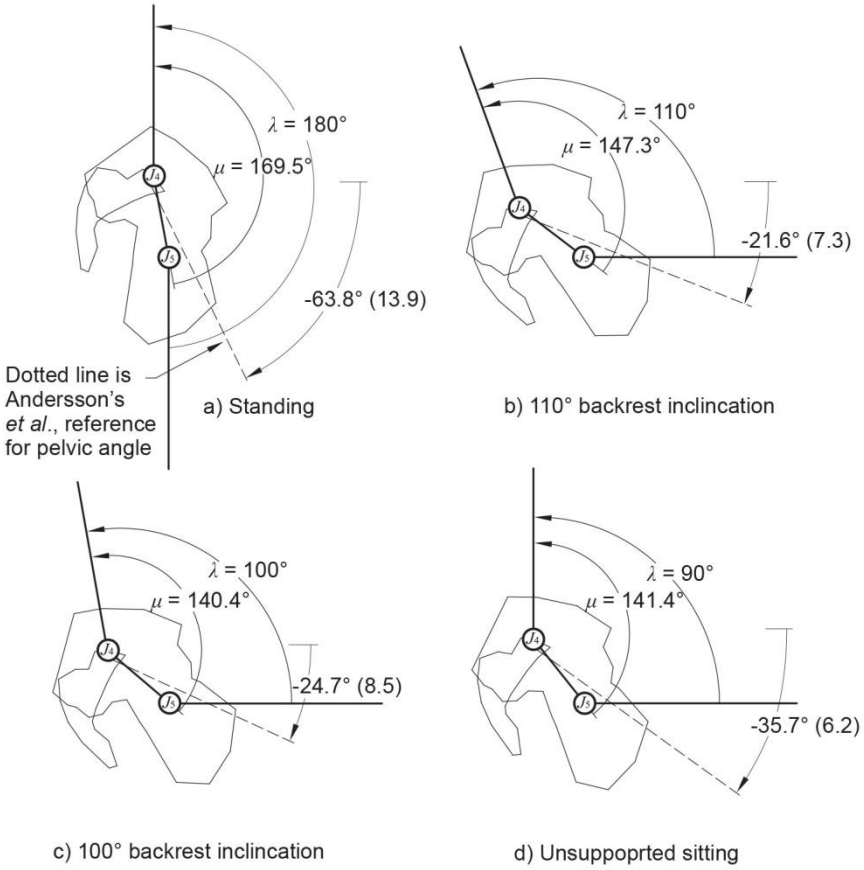

Figure 8 Diagrams showing the relationship between thigh–lumbar (λ) and pelvis–lumbar (μ) angles. Thigh–lumbar angles are assumed to correspond to seat–backrest angles which Andersson, *et al*., (1979) used to relate measurements of pelvic rotation (the dotted line). The pelvis–lumbar angles (μ) were determined from their data. Note Andersson et al.'s, data were adapted to the present coordinate system and the standard deviations, in parentheses, were calculated from the standard error of the means in their original publication.

Table 5 Polynomial interpolation of pelvis–lumbar angles (μ) with respect to thigh–lumbar angles (λ). Inclinations are anticlockwise to the horizontal and in degrees.

Thigh–lumbar angle (λ)	180	170	160	150	140	130	120	110	100
Pelvis–lumbar angle (μ)	170							147	140
Polynomial interpolation of μ	170	169	168	166	162	158	153	147	140

Note. The pelvis–lumbar angles are derived from Andersson *et al*.'s, data (1979). For $\lambda \leq 100$, $\mu = 140°$

For thigh–lumbar angles (λ) ≤ 100° the pelvis–lumbar angles (μ) are assumed to equal 140°. Equation 3 gives the third order polynomial from Table 5. Here, $\lambda = \delta - \varepsilon$, where δ (shown in Figure 7a) is the inclination of the lower lumbar segment and ε (shown in Figure 7c) is both the

thigh and seat inclination. Figures 7(a) and 7(c) show the pelvis–lumbar angles in standing (λ =180°) and sitting (λ =110°). A pelvis reference coordinate system, rather than a global coordinate system, was selected to describe pelvic rotation. Note that, although Equation 3 describes the position of the pelvis, it does not limit the range of motion of the pelvis in the biomechanical model. This was achieved with the addition of a force that represents the net effect from the posterior ligaments and is described in a Section 3.1.5.

for 180 ≥ λ >100

$$\mu = -4.66 \times 10^{-3} \times \lambda^2 + 1.67 \times \lambda + 20.13 \quad (3a)$$

for λ ≤ 100

$$\mu = 140 \quad (3b)$$

where μ and λ are in degrees.

Motion of the pelvis is complex. In sitting, the ITs contact the seat surface but the pelvis does not pivot at that point as it rotates. Neither does the pelvis pivot at a hip joint with thighs fixed. Moes (2007) describes pelvic motion as rotating about a *helical axis* that is located between the IT and skin. In the context of a two dimensional model the axis of rotation will translate in the sagittal plane as a function of pelvic rotation. Therefore, the peak contact points of the inferior ITs shift as the pelvis rotates and the ITs roll against the inner surface of the skin.

Figure 9 is an adaptation of Moes' (2007) circular disc model of the ITs. Moes found that, as the pelvis rotates, there is a related change in the distance between the ITs. This is because the ischial blades converge towards the pubic symphasis. Moes found that, for every 1° of pelvic rotation, the distance between peak IT pressures changed by an average of 0.45 mm for a group of eleven male and nine females. To account for the sagittal translation of the inferior ITs in the body link diagram, the angle between the ischial blades (z) is needed (lines AO and BO in Figure

9). This can then be used to find the radius of the ischial discs (r) in Equation 4 (adapted from Moes, 2007) to complete the model. The derivation of r follows Figure 9. To estimate the angle z, reference was made to the 3D CAD model recreated from the coordinates by Reynolds, *et al*., (1982). The chosen angle was measured between the transverse projections of lines connecting the inferior tuberosity point (the point of convergence of the medial and lateral margins of the IT) and the medial tuberosity point (the most medial point on the medial margin of the IT with the pelvis in the anatomical position). This was found to be 43° and results in an ischial disc with a radius of 35 mm. Reynolds, *et al*., also give data on female pelvises, and the data is scalable for populations not represented in his study.

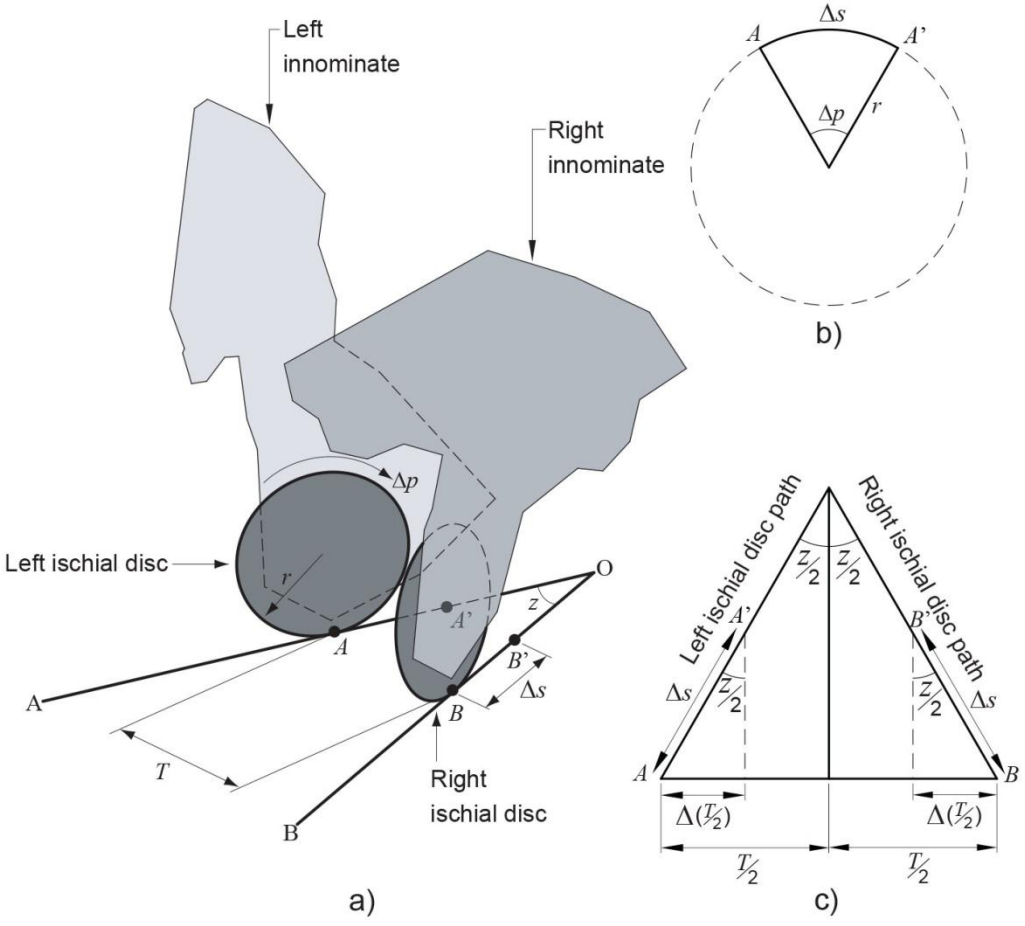

Figure 9 An adaptation of Moes (2007) circular disc model of the ischial tuberosities (ITs): a) the circular discs representing the ischial blades travel along lines AO and BO as the pelvis rotates. Δp is pelvic rotation (°), T is the distance between the inferior ITs, Δs is the distance the ischial discs travel along lines AO and BO, z is the angle between lines AO and BO and r is the radius of the ischial discs; b) the ischial blade, represented as a circular disc; c) plan view of Figure 9a

Aim: to find r in terms of T and z.

from Figure 9b,

$$\Delta s = r\Delta p \tag{4a}$$

from Figure 9c,

$$\frac{\Delta(T/2)}{\Delta s} = \sin\left(\frac{z}{2}\right)$$

$\therefore$

$$\Delta s = \frac{\Delta(T/2)}{\sin(z/2)} \tag{4b}$$

Replacing Δs from Equation 4b in Equation 4c,

$$\frac{\Delta(T/2)}{\sin(z/2)} = r\Delta p = r = \frac{\Delta(T/2)}{\Delta p \sin(z/2)} \tag{4c}$$

The sagittal projection of the ischial disc is an ellipse with a vertical semi-major axis of 35 mm and a semi-minor axis of 32.6 mm, and is shown in Figure 7a. This geometry was modelled in CAD software and the point of intersection of the ellipse against the seat was connected to the hip by the line d_9 (Figures 7a and 7c). The pelvis was then rotated in steps of 5° with respect to the seat and the change in the length of the line d_9 and its angle (χ) against the pelvis were noted (Table 6). Equations 5 and 6 give the polynomial interpolation of these values, which were calculated in Microsoft Excel after plotting in scatter graphs against σ and fitting polynomial trendlines.

Table 6 The length and angle of the line connecting the IT and hip with respect to the pelvis–seat angle. Inclinations are to the horizontal, in degrees and clockwise angles are negative

Pelvis–seat angle (σ)	100°	105°	110°	115°	120°	125°	130°	135°	140°	145°	150°	155°
IT–hip length (d_9)	77	78	78	79	79	79	79	78	78	77	77	76
Angle between the line connecting hip to IT and the pelvis(χ)	-156°	-154°	-152°	-150°	-148°	-147°	-144°	-142°	-140°	-138°	-136°	-134°

$$d_9 = -2.93 \times 10^{-3} \times \sigma^2 + 0.72 \times \sigma + 34.56 \quad (5)$$

$$\chi = 5.32 \times 10^{-04} \times \sigma^2 + 0.27 \times \sigma - 188.30 \quad (6)$$

Figure 7d shows the lower extremity linkages with dotted lines connecting the inferior IT to the hip, knee and lumbosacral joint. Additional relationships are required for the lengths of the dotted lines connecting the inferior IT to the knee (d_{10}) and lumbosacral joint (d_8) which are given in Equations 7 and 8, respectively. The inclinations of those lines (ψ and ω) are given in Equations 9 and 10. Derivations follow all equations.

$$d_{10} = \sqrt{{d_6}^2 + {d_9}^2 - 2\, d_6\, d_9\, \cos(360 - \sigma + \chi)} \quad (7)$$

where d_{10} is the length of the line connecting the IT and the knee (J_6), d_6 is the length of the thigh linkage, d_9 is the length of the line connecting the IT and the hip (J_5), σ is the thigh–pelvis angle and χ is the angle between d_9 and the pelvic linkage.

Derivation of Equation 7

From Figure 7d; where θ = 360° – $\sigma + \chi$ (note: σ and χ are labelled in Figure 7c and clockwise angles are negative)

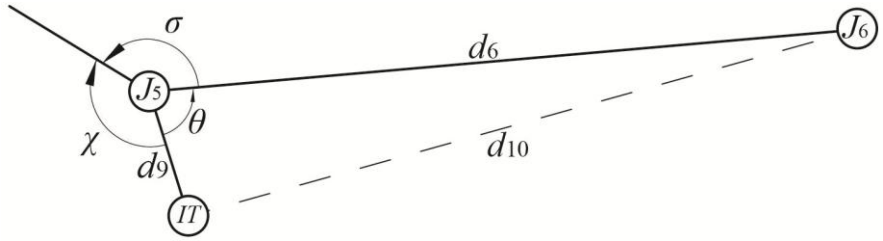

$$d_{10}{}^2 = d_6{}^2 + d_9{}^2 - 2\, d_5\, d_9\, cos\theta$$

where, θ = 360° – $\sigma + \chi$

$$d_{10} = \sqrt{d_6{}^2 + d_9{}^2 - 2\, d_6\, d_9 \cos(360 - \sigma + \chi)}$$

$$d_8 = \sqrt{d_5{}^2 + d_9{}^2 - 2\, d_5\, d_9\, cos\chi} \qquad (8)$$

where d_8 is the length of the line connecting the IT and the lumbosacral joint (J_4) and d_5 is the length of pelvic linkage.

Derivation of Equation 8

From Figure 7d; χ can be obtained from Figure 7c (note: clockwise angles are negative):

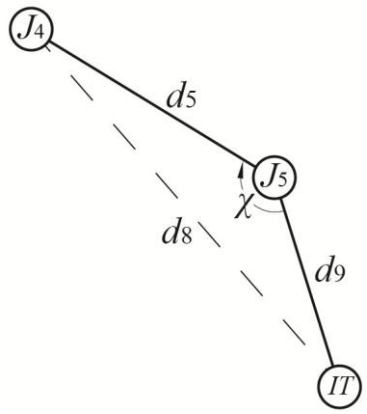

$$d_8{}^2 = d_5{}^2 + d_9{}^2 - 2\, d_5\, d_9\, cos\chi$$

$$d_8 = \sqrt{d_5{}^2 + d_9{}^2 - 2\, d_5\, d_9\, cos\chi}$$

$$\psi = -1\left[180 - \varepsilon - \cos^{-1}\left(\frac{d_{10}{}^2 + d_6{}^2 - d_9{}^2}{2\, d_{10}\, d_6}\right)\right] \quad (9)$$

where ψ is the angle of the line d_{10} and ε is the angle of the thigh linkage.

Derivation of Equation 9

From Figure 7d; the angle ψ between d_{10} and the horizontal can be derived as follows (note: clockwise angles are negative):

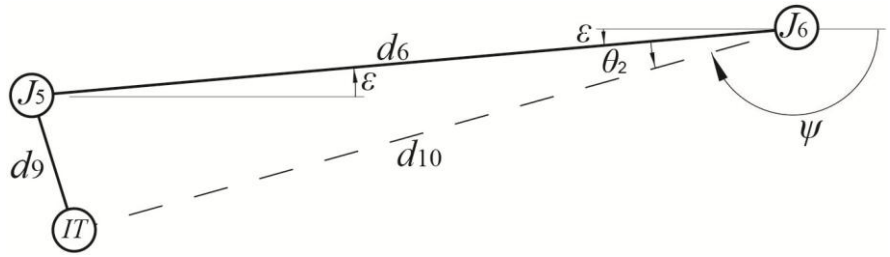

ψ = 180° – ε – θ_2, where θ_2, the angle between d_6 and d_{10}, can be derived from:

$$\theta_2 = \cos^{-1}\left(\frac{{d_{10}}^2+{d_6}^2-{d_9}^2}{2\,d_{10}\,d_6}\right)$$

Where $d9$ is given in Equation 5, $d10$ is given in Equation 7, and $d6$ is the thigh length in Table 3.

$$\therefore \quad \psi = 180 - \varepsilon - \cos^{-1}\left(\frac{{d_{10}}^2+{d_6}^2-{d_9}^2}{2\,d_{10}\,d_6}\right)$$

Since ψ is clockwise:

$$\therefore \quad \psi = -1\left[180 - \varepsilon - \cos^{-1}\left(\frac{{d_{10}}^2+{d_6}^2-{d_9}^2}{2\,d_{10}\,d_6}\right)\right]$$

$$\omega = -1\left[180 - \varphi + \cos^{-1}\left(\frac{{d_5}^2+{d_8}^2-{d_9}^2}{2\times d_5\times d_8}\right)\right] \qquad (10)$$

where ω is the angle of the line d_8 and φ is the angle of the pelvic linkage.

Derivation of Equation 10

The angle ω between d_8 and the horizontal can be derived as follows (note: clockwise angles are negative):

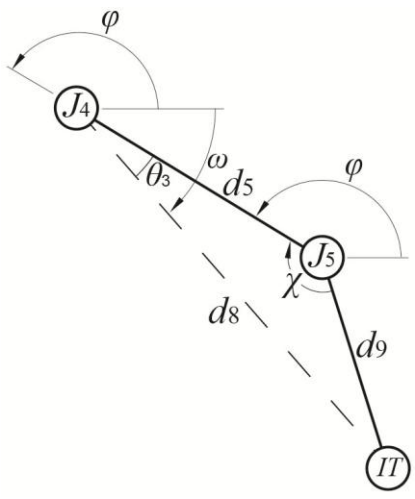

ω = 180° – ε – θ_3, where θ_3, the angle between d_5 and d_8, can be derived from:

$$\theta_2 = \cos^{-1}\left(\frac{{d_5}^2+{d_8}^2-{d_9}^2}{2\times d_5\times d_8}\right)$$

Where $d9$ is given in Equation 5, $d8$ is given in Equation 8, and $d5$ is the pelvis link length in Table 3.

$\therefore$

$$\omega = 180 - \varphi + \cos^{-1}\left(\frac{{d_5}^2+{d_8}^2-{d_9}^2}{2\times d_5\times d_8}\right)$$

Since ω is clockwise:

$$\omega = -1\left[180 - \varphi + \cos^{-1}\left(\frac{{d_5}^2+{d_8}^2-{d_9}^2}{2\times d_5\times d_8}\right)\right]$$

With these additional relationships, the inferior IT was used to ground the model on the seat. To solve for forces, the centres of gravity of the thigh (Fg_6) and pelvis (Fg_5) linkages were transferred to the dotted lines (see Figure 10). Their positions are specified in Table 4, which correspond to the body segment parameters by Pheasant (1986).

3.1.4 Force derivation

The biomechanical model is illustrated in Figure 10 which is accompanied with the nomenclature (Table 7). It is a development of the body link diagram (Figure 7) and extends the Four Link Model of the Seated Subject from Goossens and Snijders (1995). In the present model, four categories of force are assumed to be acting on the body. The first is gravitational (F_g) and results from the mass of the segments. These forces are the only predetermined forces in the model and are referenced from the body segment parameters for the 50th percentile man in Table 4. The second type of force is internal and acts parallel to the linkage in equal and opposite directions towards the linkage joints. These link forces (F_s) are derived from the equilibrium equations 11–25. The equilibrium equations correspond to Figure 10 and are developed in sequence from head to foot. The third category forms the reaction forces from the

support surfaces. The model is grounded at the heel and the ITs where the reaction forces act in horizontal and vertical directions (F_h and F_v). All reaction forces from the backrest and headrest are normal to the support surfaces (F_n). The reaction forces are derived from the equilibrium equations 11–25. For the model to be statically determinate, it is assumed that the perpendicular reaction forces (F_p) on the backrest and headrest are zero.

Table 7 Nomenclature

Segment Inclinations		**Gravitational Forces**		**Reaction Forces**	
α	Head	F_{g1}	Head	$F_{n,h}$	Normal reaction force on the head
β	Thorax	F_{g2}	Thorax	$F_{n,sh}$	Normal reaction force on the shoulder girdle
γ	Upper lumbar	F_{g3}	Upper lumbar	$F_{n,th}$	Normal reaction force on the thoracic spine
δ	Lower lumbar	F_{g4}	Lower lumbar	$F_{n,l}$	Normal reaction force on the lumbar spine
ε	Thigh	F_{g5}	Pelvis	$F_{n,cr}$	Normal reaction force on the iliac crest
η	Lower leg	F_{g6}	Thigh	F_{net}	Net pelvic force
λ	Thigh-lumbar	F_{g7}	Lower leg	$F_{h,it}$	Horizontal reaction force on the ischial tuberosity
μ	Pelvis-lumbar	**Link Forces**		$F_{v,it}$	Vertical reaction force on the ischial tuberosity
σ	Pelvis-thigh/seat	F_{s1}	Thorax	$F_{n,k}$	Normal reaction force on the knee
φ	Pelvis	F_{s2}	Upper lumbar	$F_{n,f}$	Normal reaction force on the foot
χ	Ischial-pelvis	F_{s3}	Lower lumbar		
ψ	Ischial-knee	F_{s4}	Pelvis		
ω	Ischial-L5/S1	F_{s5}	Thigh		

The model has one sliding contact (H) for the head and eight linkage joints below (J_1–J_7 and IT). Since link forces (F_s) can only exist when there is a joint at both ends of the linkage, and, since there is no shear assumed for the headrest, there are no link forces for the head segment. Linkage joint J_5 is only required for articulating the model and is redundant when calculating force. Linkage joint J_6 is not in contact with support surfaces when the feet are grounded.

To solve for forces, $F_{n,h}$ is first calculated from Equation 11. To calculate the forces at J_1, F_{s1} must first be solved from Equation 12. With F_{s1} known, $F_{n,sh}$ can be calculated from Equation 13 and F_{s2} can be calculated from Equation 14. With F_{s2} known, $F_{n,th}$ is solved in Equation 15 and F_{s3} solved

in Equation 16. This pattern repeats to find $F_{n,l}$, F_{s4} and $F_{n,cr}$. To find $F_{h,it}$ and $F_{v,it}$, Equations 22 and 23 must first be solved simultaneously to find F_{s5}. With F_{s6} being determined when calculating F_{s5}, $F_{h,f}$ and $F_{v,f}$ can be calculated in Equations 24 and 25.

All equations in this chapter are original except for Equations11–25 which are adapted from Goossens and Snidjers (1995). To verify that the model was in static equilibrium a matrix of the equations described in this chapter was created in Microsoft Excel. Additional equations were included that calculated the moments about the ITs. The only independent variables in the matrix were the inclinations of the support surfaces. To check the validity of the model, the sum of positive and negative moments were calculated. The model, and all equations, was verified when the resultant value was zero for a variety of chair configurations, which proved static equilibrium.

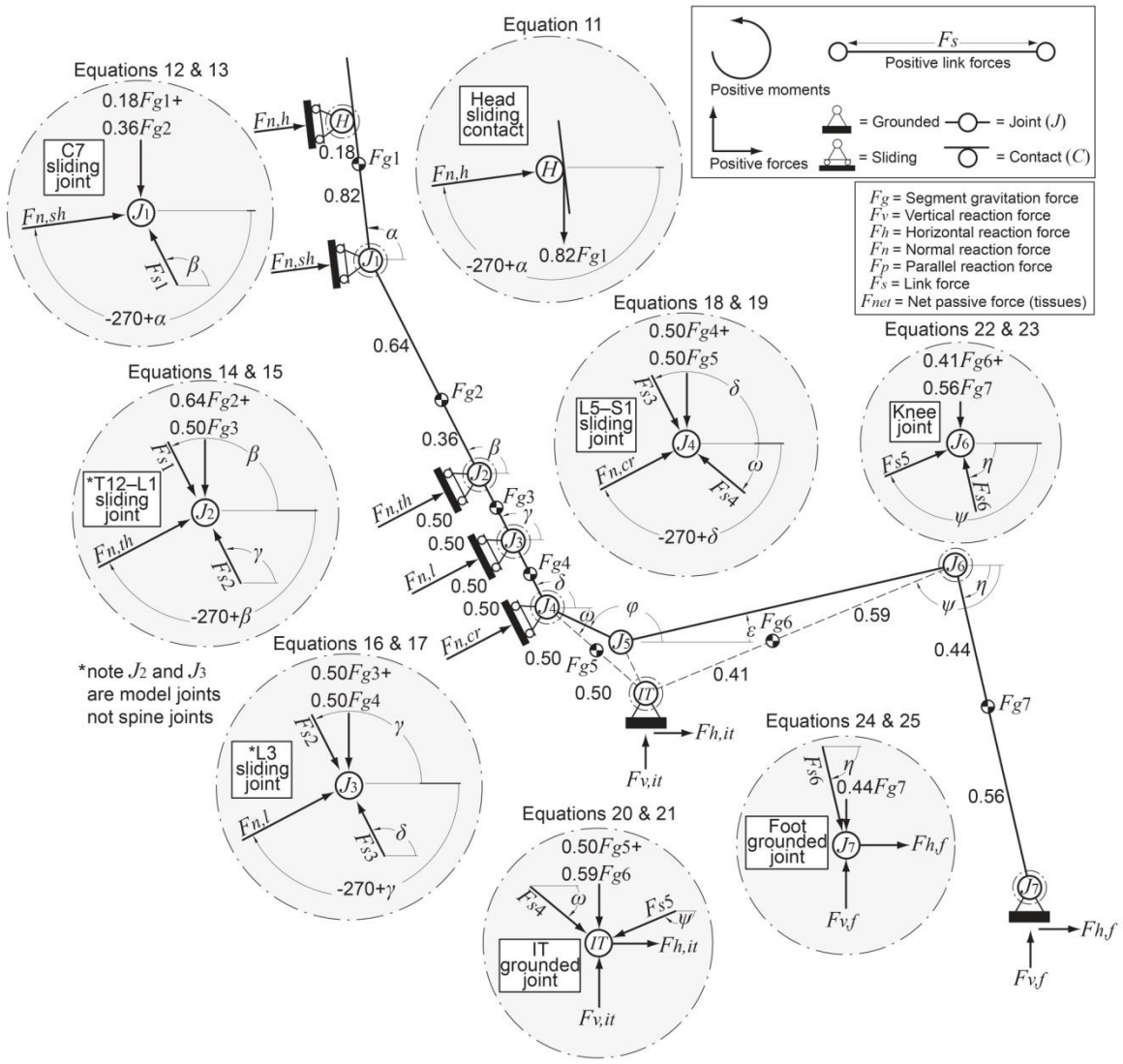

Figure 10 The biomechanical model developed from the body link diagram in Figure 7. The biomechanical model extends the Four Link Model of the Seated Subject by Goossens and Snijders (1995). The biomechanical model, which describes the forces acting on each joint and contact, has 7 linkages, 8 joints and 1 contact (H) with the addition of a force (F_{net}) to limit the range of rotation of the pelvis. The joint J_5 is an articulating joint only and is replaced by the IT joint for force

Head Joint (H) (Equation 11)

Equation 11 describes static equilibrium for the head sliding contact joint (H) with respect to normal force (F_n) and is shown in Figure 10. From Equation 11, the head normal force ($F_{n,h}$) is derived. To solve for $F_{n,h}$:

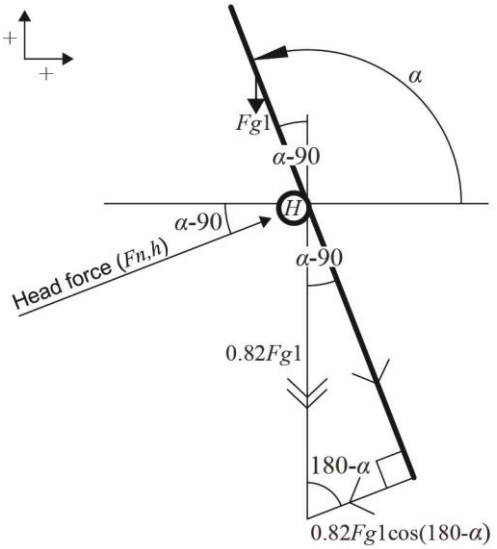

$$\sum F_n = F_{n,h} - 0.82F_{g1}\cos(180-\alpha) = 0 \tag{11}$$

$$\therefore \quad F_{n,h} = 0.82F_{g1}\cos(180-\alpha)$$

Below shows, by way of example, the calculation for the percentage of F_{g1} acting on joint H. This is not shown for the other joints, but the same principle applies. Moments are taken at joint J_1 (M_{sh}):

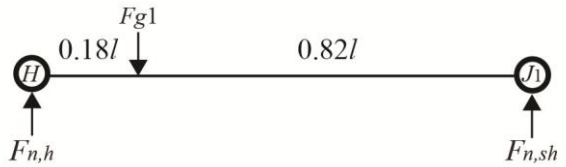

$$\sum M_{sh} = -F_{n,h}(0.18l + 0.82l) + F_{g1}(0.82l) = 0$$

$$\therefore \quad F_{n,h} = \frac{F_{g1}(0.82l)}{l} = 0.82F_{g1}$$

C7 Sliding Joint (J_1) (Equations 12 & 13)

Equation 12 describes the static equilibrium for the C7 sliding contact joint (J_1) in terms of parallel force (F_p) and is shown in Figure 10. The link force F_{s1} is derived from Equation 12. This force is needed before solving for the normal force at this joint. Note that since it is assumed that there is no parallel force and the head linkage is not connected above J_1, the entire parallel component is supported at J_1. To solve for F_{s1}:

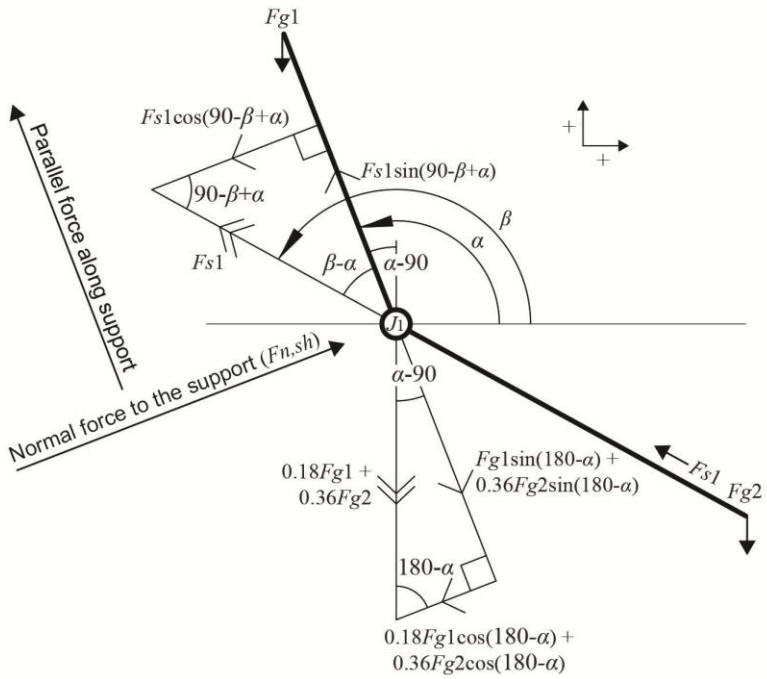

$$\sum F_p = F_{g1}\sin(180-\alpha) + 0.36F_{g2}\sin(180-\alpha) - F_{s1}\sin(90-\beta+\alpha) = 0 \qquad (12)$$

$$\therefore \qquad F_{s1} = \frac{F_{g1}\sin(180-\alpha) + 0.36F_{g2}\sin(180-\alpha)}{\sin(90-\beta+\alpha)}$$

Equation 13 describes the static equilibrium for the C7 sliding contact joint (J_1) in terms of normal force (F_n) and is shown in Figure 10. The shoulder girdle normal force ($F_{n,sh}$) is derived from Equation 13,. To solve for $F_{n,sh}$:

$$\sum F_n = F_{n,sh} - 0.18F_{g1}\cos(180-\alpha) - 0.36F_{g2}\cos(180-\alpha) - F_{s1}\cos(90-\beta+\alpha)=0 \quad (13)$$

$$\therefore \quad F_{n,sh} = 0.18F_{g1}\cos(180-\alpha) + 0.36F_{g2}\cos(180-\alpha) + F_{s1}\cos(90-\beta+\alpha)$$

T12/L1 Sliding Joint (J_2) (Equations 14 & 15) (*note this is a model joint not a spine joint*)

Equation 14 describes the static equilibrium for the T12/L1 sliding contact joint (J_2) in terms of parallel force (F_p) and is shown in Figure 10. The link force F_{s2} is derived from Equation 14. This force is needed before solving for the normal force at this joint. With F_{s1} derived from Equation 12, to solve for F_{s2}:

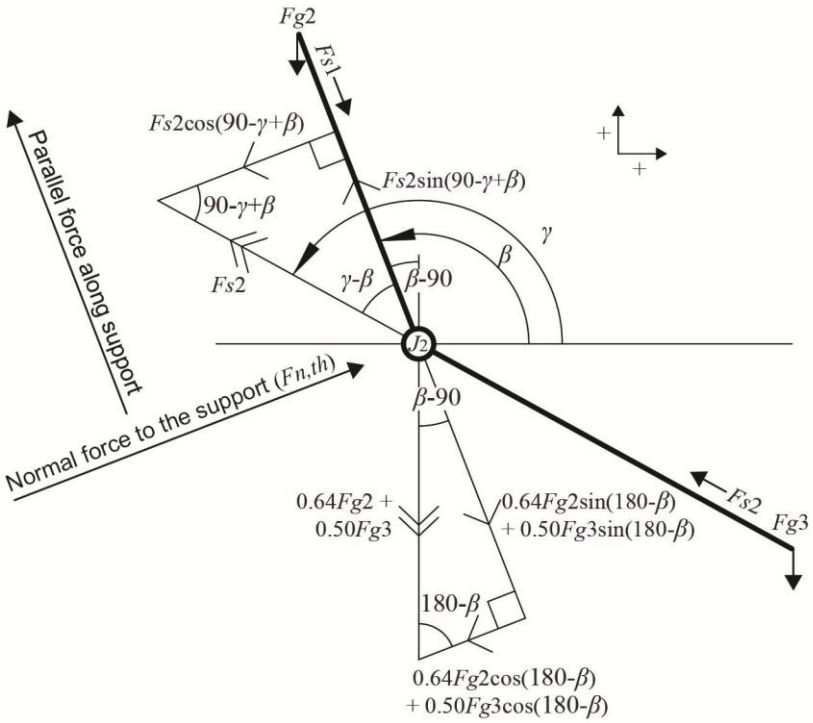

$$\sum F_p = 0.64F_{g2}\sin(180-\beta) + 0.50F_{g3}\sin(180-\beta) + F_{s1} - F_{s2}\sin(90-\gamma+\beta)=0 \quad (14)$$

$$\therefore \quad F_{s2} = \frac{0.64F_{g2}\sin(180-\beta) + 0.50F_{g3}\sin(180-\beta) + F_{s1}}{\sin(90-\gamma+\beta)}$$

Equation 15 describes the static equilibrium for the T12/L1 sliding contact joint (J_2) in terms of normal force (F_n) and is shown in Figure 10. The thoracic normal force ($F_{n,th}$) is derived from Equation 15. To solve for $F_{n,th}$:

$$\sum F_n = F_{n,th} - 0.64F_{g2}\cos(180-\beta) - 0.50F_{g3}\cos(180-\beta) - F_{s2}\cos(90-\gamma+\beta)=0 \quad (15)$$

$$\therefore \quad F_{n,th} = 0.64F_{g2}\cos(180-\beta) + 0.50F_{g3}\cos(180-\beta) + F_{s2}\cos(90-\gamma+\beta)$$

L3 Sliding Joint (J_3) (Equations 16 & 17) (*note this is a model joint not a spine joint*)

Equation 16 describes the static equilibrium for the L3 sliding contact joint (J_3) in terms of parallel force (F_p) and is shown in Figure 10. The link force F_{s3} is derived from Equation 16. This force is needed before solving for the normal force at this joint. With F_{s2} derived from Equation 14, to solve for F_{s3}:

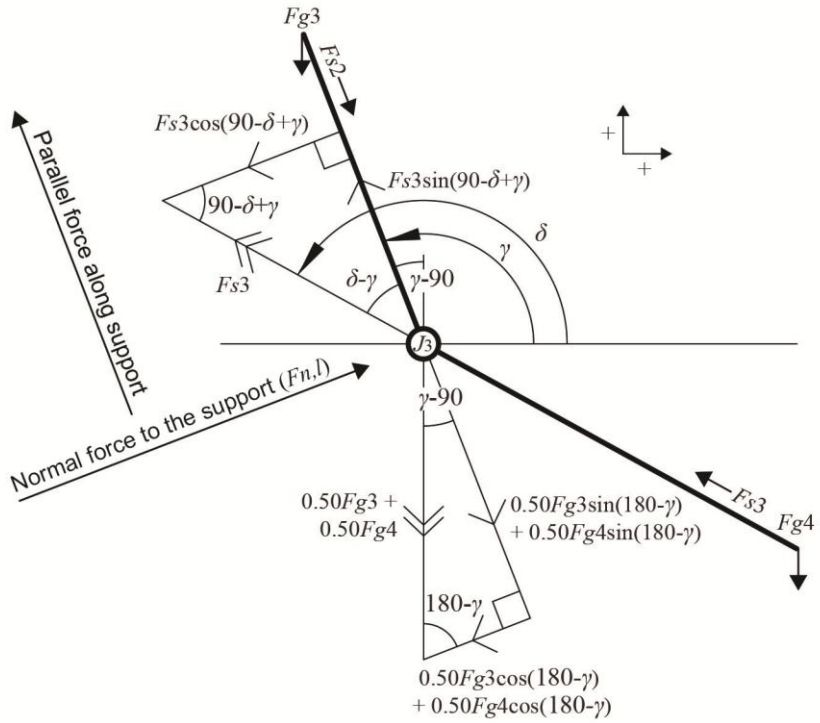

$$\sum F_p = 0.50F_{g3}\sin(180-\gamma) + 0.50F_{g4}\sin(180-\gamma) + F_{s2} - F_{s3}\sin(90-\delta+\gamma)=0 \quad (16)$$

$$\therefore \qquad F_{s3} = \frac{0.50F_{g3}\sin(180-\gamma) + 0.50F_{g4}\sin(180-\gamma) + F_{s2}}{\sin(90-\delta+\gamma)}$$

Equation 17 describes the static equilibrium for the L3 sliding contact joint (J_3) in terms of normal force (F_n) and is shown in Figure 10. The lumbar normal force ($F_{n,l}$) is derived from Equation 17. To solve for $F_{n,l}$:

$$\sum F_n = F_{n,l} - 0.50F_{g3}\cos(180-\gamma) - 0.50F_{g4}\cos(180-\gamma) - F_{s3}\cos(90-\delta+\gamma)=0 \qquad (17)$$

$$\therefore \qquad F_{n,l} = 0.50F_{g3}\cos(180-\gamma) + 0.50F_{g4}\cos(180-\gamma) + F_{s3}\cos(90-\delta+\gamma)$$

L5/S1 Sliding Joint (J_4) (Equations 18 & 19)

Equation 18 describes the static equilibrium for the L5/S1 sliding contact joint (J_4) in terms of parallel force (F_p) and is shown in Figure 10. The link force F_{s4} is derived from Equation 18. This force is needed before solving for the normal force at this joint. With F_{s3} derived from Equation 16, to solve for F_{s4}:

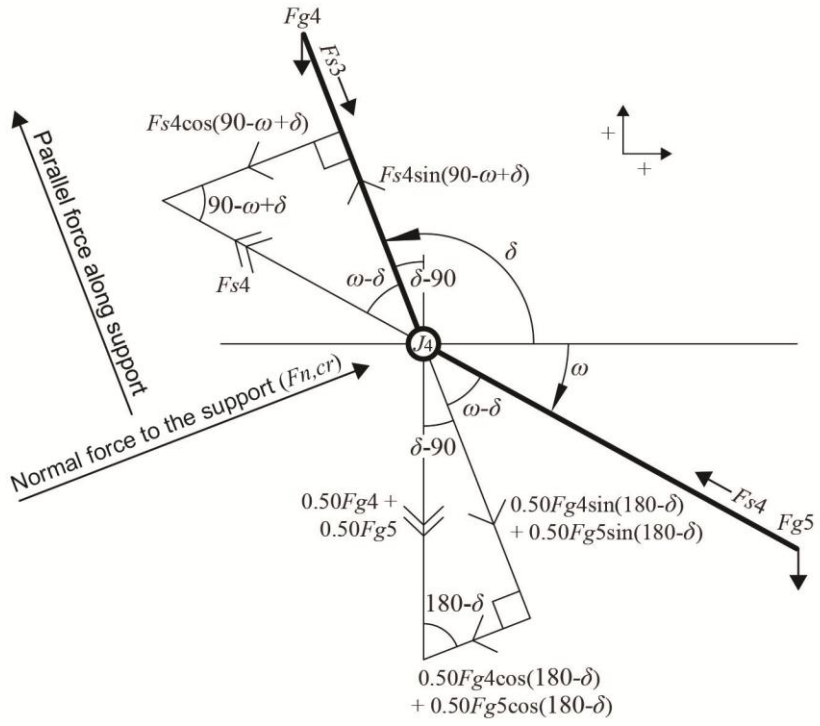

$$\sum F_p = 0.50F_{g4}\sin(180-\delta) + 0.50F_{g5}\sin(180-\delta) + F_{s3} - F_{s4}\sin(90+\omega-\delta)=0 \quad (18)$$

$$\therefore \quad F_{s4} = \frac{0.50F_{g4}\sin(180-\delta) + 0.50F_{g5}\sin(180-\delta) + F_{s3}}{\sin(-90+\omega-\delta)}$$

Equation 19 describes the static equilibrium for the L5/S1 sliding contact joint (J_4) in terms of normal force (F_n) and is shown in Figure 10. The iliac crest normal force ($F_{n,cr}$) is derived from Equation 19. To solve for $F_{n,cr}$:

$$\sum F_n = F_{n,cr} - 0.50F_{g4}\cos(180-\delta) - 0.50F_{g5}\cos(180-\delta) - F_{s4}\cos(90+\omega-\delta)=0 \quad (19)$$

$$\therefore \quad F_{n,cr} = 0.50F_{g4}\cos(180-\delta) + 0.50F_{g5}\cos(180-\delta) + F_{s4}\cos(90+\omega-\delta)$$

IT Grounded Joint (*IT*) (Equations 20 & 21)

Equation 20 describes the static equilibrium for the IT grounded joint (*IT*) in terms of horizontal force (F_h) and is shown in Figure 10. The horizontal force $F_{h,it}$ is derived from Equation 20. In order to be able to solve for $F_{h,it}$, the link force F_{s5} must first be derived from Equations 22 and 23 (see derivation following Equations 22 and 23). With F_{s4} derived from Equation 18, to solve for $F_{h,it}$:

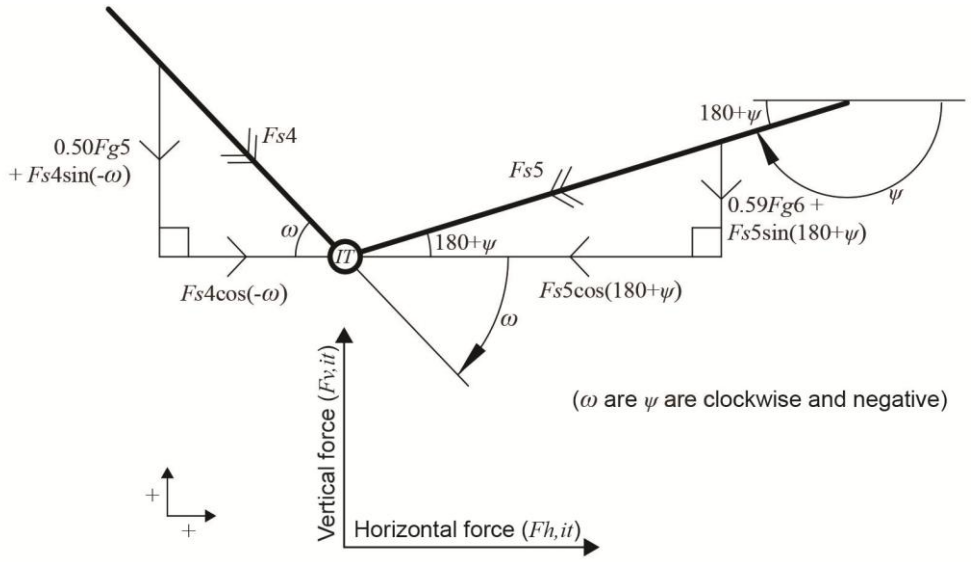

$$\sum F_h = F_{h,it} - F_{s5}\cos(180+\psi) + F_{s4}\cos(-\omega) = 0 \quad (20)$$

$$\therefore \quad F_{h,it} = F_{s5}\cos(180+\psi) - F_{s4}\cos(-\omega)$$

Equation 21 describes the static equilibrium for the IT grounded joint (IT) in terms of vertical force (F_v) and is shown in Figure 10. The IT vertical force ($F_{v,it}$) is derived from Equation 21. With F_{s5} derived from Equations 22 and 23, to solve for $F_{v,it}$:

$$\sum F_v = F_{v,it} - F_{s4}\sin(-\omega) - F_{s5}\sin(180+\psi) - 0.50F_{g5} - 0.59F_{g6} = 0 \quad (21)$$

$$\therefore \quad F_{v,it} = F_{s4}\sin(-\omega) + F_{s5}\sin(180+\psi) + 0.50F_{g5} + 0.59F_{g6}$$

Knee Joint (J_6) (Equations 22 & 23)

Equation 22 describes the static equilibrium for the knee joint (IT) in terms of horizontal force (F_h) and vertical force (F_v) and is shown in Figure 10. With the assumption that the feet are grounded, there is no support to the knee joint. Therefore, the only forces to solve for are the link forces F_{s5} and F_{s6}:

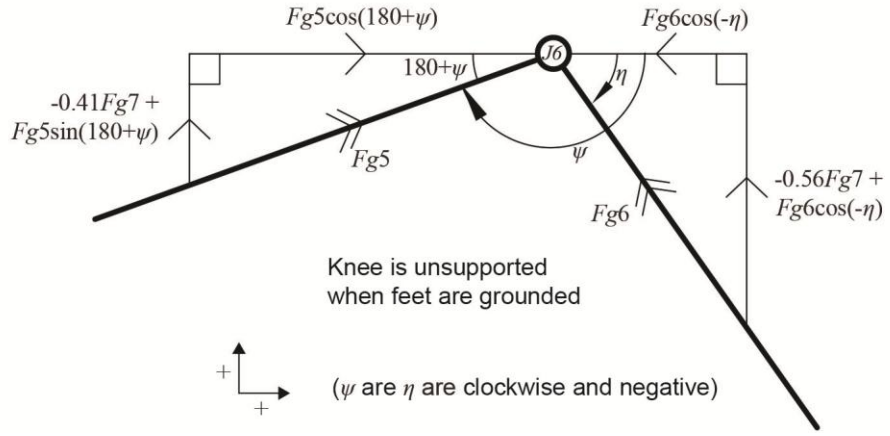

$$\sum F_h = F_{s5}\cos(180+\psi) - F_{s6}\cos(-\eta) = 0 \quad (22)$$

$$\sum F_v = -0.41F_{g6} - 0.56F_{g7} + F_{s5}\sin(180+\psi) + F_{s6}\sin(-\eta) = 0 \quad (23)$$

To find F_{s5} and F_{s6}, derived Fs_5 from Equation 22 and substitute into Equation 23:

$$\sum F_h = F_{s5}\cos(180+\psi) - F_{s6}\cos(-\eta) = 0$$

$$F_{s6}\cos(-\eta) = F_{s5}\cos(180+\psi)$$

$$\therefore \quad F_{s5} = \frac{F_{s6}\cos(-\eta)}{\cos(180+\psi)}$$

Substituting F_{s5} in Equation 23:

$$\sum F_v = -0.41F_{g6} - 0.56F_{g7} + \frac{F_{s6}\cos(-\eta)}{\cos(180+\psi)}\sin(180+\psi) + F_{s6}\sin(-\eta) = 0$$

$$F_{s6}[\cos(-\eta)\tan(180+\psi) + \cos(-\eta)] = 0.41F_{g6} + 0.56F_{g7}$$

$$\therefore \quad F_{s6} = \frac{0.41F_{g6} + 0.56F_{g7}}{\cos(-\eta)\tan(180+\psi) + \cos(-\eta)}$$

Foot Grounded Joint (J_7) (Equations 24 & 25)

Equation 24 describes the static equilibrium for the foot grounded joint (J_7) in terms of horizontal force (F_h) and is shown in Figure 10. The horizontal force $F_{h,f}$ is derived from Equation 24. With F_{s6} derived from Equations 22 and 23, to solve for $F_{h,f}$:

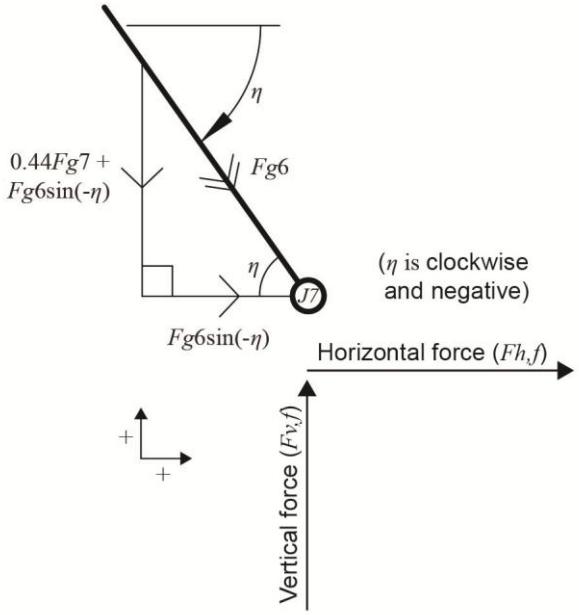

$$\sum F_h = F_{h,f} + F_{s6}\cos(-\eta) = 0 \tag{24}$$

$$\therefore \quad F_{h,f} = -F_{s6}\cos(-\eta)$$

Equation 25 describes the static equilibrium for the foot grounded joint (J_7) in terms of vertical force (F_v) and is shown in Figure 10. The vertical force $F_{v,f}$ is derived from Equation 25. With F_{s6} derived from Equations 22 and 23, to solve for $F_{v,f}$:

$$\sum F_v = F_{v,f} - 0.44F_{g7} - F_{s6}\sin(-\eta) = 0 \tag{25}$$

$$\therefore \quad F_{v,f} = 0.44F_{g7} + F_{s6}\sin(-\eta)$$

For postures where the feet are unsupported, such as when a leg rest is used, the vertical and horizontal reaction forces at the foot are replaced with a sliding contact and an additional reaction force is located behind the knee joint (Figure 11). Since the moments below the IT do not contribute to the moments above the IT, they must balance to be statically defined. This leads to the following solution for $F_{n,k}$ in Equation 26.

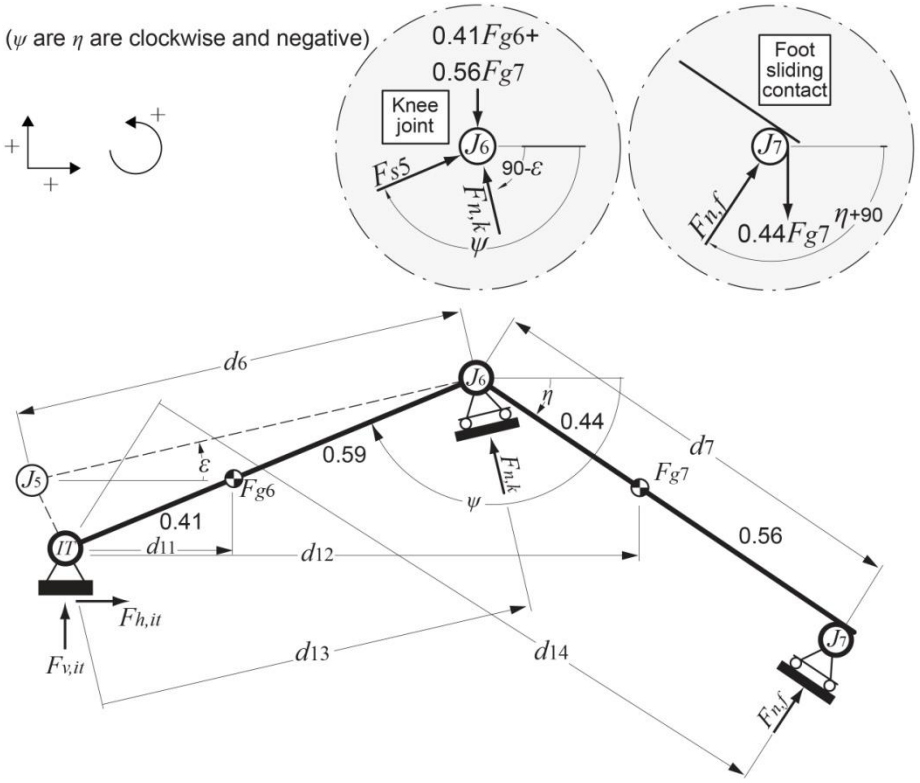

Figure 11 The model segments below the IT for postures where the feet are unsupported. A sliding contact for the foot and an additional reaction force normal to the seat surface is assumed. The lengths d_7 and d_8 are segment lengths and d_{12}-d_{15} are moment arms

$$F_{n,k} = \frac{(F_{g6} \times d_{11}) + (F_{g7} \times d_{12}) - (F_{n,f} \times d_{14})}{d_{13}} \quad (26)$$

$$F_{n,f} = 0.44 F_{g7} \cos \eta \quad (27)$$

3.1.5 Passive force on the pelvis in sitting

The only articulation in the biomechanical model that reaches the limit of its range of motion is the pelvis as it rotates posteriorly. Without any additional force to those described earlier, it is the support from the backrest to the sacrum and posterior superior iliac spines that determines the position of the pelvis in the biomechanical model. Specifically, it is the reaction force $F_{n,cr}$ that acts on the model joint J_4 (Figure 12a). $F_{n,cr}$ is defined in Equation 28 and is derived from Equation 19 (see derivation immediately after Equation 19). Here, $F_{n,cr}$ is the sum of all opposing gravitational and link forces at joint J_4, as shown in Figure 10.

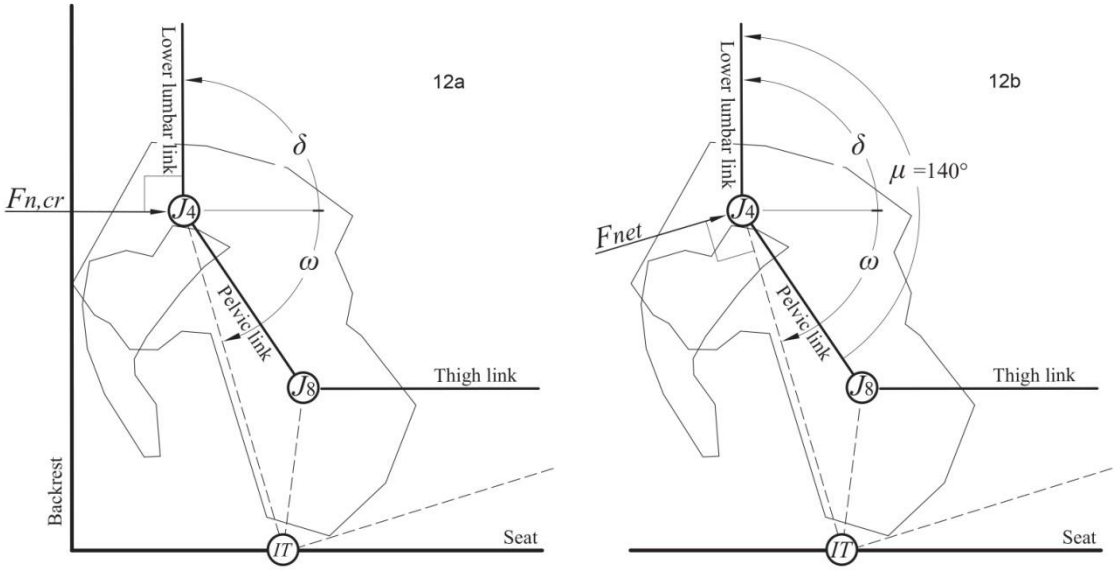

Figure 12 Illustration of the passive force on the pelvis in sitting, developed from the body link diagram (Figure 7). a) (left), sitting with a backrest and no internal force opposing pelvic rotation, the reaction force $F_{n,cr}$ positions the pelvis. b) (right), sitting with no backrest, the internal passive forces that position the pelvis are represented by the addition of F_{net} when the pelvis is at the limit of its rotation (μ = 140°)

$$F_{n,cr} = 0.50F_{g4}\,cos(180 - \delta) + 0.50F_{g5}\,cos(180 - \delta) + F_{s4}\,cos(90 + \omega - \delta) \quad (28)$$

Note: this equation was derived earlier from Equation 19.

When sitting in a relaxed upright posture and without a backrest (as with a stool), the pelvis rests in a position that is rotated by approximately 30° from standing (Andersson, *et al*., 1979, Pheasant & Haslegrave, 2006). Expressed in terms of the model coordinate system, this angle is μ = 140°. With no backrest and no reaction force acting on the posterior aspects of the pelvis, other internal passive forces must be responsible for maintaining this position. These internal passive forces are represented in Figure 12b by a single net force, F_{net}, and is related to $F_{n,cr}$:

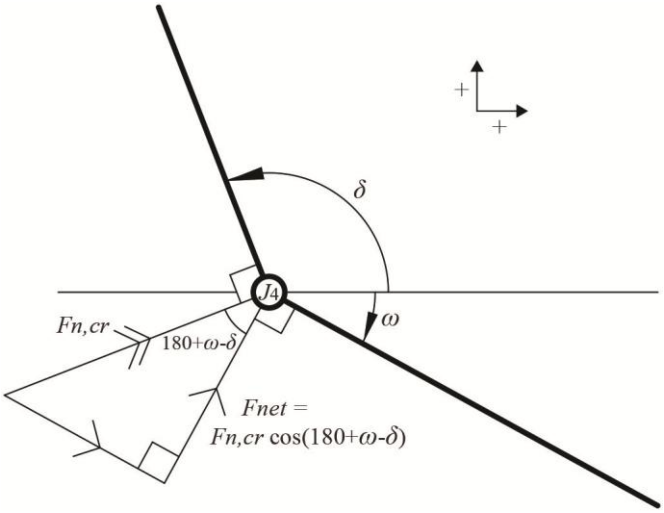

when μ = 140°,

$$F_{net} = F_{n,cr}\cos(180 + \omega - \delta) \quad (29)$$

The passive forces represented by F_{net} are assumed to predominantly arise from tension in the posterior spinal ligaments (iliolumbar ligament, ligamentum flavum, ventral portions of the interspinous ligament) (Bogduk, 1997). According to Solomonow (2006), the ligament is well established as a viscoelastic element with responses accurately estimated by exponential equations. The typical force-length relationship of a ligament, therefore, follows the exponential function $a{\cdot}e^{bt}$. So, as the pelvis approaches the limit of its range of motion there is a corresponding exponential increase in F_{net} as the posterior ligaments are stretched. When the pelvis reaches the limit of its range of motion (when the pelvis–lumbar angle μ = 140°) $F_{n,cr}$ is zero and F_{net} is highest for any given posture. Equation 29 is therefore modified to make F_{net} an exponential function of the pelvis–lumbar angle (μ). In this equation, 140 is the minimum pelvis–lumbar angle derived from Anderson, *et al*., 1976 (Figure 8) and 0.3 is an arbitrary coefficient that determines the rate at which F_{net} increases as it approaches 140°. Figure 13 shows the sensitivity of this coefficient, with additional curves having coefficients of 0.1, 0.15, 0.5 and 0.8 (dotted lines). In the absence of experimental data, the coefficient is empirically selected based on the belief that, although gradual, the forces from the posterior ligaments are likely to develop only

when the ligaments stretch, and that this would be in the last few degrees of movement before equilibrium is achieved.

$$F_{net} = F_{n,cr} \cos(180 + \omega - \delta)\, e^{-0.3(\mu - 140)} \tag{30}$$

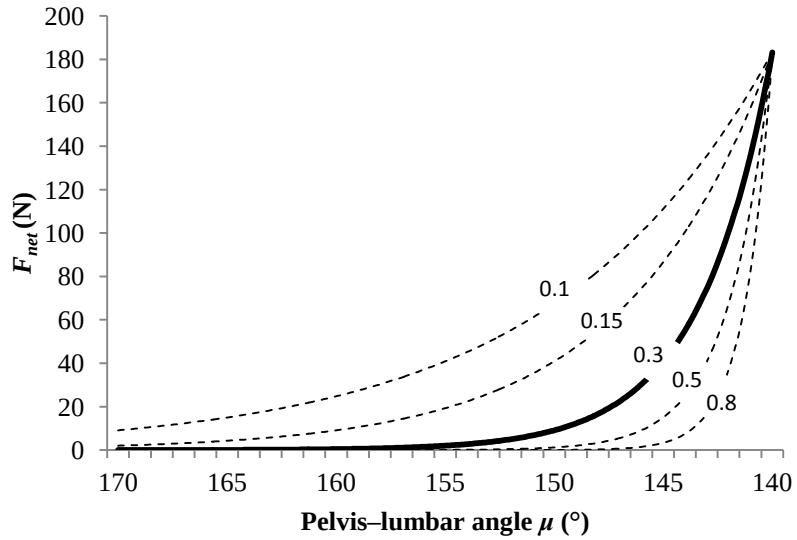

Figure 13 The relationship between the pelvis–lumbar angle μ and F_{net}. F_{net} represents the sum of passive force from the posterior spinal ligaments that oppose posterior pelvic rotation. The relationship between μ and F_{net} reflects the force-length relationship of a typical ligament and follows the exponential function $a \cdot e^{bt}$. The coefficient b is an arbitrary value. The solid line curve has a coefficient of 0.3 and was used for the model. The dotted line curves show the sensitivity of this value, with coefficients of 0.1, 0.15, 0.5 and 0.8.

Solving for F_{net}; $F_{n,cr}$ in Equation 30 is expanded using Equation 28:

$$F_{net} = \left[0.50F_{g4}\, cos(180 - \delta) + 0.50F_{g5}\, cos(180 - \delta) + F_{s4}\, cos(90 + \omega - \delta)\right] \cos(180 + \omega - \delta)\, e^{-0.3(\mu - 140)} \tag{31}$$

Note: $F_{n,cr}$ was derived earlier from Equation 19.

Solving Equation 18 for F_{s4} and inserting into Equation 31 yields:

$$F_{net} = \Big\{0.50F_{g4}\,cos(180-\delta)+0.50F_{g5}\,cos(180-\delta) + \left[\frac{0.50F_{g4}\,sin(180-\delta)+0.50F_{g5}\,sin(180-\delta)+F_{s3}}{sin(-90+\omega-\delta)}\right]cos(90+\omega-\delta)\Big\}\cos(180+\omega-\delta)\,e^{-0.3(\mu-140)} \quad (32)$$

Note: F_{s4} was derived earlier from Equation 18.

Introducing F_{net} into the biomechanical model modifies Equation 28, and Equation 18 as solved for $F_{s4,}$ so that they become Equations 33 and 34, respectively:

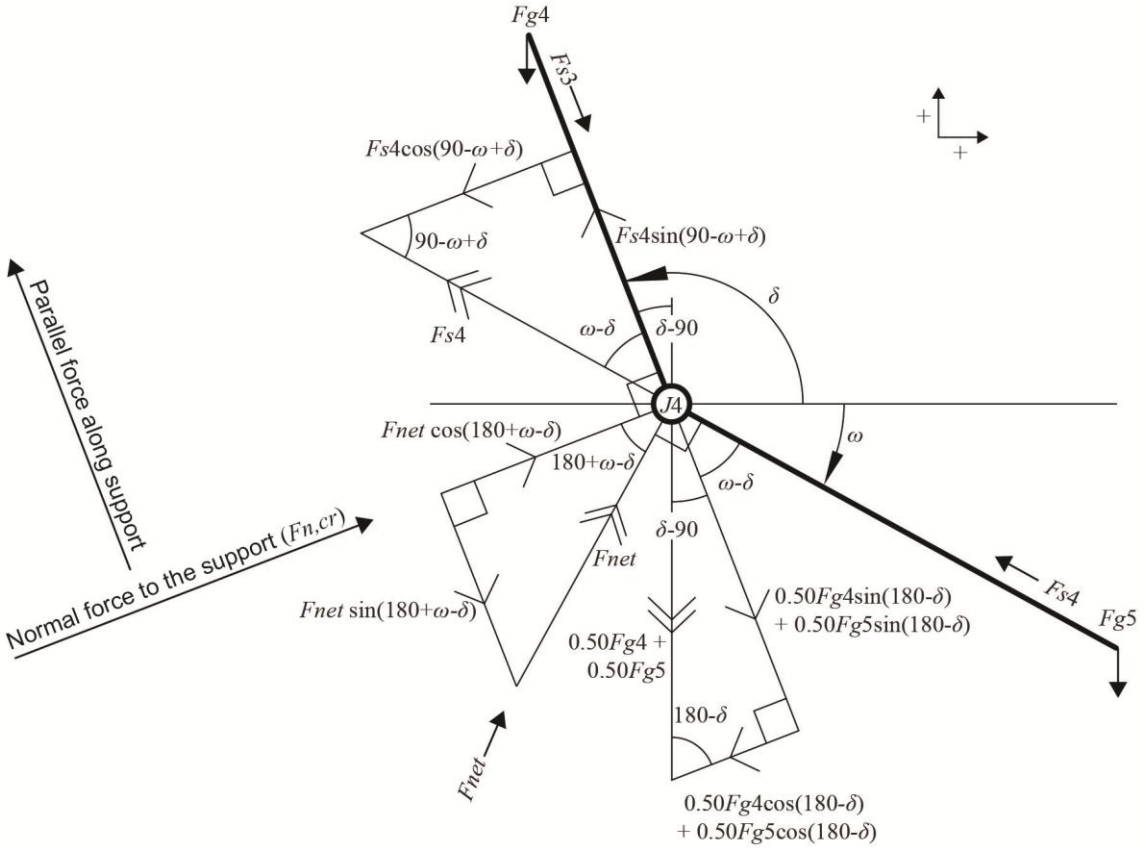

$$F_{n,cr} = 0.50F_{g4}\,cos(180-\delta)+0.50F_{g5}\,cos(180-\delta) + F_{s4}\,cos(90+\omega-\delta) - F_{net}\,cos(180+\omega-\delta) \quad (33)$$

$$F_{s4} = \frac{0.50F_{g4}\,sin(180-\delta)+0.50F_{g5}\,sin(180-\delta)+F_{s3}-F_{net}\,sin(180+\omega-\delta)}{sin(-90+\omega-\delta)} \quad (34)$$

Upon adding F_{net} into the biomechanical model, the final equations for F_{net}, $F_{n,cr}$ and F_{s4} are derived in Equations 32, 33 and 34 which are used for the remaining simulations.

3.2 Model Simulations

This section begins by explaining the process for registering the biomechanical model with the seated test postures. When configured to the test postures of this study, the model can be compared to measured data and validated. The seated test postures are illustrated on the back page of this thesis which folds out to provide a permanent reference. The remaining of this section describes the output parameters for validating the model (posture and force), and for interpreting the experimental data on interface pressure variables, stature and back muscle activity between the test postures.

3.2.1 Registering the biomechanical model to the seated test postures

In order to register the biomechanical model with the seated test postures, the support surfaces need to be modelled. Therefore, there are two conceptual models to construct: the support surface model and the human model. Details on the configuration of these models are described below, beginning with the support surface model.

Support surface model:

1. The support surfaces were first defined in a neutral configuration (horizontal seat, vertical backrest and vertical headrest) including the centres of rotations that defined the path of movement according to the specific test-rig design (Figure 14). The path of movement of support surfaces of other seating systems is likely to be different, so this should always be considered.

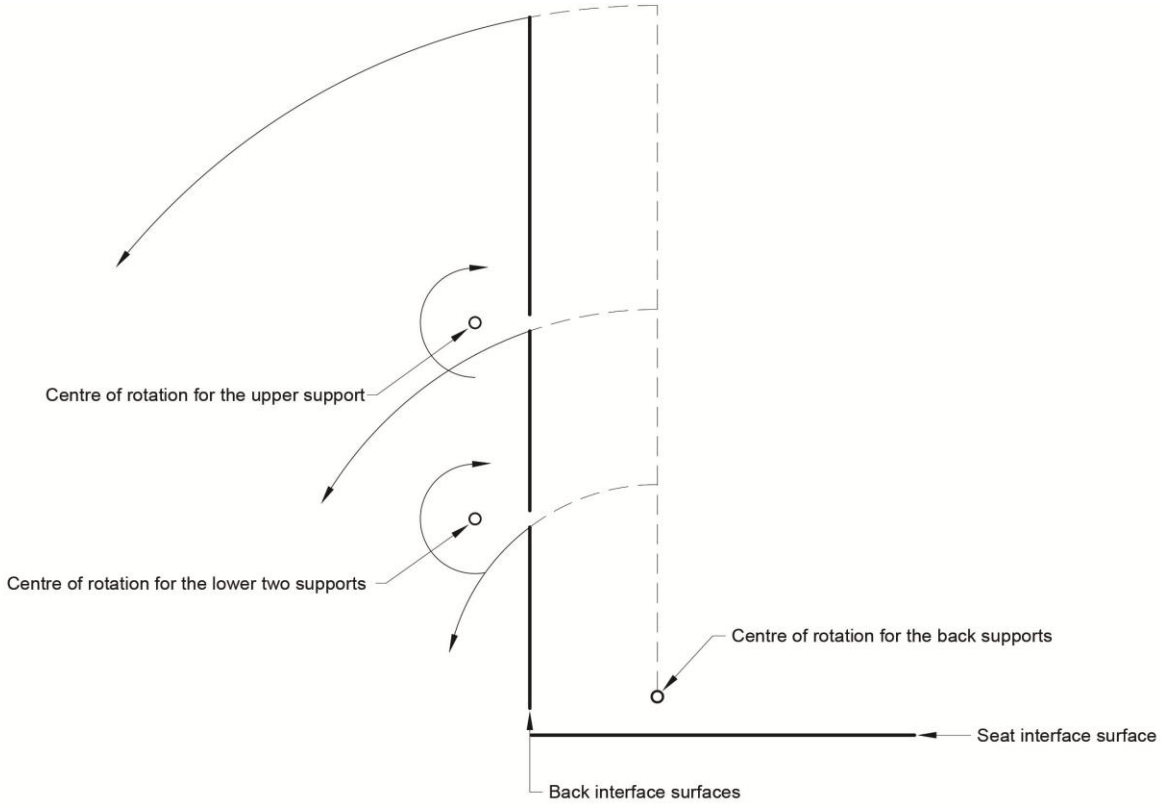

Figure 14 The support surface model in the neutral configuration showing centres of rotation and the paths of movement

2. The support surfaces were then configured for each seated test posture. For example, the support surface model configured to the standard recline test posture is shown in Figure 15. Inclinations can be based on either a design specification or direct measurements from physical support surfaces; however, the latter is likely to be more

accurate. In this study, the inclinations of the test-rig support surfaces were measured using an electromagnetic motion tracking system (see Section 4.5).

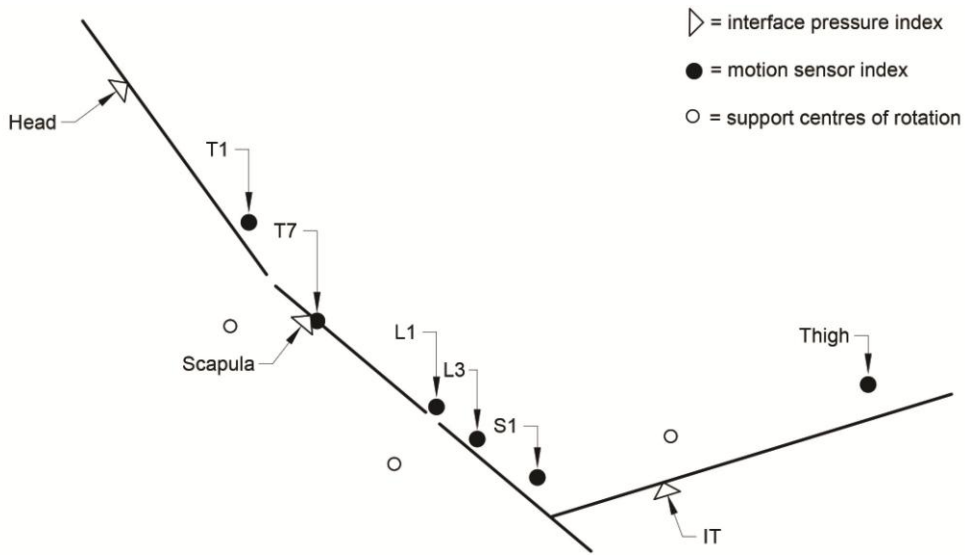

Figure 15 The support surface model configured to the standard recline test posture with the interface pressure and motion sensor indices: S1, L3, L1, T7 and T1 are the vertebral landmarks for sensor position

3. As part of this research, interface pressure and motion sensor indices were obtained. These provide data on the location of the peak pressures (associated with the ITs, scapula and head), and skin overlying S1, L1, L3, T7, T1 and the thigh. Three of the 15 test subjects who participated in this study were 50th percentile males. Each index is, therefore, the centroid of the three data points measured from these subjects. These data are included in the Support Surface Model (Figure 15)

Human model

1. The human model is defined, as described previously in Section 3.1, with the pelvis configuration and upper body linkages while in the anatomical sitting posture (no pelvic rotation) (Figure 16). Here, quantitative anthropometric data of the head (including the most posterior aspect), trunk space (as defined from the position of the tips of the scapula), thigh space (thigh thickness) and the posterior superior iliac spines (PSIS's) of the pelvis are incorporated. Pheasant (1986) explains that for this posture, the subject sits erect and pulled up to his or her full height. This would suggest active forward rotation of the pelvis. The data on the position of the PSIS's confirm that orientation of the pelvis is the same as for standing (Figure 16). All measurements are made from the seat reference point (SRP), which is the intersection of the vertical reference plane and the horizontal reference plane (Pheasant, 1986).

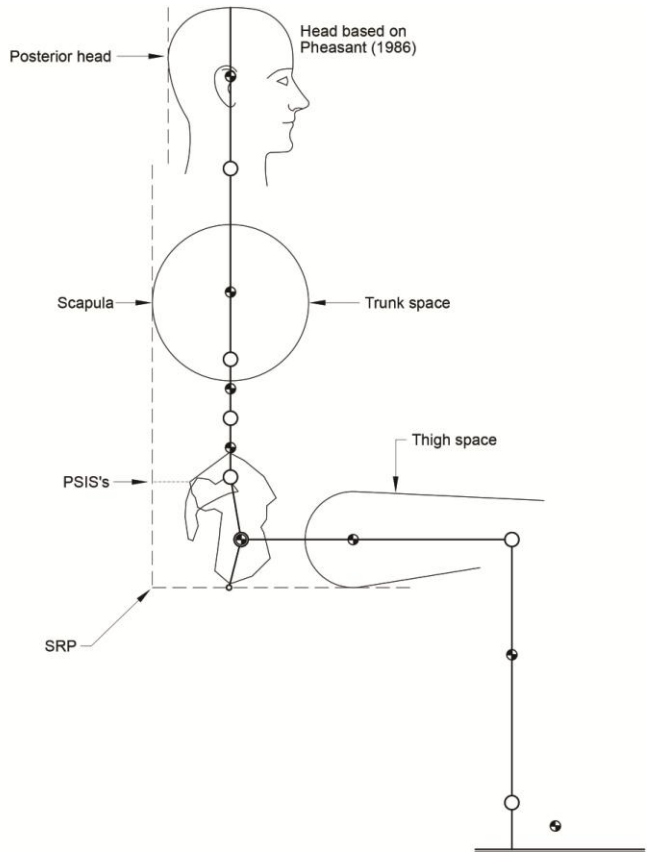

Figure 16 The human model in the anatomical sitting posture including the pelvis configuration, upper body linkages, and quantitative anthropometric data of the head, scapula, thigh and posterior superior iliac spines (PSIS's). The seat reference point (SRP) is the intersection of the vertical and horizontal reference planes

2. To configure the human model for the seated test postures, all model linkages are initially assumed to be parallel to their corresponding supports. The algorithms, previously described in Section 3.1, can then be applied to determine the orientation of the pelvis and the position of the ITs. This is shown, by way of example; in Figure 17 for the standard recline test posture.

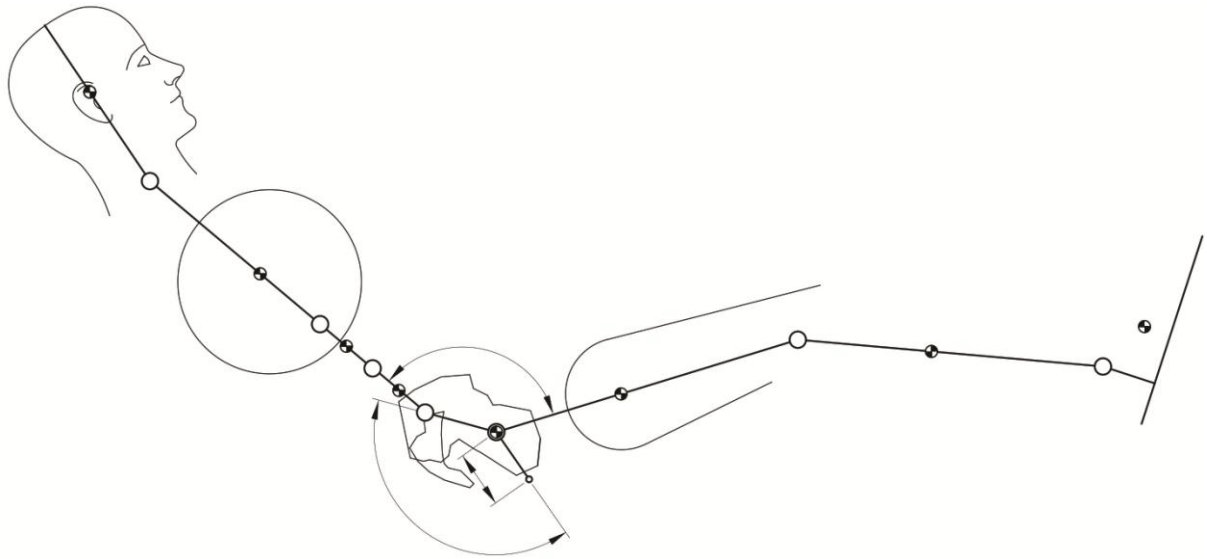

Figure 17 The human model configured to the standard recline test posture. Algorithms are applied to determine the orientation of the pelvis and the position of the inferior ischial tuberosities

3. The human model can then be registered with the support surface model where both had been previously configured to the same posture. The seat contacts the inferior ITs, the backrest contacts the trunk space and the headrest contacts the head (Figure 18). The human model is hence registered to the chair. Adjustments to the human model may be required to improve accuracy. In this study, the head segment needed inclining forwards slightly.

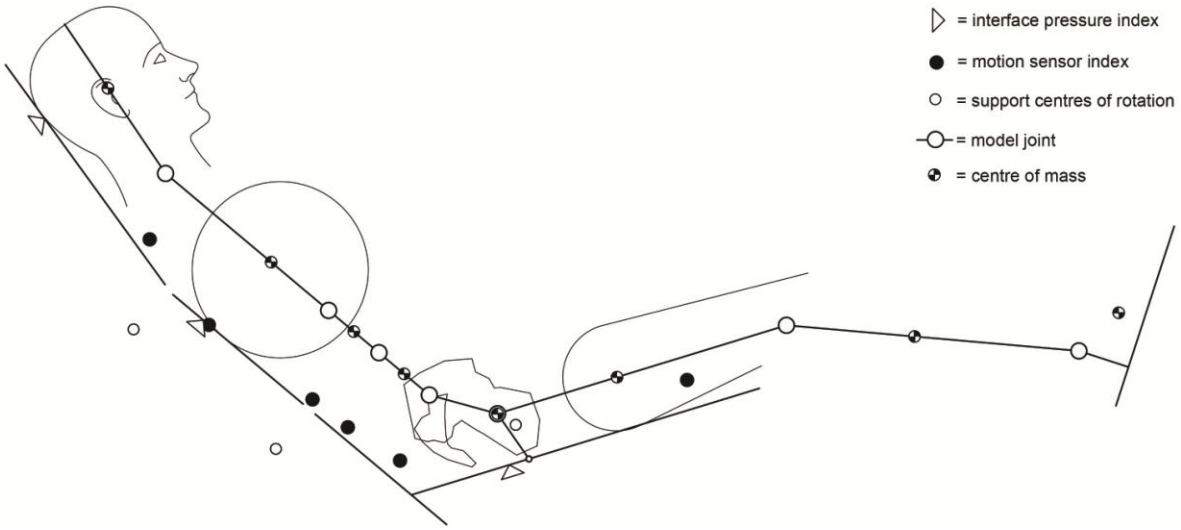

Figure 18 The human model registered with the support surface model in the standard recline test posture configuration

4. Where there are several backrest supports at different inclinations; the back supports and upper body segments are first aligned with the lowest part of the backrest to position the pelvis on the seat. The back supports and upper body segments are then articulated to the required configuration whilst preserving trunk and head space. This is illustrated with the model configured to the TIS 1 test posture in Figure 19.

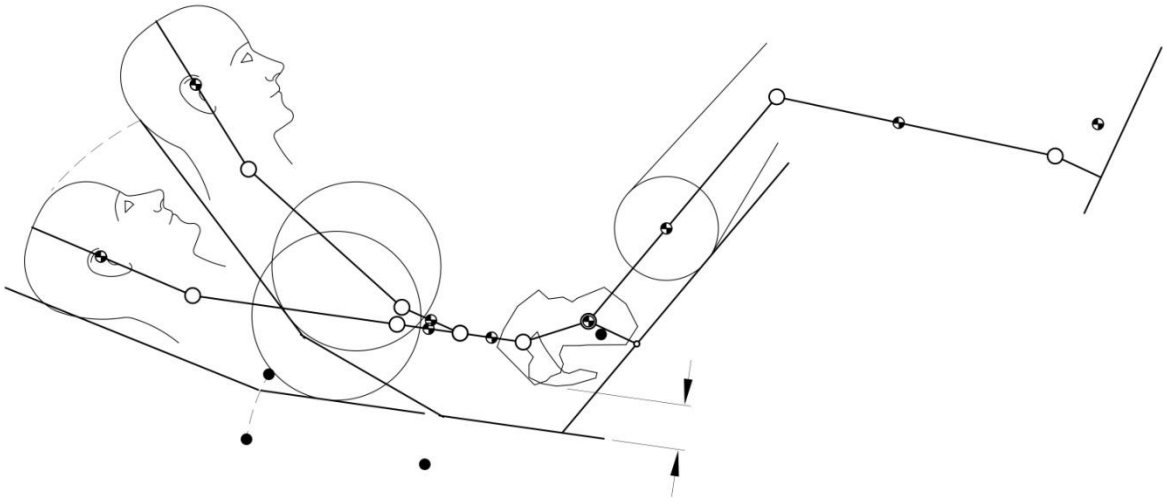

Figure 19 The human model and support surface model for the TIS 1 test posture configuration. For this posture, the backrest has several segments at different inclinations so the models are first registered with a straight back to determine the position of the pelvis on the seat before articulating the back supports and upper body segments

3.2.2 Model output parameters for validating posture

The postural accuracy of the model was evaluated against both published data to test hypothesis H1a, and experimental data collected during this study to test hypothesis H2a. In both cases the 50th percentile model was assessed so data from the three 50th percentile male subjects were used.

For comparing the model to published data, reference was made to anthropometric data on the car driver's sitting posture (Robbins, 1983). The model developed for the present study is based on anthropometric data taken from the British population (Pheasant and Haslegrave, 2006; Pheasant, 1986). The data on the car driver's posture was derived from anthropometric and stereophotogrammetric measurements at the University of Michigan. Figure 20 shows a two-dimensional side-view drawing of the midsize-male, with skeleton, that was created as part of their study, with the present model overlaid (50th percentile man). The configuration of the model was approximated. For this comparison, the accuracy was estimated using percent difference (Equation 35) for the vertical distance from the horizontal plane touching the inferior surface of the buttocks to the horizontal plane touching the superior surface of the head. For comparing the model to the experimental data, the distance from the intersection of the backrest and seat, along all support surfaces, to the most posterior aspect of the head that connects the support (peak head pressure in the experimental data) was chosen (Figure 21). The difference for the two measures of sitting height being difference in the quality of the data. The error for the comparison with experimental data was also expressed as percent difference (Equation 35).

$$\%\, Difference = \frac{(x_1 - x_2)}{\left(\frac{x_1 + x_2}{2}\right)} \times 100 \tag{35}$$

x_1 is the model distance and x_2 is the reference distance (measured from published data or experimentally)

Other secondary parameters for assessing accuracy were the distances from the intersection of the backrest and seat to the modelled position of the ITs, L3 vertebrae, and scapula. These model parameters were compared to measured peak pressure and motion sensor indices, and expressed as percent differences (Equation 35). Figure 21 illustrates the model measured against the interface pressure and motion sensor indices for the standard recline test posture configuration.

An additional analysis was performed to test hypothesis H2b, which states that the model predictions of the support surface motion paths will agree with at least 95% of measured data across the seated test postures. The modelled displacement of the motion tracking sensors relative to the modelled test-rig support surfaces across the seated test postures were compared with the measured displacement using the motion tracking system. The error for the comparison was expressed as percent difference (Equation 35). For this analysis, three biomechanical models were created representing the 5th percentile female, 50th percentile male and 95th percentile male populations. Data from Reynolds, *et al*., (1982) were used for the model pelvises (small female, medium male and large male) and Pheasant (1986) for the linkages. The torso segments that were derived from Reynolds' (1978) data in Section 3.1.2 were scaled from 50th percentile man.

The three human models (5th percentile female, 50th and 95th percentile male) were registered to the support surface models, as described in Section 3.2.1, for the upright, standard recline and TIS 1 test seating configurations (Figure 22). The positions of the motion sensors were incorporated into the human models in the upright posture, and then the models were reconfigured for standard recline posture and TIS 1 whilst maintaining the relative position of the motion sensors to the torso. Their displacements relative to the support surface model were then measured (positive values indicate the body sliding down the backrest). Measurements were made from the top of the either lower, middle or upper backrest segment, depending on which

motion sensor (Figure 22). Since the only change to the TIS 2 and TIS 3 seating configurations is the whole system tilt, it is assumed that there is no displacement between the human model and the support surfaces model. The sensor displacements are also shown in Table 8.

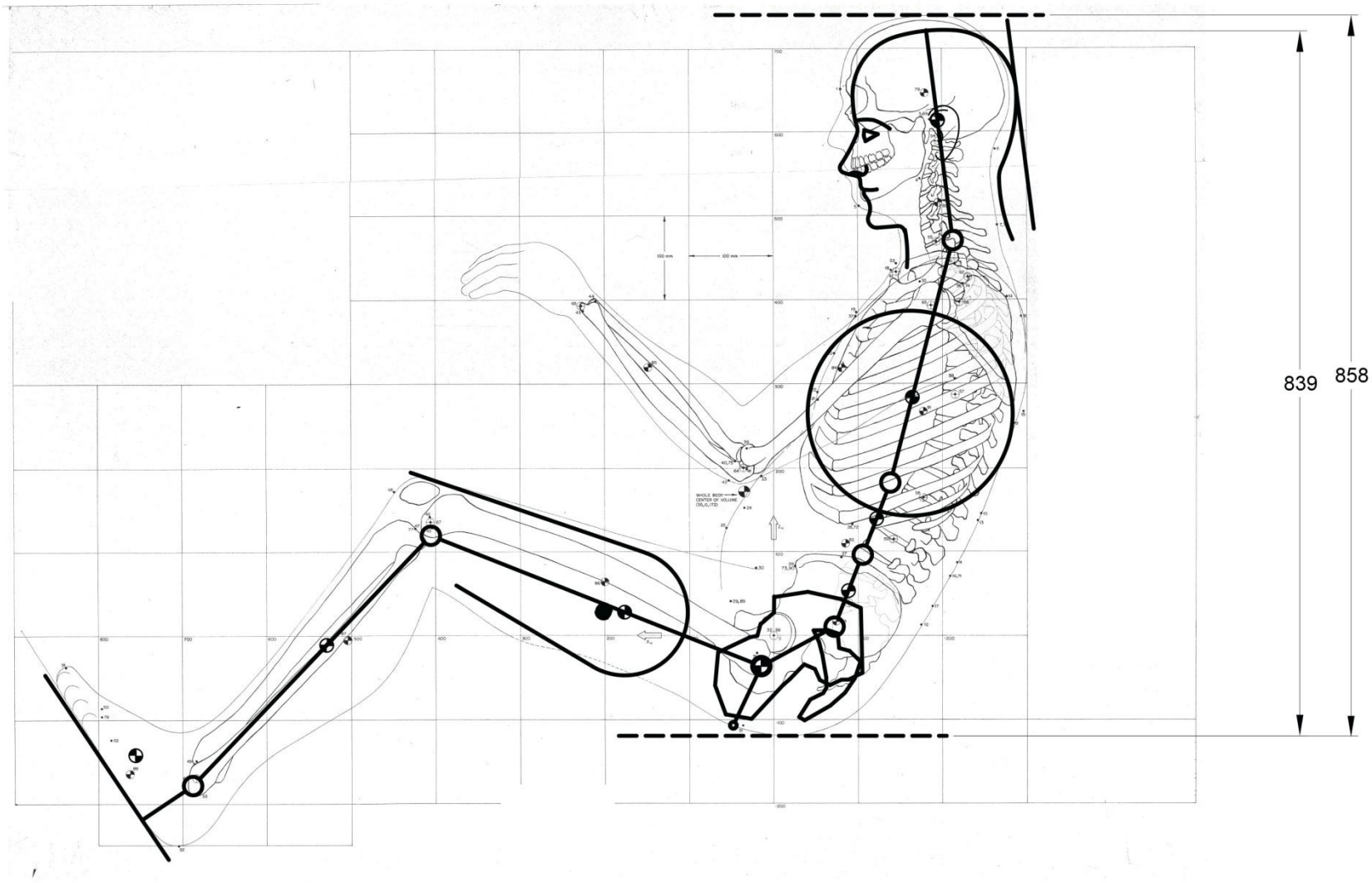

Figure 20 A two dimensional side-view drawing of the midsize-male, with skeleton, in a car driver's seat (Robbins, 1983). The 50th percentile male model is configured to the driver's posture, scaled and overlaid, with the sitting heights of both measured.

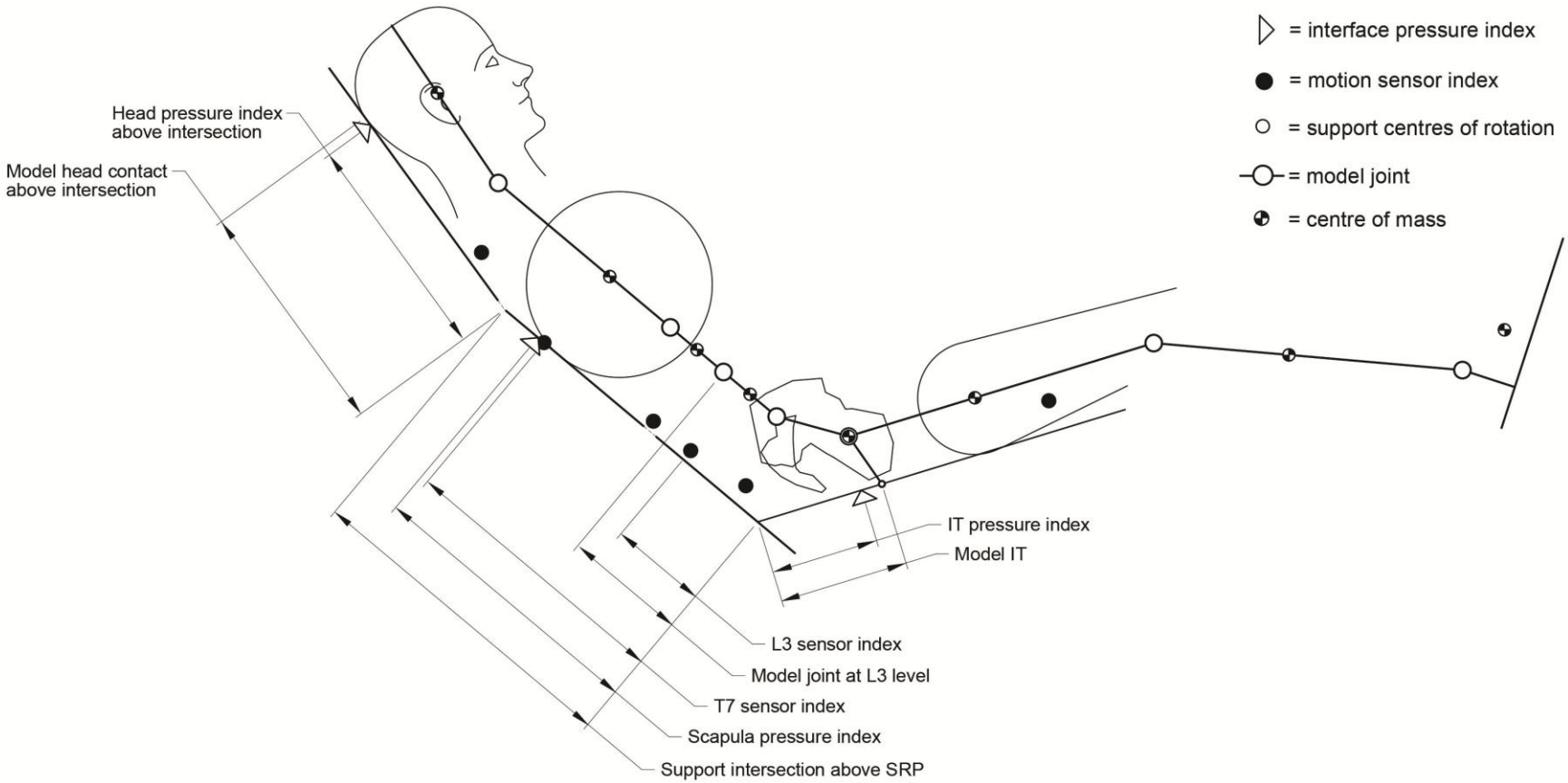

Figure 21 The 50th percentile male model and support surface model configured and registered to the standard recline test posture. All interface pressure, motion sensor and model indices are measured from the intersection of the backrest and seat, and along the support surfaces

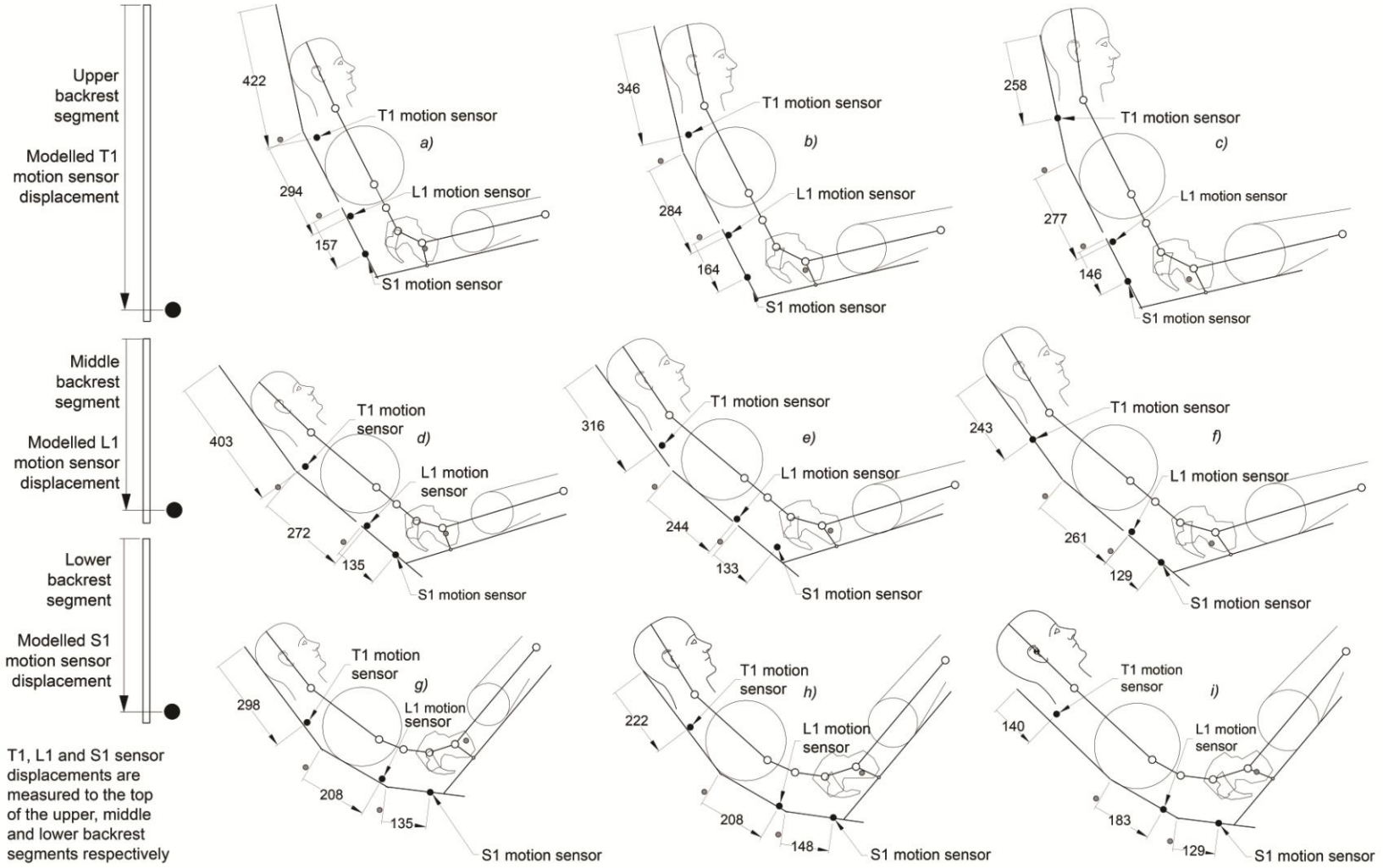

Figure 22 5th percentile female (*a,d,g*), 50th percentile male (*b,e,h*) and 95th percentile male (*c,f,i*) models in the upright (*a-c*), standard recline (*d-f*) and TIS 1 (*g-i*) test configurations, showing the modelled displacement of the S1, L1 and T1 motion sensors

Table 8 Modelled motion sensor displacements from Figure 22

	Sensors	Upright	Standard	TIS 1
5th percentile female	T1	422	403	298
	L1	294	272	208
	S1	157	135	135
50th percentile male	T1	346	316	222
	L1	284	244	208
	S1	164	133	148
95th percentile male	T1	258	277	140
	L1	277	261	183
	S1	146	129	129

3.2.3 Model output parameters for validating force

An initial verification was carried out to evaluate the model against a previously published biomechanical model in terms of force to test hypothesis H1b. Goossens and Snidjers' model (1995) was chosen for comparison. The model developed during this research is a modification of the Goossens and Snidjers model, so this comparison permits an evaluation of the changes made, such as sensitivity. Furthermore, Goossens and Snidjers validated their model in terms of parallel force at the ITs with experimental data collected using a force plate. Parallel force was not evaluated in the experiments from this study so this provides some interesting insight into different aspects of the model.

The Goossens and Snidjers original four link model was reconstructed and scaled to each test subject who participated in this study (based on their weight and height). Figure 23 shows the model from this research, the Goossens and Snidjers model in the context of this research and the Goossens and Snidjers model showing just the reaction forces and specific inclinations of the pelvis and upper body. Goossens and Snidjers modelled a relationship between posture and the position of the pelvic linkage based on Equation 36, by Stumbaum (1983), where ρ was the backrest inclination and κ was the inclination of the pelvic link (Figure 23). The inclination of the pelvis was therefore a function of the backrest inclination to the ground. Note that this coordinate

system is from Goossens and Snidjers, not the present study. The resulting model was then configured to simulate the seated test postures reported in their publication (Goossens & Snidjers, 1995). The model developed during this research was registered to the Goossens and Snidjers model and the same simulations were performed. The model output parameter for verification was seat parallel force ($F_{p,st}$) and is defined in Equation 37. Equation 37 is adapted from Goossens and Snidjers (1995).

$$\kappa = \frac{17}{18}\rho \tag{36}$$

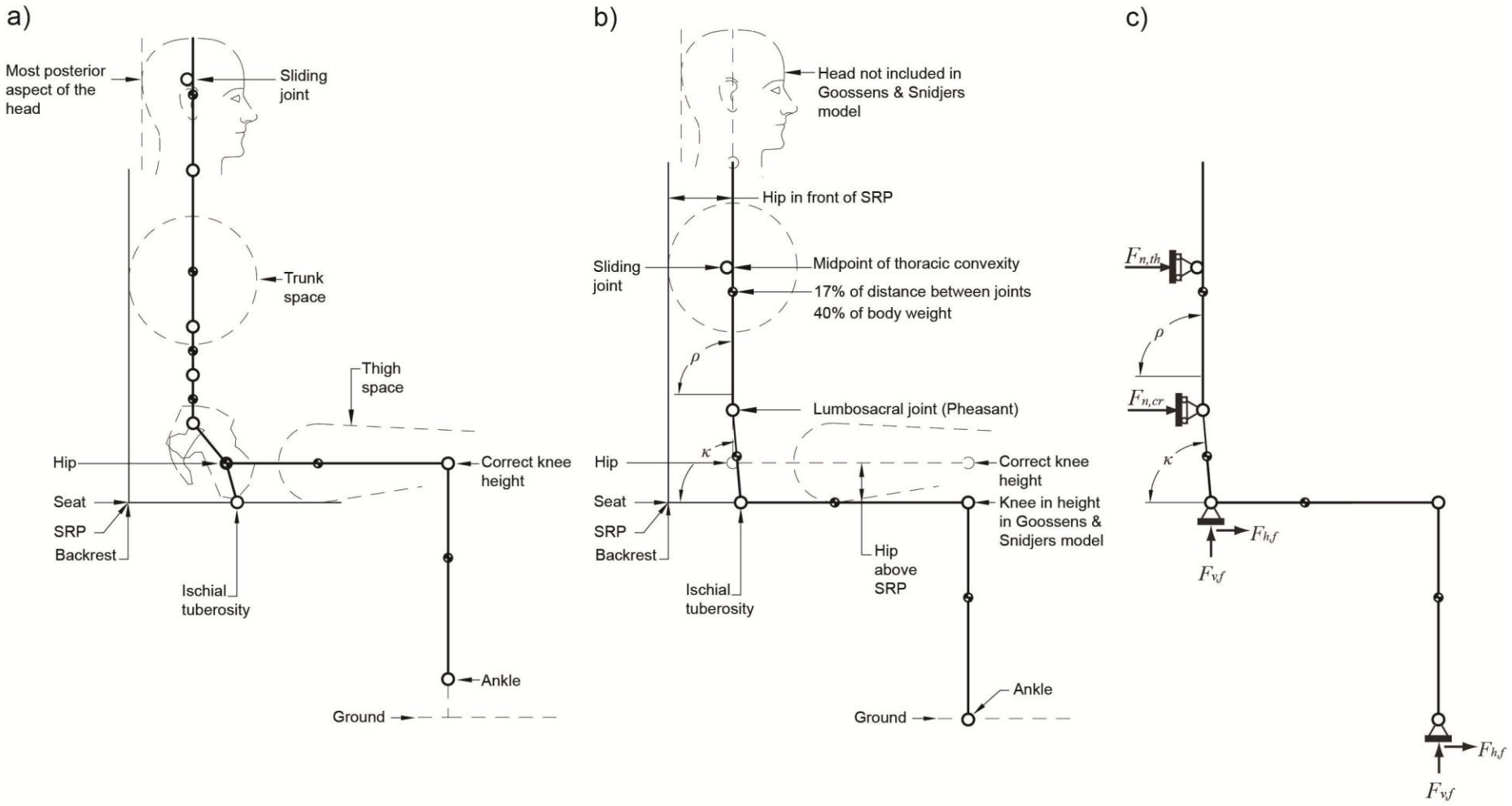

Figure 23 a) The biomechanical model developed during this research; b) Goossens and Snidjers four link model (1995) shown in the context of this study; c) Goossens and Snidjers four link model (1995) showing reaction forces. In their model, the inclination of the pelvis link (κ) is a function of the inclination of the upper body link (ρ): $\boldsymbol{\kappa = \frac{17}{18}\rho}$

For validating the model force predictions using experimental data collected during this study, model predictions were compared to the force measured from the seat, lumbar, thoracic and head supports. There are two options for calculating the total force of the seat. The choice depends on the seating configuration being modelled. If the feet are grounded on the floor, the seat total force ($F_{n,st}^{1}$) is defined in Equation 38. Equation 18 is adapted from Goossens and Snidjers (1995). If the seating configuration reclines with the feet unsupported, then the seat total force ($F_{n,st}^{2}$) is defined in Equation 39. Here, $F_{n,st}$ has the addition of the reaction force behind the knee ($F_{n,k}$) which was derived from Equation 26. The prediction for the total force by region of the backrest is the sum of corresponding normal reaction forces. These are $F_{n,cr} + F_{n,l}$ for the lumbar region, $F_{n,th} + F_{n,sh}$ for the thoracic region and $F_{n,h}$ for the head. $F_{n,cr}$ was derived from Equation 19 and modified with Equation 33, $F_{n,l}$ was derived from Equation 17, $F_{n,th}$ was derived from Equation 15, and $F_{n,sh}$ was derived from Equation 13.

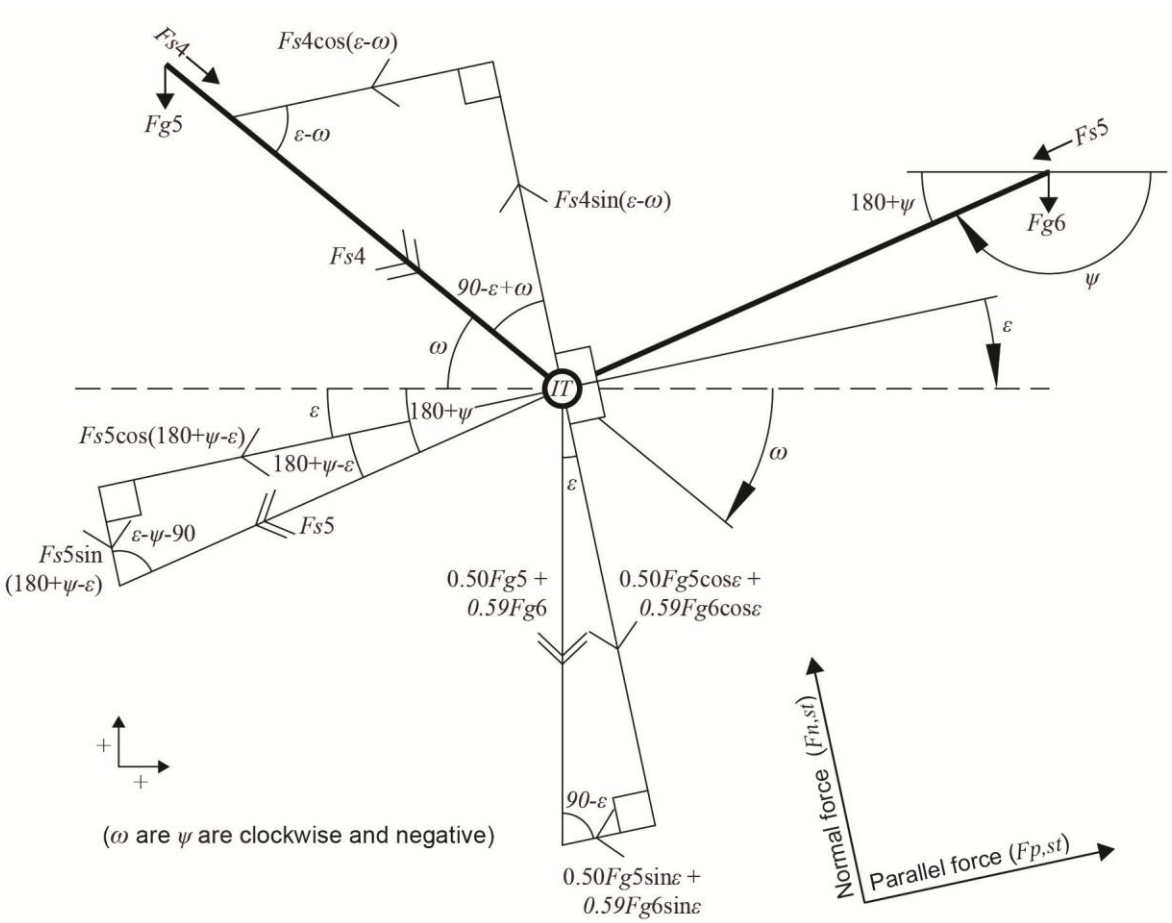

$$F_{p,st} = 0.50F_{g5}\,sin(\varepsilon) + 0.59F_{g6}\,sin(\varepsilon) + F_{s4}\,cos(\varepsilon - \omega) + F_{s5}\,cos(180 + \psi - \varepsilon) \quad (37)$$

$$F_{n,st}{}^{1} = 0.50F_{g5}\,cos(\varepsilon) + 0.59F_{g6}\,cos(\varepsilon) + F_{s4}\,sin(\varepsilon - \omega) + F_{s5}\,sin(180 + \psi - \varepsilon) \quad (38)$$

$$F_{n,st}{}^{2} = 0.50F_{g5}\,cos(\varepsilon) + 0.59F_{g6}\,cos(\varepsilon) + F_{s4}\,sin(\varepsilon - \omega) + F_{s5}\,sin(180 + \psi - \varepsilon) + F_{n,k} \quad (39)$$

3.2.4 Model output parameters for interpreting experimental data

Model force predictions for the support surfaces were tested for a relationship with the measured interface pressure variables (seat peak pressure, average pressure and contact area, and back average pressure and contact area). Using a wheelchair, Peters (1999) showed that, whilst keeping the thighs parallel to the seat, support to the feet from footplates resulted in an 11% increase in ischial interface pressure compared with the feet unsupported. He argued that this was a result of decreasing the contact area of the thighs by raising the knees and offloading the thighs to the ischial zones. In the present study, the feet where supported on the ground for the upright posture only, so for this posture Equation 37 is used for all comparisons. When the feet are unsupported, the model predicts an additional force at the knee joint which represents force from the front of the seat to the anterior thighs ($F_{n,k}$). For postures where the feet are unsupported, Equation 38 is used, however the additional force ($F_{n,k}$) at the front edge of the seat is omitted when comparing seat force to peak and average pressures and is only included for contact area. The sum of backrest force is tested for a relationship with the backrest pressure.

For spinal loading, the model link forces acting along the axis of the thoracic (F_{s1}), upper lumbar (F_{s2}) and lower lumbar (F_{s3}) linkages, and the sum of these predicted forces (total torso link force), were analysed and compared to the stadiometry data. F_{s1} was derived from Equation 12, F_{s2} was derived from Equation 14 and F_{s3} was derived from Equation 16. For muscle activity, it was hypothesised that muscle recruitment would reduce as support from the test-rig increases. Therefore, model force predictions acting on the pelvis ($F_{n,cr}$), lumbar spine ($F_{n,l}$), thoracic spine ($F_{n,th}$), and shoulder girdle ($F_{n,sh}$) were tested for a relationship with corresponding proximal surface electromyographic activity. Model predictions of passive force acting on the pelvis (F_{net}) were also evaluated with respect to neighbouring surface electromyographic activity. F_{net} was derived in Section 3.1.5 and defined in Equation 32, $F_{n,cr}$ was derived from Equation 19 and modified with Equation 33, $F_{n,l}$ was derived from Equation 17, $F_{n,th}$ was derived from Equation 15, and $F_{n,sh}$ was derived from Equation 13.

4 Data collection

This chapter describes the methods of four experiments aimed at quantifying a subset of the biomechanical effects of tilt-in-space (TIS), reclined and combination postures, in order to test the thesis hypotheses listed in Section 1.4 of the introduction. The methods described are: 1) interface pressure measurement; 2) stature measurement; 3) electromyography measurement; and 4) posture measurement.

The same test-rig and seated test postures, as described in Section 2.3, Chapter 2, were used throughout. For measurements of interface pressure and posture, additional measures of the TIS 1 configuration were performed with the backrest articulated after the subject had been seated in the test-rig (TIS 1a).

4.1 Subjects

A cohort of 15 asymptomatic healthy subjects, seven male and eight female, mean age 43 years (29-56 years) was recruited for this investigation. Table 8 gives the basic anthropometric information for the subjects included. All subjects completed consent forms before participating (Appendix A-1). Ethical approval was sought from Anglia Ruskin University and approved.

Table 8 Basic anthropometric data of test subjects

Subject	Sex	Height (cm)	Mass (kg)	Age (years)
1	Female	171	76	51
2	Female	157	69	34
3	Female	152	59	41
4	Female	154	58	45
5	Male	173	72	36
6	Female	152	60	62
7	Female	181	70	29
8	Male	173	84	46
9	Female	166	77	56
10	Male	180	95	46
11	Male	182	67	53
12	Female	162	75	31
13	Male	173	101	32
14	Male	186	87	32
15	Male	167	66	48

4.2 Interface pressure

4.2.1 Test apparatus and set up

An XSENSOR pressure mapping system (XSENSOR Technology Corporation, Calgary, Canada) was used to measure the body/support interface pressures. The system consists of two pressure mats (seat and backrest) and an X3 sensor platform to provide a signal interface and power for the pressure mats. The XSENSOR 4.3 Industrial software was used for calibration, data collection and file archiving.

The pressure mats for the seat and backrest were thin and flexible, containing capacitance sensors. The seat mat consisted of a 36 x 36 array of sensors (1296 measuring points in total) and covers a sensing area of 457 x 457 mm. The backrest mat consisted of an array of 40 x 64 sensors (a total of 2560 sensors) and covered a sensing area of 508 mm x 813 mm. The advantages of capacitance sensors over other sensor types, such as the resistive sensor, are high repeatability, high accuracy, low hysteresis, and no need for frequent calibration, as is the

case for resistive sensors (Mootanah & Bader, 2006). In addition, the study by Pipkin and Sprigle (2008) suggested a low perturbation error for the XSENSOR mats. The pressure range was 10–200 mmHg, with a corresponding accuracy of ±10% (XSENSOR Technology Corporation, 2012).

Prior to testing, the sensor mats were calibrated according to the manufacturer's guidelines. In this process, the sensor mats were placed in a calibration jig with an air filled bladder. The bladder was then inflated and measured, assuming the pressure was evenly distributed over the mat. With the mat subjected to known forces, the sensor responses were monitored and modelled. A record of this response was obtained and stored as the calibration file.

4.2.2 Protocol

Subjects wore thin, light weight fabrics, were given a pair of Jersey shorts and allowed to change in privacy (Jersey is a highly conformable material which should have negligible impact on the pressure readings). The subjects were allowed to keep on their upper garment because they were thin, lightweight fabrics. Although underwear could affect the data (i.e. bra straps), subjects were allowed to keep them on. Since the aim of the investigation was to assess the general weight shift from seat to backrest, preservation of dignity was considered to outweigh the benefits of removing underwear. The examiner then set up the test-rig so that the seat height and seat length were the correct size for the subject. With the subject sitting within the test-rig and the pelvis touching the backrest, the seat length was set to the maximum position before the front edge of the seat touched the calves. Seat height was determined by setting the height to a level where the subject reported comfortable pressure beneath the entire thigh contact area. The subject was then asked to stand whilst the pressure mats were placed on the test-rig. The seat foam was removed from the test-rig and placed central to the sensor area and held in place with masking tape (Figure 24). The cushion and pressure mat was then transferred back to the test-

rig and fixed to the seat base with masking tape. The backrest pressure mat was first placed so that the edge of the sensing area was in line with the lower edge of the backrest foam. The mat was not large enough to cover the entire backrest for the taller subjects. In these cases, two recording sessions were carried out moving the backrest pressure map upwards between measurements, with the data concatenated during the analysis.

The investigator set the test-rig to the required posture. For the TIS postures, the subject entered the test-rig in its upright position prior to tilting by the investigator. For the TIS 1 posture, the backrest was articulated before the subject entered the test-rig. For the TIS 1a posture, the backrest was articulated after the subject was tilted in the test-rig. Subjects were asked to be as still as possible, with arms rested on their laps for a one minute stabilisation period to reduce creep in the cushion, pressure mat and body tissues (Figure 25). The seat cushion was found to stabilise adequately after approximately 60 seconds in a pilot test with one investigator acting as the test subject. Figure 26 gives the results for peak pressure and Figure 27 gives the results for average pressure from this pilot test. The seat cushion stabilised quicker for peak pressure, with 87% of the pressure change over 3 minutes occurring within the first 60 seconds. There was a pressure change of 2 mmHg for the remaining 2 minutes of the measurement. For average pressure, 73% of the pressure change of the over 3 minutes occurred within the first 60 seconds. The pressure change for the remaining 2 minutes was 3 mmHg.

After the stabilisation period, interface pressure was recorded for 30 seconds, whilst the subject remained as still as possible. This protocol was repeated for all postures to complete the trial. The subject stood for one minute between each test to allow for recovery in the cushion, pressure mat and body tissue.

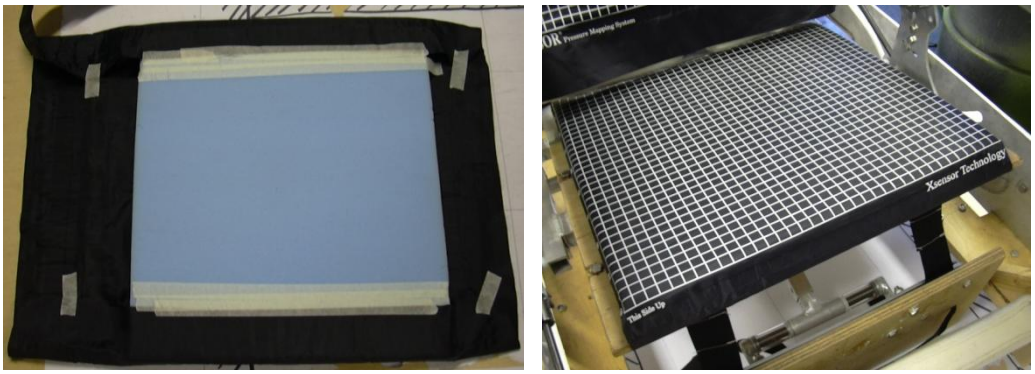

Figure 24 Fixture of pressure mats on the test-rig

Figure 25 Subject positioned in the test-rig

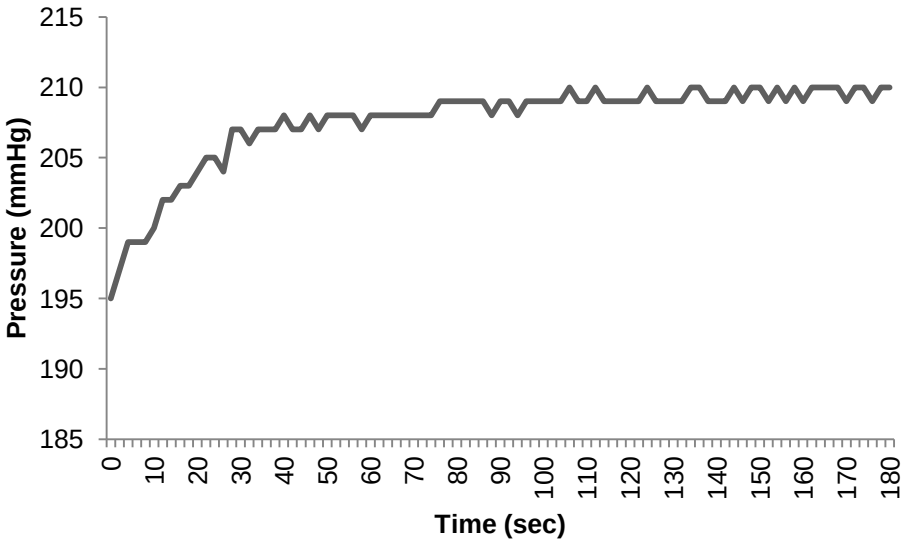

Figure 26 Results from the pilot test showing peak pressure creep

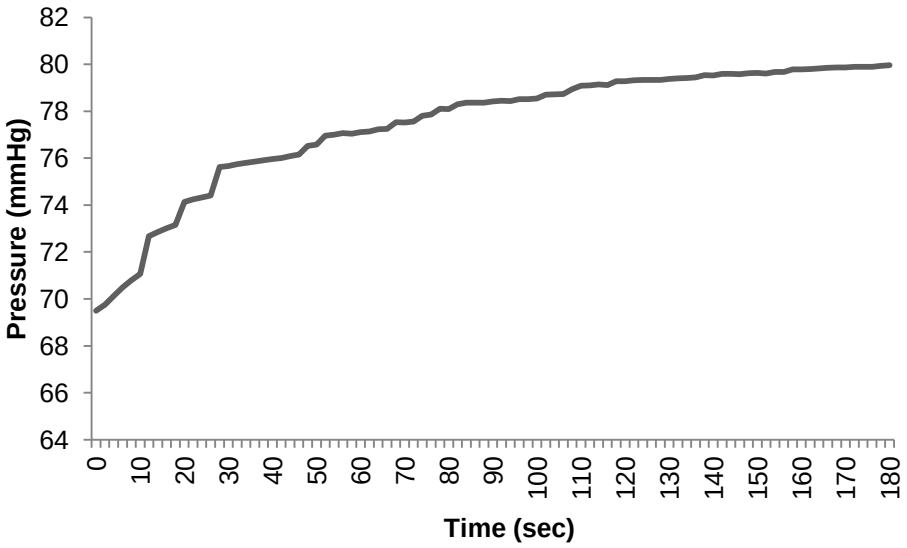

Figure 27 Results from the pilot test showing average pressure creep

4.2.3 Data collection and interpretation

Each 30 second recording resulted in 100 pressure distribution frames. The average of all frames was exported from the XSENSOR software to Excel for further analysis. There are many ways of interpreting interface pressure distributions. The ISO Working Group 11 have considered Total Force, Percent total Force, Dispersion Index, and Contact Area, in developing standards for tissue integrity (International Organisation for Standardisation, 2001). In addition to these, Contact Area Threshold, Peak Pressure Index, and Seat Pressure Index were also considered (Sprigle, *et al*, 2003).

For model validation, total force was required for the seat, lumbar, thoracic, and head regions, as these corresponded to the model force predictions. In Excel, the pressure distribution of a given region was converted into a single total force value (expressed in Newtons) by multiplying the sum of pressure readings by the conversion factor of 0.013332239 (mmHg to N/cm^2) and dividing by 1.61 (the sensor area) (Sprigle, *et al*., 2010). For the seat region, the sum of all pressures measured by the seat mat was converted to force. Figure 28 shows a typical backrest pressure

distribution. Here, it can be seen that the lumbar, thoracic and head regions correspond to different foam segments in the backrest of the test-rig, making them easily identifiable.

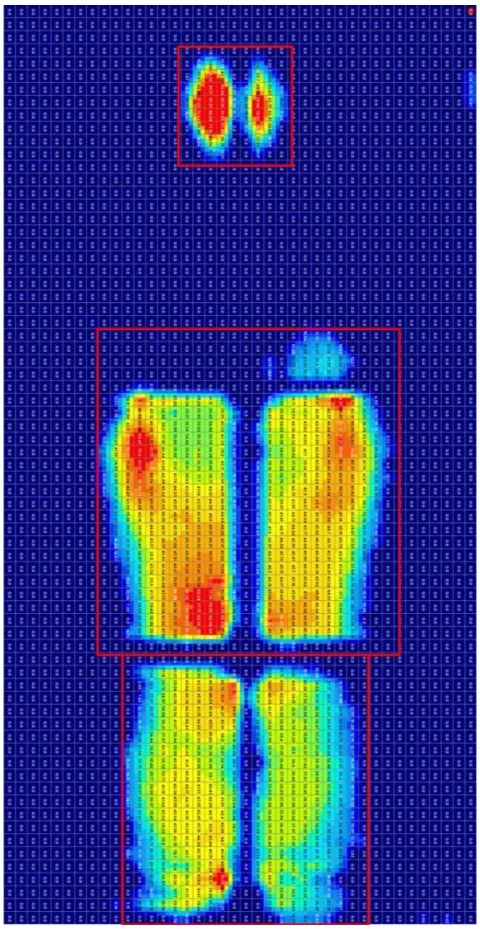

Figure 28 Example of a backrest pressure where the lumbar, thoracic and head regions are clearly defined from the supporting foam segments

Sprigle, *et al*. (2003) carried out a study to determine the test-retest reliability of the interface pressure measurements as defined by the draft ISO document. This study confirmed that single sensor peak pressure readings were unstable measures that exhibited poor repeatability. To overcome this, some researchers have reported the average of a small area in the region of the bony prominence (Henderson, *et al*., 1994; Burns & Betz, 1999; Giesbrecht, *et al*., 2011). Sprigle, *et al*., (2003) called this Peak Pressure Index and demonstrated that it was a reliable interface pressure parameter. Localised areas of high pressure may affect tissue mechanics,

alter blood perfusion and lead to discomfort levels. From reviewing the literature, Peak Pressure Index may best describe this. The amount of contact area was also of interest. In addition to mechanically redistributing load across a greater area, and hence reducing areas of localised high pressure, it may also physiologically have altered how comfort was perceived. Subjective ratings were not included in this dissertation; however, how Peak Pressure Index and contact area change with respect to the test postures was of interest, as well as the relationship with force predictions from the biomechanical model. Sprigle, *et al*., (2003) defined "contact" as pressure readings equal to or exceeding 5 mmHg, and called this pressure parameter Contact Area Threshold. In the present study, the calibration of the pressure mats was over the range of 10-200 mmHg. The Contact Area Threshold was therefore modified to include all pressures equal to or above 10 mmHg.

Peak Pressure Index was calculated in the XSENSOR 4.3 Industrial software. An area of 9.66 cm^2 (2 x 3 sensors, each sensor being 1.61 cm^2) was selected that gave the highest mean value. This value was noted down and later tabulated in Excel. Peak Pressure Index was taken for the seat only, in the areas of the ischial tuberosities.

For Contact Area Threshold, the average of all frames for each recording session was exported into Excel for analysis. These data were inspected visually to identify any obvious values that were not associated with the test subject, such as creases in the pressure mat. These values were then replaced with zero. Contact Area Threshold was obtained for both the seat and backrest by establishing the ratio of sensors giving values equal to or above 10 mmHg against all sensors, and then applying this ratio to the area of the mat containing the sensors (Equation 40).

$$C = A \times \left(n / N_{mat} \right) \tag{40}$$

Where,

$C =$ contact area

$A =$ area of pressure mat containing sensors

$N_{mat} =$ the number of sensors in the mat

$n =$ the number of sensors with pressure readings $\geq$ 10mmHg

4.3 Stature

4.3.1 Test apparatus and set up

The stadiometer used for stature measurements (Figure 29) is the version modified by Bonney (1988). The stadiometer consisted of a column and a base plate. A measuring head and frame for locating points on the back and neck was attached to the column. The base plate positioned and supported the heels, and a weighing scale supported the soles of the feet. This allowed for control of the distribution of weight between the heels and soles. Tape was fixed to the weighing scales to align the feet. Adjustable lateral supports located the knees and hips. The frame attached to the column had five adjustable rods to register the spine to the testing device. Two adjustable rods also located the back of the knees. The adjustable rods had a microswitch at their ends, with a displacement of 1mm, and connected to a light box giving visual feedback on the pressures for each microswitch. The head was located in a V-shaped support, and the head orientation was controlled by a nose pointer. A mirror, fixed to the nose pointer, assisted the subject to align their head. The position of the test-rig relative to the stadiometer was recorded for repeatable transfer of the subject. Measurements were also taken for heart rate during this experiment as a quality control for the sEMG study with respect to potential electrocardiographic

(ECG) contamination. A wireless heart rate sensor/transmitter was used that straps around the chest (www.polar.fi).

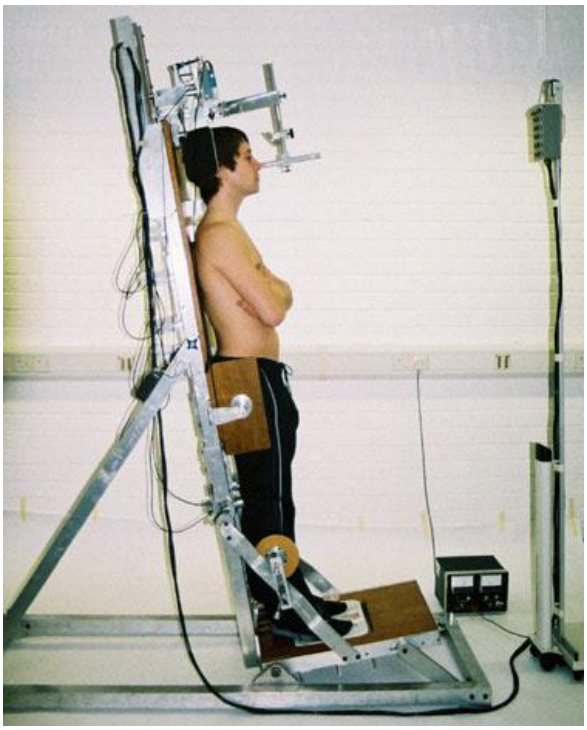

Figure 29 A subject standing in the stadiometer for height measurement

4.3.2 Protocol

Subjects were instructed to wear loose T-shirts, light weight trousers, to remove belts, and empty pockets. Subjects were allowed to keep their shoes on (Bonney, 1988). Subjects with long hair were asked to tie their hair up so the back of their necks could be easily accessed. The wireless heart rate sensor/transmitter was given to the volunteers at the beginning of the investigation. Subjects were asked to follow the same daily routine for the day prior to the testing, not to drink alcohol and to ensure they had 8 hours sleep. At the beginning of each test the scales were calibrated and the supports removed.

A training session was provided prior to testing. This lasted approximately 40 minutes. Firstly, an explanation of the stadiometer was provided. The subjects were then asked to step into the stadiometer, ensuring the heels were touching the back of the base and the feet were angled approximately 25° to each other (masking tape was placed on the scales to assist). The subjects were then instructed to stand as tall as possible without stretching, and relax with arms folded. The lateral supports for the knees and hips were then moved until acceptable pressure was applied to both sides of the subject, with both sides measuring the same distance, and perceived comfortable by the subject. The rods for behind the knees were then moved until the lights showed green and fixed. Following this, the rods for the spine were moved in place in the order of S1, centre of concavity of lumbar spine, T12, centre of thoracic convexity, and centre of cervical concavity. Finally the nose pointer was positioned. The subjects were then asked to step out of the stadiometer and shake their arms and legs to relax muscular tension. The subjects were then instructed to step into the stadiometer and amendments were made so all lights went to green (if the light was red, too much pressure was being applied to the rods). If it took too long to get the lights to green the subjects were again asked to step out, shake their limbs and return. Only when the subjects got all lights onto green immediately was the stadiometer considered to be set correctly, and the subjects fully trained on how to make the correct movements to repeat their posture precisely. A short practice session commenced the training. Subjects were instructed as follows:

- feet in position;
- roll into position (rolling back into the stadiometer was found to be a more accurate method of ingress);
- fold arms;
- stand tall without stretching;
- contact probes until all lights show red;
- adjust head angle to the nose pointer;

- control weight distribution – observer to check;
- relax and try to get as many lights to green as possible.

The procedure was repeated until consecutive results did not differ by more than 0.5 mm.

Pre-test:

Subjects were asked to stand comfortably or walk slowly around the laboratory for one hour. Two of the six pre-test periods lasted for 40 minutes to ensure all testing would be completed within two days for each subject. The test order was randomised. During this pre-test period, measurements were taken every 5 minutes (12 measurements in total). Three sets of measurements were taken each time with the subject repositioning themselves between measurement sets. For each set a series of 5 readings were taken. If an outlier was found (more than 0.5 mm between consecutive readings), it was disregarded and replaced. This pre-test obtained the data that was subsequently used to fit the exponential function to predict the natural height change during the test period (Alfthoff, *et al*., 1992).

Test:

Immediately following the final measurement of the pre-test period, subjects were asked to sit in the test-rig, relax into their posture and to not fold arms or cross legs. The test period corresponded to the pre-test period such that a one hour test followed a one hour pre-test, and a 40 minute test followed a 40 minute pre-test. The test-rig was adjusted to the posture under investigation by the examiner. Sitting was interrupted for approximately 3 minutes at 10 minute intervals for measurements as described for the pre-test period. Once the subject was in the test position, heart rate was measured three times using the monitor fitted to the subject's chest, and archived for analysis with the sEMG data.

4.3.3 Data collection and interpretation

An average was taken of the three data sets recorded at each measurement interval. The values were then plotted on a graph. Separate exponential curves for the pre-test and test period were made by inverting the data and normalising to the initial value. An exponential as defined by Equation 41 was fitted to the data.

$$\text{Relative height} = A \times \left(1 - e^{-bt}\right) \tag{41}$$

In this curve coefficient A stands for the equilibrium deformation, while b stands for the creep rate, that is, the rate at which this equilibrium deformation is approached (van Dieen, *et al*., 1994). If an exponential curve could not be fitted, the protocol resorted to linear regression. Figure 30 shows an example of the curve fitting. For each posture studied, a single value was obtained for the change in stature for each subject after 40 minutes of testing.

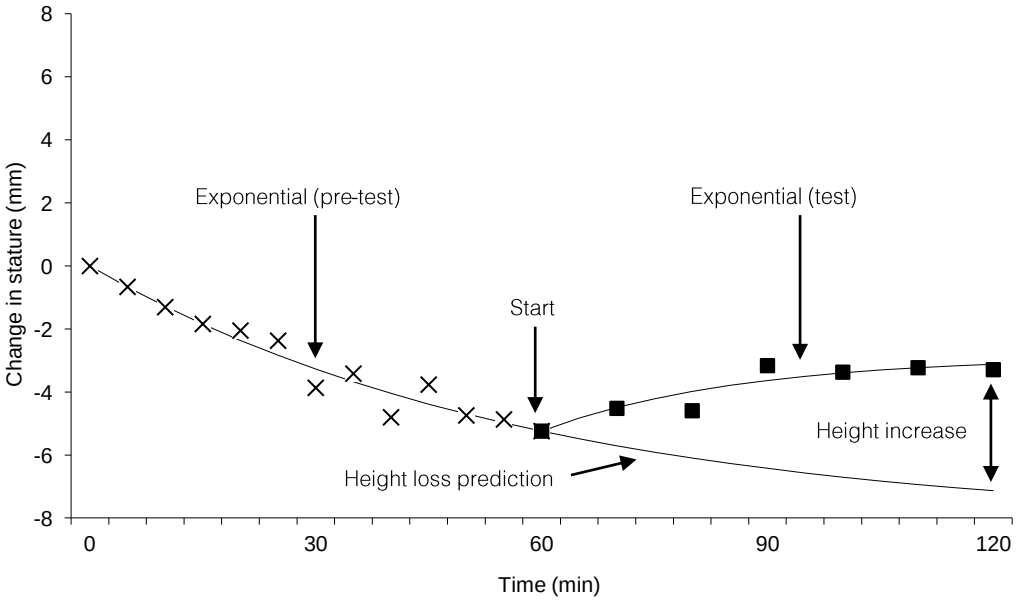

Figure 30 An example of the mathematical treatment of experimental data (here it can be seen that shrinkage occurs during the pre-test period, followed by recovery)

4.4 sEMG

4.4.1 Test apparatus and set up

The MESPEC8000 8-channel system and the MegaWin software[1] were used in this study. The system consists of two snap connectors for the active surface electrodes and one snap connector for the ground electrode located below an analogue differential pre-amplifier (375 gain). The surface electrodes were disposable pre-filled Ag/AgCI electrodes (Vermed Inc, USA). The pre-amplified signal was transmitted to the main differential amplifier with a Common Mode Rejection Ratio (CMRR) value of 110 dB. The frequency range of the amplifier is 8–500 Hz. The low pass filtered analogue voltage was converted to a digital signal via a 12 bit A/D converter for display and analysis in the computer. The sampling rate at which the A/D converter acquired the input signal was 1000 Hz. This specification met the requirements established by the SENIAM project (Hermens, *et al*., 1999) for surface electromyography (sEMG) signal processing. The SENIAM project is a European Commission initiative to build and disseminate the state of the art in sEMG.

The same 15 subjects who participated in the other investigations were invited for this test, however, one candidate declined, leaving 7 male and 7 female participants. Unfortunately, prior to the analysis being carrying out, the data from 3 subjects were accidentally deleted from the PC used to carry out the investigation. The measurements on these 3 subjects could not be repeated due to time constraints. Therefore, 11 samples were available for analysis.

4.4.2 Protocol

Subjects were given a pair of linen shorts and a surgical gown that opened from the back to wear for the experiment. Standard palpation techniques were used to identify anatomical landmarks. Training was provided by a Senior Physiotherapist from the Mid Essex Hospital Services NHS

[1] Mega Electronics Ltd, Savilahdentie 6, P.O. Box 1750, FIN-70211 Kuopio, Finland. http://www.meltd.fi

Trust, Broomfield Hospital in Chelmsford. Subjects with long hair were provided with bands to tie their hair back. Each subject was asked to sit on a wooden stool and assume a semi-flexed posture. The surgical gown was opened at the back and shorts lowered if too high. The first bony landmarks to locate were the Posterior Superior Iliac Spines (PSISs). These were relatively easy to find, and often seen by eye next to the 'Dimples of Venus'. Once the PSISs were identified, they were marked with a China pencil (recommended by Physiotherapists). A line was drawn between the PSISs and the line bisection defined the interspace of S1 and S2. The interspace of L4 and L5 was located by bisecting the line joining the highest point of the iliac crest. The spine was then counted up from L5 and each bony prominence was marked (Figure 31). The location of C6 was then identified by palpation. C6 was the first obvious bony prominence when palpating down the cervical spine. C6 protrudes and retracts when the head moves forwards and backwards. The spine was then counted down from C6 by palpation. If the counts down the spine agreed with the counts up, the locations were deemed correct. Reference marks were then made on all spinous processes.

Figure 31 Identification of the bony landmarks by palpation (marks 1 and 3 denote the 1st and 3rd lumbar vertebral prominences)

The electrode location and placement procedure followed the recommendations published by the SENIAM project (Hermens, *et al*., 1999). Reference lines were first drawn on the subject's back for electrode placement. The location for the electrodes were over the following muscles on both sides of the spine (Figure 32): multifidus (Figure 32a) (aligned from the caudal tip of the PSIS to the interspace between L1 and L2 at the level of L5 spinous process); erector spinae iliocostalis (Figure 32b) (1 finger width medial from the line connecting the PSIS to the lowest point of the lower rib, at the level of L2); erector spinae longissimus (Figure 32c) (2 fingers width lateral from the spinous process of L1). Vertical reference lines were also drawn for two additional electrodes to be placed on the left side of the erector spinae at the levels of T8 and T4, and at a 2 fingers width distance lateral to the spinous process. The terms 'erector spinae iliocostalis' and 'erector spinae longissimus' will be abbreviated to 'iliocostalis' and 'longissimus' for future reference.

In order to get a good electrode-skin contact, the subject was shaved with a vibrating razor at the skin surface where the electrode was to be placed to remove hair. This method was also likely to remove dead skin which can produce high impedance. The skin surface was then cleaned with alcohol and allowed to dry before electrodes were placed. In general, the skin preparation left the skin slightly reddened which indicates a good skin impedance condition. The electrodes were then attached to the skin at the locations described previously. The inter-electrode distance was 2 cm and the reference electrodes were attached 2 cm lateral to the recording electrode pairs (Figure 32).

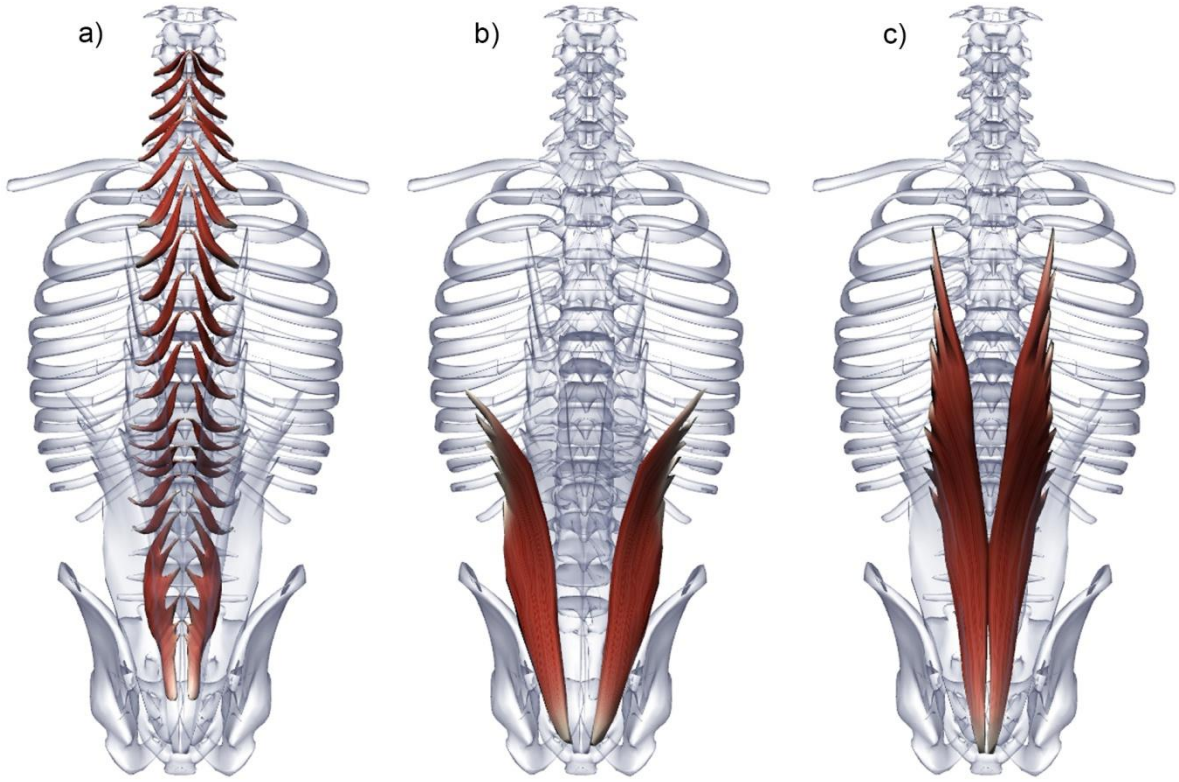

Figure 32 The back muscle groups: a) the multifidus; b) the erector spinae iliocostalis; c) the erector spinae longissimus (images from www.biodigitalhuman.com)

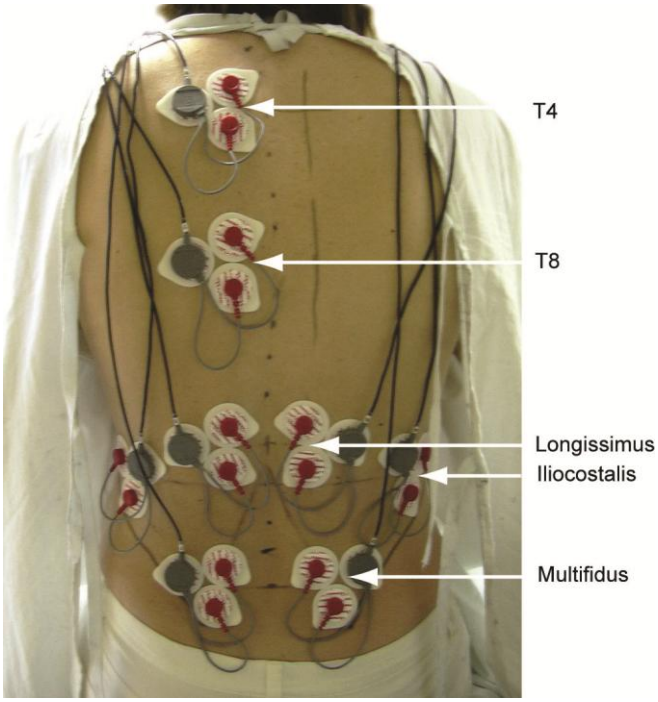

Figure 32 Electromyographic electrode arrangement (over the multifidus, the erector spinae iliocostalis, the erector spinae longissimus, and at T8 and T4 levels)

Subjects were instructed to stand tall and then relax, look straight ahead and to remain still for the first recording session. The recording session lasted for precisely 2 minutes and 30 seconds. The subjects were then taken through the 4 sitting postures; each recorded for the same measurement period as for standing. The subjects were asked to relax and remain still for each recording session to reduce the potential for noise due to friction between the electrodes and the upholstery fabric on the test-rig (dues to skin-motion artefact). Lying supine on a firm closed cell foam mat was also included to provide additional a reference data. After testing, the electrodes were removed and any gel, adhesive and reference marks were cleaned off the subject's back using pre-impregnated skincare wipes.

4.4.3 Data collection and interpretation

Five 30 second measurements were recorded for each posture, with each measurement corresponding to a different signal processing protocol as specified by the software. This

provided a record of the sEMG data processed by five different methods and afforded the investigator the choice post hoc. The ‘raw free’ measurement data was ultimately selected because no mathematical treatment was applied for this protocol.

On inspection of the raw data, it was clear that, for some muscles, the baseline had shifted from zero. The most significantly affected was the longissimus left side (Figure 33). It was noted that this happened for all measurements and so this was considered to be a systematic error attributed to the sEMG hardware. This was corrected by shifting the mean of the data to zero (Figure 34).

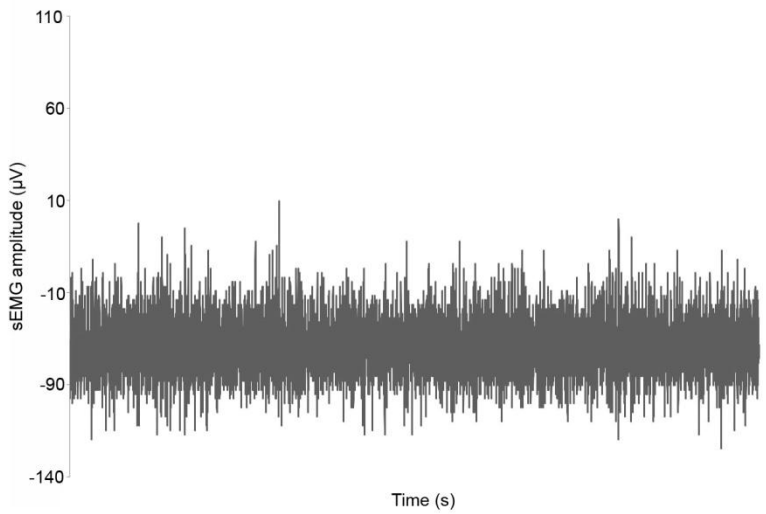

Figure 33 Raw sEMG data for the longissimus left side (graph shows the baseline is significantly shifted from zero)

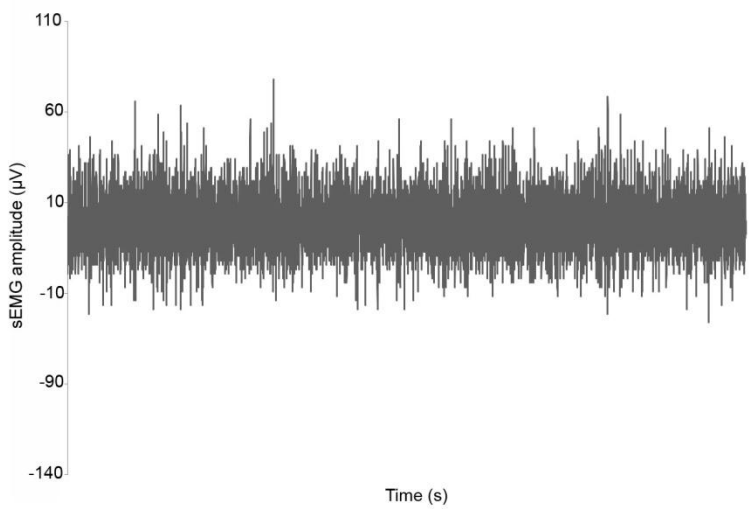

Figure 34 sEMG data for the longissimus left side after setting the mean to zero

For some muscles it was evident that there was ECG contamination. Figure 35 gives the example of the iliocostalis left side where very little muscle (almost silent) activity was measured. Here, ECG contamination is most apparent. Heart rate was measured during the stadiometry investigation as a quality control. The average heart rate for lying was 61 beats per minute, and for the TIS 2 posture the average heart rate was 66 beats per minute. The raw sEMG data for these two postures were explored visually and the ECG spikes were counted. On average, 60 spikes were counted for the lying posture, and 66 for the TIS 2 posture. The strong correlation between the measured heart rate and the number of spikes counted in the sEMG data, as well as their periodicity, strongly implicates the heart.

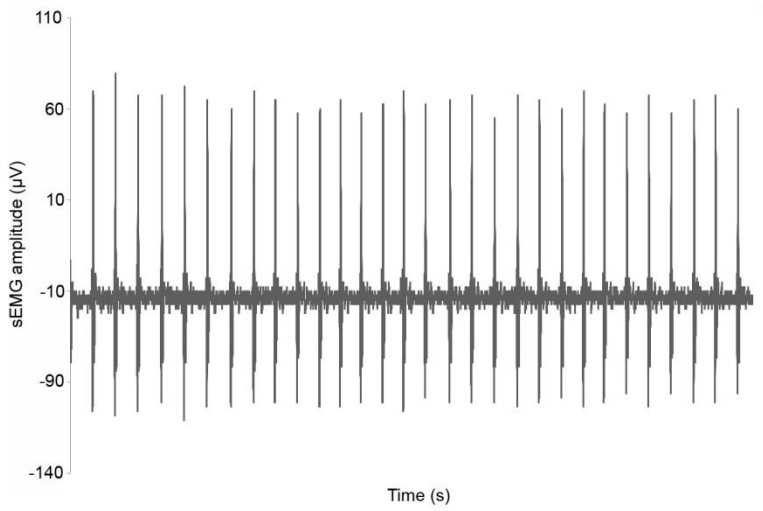

Figure 35 Raw sEMG data of the iliocostalis left side (data suggests muscular silence, spikes indicate ECG contamination)

In order to reduce the effect of ECG, assistance was provided by Professor Howard Hillstrom's research team at the Hospital for Special Surgery (HSS) in New York. Mark Lenhoff, Chief Engineer of the Motion Analysis Lab at HSS, reviewed the data and developed a programme using LabVIEW to remove some of the ECG. The method the researchers at HSS selected was to create a Linear Envelope (Winter, 1979) after high-pass filtering. For this, the raw data was high-pass filtered, rectified (analogous to the absolute value function), and low-pass filtered using a pre-determined time-constant. ECG spectra were contained within the low frequency spectra of the sEMG. The challenge was to set the cut-off frequency of the high-pass filter such that it adequately removed the ECG whilst retaining as much sEMG information as possible. The researchers at HSS ran some preliminary signal processing experiments to determine which high-pass filter cut-off frequency minimised the ECG artefact while maximising sEMG spectra. Two extremes were used to assess the best frequency for one subject. For the maximum muscle activity (minimal ECG contamination) data was taken from the left side of the paraspinal muscle at the T8 level. For the lowest muscle activity (maximal ECG contamination) data was taken from the left side of the iliocostalis muscle. Both measurements were taken for the lying posture. The results can be seen in Appendix B. The graphs show the raw sEMG data, the raw sEMG data filtered at high-pass frequencies of 10, 20, 30 and 50 Hz, and the linear envelopes with high-pass

filters of 10, 20, 30 and 50 Hz and subsequent low-pass filtering with a time-constant of 50 ms. The researchers at HSS found that the best compromise for removing as much ECG whilst retaining as much sEMG as possible to be a linear envelope with a high-pass filter of 25 Hz followed by full wave rectification and a low-pass filter time-constant of 50 ms. Note that, for this investigation, static muscle activity was measured. Therefore, the mean value of the linear envelope was used to represent the magnitude of myoelectrical activity.

In order to compare muscle activities across subjects and between postures, the mean of the linear envelope required normalising (Mirka, 1991). Typically, the maximum voluntary contraction (MVC) serves as the normalisation factor. A problem with using MVC is that it depends on the motivation and sincerity of the individual, which can lead to varying MVCs in individuals and between individuals. This variability could result in substantial MVC variability and influence the interpretation of the sEMG signal (Marras & Davis, 2001). Various alternatives to MVC have been previously proposed. As an attempt to remove the subjective nature of MVC, Baratta, *et al.* (1998) developed a method whereby subjects were required to perform a maximum exertion, followed by a series of successive exertions that increase by 10%. Once the subject was no longer able to achieve a targeted exertion, the previous successful level was identified as the MVC. A limitation to this technique is that it requires significant time due to substantial rest periods. Yang and Winter (1983) used sub-maximal exertions to normalise muscle activity and found them to be more reliable than maximum exertions. Marras and Davis proposed a method involving various sub-maximal muscle exertions to build a series of data that could be used to establish an sEMG-force relationship to predict a reference point. A limitation to this technique, as with that proposed by Baratta, *et al*. (1998) is the complexity and time required.

For this study, the relaxed standing posture was selected for the relative reference point for normalisation since it was considered to provide an exertion that is quick and simple to obtain, and is relatively consistent across the muscles, and across subjects. It was envisaged that all sitting postures and lying supine would produce lower sEMG values based on previous work by

Andersson and colleagues which showed that sitting with a backrest always resulted in less myoelectric muscle activity than standing (Andersson, *et al*., 1974[a-f]). Therefore, all data is reported as the percentage of the mean of the linear envelope relative to the mean of the linear envelope for the standing posture.

The raw data was exported from the MegaWin software to Excel for flexibility of calculations. The baseline of the data was then set to zero by first taking the mean of the measurement phase and then subtracting it from all of the data of that phase. The resulting data was then saved as a text file. The programme created by the scientists at HSS specifically for this investigation was used to create the linear envelopes for all of the data. After rectified and smoothed, the replicated data trials were averaged in Excel and tabulated for statistical analysis.

4.5 Posture

4.5.1 Apparatus and set up

A Flock of Birds electromagnetic motion capture system (Ascension Technology Inc. Burlington, VT, USA), consisting of an extended range transmitter (range ± 3.05 m) and eight sensors, was used. Each sensor measured 25.4 mm x 25.4 mm x 20.3 mm. All settings were in default mode (103 Hz, AC wide filter on, DC low pass filter on). Training on the use of the Flock of Birds motion capture system was provided by a representative from Ascension Technology Inc.

The test-rig used for data collection was built with aluminium parts instead of steel to avoid electromagnetic interference. Where steel was unavoidable, such as screws, stainless steel was used. Preliminary tests into the effect of introducing aluminium into the measuring space of the Flock of Birds showed data collection was not affected. In addition to our own experiments, a GPM anthropometer (SiberHegner, Zurich, Switzerland) is recommended by the Flock of Birds supplier for calibrating the measurement space which is made of aluminium.

A room was selected to be used for the laboratory which had the least amount of metal in the space. The foot print for the measuring space required for the testing was 3.2 m x 1.6 m. Consideration was given to the position and orientation of the measurement space to minimise the impact of metal in the environment. Neighbouring rooms were checked to see if any large pieces of metal furniture were present and, if so, they were removed. The ground level of the measuring space was built up by 200 mm with the use of polyethylene foam sheets to reduce the risk of interference from metal underneath the floor (Figure 36). A plywood base was then placed on top of the polyethylene sheet to create a firm, rigid surface. The foam was taped together and the location of the plywood base was marked onto the foam in case of movement during the testing. A grid was plotted onto paper for calibration of the measurement space and fixed to the plywood board with spray mount. The location of the test-rig was marked onto the grid so that it could be removed and replaced accurately. The transmitter was placed on a plastic bin that was turned upside down. This was determined to be ideal because it was the correct size to support the transmitter, it had no metal fixtures and it gave the required height of 650 mm.

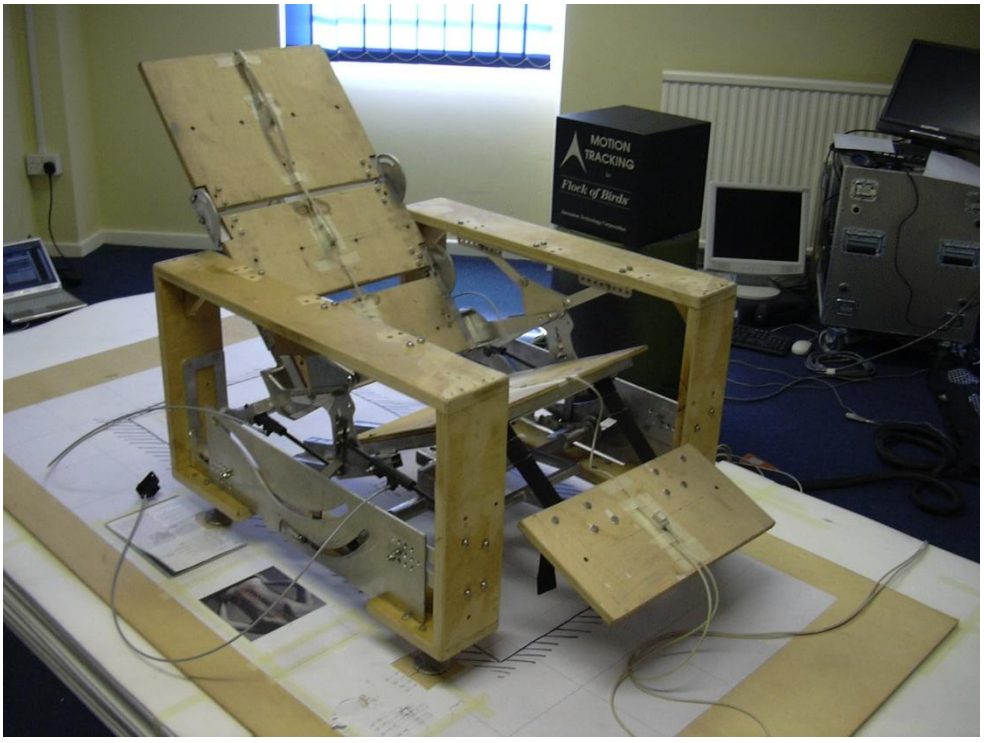

Figure 36 Laboratory set up for the electromagnetic motion capture study

A triangular flat piece of rigid ABS plastic was used for the stylus in this study. The point of the triangle was sharpened with a scalpel. A sensor was fixed to the stylus with double sided tape and the location marked on the stylus. The stylus was first used for establishing the world axis, and then for digitising the test-rig and test subjects.

By default, the world axis is set to the centre of the transmitter. For this study, the origin of the world axis was chosen to be located on the grid of the plywood base. The x-axis was set to the length of the measurement space in the direction of the test-rig, the y-axis was set to the width of the measurement space and the z-axis was set to the line perpendicular to the x and y-axis. To determine the origin of the world axis, the tip of the stylus was place on the grid and then a number of data points were collected with the stylus at various orientations with the tip remaining in the same place for each data point. The software then estimated the location of the tip of the stylus and thus the origin of the world axis. The stylus was then relocated along the grid on the plywood base to determine the x-axis, and then again to locate the y-axis. The tolerance for setting up the world axis was set to 0.015 m (this was found to be the highest tolerance that was practically achievable). This process was repeated at the beginning of each test day in case the test-rig or transmitter had been moved.

In order to determine the accuracy of the equipment in the measurement space, two sensors were fixed at approximately 200 mm apart on a rigid wooden beam. The software was set-up to output the raw data on the inter-sensor distance in real time. With the test-rig removed from the laboratory, the beam was held as close to the transmitter as possible before saturation occurred. This gave the absolute value. The beam was then moved randomly around the measurement volume to obtain $\pm$ error values, and the optimum location for the test-rig was identified. The location of the test-rig, saturation parameter and the range of the transmitter were marked onto the plywood base.

The absolute value for the inter-sensor distance was found to be 202 mm. Table 9 presents the values obtained in the measurement space without the test-rig present, and with the test-rig introduced. The RMS error without the test-rig was 5.37 mm and with the test-rig the RMS error was 6.42 mm. The Flock of Birds system specification states that for an extended transmitter at a distance of 1.52 m the RMS error is 7.62 mm (Ascension Technology Inc, 1999). The accuracy of the measurement space with the test-rig present was within the quoted accuracy, so calibration of the test environment was considered unnecessary.

Table 9 Values from testing the measurement space for accuracy (Root Mean Square (RMS) error calculation)

Test-rig not present			Test-rig present		
202 absolute	Error	Error ²	202 absolute	Error	Error ²
201	-1	1	213	11	121
204	2	4	191	-11	121
200	-2	4	190	-12	144
194	-8	64	205	3	9
193	-9	81	199	-3	9
195	-7	49	201	-1	1
202	0	0	199	-3	9
197	-5	25	201	-1	1
210	8	64	215	13	169
210	8	64	202	0	0
212	10	100	207	5	25
207	5	25	202	0	0
203	1	1	200	-2	4
199	-3	9	201	-1	1
197	-5	25	200	-2	4
200	-2	4	197	-5	25
203	1	1	195	-7	49
201	-1	1	195	-7	49
204	2	4			
199	-3	9			
197	-5	25			
196	-6	36			
197	-5	25			
198	-4	16			
196	-6	36			
199	-3	9			
200	-2	4			
194	-8	64			
198	-4	16			
192	-10	100			
	Mean	28.87		Mean	41.17
	RMS error	**5.37**		**RMS error**	**6.42**

The test-rig was digitised so that the position of the subject relative to the support surfaces could be calculated. With the upholstery removed and the sensors fixed to the centre of the supporting surfaces (Figure 37), the orientation and position of the sensors were captured. Using this data, the support surfaces were recreated in 3D CAD software (Figure 38). This was done for all of the configurations of the test-rig. Digitisation of the test-rig was done only once at the beginning of the testing.

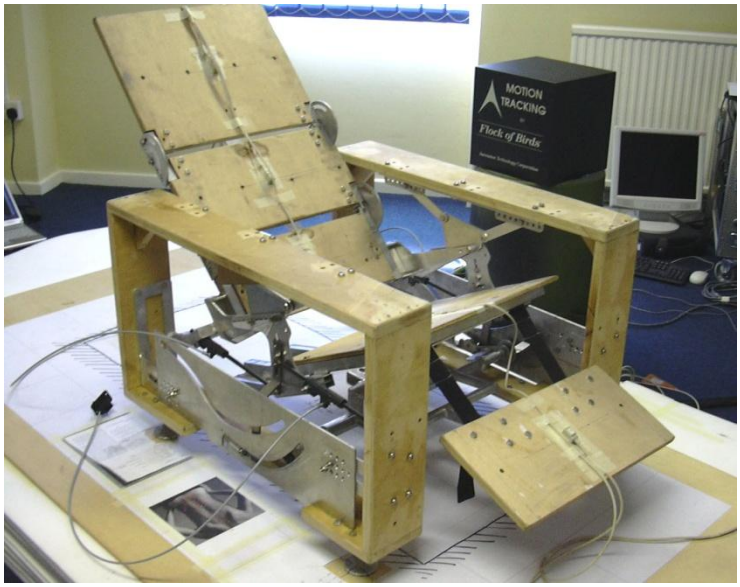

Figure 37 Test-rig set up for digitisation

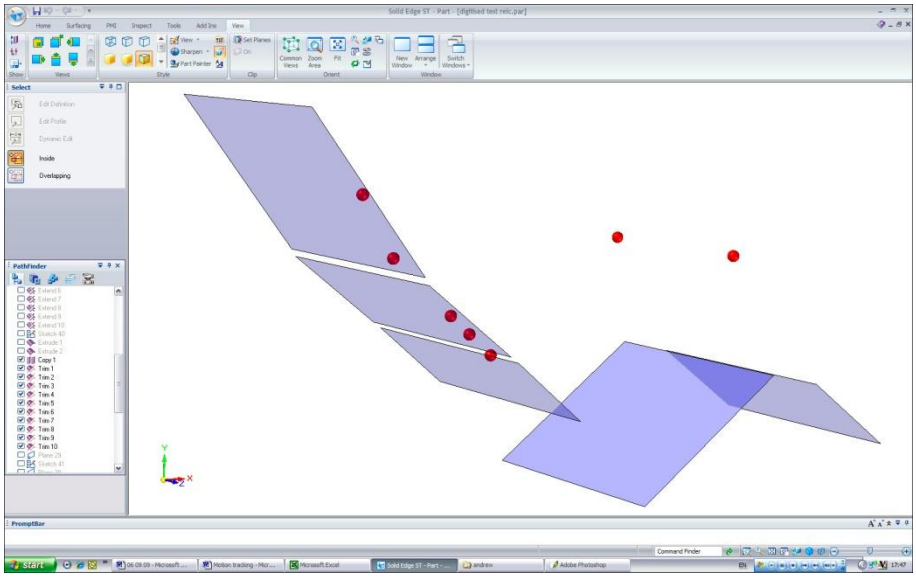

Figure 38 Test-rig digitised and recreated in Solid Edge ST CAD programme (the red dots represent the sensors on the subject's back and thighs)

A test was first carried out using two subjects (not included in the main investigation) to assess the reliability of the motion capture system. For this, the test-rig was not used. The Flexicurve technique was chosen to validate the data, so postures were selected where the back could be easily accessed. The Flexicurve technique has been established as a reliable and valid method for measuring spinal profiles (Hart & Rose, 1986; Burton, 1986). Following the protocol procedure described below in Section 4.5.2, two subjects were asked to assume the postures of

standing, unsupported sitting, maximum extension and maximum flexion. For maximum extension, the subject was asked to assume a prone position supporting the upper trunk on the elbows (Figure 39). For maximum flexion, the subject was asked to sit on a chair (with feet on the floor) so that the trunk could pass between the knees (Figure 41). These postures are described by Burton (1986). Two sets of measurements were taken for each posture, with each measurement period lasting for approximately 30 seconds. Each recording resulted in approximately 2,500 measurements, which was saved in the Flock of Birds software for further analysis.

Figure 39 Position of maximum extension

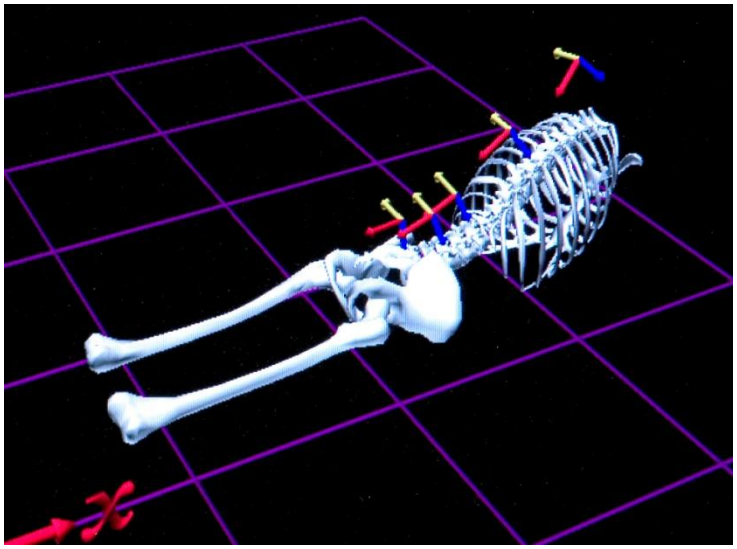

Figure 40 The Flock of Birds visual display showing maximum extension (arrows denote sensor position and orientation)

Figure 41 Position of maximum flexion

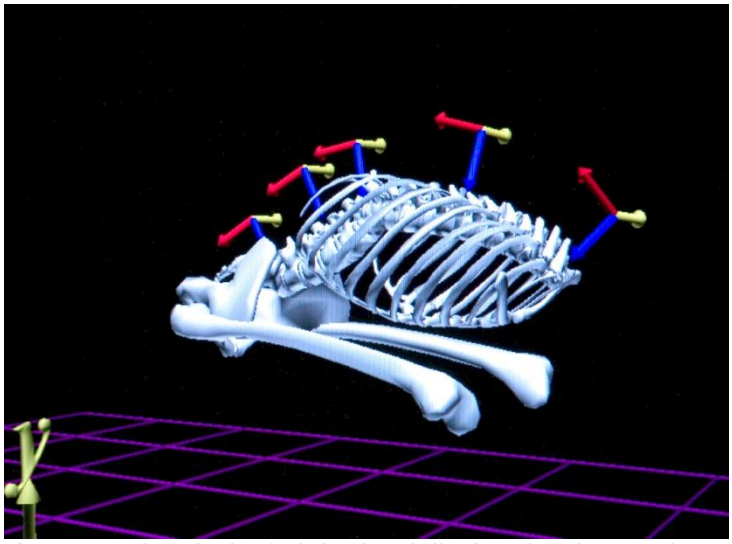

Figure 42 The Flock of Birds visual display showing maximum flexion (arrows denote position and orientation of sensors)

4.5.2 Protocol

The subjects were given surgical gowns to wear so that their backs could be easily accessed, and a pair of shorts. The subjects were asked to remove any watches and jewellery. The subjects wearing bras were asked to undo the strap if it was in the area of sensor location. Subjects with long hair were provided with bands to tie their hair back. Standard palpation techniques (see Section 4.4.2) were used to identify the spinous processes of S1, L3, L1, T7, and T1. These correspond to the sacrum (and pelvis), the apex of concavity of the lumbar spine (L3) and apex of convexity of the thoracic spine (T7) (Frigo, *et al*., 2003). T1 was chosen over C7 because the software excluded the cervical spine and head. Once these landmarks were marked on the subject's back, a horizontal and vertical line was drawn to aided placement of the sensors (Figure 43).

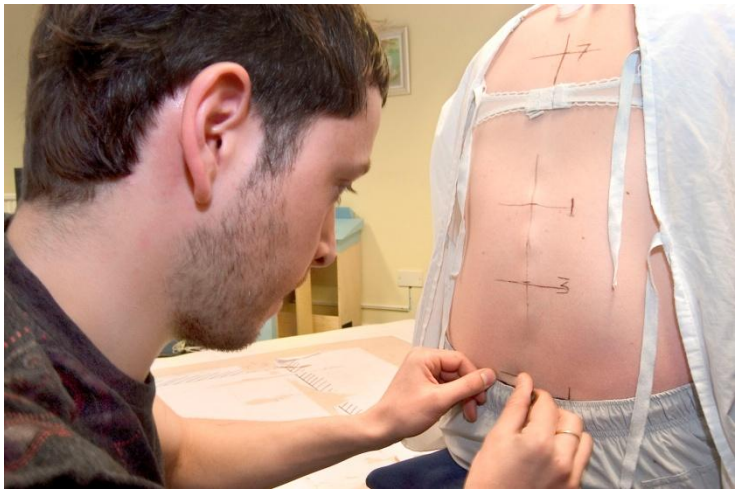

Figure 43 Reference lines to aid sensor placement

Strips of HypaFix tape were placed over the area of the skin where the sensors were to be positioned (Figure 44). This was done to protect the skin from the adhesive on the double sided tape. The double sided tape was fixed to the back of the sensors to directly secure them to the HypaFix tape on the skin. Additional HypaFix tape was used to secure the sensor on the sides and top (Figure 45). Finally, drinking straws were used to manage the cables. Pieces of straw were cut and slit along lengthwise. The pieces of straw were placed around the cable and then fixed to the back of the subject such that the cable could move freely inside. This aided in reducing the effect from the weight of the cables on the sensors. The sensors on the subject's back were positioned so that the cables ran vertically. Although it has been previously shown that this is likely to result in more sensor movement than cables running horizontally, it was necessary so that the cables could be located in the vertical channel in the backrest upholstery (Figure 49). Two additional sensors were placed on the thighs with straps and rigid moulded plastic sensor holders. A research assistant held the cables above the subject's head throughout the testing to reduce the effects from the weight of the cables and to monitor the sensors.

Figure 44 Fixation of the sensors: use of protective HypaFix tape

Figure 45 Fixation of the sensors (sensors fixed to HypaFix tape with double-sided tape, reinforce with additional HypaFix tape on side and top. Drinking straws used for cable management and to reduce the effect of the weight of the cables on sensors)

The next step was to digitise the subject. The subject was asked to stand in a specific position marked on the base of the measurement space in front of the transmitter. This was facing down the x-axis and the back towards the world axis origin. The subject was asked to assume an anatomical stance position with their feet at shoulder width apart, legs straight, arms straight with palms facing forwards, straight back and facing straight ahead. In this position, digitisation began. With the stylus, and a hand held event marker, the S1, L1, and T1 landmarks were digitised (Figure 46). The point of the stylus was placed over the spinous process, and the event

marker was pressed several times, with the orientation of the stylus being altered about the point each time. Once the digitisation of the spine was accepted, the software moved to the legs and pelvis. The knee joints were digitised by capturing the location of the stylus when touching the front, sides and back of the knee (Figure 47). The software calculates a single point defined by the several locations around the knee. The manufacturer recommended using the Leonardo method (a functional axis approach) to identify the hip joint centres. For this method, the subject's data were captured in the anatomical position. The subject was asked to kick their legs forwards and hold, to the side and then back. In each position the subject's posture was captured. This was used to calculate the hip joint centre based on the relative orientations of the thigh marker. Figure 48 shows the visual display after digitisation.

Figure 46 Digitisation of the spine

Figure 47 Digitisation of the knee

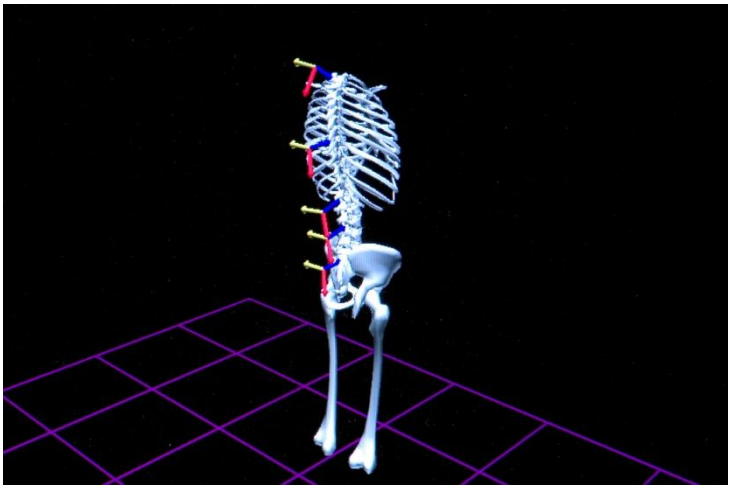

Figure 48 Visual display after digitisation – animation in real time

The subjects then carefully sat in the test-rig, first leaning forwards and then slowly rolling into backrest. During this the examiner ensured all sensors and cables fell in the channel in the upholstery (Figure 49). The test-rig was then adjusted to the seated position. As with the interface pressure measurement, additional measures were made of the TIS 1 configuration where the backrest was articulated after the subject had sat in the test-rig (TIS 1a). In addition to the seated test postures described earlier, standing and maximum flexion were captured for normalisation. The method for achieving maximum flexion was described previously (Figure 41). Motion data were captured over a 30 second recording epoch for each posture. Each trial resulted in approximately 2,500 data points, which were saved in the motion monitor computer for further analysis.

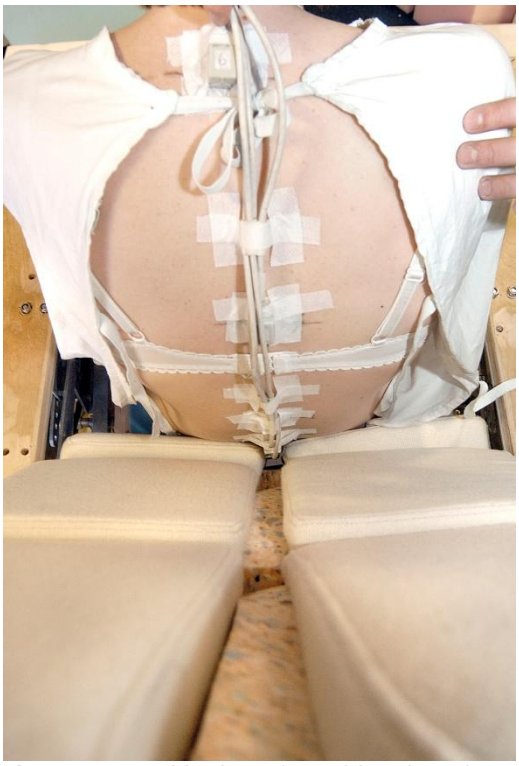

Figure 49 Positioning of a subject into the test-rig (with assistance from the investigator to ensure that sensors and cables fall into the channel in the backrest upholstery)

4.5.3 Data collection and interpretation

The greatest source for error was expected from sensors being displaced due to pressure on either the sensors, or on the sensor cables. If the sensors were to move, their orientation would be more likely to be affected than their position. As an attempt to reduce error associated with sensor movement, analysis was performed on position data only. This is the x, y, z coordinates relative to the world axis.

The raw position data was exported to a spreadsheet in Excel, and the average for each recording was calculated. The standard deviation of the data was less than 0.02 mm. The mean data for the coordinates of each sensor were then plotted in 3D CAD software and overlaid with the CAD models of the test-rig surfaces for further analysis (Figure 38).

Two methods were used previously to calculate a value that represented lumbar curvature. Both methods were based on obtaining a profile using a Flexicurve (Burton 1986; Hart & Rose, 1990). The method developed by Burton measures lumbar curvature from tangents drawn from the Flexicurve profile. This method was also used by Dolan and Adams (1993) in their studies using the Isotrak electromagnetic motion capture system. However, for data obtained from motion capture systems, the method requires orientation data which was not chosen for the reasons outlined above. The trigonometric method validated by Hart and Rose (1986) only requires position data so this approach was chosen as a basis to calculate lumbar and thoracic curvature.

The data required to calculate lumbar curvature was obtained from the CAD model of the sensor positions. A plane was created from 3 points; S1, the midpoint of the line connecting L1 and T7, and T1. In this plane, the position of the S1 and L1 sensors were connected by a line (l). A second line (h) was drawn perpendicular to line l and connected to the L4 sensor position

(Figure 50). The length of each line was determined and the values were inserted into Equation 2 (Hart & Rose, 1986), shown again below:

$$\theta = 4 \times \arctan(2h / l)$$

This gave the lumbar curvature (θ). Positive values represented lumbar extension and negative values represented flexion. The same calculation was used to determine thoracic curvature in the same plane created for lumbar curvature. Figure 50a illustrates the method for determining lumbar and thoracic curvature. The lumbar and thoracic curvature data was then expressed as percentage lumbar and percentage thoracic flexion, which is a measure of changes in curvature (Dolan & Adams, 1993). The curvature in erect standing was taken to represent 'zero flexion' (Figure 50b). Dolan and Adams found this posture to be more reproducible than curvature in maximum extension. Equation 42 defines percentage lumbar and percentage thoracic flexion, which are expressed as a percentage of the full range of movement between erect standing (Figure 50b) and maximum flexion (Figure 50c).

$$\% \text{ flexion} = 100 \text{ x } (\theta - \theta_0) / (\theta_F - \theta_0) \quad (42)$$

Where,

θ = Lumbar or thoracic curvature

θ_0 = Lumbar or thoracic curvature in erect standing, representing zero curvature

θ_F = Maximum lumbar or thoracic flexion

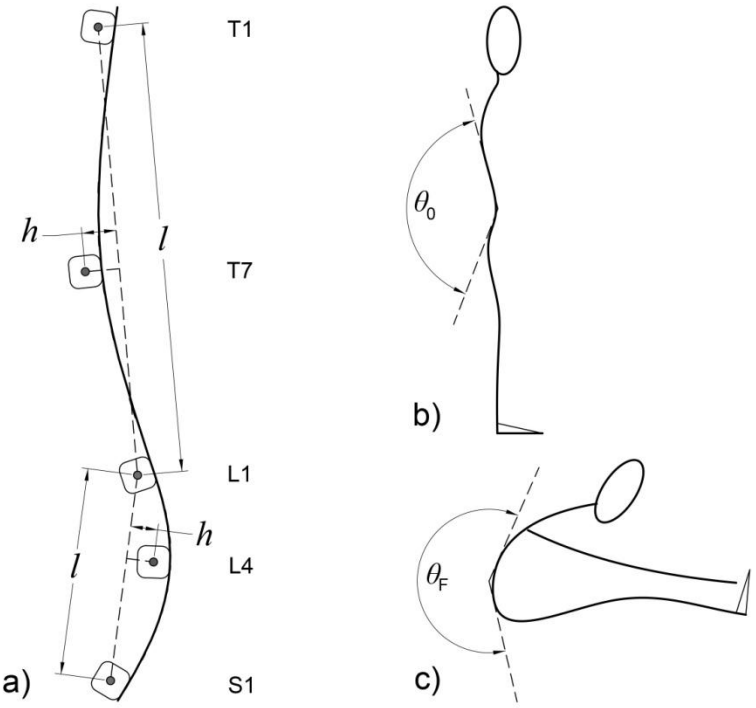

Figure 50 a) method for determining the degree of lumbar and thoracic curvature (θ), b) the erect standing position for percentage flexion, and c) the maximum flexion position for percentage lumbar flexion

5 Results and Analysis

This chapter gives the results and analysis from the model simulations and the experimental data collection in the order of the thesis hypotheses. For each experiment, the statistics are described with histograms, typically followed by a comparative analysis and then relationships. Examples of the workings for the statistical tests are given for the interface pressure data in Section 5.3.2, and summarised thereafter. The histograms typically contain the mean data, standard deviations, the Friedman's ANOVA result and the markings denoting the *post hoc* test results on significant differences. Where possible, the descriptive statistics of the model predictions and corresponding measured data are presented side by side for ease of comparison. In this endeavour it was necessary to show some of the histograms more than once. For some of the experiments, additional test postures have been included which are identified in the histograms with no shading.

5.1 Model verification with published data

The comparison between the model prediction of the car driver's seat posture and the published anthropometric data for this posture give initial verification on the accuracy, with a percent difference in sitting height of 2.2%. Verification is different to validation in that it is a quick check on the results that they meet initial requirements using published data. Validation uses original experimental data and is more robust and controlled than verification. The validity of the model is assessed in Section 5.2. For verification, hypothesis H1a required the model to agree with at least 95% of published data, so the hypothesis is supported by this comparison.

The Goossens and Snidjers model (1995) was used for initial verification on the accuracy of the force predictions. Goossens and Snidjers evaluated their model based on parallel force only, so this parameter was used to assess the new model. Table 10 gives the results from the simulations of the seated test postures validated in Goossens and Snidjers' study, for both the Goossens and Snidjers model that was recreated and the new model. It can be seen that there is a substantial difference in the predictions of parallel force between the two postures, and hence the hypothesis H1b is not supported by these data. It can be seen from Figure 23 that the greatest difference between the two models is the IT position suggesting that this is a sensitive feature of the model.

Table 10 IT parallel force predictions from the Goossens and Snidjers model and the model developed during this research for the seated test postures described by Goossens and Snidjers (1995)

Inclination (°)		IT Parallel Force (N)	
Backrest	Seat	Goossens & Snidjers	New model
70	14.4	-9	-174
72	13.18	-9	-174
74	11.96	-9	-174
76	10.74	-9	-174
78	9.52	-10	-174
80	8.3	-10	-173
82	7.08	-10	-172
84	5.86	-10	-170
86	4.64	-10	-169

5.2 Model validation with experimental data

5.2.1 Descriptive statistics

Table 11 presents the results for evaluating the postural accuracy of the model against experimental data collected during this research. Hypothesis H2a required the model to agree with at least 95% of measured data. The primary index for assessing postural accuracy was

sitting height which showed a percent difference of 1.2% and, hence, hypothesis 2a was supported. Larger differences can be seen for the secondary indices, which are discussed in Chapter 6.

Table 11 Posture indices (mm) and the resulting percent differences of measured and predicted data for the assessment of model postural accuracy. Interface pressure indices (IPI) and motion sensor indices (MSI) were derived from measurements of three 50th percentile male subjects. Percent difference is defined in Equation 35

		Head IPI	**IT IPI**	**L3 MSI**	**Scapula MSI**	**Scapula IPI**
Measured indices (mm)	Upright	772	181	151	392	415
	Standard	740	143	129	370	380
	TIS 1	797	142	166	423	511
	TIS 2	786	181	179	420	409
	TIS 3	788	168	174	416	458
Modelled indices (mm)	Upright	795	182	205	386	386
	Standard	753	172	163	343	343
	TIS 1	797	168	112	439	439
	TIS 2	794	185	204	389	389
	TIS 3	784	178	204	376	376
% difference	Upright	2.9%	0.6%	30.3%	1.5%	7.2%
	Standard	1.7%	18.4%	23.3%	7.6%	10.2%
	TIS 1	0.0%	16.8%	38.8%	3.7%	15.2%
	TIS 2	1.0%	2.2%	13.1%	7.7%	5.0%
	TIS 3	0.5%	5.8%	15.9%	10.1%	19.7%
	Average	**1.2%**	**8.7%**	**24.3%**	**6.1%**	**11.5%**

The displacement of the motion tracking sensors (modelled and measured) were used to verify the model's ability to predict the motion paths of the support surfaces, and test hypothesis H2b. Hypothesis H2b requires that the model agrees with at least 95% of measured data. The percent differences in Table 12 do not support this.

Table 12 Mean displacement (mm) of motion sensors from their position in the upright test posture for the group of 15 subjects with standard deviations and the modelled displacement during simulation of the same test postures, for 5th percentile woman, 50th percentile man and 95th percentile man. Percent difference between modelled average and measured data is given and is defined in Equation 35

			Motion sensor displacement (mm)		
			S1	L1	T1
Standard	Modelled	5th%ile woman	-22	-22	-19
		50th%ile man	-18	-19	-19
		95%ileman	-17	-16	-15
	Modelled average		-19	-19	-18
	Measured		-18 (20)	-26 (19)	-25 (20)
	Difference between modelled average and measured data		1	7	7
	Percent difference		**5%**	**31%**	**33%**
TIS 1	Modelled	5th%ile woman	-22	-86	-124
		50th%ile man	-18	-76	-124
		95%ileman	-17	-94	-118
	Modelled average		-19	-85	-122
	Measured		-9 (29)	-79 (22)	-136 (20)
	Difference between modelled average and measured data		10	6	14
	Percent difference		**71**	**7**	**-11**
TIS 2	Modelled (all percentiles)		0	0	0
	Measured		5 (27)	-18 (12)	-30 (16)
	Percent difference		**N/A**	**N/A**	**N/A**
TIS 3	Modelled (all percentiles)		0	0	0
	Measured		5 (38)	-11 (12)	-32 (15)
	Percent difference		**N/A**	**- N/A**	**N/A**

Figures 51-54 give the model force predictions and the measured force for the seat, lumbar, thoracic and head supports respectively, for all 15 subjects, with standard deviations. The model force predictions include each individual's height, mass and gender, which modify the proportions, lengths and masses of the body segments. Model predicted and known experimental force data are summarised as histograms stratified by seated test postures. The raw experimental force values are typically half of the predicted values, but the relative differences across the test postures are qualitatively similar.

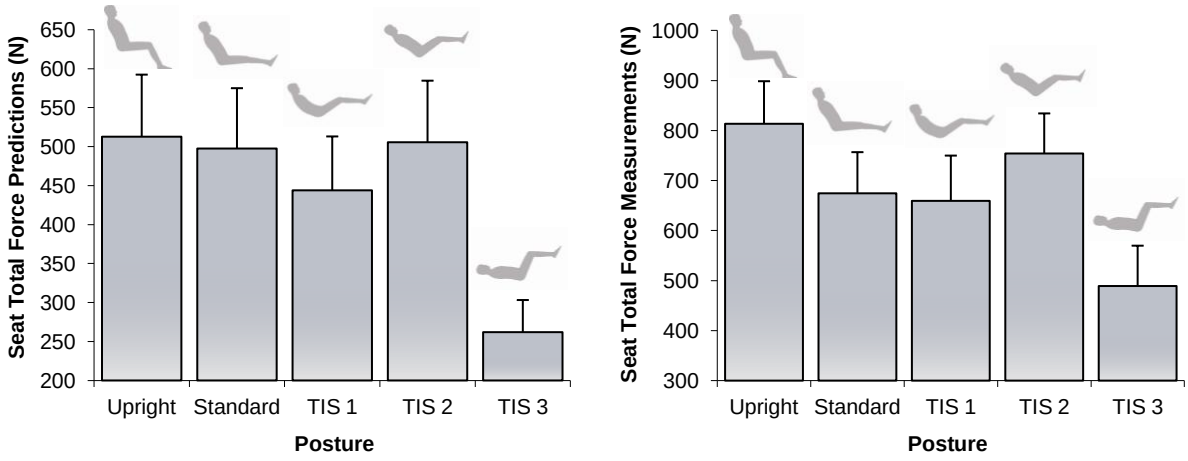

Figure 51 Seat Total Force predictions (left) and Seat Total Force measurements (right) showing means and standard deviations for the 15 subjects

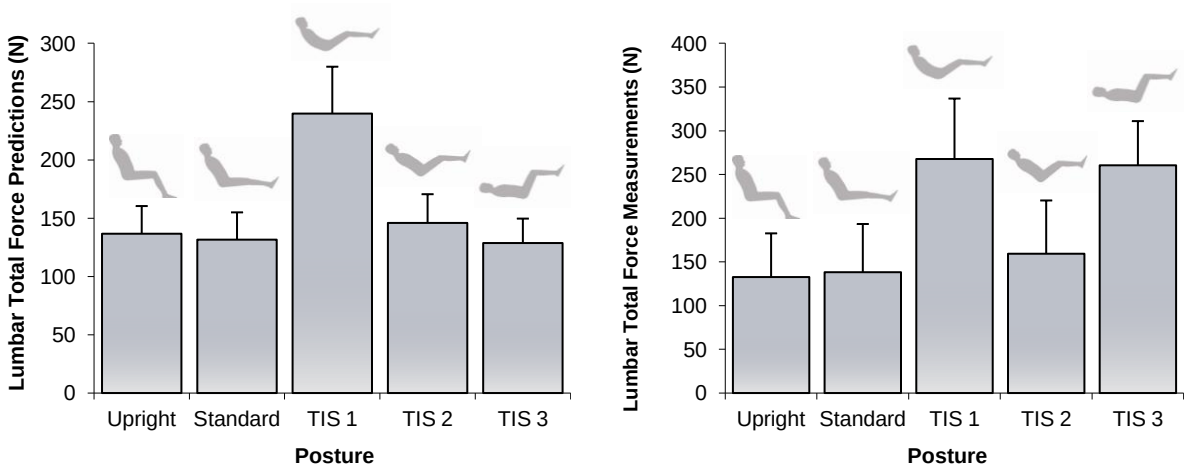

Figure 52 Lumbar Total Force predictions (left) and Lumbar Total Force measurements (right) showing means and standard deviations for the 15 subjects

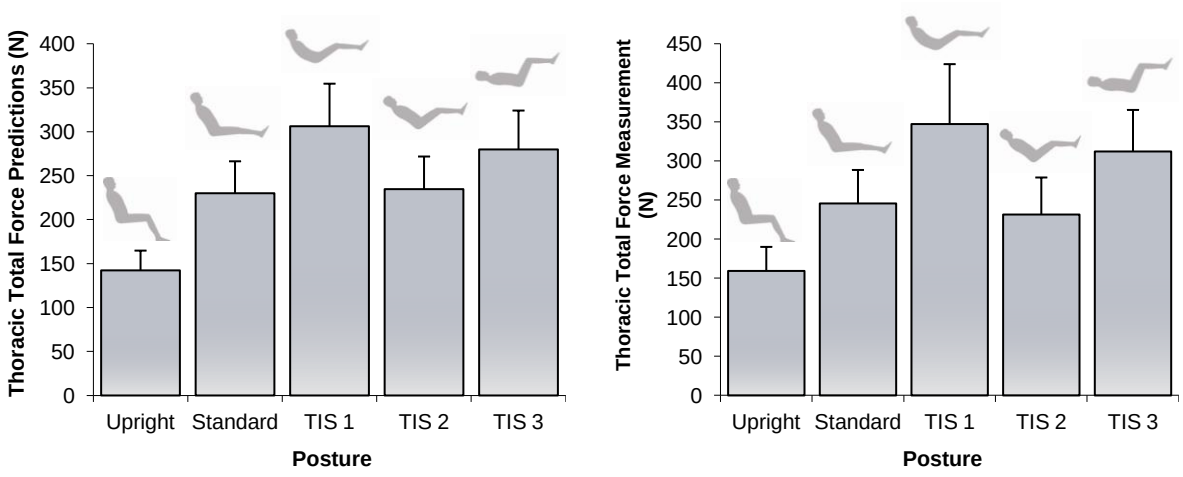

Figure 53 Thoracic Total Force predictions (left) and Thoracic Total Force measurements (right) showing means and standard deviations for the 15 subjects

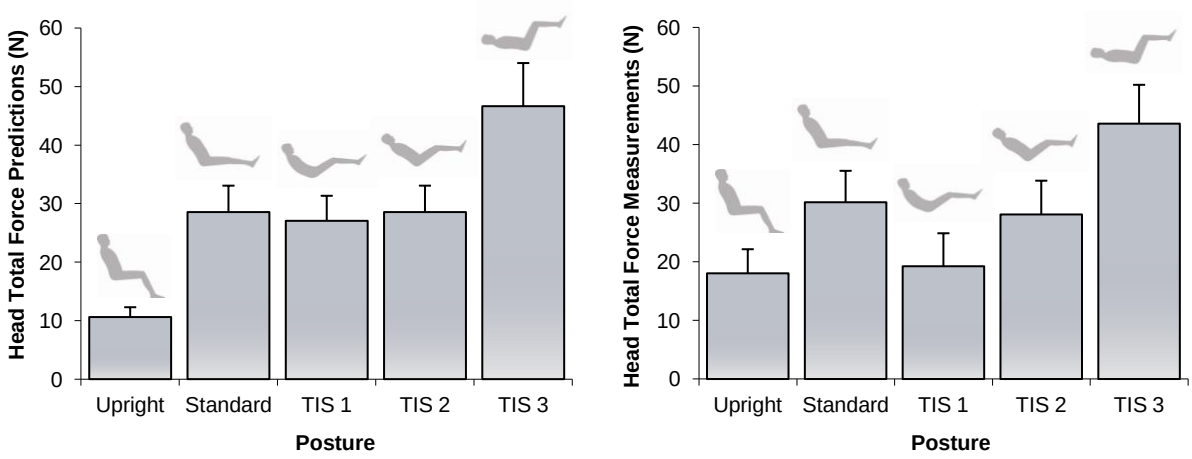

Figure 54 Head Total Force predictions (left) and Head Total Force measurements (right) showing means and standard deviations for the 15 subjects

5.2.2 Relationships

A significant relationship ($p < .001$) and a strong correlation ($r = 0.92$) was found between predicted and measured force across all subjects, supports and postures, using a linear regression model, which supports hypothesis H2d. Hypothesis H2d requires significance to be $p < .05$ and the correlation coefficient to be $r > 0.7$. The overall root mean square error (RMSE) was 143 N, with a full scale error of 15%. Full scale error (FSE) was calculated to provide a standardised measurement of the error, and is the RMSE divided by the highest unit of force

measured. The RMSE and FSE for the individual support surfaces for each posture are given in Table 13. This does not support hypothesis H2c, which requires the full scale error to be within 10%.

Table 13 Root mean square error (RMSE) and full scale error (FSE) between measured and predicted force, for each test posture and support surface

Test posture		Support surface			
		Seat	Lumbar	Thoracic	Head
Upright	RMSE	321	55	43	9
	FSE	33%	26%	20%	37%
Standard	RMSE	209	61	62	9
	FSE	26%	21%	19%	22%
TIS1	RMSE	250	62	109	11
	FSE	28%	17%	22%	39%
TIS 2	RMSE	277	57	61	8
	FSE	30%	21%	19%	22%
TIS 3	RMSE	246	140	82	11
	FSE	38%	40%	19%	19%

The measured data, and predictions using only the 50th percentile male model, were normalised to investigate the feasibility of a simpler analysis that does not require individual anthropometric data. The force data were normalised by dividing into the sum of force measured from all support surfaces, and expressed in percent. The resulting normalised measured and predicted forces are shown in Figure 55. A significant relationship exists (p < .001) across all subjects, supports and postures, with a strong correlation at r = 0.97. The overall RMSE for the normalised data is 6%, with an FSE of 8%. This supports hypothesis H2c.Table 14 gives the RMSE breakdown for all support surfaces. The variance in the normalised data was assessed against both gender and height. A one-way analysis of variance (ANOVA) model was used to test for differences in RMSE values between male and female subjects. A linear regression model was used to test for a relationship between RMSE values and height. There was no difference in RMSE values across gender (p = 0.619) and no relationship between RMSE values and height (R^2 = 0.028, p = 0.549). This confirms that the process of normalisation provides a common means of comparison of

relative load regardless of height, weight and gender, and that the model is robust against long-tail anthropometric variation.

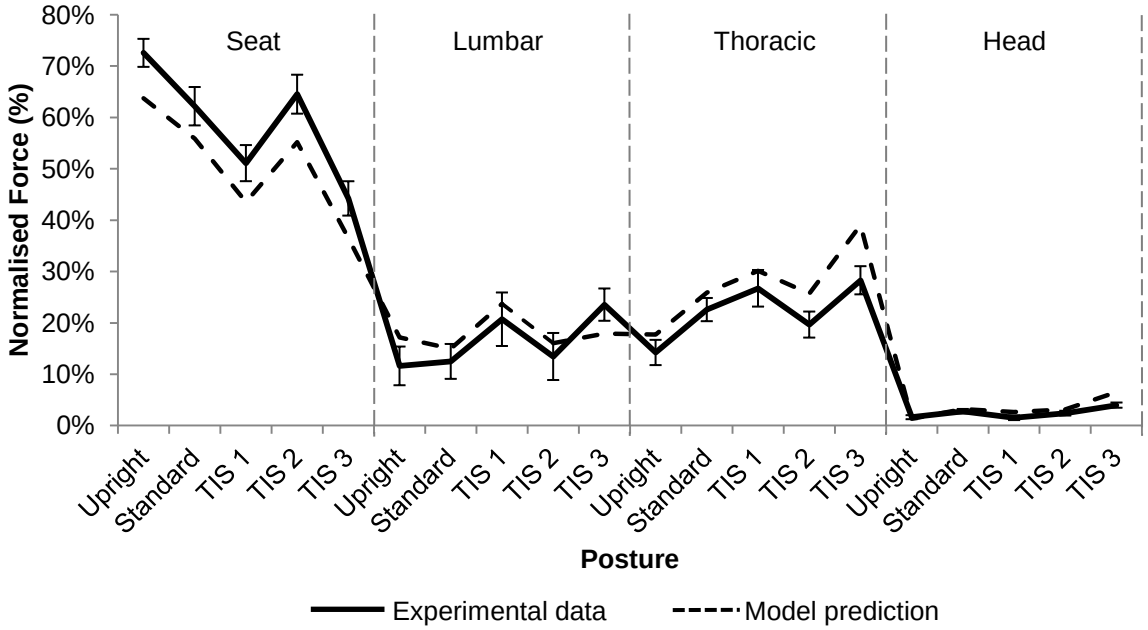

Figure 55 Average normalised force (with standard deviation) and normalised predicted force from the seat, lumbar, thoracic and head supports, for different seating configurations

Table 14 Root mean square error (RMSE) and full scale error (FSE) for normalised measured and predicted force, for each posture and support surface

Test posture		Support surface			
		Seat	Lumbar	Thoracic	Head
Upright	RSME	9%	7%	4%	0%
	FSE	12%	38%	22%	20%
Standard	RSME	7%	4%	4%	1%
	FSE	11%	20%	15%	16%
TIS 1	RSME	8%	6%	5%	1%
	FSE	14%	20%	16%	59%
TIS 2	RSME	10%	5%	7%	1%
	FSE	14%	22%	26%	26%
TIS 3	RSME	8%	6%	11%	3%
	FSE	17%	21%	34%	52%

5.3 Interface pressure

5.3.1 Descriptive statistics

The means and standard deviations from the interface pressure mapping tests are shown in Figures 56–60, with the corresponding model force predictions, in the order of: seat peak pressure index, seat average pressure, seat contact area threshold; back average pressure; and back contact area threshold. The histograms showing force predictions repeat for side by side comparison with the interface pressure histograms. The unshaded columns give the results for an additional posture (TIS 1a), which is TIS 1 but with the back supports articulated after the subject is tilted in the test-rig. The results from the Friedman's ANOVA are included in interface pressure histograms. Since significant effects were found for most paired comparisons, there was not enough space in Figures 56-60 to denote significance.

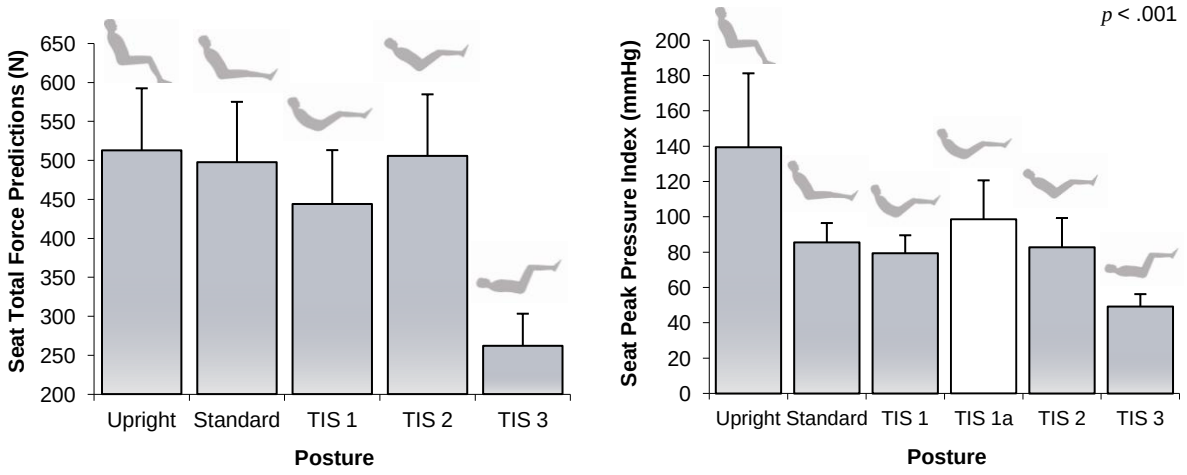

Figure 56 Seat Total Force predictions (left) and Peak Pressure Index measurements (right) showing means and standard deviations for the 15 subjects, and the Friedman's ANOVA result. The unshaded data column is an additional reference posture

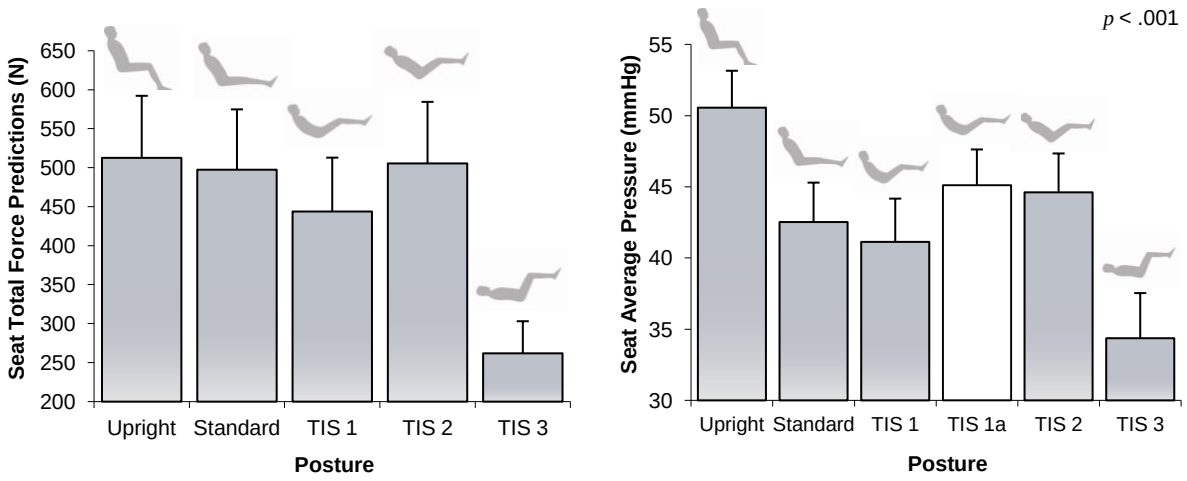

Figure 57 Seat Total Force predictions (left) and Seat Average Pressure measurements (right) showing means and standard deviations for the 15 subjects, and the Friedman's ANOVA result. The unshaded data column is an additional reference posture

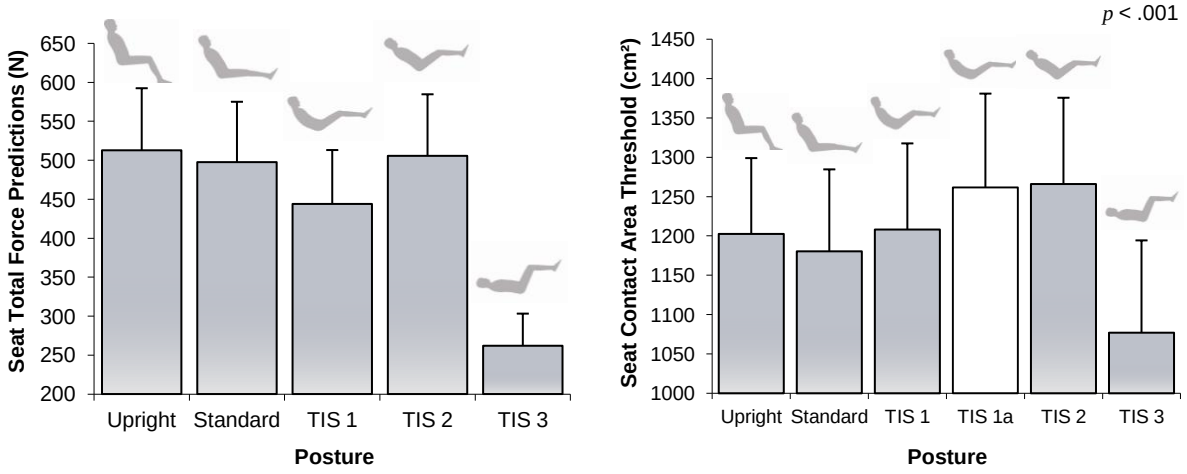

Figure 58 Seat Total Force predictions (left) and Seat Contact Area Threshold measurements (right) showing means and standard deviations for the 15 subjects, and the Friedman's ANOVA result. The unshaded data column is an additional reference posture

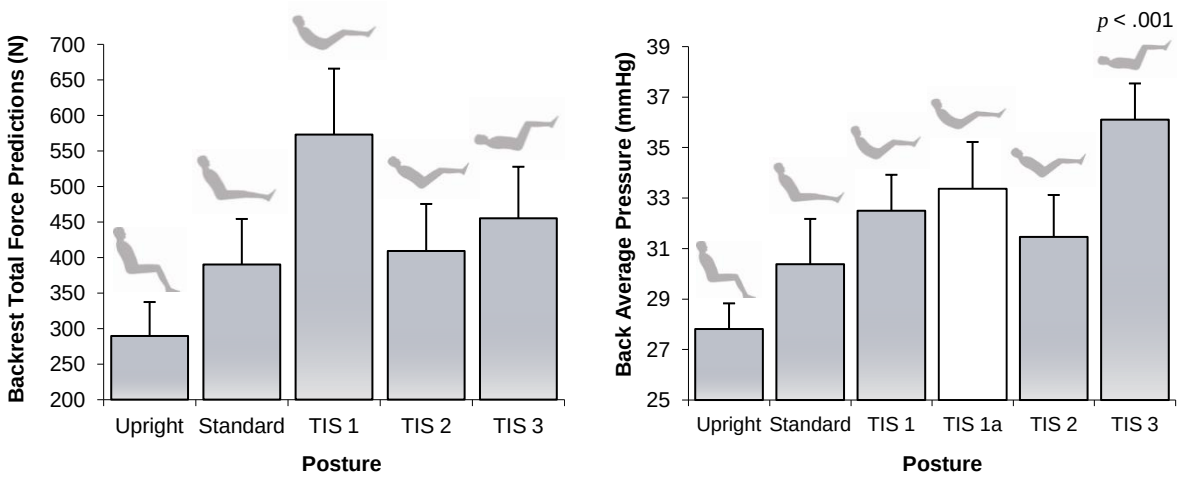

Figure 59 Back Total Force predictions (left) and Back Average Pressure measurements (right) showing means and standard deviations for the 15 subjects, and the Friedman's ANOVA result. The unshaded data column is an additional reference posture

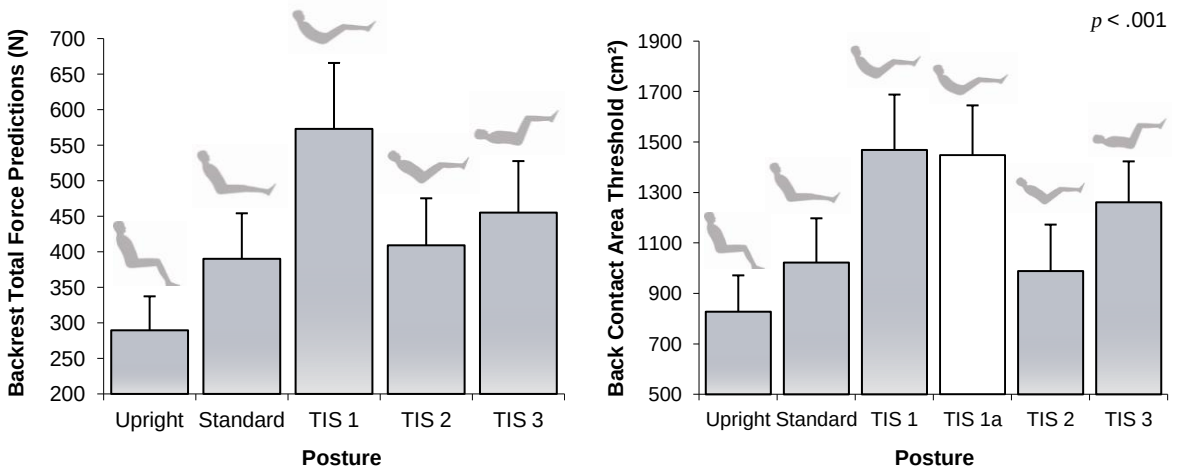

Figure 60 Back Total Force predictions (left) and Back Contact Area Threshold measurements (right) showing means and standard deviations for the 15 subjects, and the Friedman's ANOVA result. The unshaded data column is an additional reference posture

5.3.2 Comparative statistics

The following statistical analysis was carried out on the experimental data to test the hypothesis H3a stating that there will be a significant difference ($p < .05$) in peak pressure, average pressure and contact area between the seated test postures, with increasing back pressure and contact area, and decrease seat pressure and contact area, as the upper body approaches the horizontal.

Before the testing was carried out, an *a priori* power analysis was performed to determine the minimum number of subjects to include in the investigation. G*Power 3.1.0 software was used to calculate the sample size, based on the type of statistical tests to be performed, the estimated effect size likely to be encountered in the investigation (d), the probability of making a Type I error (α), and the statistical power level (1-β) where β is the probability of making a Type II error. Fisher (1925) recommends a 95% confidence level for accepting a result as being true. Based on this recommendation, the probability of a Type I error was set to .05 (the α-level). A Type I error occurs when it is believed that there is a genuine effect in a population, when in fact there is not. Cohen (1992) suggests that the maximum acceptable probability of a Type II error would be .2 (the β-level). A Type II error occurs when it is believed that there is no effect in the population when, in reality, there is. It follows that the probability of detecting an effect if one exists is the opposite of the probability of not detecting that effect (i.e. 1 - β), which is the statistical power of the test. This is 1 - .2, or .8 (Cohen, 1992). Matched pairs t-tests were selected for the type of tests, and the one-tailed test was chosen based on the direction of the hypothesis. To estimate the effect size, data was taken from a similar study measuring interface pressure for recline postures by Aissaoui (2001). Two postures were compared; one upright sitting posture (the condition c) and a tilt-in-space posture with 45° of tilt (the treatment t). The peak pressure averaged across 10 subjects and standard deviations were 90.3 mmHg (12.4) and 65.8 mmHg (11.1) respectively. To calculate the effect size, the pooled standard deviation is needed. This is defined by Equation 43.

$$s_{pooled} = \sqrt{\frac{(n_t - 1)s_t^{\ 2} + (n_c - 1)s_c^{\ 2}}{n_t + n_c}} \tag{43}$$

Therefore,

$$s_{pooled} = \sqrt{\frac{(10-1)11.1^2 + (10-1)12.4^2}{10+10}}$$

$$s_{pooled} = \sqrt{\frac{9980.01 + 12454.56}{20}}$$

$$s_{pooled} = 33.49$$

The effect size is Cohen's d, where an effect size of .2 to .3 is a small effect, around .5 a medium effect and .8 to infinity is a large effect (Cohen, 1988). The effect size is defined by Equation 44.

$$d = \frac{\bar{x}_t - \bar{x}_c}{s_{pooled}} \tag{44}$$

Therefore,

$$d = \frac{68.3 - 90.4}{33.49}$$

$$d = -0.7$$

where,

d = Cohen's d effect size

$\bar{x}$ = mean (average of treatment or comparison conditions)

s = standard deviation

n = number of subjects

Subscripts: t refers to the treatment condition and c refers to the comparison condition (or control condition).

The data was entered into G*Power which calculated that a sample size of 14 subjects would be required as a minimum to detect a significant effect in interface pressure. The remaining of the analysis was carried out in Excel and SPSS version 16.0. For guidance on statistical analysis, reference was made to Field (2005). Data and examples of the statistical processes can be found in Appendix C.

The interface pressure data were explored to assess whether they fitted parametric assumptions. The frequency histograms for the Seat Contact Area data for the TIS 3 posture, and the Peak Pressure Index data for the TIS 3 posture, indicated that those data were non-normal in their distribution (Appendix C-2).

The Kolmogorov-Smirnov statistical test was performed on the data sets to decide on normality of distribution. It was found that the Seat Contact Area Threshold and Seat Average Pressure parameters were normally distributed for all postures (Appendix C-3). However, the Back Contact Area Threshold data for the standard recline posture, the Back Average Pressure data for the TIS 2 posture and the Peak Pressure Index Pressure data for the TIS 2 and TIS 3 postures were found to be significantly non-normal in their distribution of data. The Levene's test was carried out to test the data for homogeneity of variance. The Peak Pressure Index data was found to be significantly heterogeneous in its variance (Appendix C-3).

Attempts were made to transform the data to correct the problems with the distribution and variance using square root and logarithm (to base 10) functions (Appendix C-3). A constant of 1 was added to the original data before applying the function since there is no logarithm or square root of values at or below zero. Logarithm transformation corrected normality of distribution for the Back Contact Area data and for the Peak Pressure Index data but not for the Back Average Pressure data. Logarithm transformation did not correct the variance for the Peak Pressure Index data. Since the transformed data failed to correct the problems, the original data was used for the analysis, and as this has violated parametric assumptions, the statistical analysis was carried out using non-parametric methods.

The Friedman's ANOVA is the non-parametric equivalent to the repeated measures ANOVA and hence was chosen to test for differences between postures. The test works by ranking the data. For example, Table 15 gives the ranks for the seat average data where the lowest value is given the rank of 1 and the highest value is given the rank of 6. The sum of ranks calculated for each posture is then used to calculate the test statistic χ^2 using Equation 45.

Table 15 Seat average pressure (mm Hg) example with ranks

Subject	Posture						Posture					
	Upright	Standard	TIS 1a	TIS 1	TIS 2	TIS 3	Upright (Ranks)	Standard (Ranks)	TIS 1a (Ranks)	TIS 1 (Ranks)	TIS 2 (Ranks)	TIS 3 (Ranks)
1	52.31	42.61	45.24	38.9	47.81	37.37	6	3	4	2	5	1
2	48.97	43.2	43.36	38.55	43.04	33.47	6	4	5	2	3	1
3	46.36	41.14	45.08	43.22	43.39	34.44	6	2	5	3	4	1
4	54.5	42.48	42.67	39.34	44.49	32.94	6	3	4	2	5	1
5	51.02	47.18	46.67	42.87	46.84	37.9	6	5	3	2	4	1
6	49.51	42.29	41.92	40.64	41.29	29.88	6	5	4	2	3	1
7	54.56	45.5	48.3	43.5	45.79	35.72	6	3	5	2	4	1
8	53.24	45.12	42.88	40.58	45.93	36.89	6	4	3	2	5	1
9	50.22	41.62	51.13	48.84	50.16	40.09	5	2	6	3	4	1
10	50.89	44.28	46.93	41.28	42.84	31.86	6	4	5	2	3	1
11	53.11	40.88	47.14	42.94	44.4	34.58	6	2	5	3	4	1
12	49.85	44.98	44.3	41.5	46.39	36.67	6	4	3	2	5	1
13	47.98	37.28	44.29	38.99	44.01	32.75	6	2	5	3	4	1
14	46.7	37.31	42.95	35.39	38.86	28.15	6	3	5	2	4	1
15	49.13	42.01	43.86	40.48	43.94	32.81	6	3	4	2	5	1
						$\boldsymbol{R_i}$	**89**	**49**	**66**	**34**	**62**	**15**

$$\chi^2 = \left[\frac{12}{Nk(k+1)} \sum_{i=1}^{k} R_i^2 \right] - 3N(k+1) \quad (45)$$

In this equation, R_i is the sum of ranks for each posture, N is the total sample size (in this case 15) and k is the number of postures (in this case 6). The test statistic had a chi-square distribution due to the number of people tested (i.e. more than 10).

The calculation for the test statistic for the seat average pressure is presented below:

$$\chi^2 = \left[\frac{12}{(15 \times 6)(6+1)} \left(89^2 + 49^2 + 66^2 + 34^2 + 62^2 + 15^2\right) - (3 \times 15)(6+1) \right]$$

$$= \frac{12}{630} \left(7921 + 2401 + 4356 + 1156 + 3844 + 225\right) - 315$$

$$= 0.019047619(19903) - 315$$

$$= 64.105$$

The analysis was carried out in SPSS where there is a choice for the method for computing the test statistics. By default SPSS calculates the significance of the Friedman's ANOVA test by using a method that is accurate with large samples called the Asymptotic method. However, since the interface pressure samples are small, there are two other choices. The most accurate method is the Exact test, which calculates the Friedman's test exactly. However, a computer was not available with sufficient memory to perform this analysis because of the complexities of the computation. A slightly less demanding method to estimate the significance is the Monte Carlo method. This involves creating a distribution similar to that found in the sample and then taking several samples (the default is 10,000) from this distribution and from those samples the mean significance value and confidence interval around it is created. This method is recommended

when the Exact method is too labour-intensive (Field, 2005). A significant difference was found for all interface pressure parameters (Table 16) and hence hypothesis H3a is supported.

Table 16 Results from the Friedman's ANOVA ($p < .05$, χ^2 denotes the Friedman's ANOVA test statistic)

Seat Contact Area Threshold	$\chi^2(5) = 52.5$, $p < .001$
Back Contact Area Threshold	$\chi^2(5) = 68.5$, $p < .001$
Seat Average Pressure	$\chi^2(5) = 64.1$, $p < .001$
Back Average Pressure	$\chi^2(5) = 60.9$, $p < .001$
Peak Pressure Index	$\chi^2(5) = 53.4$, $p < .001$

The Wilcoxon signed-rank test is the non-parametric equivalent to the dependent *t*-test and can be used for *post hoc* tests by correcting for the number of comparisons (Field, 2005). The test works by first ranking the difference between conditions and applying the sign of the difference (positive or negative). For example, Table 17 gives the ranks for the seat average pressure for the comparison between the standard reclined posture and TIS 1a. The sum of the positive ranks and the sum of the negative ranks are calculated. The test statistic, T, is the smaller of these two values so in the example below the test statistic is 19.

Table 17 Ranks for seat average pressure (standard recline and TIS 1a postures)

						Positive	Negative
Subject	Standard	TIS 1a	Difference	Sign	Rank	Ranks	Ranks
1	42.61	45.24	2.64	-	8		8
2	43.2	43.36	0.16	-	1		1
3	41.14	45.08	3.93	-	11		11
4	42.48	42.67	0.2	-	2		2
5	47.18	46.67	0.51	+	4	4	
6	42.29	41.92	0.36	+	3	3	
7	45.5	48.3	2.81	-	10		10
8	45.12	42.88	2.24	+	7	7	
9	41.62	51.13	9.51	-	15		15
10	44.28	46.93	2.65	-	9		9
11	40.88	47.14	6.26	-	13		13
12	44.98	44.3	0.68	+	5	5	
13	37.28	44.29	7.02	-	14		14
14	37.31	42.95	5.64	-	12		12
15	42.01	43.86	1.85	-	6		6
					Total	**19**	**101**

To calculate the significance of the test statistic (T), the mean of test statistics ($\bar{T}$ in Equation 46) and the standard error (SE in Equation 47) are needed which are functions of the sample size. The test statistic is converted into a z-score using Equation 48. If the z-score is greater than 1.96 (ignoring the minus sign) then it is significant at $p < .05$. The 95% confidence level is recommended by Fisher (1925). The workings to test for significant differences between the standard recline posture and TIS 1a for seat average pressure are given as an example. Here it can be seen that the z-score is -2.329, so the effect is significant at the .05 level.

$$\bar{T} = \frac{n(n+1)}{4} \tag{46}$$

Therefore,

$$= \frac{15(15+1)}{4} = 60$$

$$SE = \sqrt{\frac{n(n+1)(2n+1)}{24}} \tag{47}$$

$\therefore$

$$= \sqrt{\frac{15(15+1)(30+1)}{24}} = 17.60681686$$

$$z = \frac{T - \bar{T}}{SE_T} \tag{48}$$

$\therefore$

$$= \frac{19 - 60}{17.60681686} = -2.329$$

where,

T = test statistic for Wilcoxon's matched-pairs signed-ranks test

$\bar{T}$ = mean of test statistics for Wilcoxon's matched-pairs signed-ranks test

SE = standard error

z = z-score

Because the Wilcoxon signed-rank test is being used as a *post hoc* test on a study that is a repeated measures design, the significance value needs to be corrected for the number of comparisons. The Bonferroni correction is used which is α/number of comparisons (α is the level of significance). In this case, there were 6 postures tested but 15 comparisons so the significance value (.05) is divided by 15, giving an adjusted significance of $p < .0033$. This is important to ensure that an overall Type 1 error rate across all comparisons remained at .05. In other words, the Bonferroni correction ensures that the overall probability of falsely rejecting the null hypothesis remained at 5%. Without applying this correction, the probability of making at least one Type 1 error on the interface pressure data would be 54%. This is known as the familywise error rate, and is defined by $1 - (.95)^{15}$. Here, $(.95)^{15}$ gives the overall probability of making no Type 1 errors which is the probabilities of each comparison making no Type 1 errors multiplied together, in this case giving .46 or 46%. It follows then that the probability of making a Type 1 error is 1 - .46, giving .54 or 54%.

The Exact method successfully calculated the significance of effects for the *post hoc* tests. Although this did not compute for the Friedman's ANOVA, it is the *post hoc* tests that establish between which variables there is an effect, at what size and the significance. The Friedman's ANOVA is used to see if there is an overall effect in the samples. Therefore, the problems with

computing the Exact test for the Friedman's ANOVA will not affect the results providing it does not miss an effect where one actually exists (a Type II error).

The effect size is the Pearson's correlation coefficient r and is calculated from the z-score which was defined in Equation 49. The equation to convert the z-score into the effect size estimate r is as follows:

$$r = \frac{Z}{\sqrt{N}} \tag{49}$$

Taking the example above for the comparison between the standard recline posture and TIS 1a for the average seat pressure:

$$r = \frac{-2.329}{\sqrt{15}} = -.60$$

For the Pearson's correlation coefficient r, .10 is a small effect, .30 is a medium effect and .50 is a large effect (Cohen 1988, 1992). So, here it can be seen that there is a large effect between the standard recline and TIS 1a postures.

The results from the *post hoc* tests on all pressure variables are presented in Table 18.

Table 18 Results from the *post hoc* tests ($p < .0033$). T = Wilcoxon's matched pairs signed-ranks test statistic; r = Pearson's correlation coefficient (effect size); NS = non-significant result

	Seat Contact Area Threshold	Back Contact Area Threshold	Seat Average Pressure	Back Average Pressure	Peak Pressure Index
Upright – standard	NS	$T = 0$, $p < .001$, $r = .88$	$T = 0$, $p < .001$, $r = .88$	$T = 1$, $p < .001$, $r = .87$	$T = 3$, $p < .001$, $r = .84$
Upright – TIS 1	NS	$T = 0$, $p < .001$, $r = .88$	$T = 1$, $p < .001$, $r = .87$	$T = 0$, $p < .001$, $r = .88$	$T = 4$, $p < .001$, $r = .82$
Upright – TIS 1a	NS	$T = 0$, $p < .001$, $r = .88$	$T = 0$, $p < .001$, $r = .88$	$T = 0$, $p < .001$, $r = .88$	$T = 1$, $p < .001$, $r = .87$
Upright – TIS 2	NS	$T = 7$, $p < .001$, $r = .78$	$T = 0$, $p < .001$, $r = .88$	$T = 0$, $p < .001$, $r = .88$	$T = 0$, $p < .001$, $r = .88$
Upright – TIS 3	$T = 8$, $p < .001$, $r = .76$	$T = 0$, $p < .001$, $r = .88$	$T = 0$, $p < .001$, $r = .88$	$T = 0$, $p < .001$, $r = .88$	$T = 0$, $p < .001$, $r = .88$
Standard – TIS 1	$T = 13$, $p < .01$, $r = .69$	$T = 0$, $p < .001$, $r = .88$	NS	$T = 0$, $p < .001$, $r = .88$	NS
Standard – TIS 1a	NS	$T = 0$, $p < .001$, $r = .88$	NS	$T = 11$, $p < .01$, $r = .72$	NS
Standard – TIS 2	$T = 0$, $p < .001$, $r = .88$	NS	NS	NS	NS
Standard – TIS 3	$T = 1$, $p < .001$, $r = .87$	$T = 0$, $p < .001$, $r = .88$	$T = 0$, $p < .001$, $r = .88$	$T = 0$, $p < .001$, $r = .88$	$T = 0$, $p < .001$, $r = .88$
TIS 1 – TIS 1a	$T = 7$, $p < .001$, $r = .78$	NS	$T = 0$, $p < .001$, $r = .88$	NS	$T = 3$, $p < .001$, $r = .84$
TIS 1 – TIS 2	NS	$T = 0$, $p < .001$, $r = .88$	NS	$T = 10$, $p < .001$, $r = .73$	NS
TIS 1 – TIS 3	$T = 0$, $p < .001$, $r = .88$	$T = 0$, $p < .001$, $r = .88$	$T = 0$, $p < .001$, $r = .88$	$T = 1$, $p < .001$, $r = .87$	$T = 0$, $p < .001$, $r = .88$
TIS 1a – TIS 2	$T = 3$, $p < .001$, $r = .84$	$T = 0$, $p < .001$, $r = .88$	$T = 0$, $p < .001$, $r = .88$	NS	NS
TIS 1a – TIS 3	$T = 0$, $p < .001$, $r = .88$	$T = 1$, $p < .001$, $r = .87$	$T = 0$, $p < .001$, $r = .88$	$T = 0$, $p < .001$, $r = .88$	$T = 0$, $p < .001$, $r = .88$
TIS 2 – TIS 3	$T = 0$, $p < .001$, $r = .88$	$T = 0$, $p < .001$, $r = .88$	$T = 0$, $p < .001$, $r = .88$	$T = 0$, $p < .001$, $r = .88$	$T = 0$, $p < .001$, $r = .88$

5.3.3 Relationships

Linear regression was used to test for relationships across the model predictions of force at the seat and sum of forces at the backrest, and the measured interface pressure variables. The results from this analysis support hypothesis H3b (Table 19). Hypothesis H3b required significant relationships, where $p < .05$.

Table 19 Relationships across model predictions of force from the seat and backrest with various interface pressure variables

Modelled data	Experimental data	Relationship	
		Significance	R^2
Seat Total Force	Seat Peak Pressure Index	$p < .001$	.291
	Seat Average Pressure	$p < .001$	.550
	Seat Contact Area Threshold	$p < .001$	.531
Back Total Force	Back Average Pressure	$p < .001$	.315
	Back Contact Area Threshold	$p < .001$	.833

5.4 Stadiometry

5.4.1 Descriptive statistics

Figures 61-64 show the predicted link forces for the thoracic, upper lumbar, lower lumbar, and the total torso with the measured height change results from the stadiometry investigation. Note that the height change histograms are repeated for side by side comparison with the different model predictions. The unshaded data columns give the results for lying supine which is an additional reference posture for this experiment. The results from the Friedman's ANOVA and the *post hoc* tests are included.

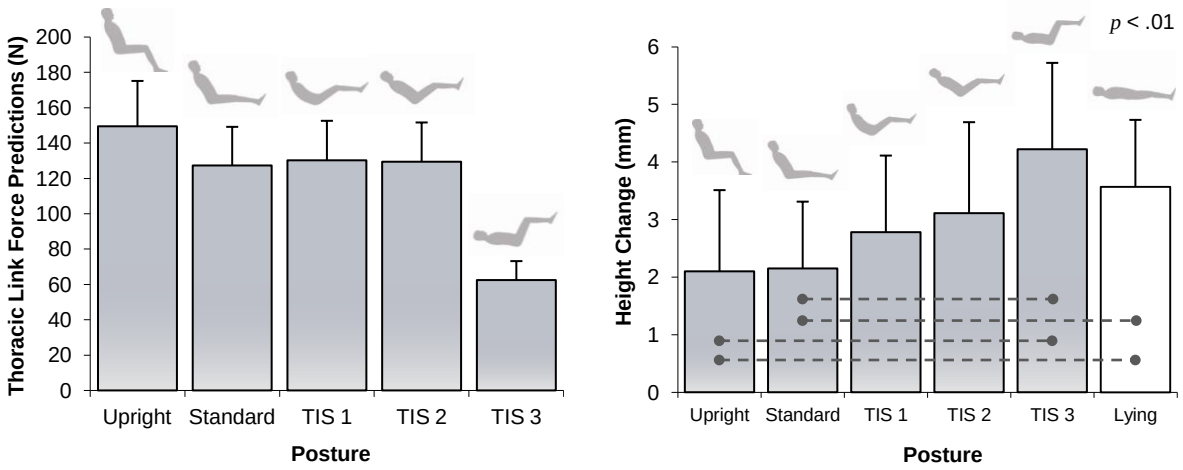

Figure 61 Thoracic Link Force predictions (left) and Height Change measurements (right) showing means and standard deviations for the 15 subjects, and the Friedman's ANOVA result. The unshaded data column is an additional reference posture. Dotted lines denote statistical *post hoc* significance

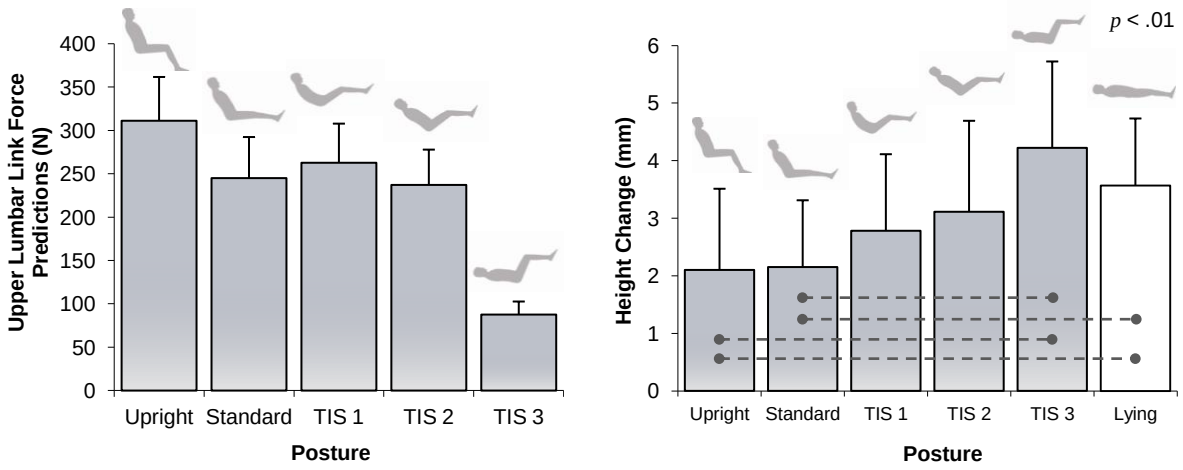

Figure 62 Upper Lumbar Link Force predictions (left) and Height Change measurements (right) showing means and standard deviations for the 15 subjects, and the Friedman's ANOVA result. The unshaded data column is an additional reference posture. Dotted lines denote statistical *post hoc* significance

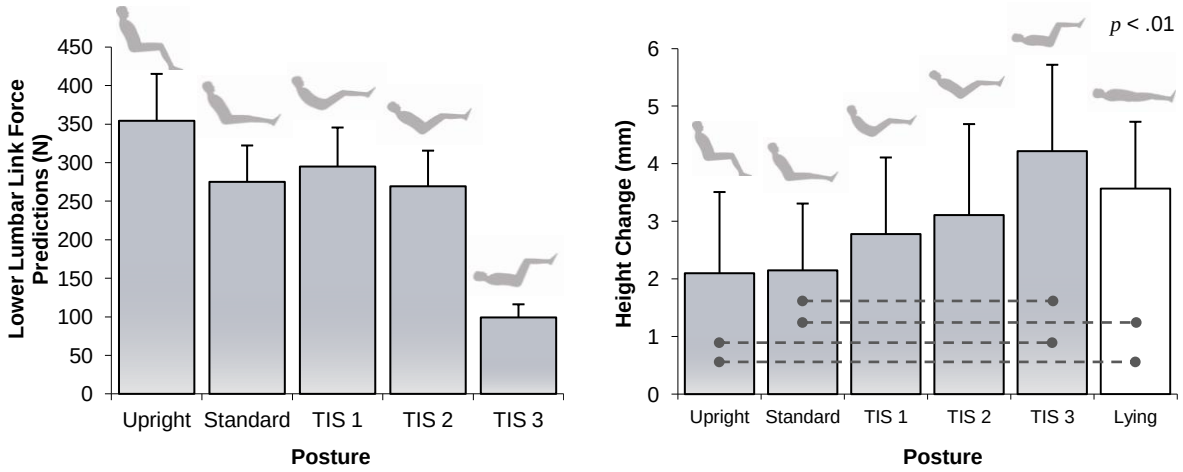

Figure 63 Lower Lumbar Link Force predictions (left) and Height Change measurements (right) showing means and standard deviations for the 15 subjects, and the Friedman's ANOVA result. The unshaded data column is an additional reference posture. Dotted lines denote statistical *post hoc* significance

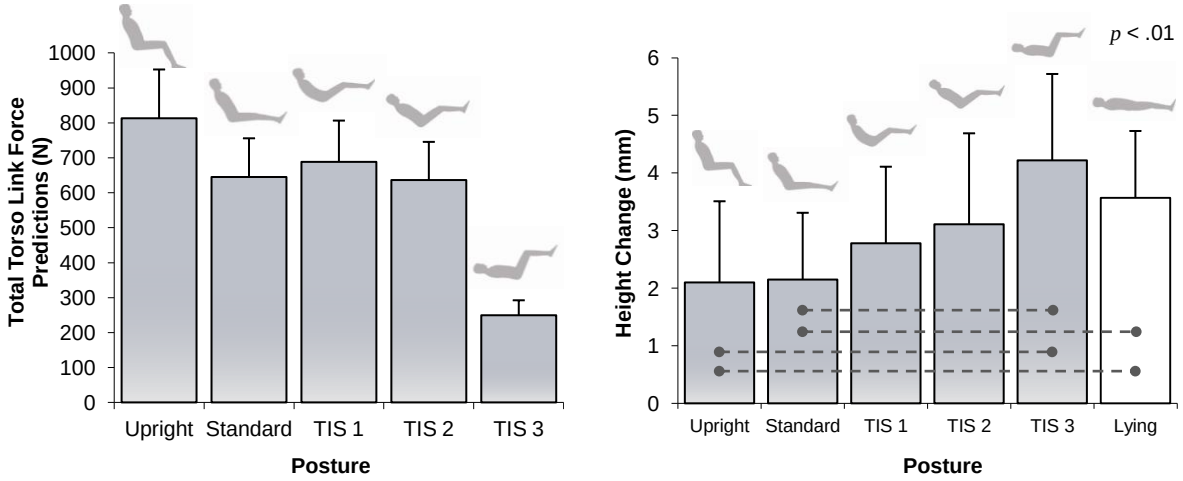

Figure 64 Total Torso Link Force predictions (left) and Height Change measurements (right) showing means and standard deviations for the 15 subjects, and the Friedman's ANOVA result. The unshaded data column is an additional reference posture. Dotted lines denote statistical *post hoc* significance

5.4.2 Comparative statistics

The following statistical analysis was carried out on the experimental data to test the hypothesis H4a stating that there will be a significant difference ($p < .05$) in stature change between the seated test postures, with stature gain greater for those postures where the upper body approaches the horizontal.

Before testing was carried out, an *a priori* power analysis was performed to determine the sample size for the investigation into the effects of reclined posture on stature. The calculations are explained in full in Section 5.3.2. Data from Althoff, *et al*. (1992) were used to estimate the effect size. The two postures that were compared are described by Althoff, *et al*. as an office chair with lumbar support (the control) and an office chair with a 120° backrest angle with arm support (the treatment). The mean height change and standard deviations were 2.1 mm (0.8) and 4.3 mm (0.9) respectively, giving an effect size of .9. All other data required for the calculation are the same as described in Section 5.3.2. The results indicate that a minimum of 9 subjects would be required to detect an effect in height change.

Table 20 presents the data obtained from a total of 25,000 readings after the curve fitting (see Section 4.3.3), including the mean, standard deviation and coefficient of variation. 5 cases are missing due to incomplete tests for three subjects.

Table 20 Height change (mm) data after curve fitting (with outlier removed)

Subject	Upright	Standard	TIS 1	TIS 2	TIS 3	Lying
1	2.5	2.6	1.37	2.82	5.08	2.92
2	0.54	1.1	0.74	5.56	4.26	2.83
3	2.05	2.13	2.59	2.82	4.39	4.5
4	3.44	/	/	2.58	4.44	/
5	3.24	2.46	3.01	/	2.37	4.24
6	3.04	3.57	2.82	3.33	6.01	3.14
7	0.23	-0.86	2.68	0.91	2.73	2.77
8	1.48	2.43	3.02	4.05	5.23	3.17
9	1.92	3.4	3.12	3.3	5.37	2.47
10	1.52	0.66	2.19	2.72	5.45	1.8
11	/	2.91	6.14	5.39	3.45	4.67
12	0.02	2.6	2.17	0.41	1.47	4.22
13	1.39	1.91	4.25	1.39	4.33	4.07
14	2.79	2.81	/	2.95	6.55	6.32
15	5.19	2.36	2.09	5.22	2.18	2.8
Mean	2.1	2.15	2.78	3.11	4.22	3.57
Standard deviation	1.41	1.16	1.33	1.58	1.5	1.16
Coefficient of variation	67%	54%	48%	51%	35%	33%

It was apparent from the coefficient of variation that there was a high variance in the data. Box plots were used to search for obvious outliers. One case was identified and removed from the data set. This was from one subject for the TIS 2 posture. The case suggested 9.83 mm of height increase. The mean for this posture (with the case removed) is 3.11 mm. The decision to remove this case was based on the possibility that it might bias the results leading to a Type I error. The resulting box plots and histograms for the distribution of data before and after the outlier was removed are presented in Appendix D-1.

The remaining data were then assessed for normality of distribution and homogeneity of variance using the Kolmogorov-Smirnov and Levene statistical tests respectively (Appendix D-2). The data were not normally distributed so attempts were made to transform the data (Appendix D-2). Square root and logarithm transformations were applied to the data, however the data remained non-normal. Therefore, the statistical analysis was carried out using non-parametric methods (see Section 5.3.2).

A significant difference was found for height change ($\chi^2(5) = 21.8, p < .001$) and hence hypothesis H4a is supported from these data. Wilcoxon tests were used to follow up this finding. Since a prediction was made as to the order of differences between postures, the one-tailed significance value was taken. A Bonferroni correction was applied and so all effects are reported at a .0033 level of significance (Table 21).

Table 21 *Post hoc* test statistics for height change ($p < .01$)

	Test statistics for height change
Upright - standard	NS
Upright - TIS 1	NS
Upright - TIS 2	NS
Upright - TIS 3	$T = 10$, $p < .01$, $r = .69$
Upright - Lying	$T = 8$, $p < .01$, $r = .68$
Standard - TIS 1	NS
Standard - TIS 2	NS
Standard - TIS 3	$T = 7$, $p < .001$, $r = .74$
Standard - Lying	$T = 7$, $p < .001$, $r = .74$
TIS 1 - TIS 2	NS
TIS 1 - TIS 3	NS
TIS 1 - Lying	NS
TIS 2 - TIS 3	NS
TIS 2 - Lying	NS
TIS 3 - Lying	NS

5.4.3 Relationships

Linear regression was used to test for relationships across the model predictions of link forces and the measured height change. The results from this analysis support hypothesis H4b (Table 22). Hypothesis H4b required significant relationships, where $p < .05$.

Table 22 Relationships between link forces and height change

Modelled data	**Experimental data**	**Relationship**	
		Significance	R^2
Thoracic Link Force	Height Change	$p < .01$	.091
Upper Lumbar Link Force		$p < .05$	.065
Lower Lumbar Link Force		$p < .01$	.094
Total Torso Link Force		$p < .01$	.097

5.5 sEMG

5.5.1 Descriptive statistics

The sEMG results are organised slightly differently to the other experimental data for economy. Figures 65-67 give the model force predictions and Figures 68-71 give the measured sEMG results, including the results from the Friedman's ANOVA and *post hoc* tests. Table 23 lists the measured muscle groups and their corresponding model forces to aid comparison. Lying supine was also included in this investigation, and is represented by unshaded data columns. When inspecting the raw sEMG data, ECG spikes were found which were corroborated with heart rate data that were collected as a quality control. The heart rate data are presented in Figure 72 with the Friedman's ANOVA and *post hoc* test results.

Table 23 Muscle groups and corresponding model forces

Muscle group	**Corresponding model forces**		
Multifidus left	$F_{n,cr}$	F_{net}	
Multifidus right	$F_{n,cr}$	F_{net}	
Iliocostalis left	$F_{n,cr}$	F_{net}	$F_{n,l}$
Iliocostalis right	$F_{n,cr}$	F_{net}	$F_{n,l}$
Longissimus left	$F_{n,l}$	$F_{n,th}$	
Longissimus right	$F_{n,l}$	$F_{n,th}$	
T8 left	$F_{n,th}$		
T4 right	$F_{n,sh}$		

$F_{n,cr}$: Force on the iliac crest, normal to the support

F_{net} : Pelvic stabilising force acting on L5/S1, normal to the pelvis linkage

$F_{n,l}$: Force on the L3 vertebrae, normal to the support

$F_{n,th}$: Force on the T12/L1 vertebrae, normal to the support

$F_{n,sh}$: Force on the C7 vertebrae, normal to the support

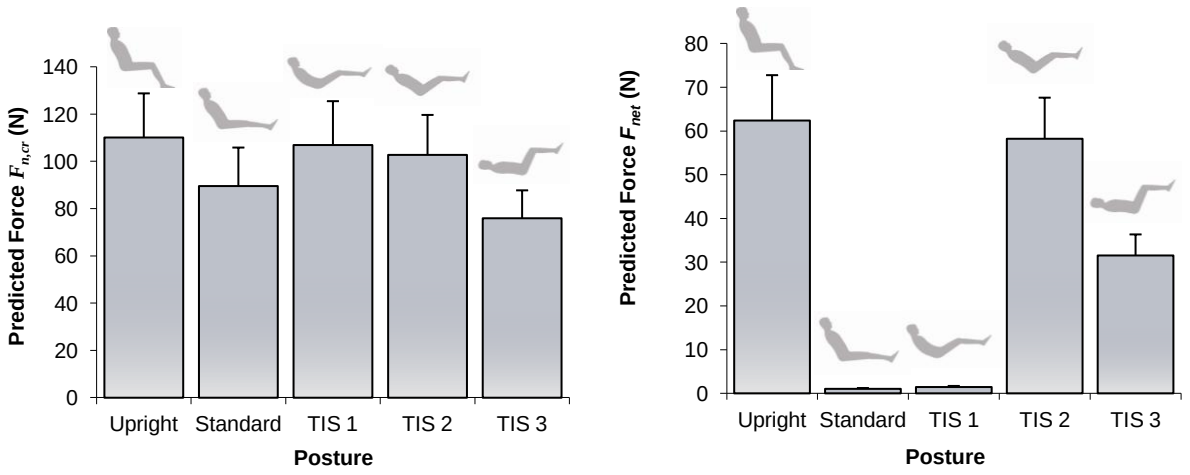

Figure 65 $F_{n,cr}$ force predictions (left) and F_{net} force predictions (right) showing means and standard deviations for the 15 subjects. $F_{n,cr}$ is the Force on the iliac crest, normal to the support. F_{net} is the pelvic stabilising force acting on L5/S1, normal to the pelvis linkage (net force representing posterior spinal ligaments)

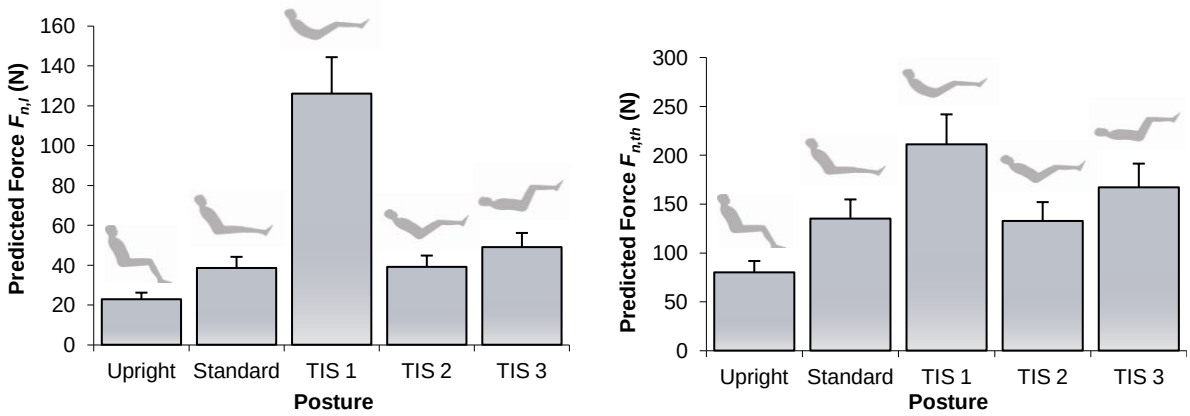

Figure 66 $F_{n,l}$ force predictions (left) and $F_{n,th}$ force predictions (right) showing means and standard deviations for the 15 subjects. $F_{n,l}$ is the force on the L3 vertebrae, normal to the support. $F_{n,th}$ is the force on the T12/L1 vertebrae, normal to the support

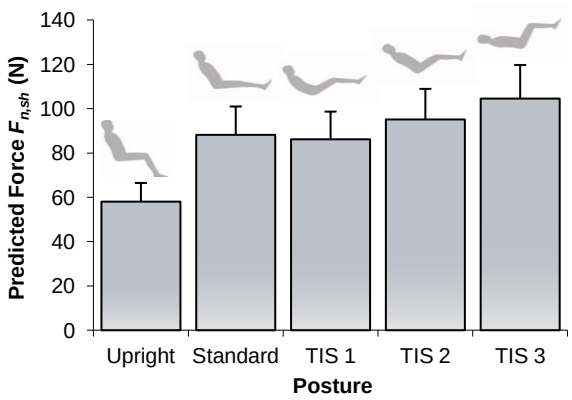

Figure 67 $F_{n,sh}$ force predictions showing means and standard deviations for the 15 subjects. $F_{n,sh}$ is the force on the C7 vertebrae, normal to the support

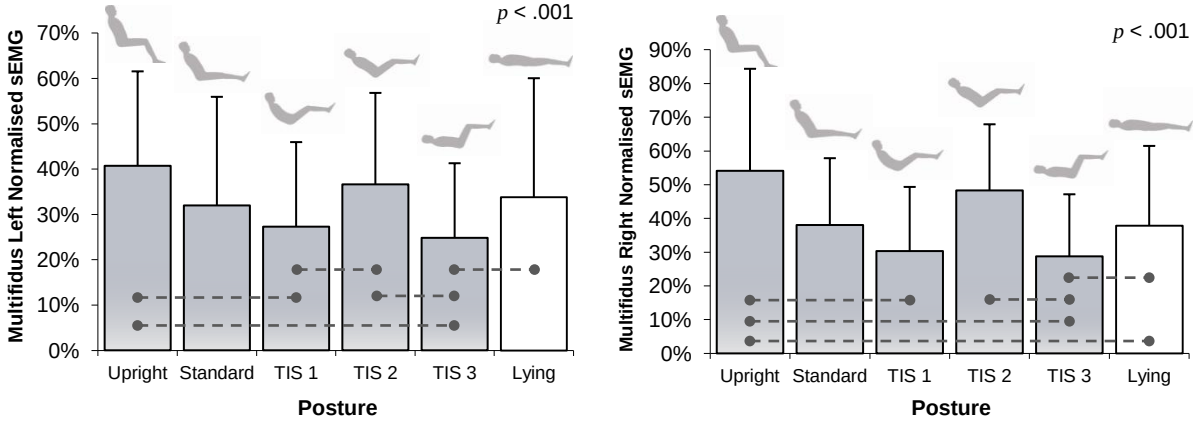

Figure 68 Mean linear envelope for the multifidus left side (left) and right side (right) normalised to the standing posture showing means and standard deviations for the 15 subjects, and the Friedman's ANOVA result. Dotted lines denote statistical *post hoc* significance

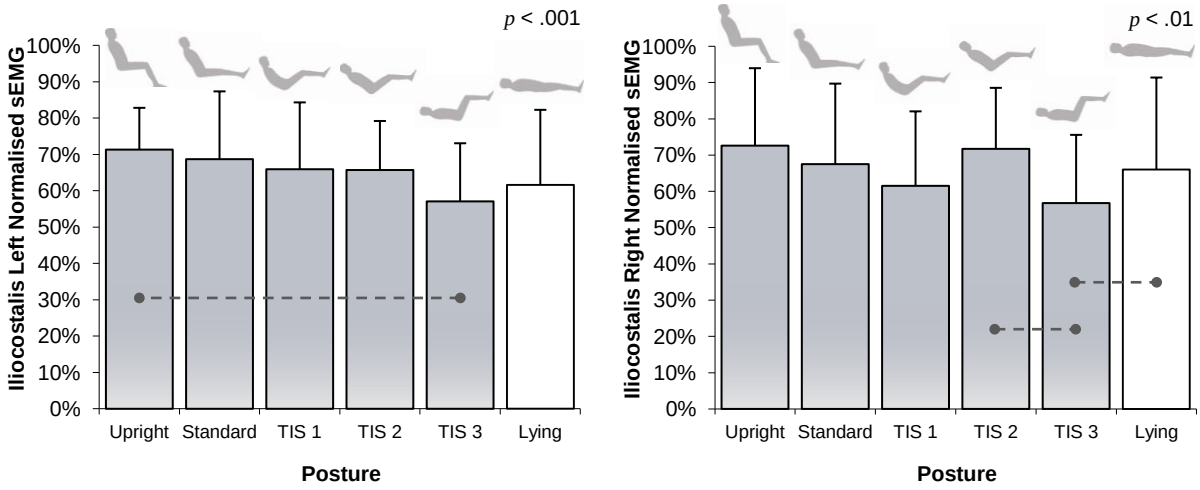

Figure 69 Mean linear envelope for the iliocostalis left side (left) and right side (right) normalised to the standing posture showing means and standard deviations for the 15 subjects, and the Friedman's ANOVA result. Dotted lines denote statistical *post hoc* significance

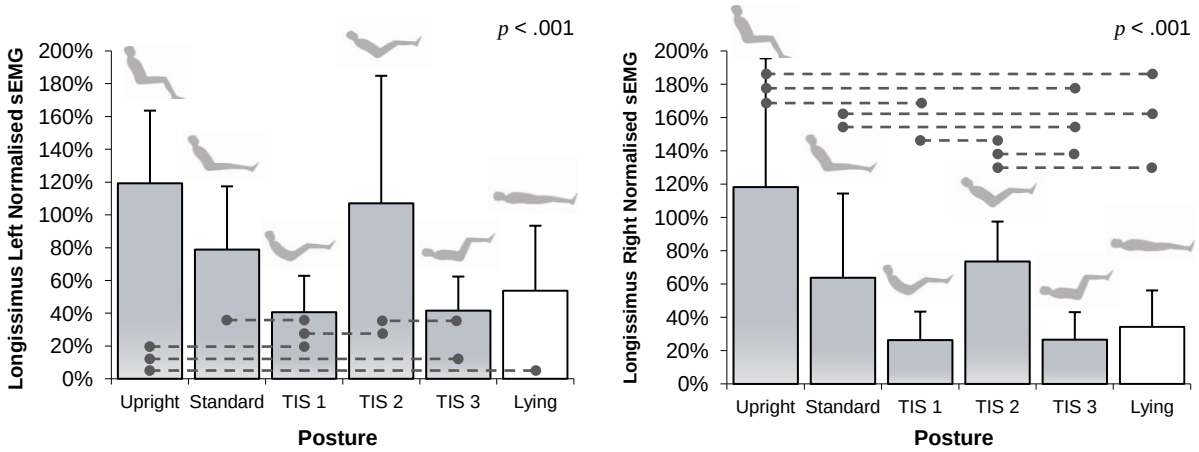

Figure 70 Mean linear envelope for the longissimus left side (left) and right side (right) normalised to the standing posture showing means and standard deviations for the 15 subjects, and the Friedman's ANOVA result. Dotted lines denote statistical *post hoc* significance

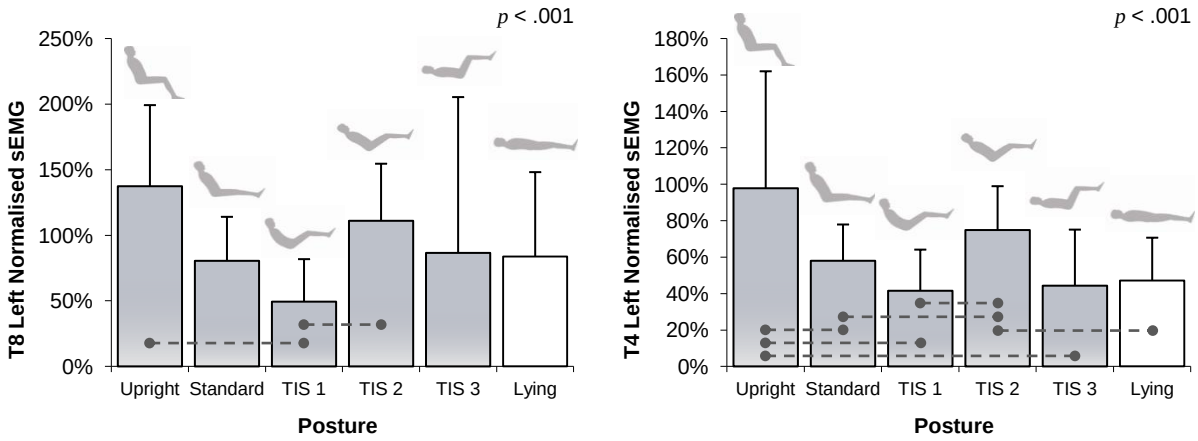

Figure 71 Mean linear envelope for the T8 level left side (left) and the T4 level left side (right) normalised to the standing posture showing means and standard deviations for the 15 subjects, and the Friedman's ANOVA result. Dotted lines denote statistical *post hoc* significance

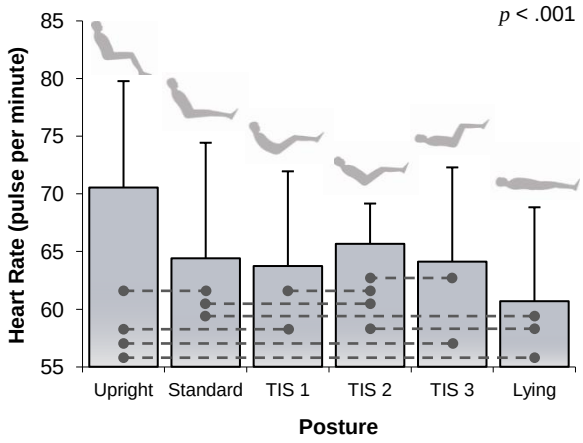

Figure 72 Heart rate showing means and standard deviations for the 15 subjects, and the Friedman's ANOVA result. Dotted lines denote statistical *post hoc* significance

5.5.2 Comparative statistics

The following statistical analysis was carried out on the experimental data to test the hypothesis H5a stating that there will be a significant difference ($p < .05$) in back muscle EMG activity between the seated test postures, with less activity for those postures where the upper body approaches the horizontal.

Before the testing was carried out, the data from Andersson and Örtengren (1974[a]) were used to estimate the effect size for the *a priori* analysis for the electromyography experiments. The two postures that were compared were a sitting posture with a 100° backrest recline (the control) and a sitting posture with a 130° backrest recline (the treatment). The full-wave rectified and average values, and standard deviations, are 4.93 μV (1.16) and 2.5 μV (0.21) respectively, giving an effect size of .7. All other data required for the calculation are the same as described in Section 5.3.2. The results indicate that a minimum of 15 subjects would be required to detect a significant effect in muscle activity.

The mean data from the linear envelopes, normalised to the standing posture, are given in Appendix E-1. The data were explored, using histograms, and for the longissimus, T8 and T4, the data were clearly skewed. On examination of box plots, there appeared to be no obvious outliers that could not be explained by individual responses to the sitting postures. The histograms and box plot are presented in Appendix E-3. Statistical tests were carried out to objectively assess whether distributions were normal and that there is homogeneity of variance in the data. Full wave rectification is a non-linear operation, which is why the data is not normally distributed. The results of these tests confirmed that the distribution of data is non-normal, and that the variability in the data is heterogeneous (Appendix E-3). Since the original raw data had been rectified, smoothed and normalised, it was considered that the potential statistical benefit of applying additional transformations was outweighed by the negative implications for interpreting the results, that is, the fewer transformations applied to the original data, the more meaningful the results. Therefore, all subsequent analysis was performed using non-parametric methods.

There was a significant difference for the sEMG and hence hypothesis H5a is supported from this study. The results from the Friedman's ANOVA are presented in Table 24. Wilcoxon tests were used for *post hoc* evaluations. Since a prediction was made on the order of differences between postures, the one-tailed significance value was taken. A Bonferroni correction was

applied and so all effects are reported at a .0033 level of significance. The results of the *post hoc* tests are given in Table 25. Heart rate data were collected as a quality control for potential ECG contamination. Differences were observed in the data so the results were analysed using the same statistical tests as for the sEMG data. A significant effect was found for heart rate $(\chi^2(5) = 30.7, p < .001)$. The results from the *post hoc* tests are reported in Table 26.

Table 24 Results from the Friedman's ANOVA ($p < .05$)
(χ^2 denotes the Friedman's ANOVA test statistic)

Multifidus left	$\chi^2(5) = 32.662$, $p < .001$
Multifidus right	$\chi^2(5) = 34.013$, $p < .001$
Iliocostalis left	$\chi^2(5) = 20.039$, $p < .001$
Iliocostalis right	$\chi^2(5) = 15.987$, $p < .01$
Longissimus left	$\chi^2(5) = 35.779$, $p < .001$
Longissimus right	$\chi^2(5) = 40.351$, $p < .001$
T8 left	$\chi^2(5) = 28.558$, $p < .001$
T4 left	$\chi^2(5) = 19.935$, $p < .001$

Table 25 Results from the *post hoc* tests ($p < .0033$). T = Wilcoxon's matched pairs signed-ranks test statistic; r = Pearson's correlation coefficient (effect size); NS = non-significant result

	Multifidus left	Multifidus right	Iliocostalis left
Upright - Standard	N/S	N/S	N/S
Upright - TIS 1	$T = 0$, $p < .001$, $r = .76$	$T = 0$, $p < .001$, $r = .76$	N/S
Upright - TIS 2	N/S	N/S	N/S
Upright - TIS 3	$T = 0$, $p < .001$, $r = .76$	$T = 0$, $p < .001$, $r = .76$	$T = 2$, $p < .001$, $r = .71$
Upright - Lying	N/S	$T = 2$, $p < .01$, $r = .71$	N/S
Standard - TIS 1	N/S	N/S	N/S
Standard - TIS 2	N/S	N/S	N/S
Standard - TIS 3	N/S	N/S	N/S
Standard - Lying	N/S	N/S	N/S
TIS 1 - TIS 2	$T = 0$, $p < .001$, $r = .76$	N/S	N/S
TIS 1 - TIS 3	N/S	N/S	N/S
TIS 1 - Lying	N/S	N/S	N/S
TIS 2 - TIS 3	$T = 0$, $p < .001$, $r = .76$	$T = 0$, $p < .001$, $r = .76$	N/S
TIS 2 - Lying	N/S	N/S	N/S
TIS 3 - Lying	$T = 0$, $p < .001$, $r = .76$	$T = 3$, $p < .01$, $r = .69$	N/S

Table 25 *continued*

	Iliocostalis right	Longissimus left	Longissimus right
Upright - Standard	N/S	N/S	N/S
Upright - TIS 1	N/S	$T = 0$, $p < .001$, $r = .76$	$T = 0$, $p < .001$, $r = .76$
Upright - TIS 2	N/S	N/S	N/S
Upright - TIS 3	N/S	$T = 0$, $p < .001$, $r = .76$	$T = 0$, $p < .001$, $r = .76$
Upright - Lying	N/S	$T = 1$, $p < .001$, $r = .73$	$T = 1$, $p < .001$, $r = .73$
Standard - TIS 1	N/S	$T = 3$, $p < .01$, $r = .69$	$T = 1$, $p < .001$, $r = .73$
Standard - TIS 2	N/S	N/S	N/S
Standard - TIS 3	N/S	N/S	$T = 1$, $p < .001$, $r = .73$
Standard - Lying	N/S	N/S	$T = 2$, $p < .001$, $r = -.71$
TIS 1 - TIS 2	N/S	$T = 0$, $p < .001$, $r = .76$	$T = 0$, $p < .001$, $r = .76$
TIS 1 - TIS 3	N/S	N/S	N/S
TIS 1 - Lying	N/S	N/S	N/S
TIS 2 - TIS 3	$T = 1$, $p < .001$, $r = .73$	$T = 0$, $p < .001$, $r = .76$	$T = 0$, $p < .001$, $r = .76$
TIS 2 - Lying	N/S	N/S	$T = 0$, $p < .001$, $r = .76$
TIS 3 - Lying	$T = 2$, $p < .001$, $r = .71$	N/S	N/S

Table 25 *continued*

	T8 left	T4 left
Upright - Standard	N/S	$T = 3$, $p < .01$, $r = .69$
Upright - TIS 1	$T = 0$, $p < .001$, $r = .76$	$T = 2$, $p < .001$, $r = .71$
Upright - TIS 2	N/S	N/S
Upright - TIS 3	N/S	$T = 1$, $p < .001$, $r = .73$
Upright - Lying	N/S	N/S
Standard - TIS 1	N/S	N/S
Standard - TIS 2	N/S	$T = 3$, $p < .01$, $r = .69$
Standard - TIS 3	N/S	N/S
Standard - Lying	N/S	N/S
TIS 1 - TIS 2	$T = 0$, $p < .001$, $r = .76$	$T = 3$, $p < .01$, $r = .69$
TIS 1 - TIS 3	N/S	N/S
TIS 1 - Lying	N/S	N/S
TIS 2 - TIS 3	N/S	N/S
TIS 2 - Lying	N/S	$T = 3$, $p < .01$, $r = .69$
TIS 3 - Lying	N/S	N/S

Table 26 *Post hoc* test statistics for heart rate ($p < .0033$). T = Wilcoxon's matched pairs signed-ranks test statistic; r = Pearson's correlation coefficient (effect size); NS = non-significant result

	Heart rate
Upright - Standard	T =60, $p < .001$, r = .95
Upright - TIS 1	T =162, $p < .01$, r = .74
Upright - TIS 2	N/S
Upright - TIS 3	T =67.5, $p < .001$, r = .97
Upright - Lying	T =69.5, $p < .001$, r = .97
Standard - TIS 1	N/S
Standard - TIS 2	T =161, $p < .01$, r = .74
Standard - TIS 3	N/S
Standard - Lying	T =247, $p < .001$, r = .83
TIS 1 - TIS 2	T =162, $p < .001$, r = .97
TIS 1 - TIS 3	N/S
TIS 1 - Lying	N/S
TIS 2 - TIS 3	T =347, $p < .01$, r = .72
TIS 2 - Lying	T =100.5, $p < .001$, r = .97
TIS 3 - Lying	N/S

5.5.3 Relationships

Linear regression was used to test for relationships across the model predictions of link forces and the measured sEMG. The results from this analysis support hypothesis H5b (Table 27). Hypothesis H5b required significant relationships, where $p < .05$.

Table 27 Relationships between model forces and sEMG

Modelled data	**Experimental data**	**Relationship**	
		Significance	R^2
$F_{n,cr}$	Multifidus left	N/S	
F_{net}		N/S	
$F_{n,l}$		N/S	
$F_{n,cr}$	Multifidus right	$p < .01$	.135
F_{net}		$p < .01$	.159
$F_{n,l}$		N/S	
$F_{n,l}$	Iliocostalis left	N/S	
$F_{n,l}$	Iliocostalis right	N/S	
$F_{n,l}$	Longissimus left	$p < .001$	.186
$F_{n,th}$		$p < .001$	.266
$F_{n,l}$	Longissimus right	$p < .001$	.185
$F_{n,th}$		$p < .001$	.287
$F_{n,th}$	T8	$p < .001$	.212
$F_{n,sh}$	T4	$p < .01$	.173

5.6 Posture

5.6.1 Descriptive statistics

Pilot tests were initially performed to assess the accuracy of the Flock of Birds electromagnetic motion tracking system. Lumbar and thoracic curvatures were measured twice from two subjects for standing, unsupported sitting, maximum extension and maximum flexion (Section 4.5.1). For maximum extension and maximum flexion, lumbar and thoracic curvatures were also measured using the flexicurve technique (Hart & Rose, 1986; Burton, 1986). Table 28 gives the results for lumbar curvature and Table 29 gives the results for thoracic curvature.

Table 28 Results for lumbar curvature from the pilot test (including Flexicurve measurements of extension and flexion)

Posture	Subject 1 Lumbar curvature (°)	Subject 2 Lumbar curvature (°)
Standing 1	28	67
Standing 2	31	60
Mean standing	29	64
Standard deviation	2	5
Sitting 1	-37	27
Sitting 2	-32	/
Mean sitting	-35	/
Standard deviation	3	/
Extension 1	68	102
Extension 2	65	92
Mean extension	67	97
Standard deviation	3	7
Flexicurve extension	24	61
RMS error	43	36
Flexion 1	-36	-28
Flexion 2	-34	-26
Mean flexion	-35	-27
Standard deviation	2	2
Flexicurve flexion	-32	-25
RMS error	3	2

Table 29 Results for thoracic curvature from the pilot test, with means and standard deviations for each posture

Posture	Subject 1 Thoracic curvature (°)	Subject 2 Thoracic curvature (°)
Standing 1	-27	-33
Standing 2	-38	-42
Mean standing	-32	-38
Standard deviation	8	6
Sitting 1	-29	-45
Sitting 2	-33	/
Mean standing	-31	/
Standard deviation	3	/
Extension 1	-20	-16
Extension 2	-19	-18
Mean standing	-19	-17
Standard deviation	1	2
Flexion 1	-61	-55
Flexion 2	-62	-52
Mean standing	-61	-54
Standard deviation	0	2

The mean and standard deviations for lumbar and thoracic curvatures from the group of 15 subjects for the test postures, including the additional unsupported sitting posture, are given in Figure 73, including the results from the Friedman's ANOVA and the *post hoc* tests. There are no model predictions for spinal curvature.

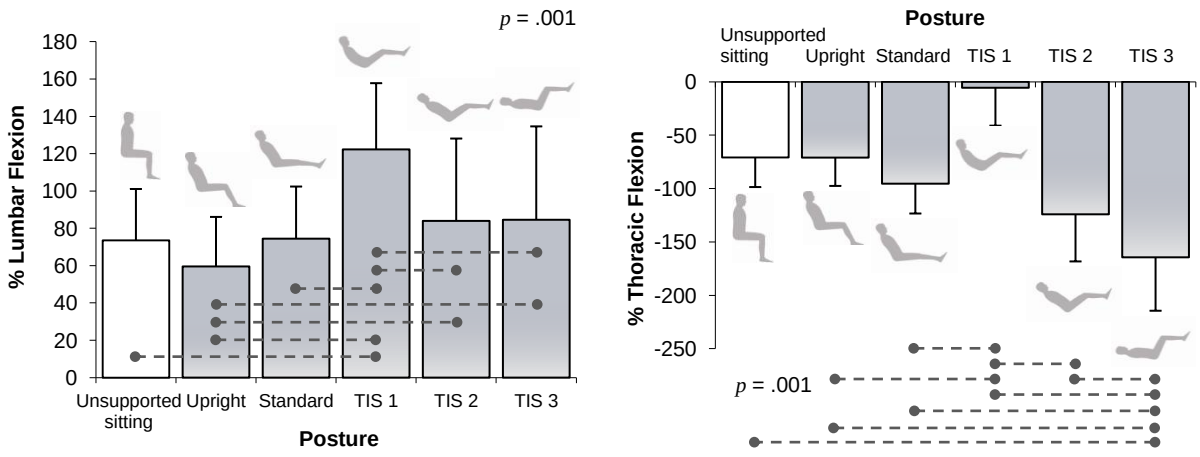

Figure 73 % lumbar flexion and % thoracic flexion (right) showing means and standard deviations for all 15 subjects, and the Friedman's ANOVA result. Dotted lines denote *post hoc* statistical significance

5.6.2 Comparative statistics

The following statistical analysis was carried out on the experimental data to test the hypothesis H6 stating that there will be a significant difference ($p < .05$) in spinal curvature between the seated test postures.

Before the testing was carried out, data from Dolan, *et al*. (1988) were used to estimate the effect size for the *a priori* power analysis. The two postures that were compared were an unsupported relaxed sitting posture (the control) and sitting in a low, firm chair with a seat tilt of 30° (the treatment). Mean lumbar flexion and standard deviations were 30° (8) and 23° (8) respectively, giving an effect size of .3. The results indicate that a minimum of 90 subjects would be required to detect a significant effect in spinal curvature. A study involving 90 subjects is outside the scope of this pilot investigation. It is possible that larger effects will be observed in this investigation, particularly with the TIS 1 posture where the backrest articulates to flex the spine. Given the time and resources available, and the possible effect sizes between postures, it was decided to proceed with the same 15 subjects who participated in the previous investigations.

The results for lumbar and thoracic curvature data were tested for normality of distribution and homogeneity of variants. The findings are in Appendix F-1 and show that the data is non-normal in its distribution and therefore violates parametric assumptions. The data from one subject was rejected from the analysis because the standing and maximum curvature data required for calculating % flexion appeared erroneous.

A significant difference was found for the % lumbar and % thoracic flexion (Table 30), which supports hypothesis H6. Wilcoxon tests were used to follow up this finding. Since no direction was given to the differences between postures, the two-tailed significance value was taken. A Bonferroni correction was applied and so all effects were reported at a .0033 level of significance (Table 31).

Table 30 Results from the Friedman's ANOVA ($p < .05$)
(χ^2 denotes the Friedman's ANOVA test statistic)

% Lumbar Flexion	$\chi^2(5) = 31.571$, $p < .001$
% Thoracic Flexion	$\chi^2(5) = 28.558$, $p < .001$

Table 31 Results for lumbar and thoracic flexion from the *post hoc* tests ($p < .0033$). T = Wilcoxon's matched pairs signed-ranks test statistic; r = Pearson's correlation coefficient (effect size); NS = non-significant result

	% Lumbar Flexion	% Thoracic Flexion
Unsupported Sitting - Upright	N/S	N/S
Unsupported Sitting - Standard	N/S	N/S
Unsupported Sitting - TIS 1	$T = 0$, $p < .001$, $r = .76$	N/S
Unsupported Sitting - TIS 2	N/S	N/S
Unsupported Sitting - TIS 3	N/S	$T = 1$, $p < .01$, $r = .73$
Upright - Standard	N/S	N/S
Upright - TIS 1	$T = 0$, $p < .001$, $r = .82$	$T = 1$, $p < .001$, $r = .83$
Upright - TIS 2	$T = 1$, $p < .001$, $r = .80$	N/S
Upright - TIS 3	$T = 2$, $p < .001$, $r = .78$	$T = 3$, $p < .001$, $r = .80$
Standard - TIS 1	$T = 0$, $p < .001$, $r = .82$	$T = 3$, $p < .001$, $r = .77$
Standard - TIS 2	N/S	N/S
Standard - TIS 3	N/S	$T = 3$, $p < .001$, $r = .77$
TIS 1 - TIS 2	$T = 0$, $p < .001$, $r = .85$	$T = 1$, $p < .001$, $r = .83$
TIS 1 - TIS 3	$T = 1$, $p < .001$, $r = .83$	$T = 1$, $p < .001$, $r = .83$
TIS 2 - TIS 3	N/S	$T = 2$, $p < .001$, $r = .82$

6 Discussion

This chapter discusses the main findings from this research in the wider context of the literature. The chapter begins with a discussion on the biomechanical model; its postural accuracy, its validation, its use for interpreting the published literature and how it relates to digital human models, and future developments. Following this, a discussion on the effectiveness of the test postures is given, where the model is applied to help to understand the observed effects. Consideration is given to how the findings and concepts developed during this study might be applied to various contexts of use such as back care, long term care and long haul flights, and future research.

6.1 Biomechanical model

The biomechanical model developed is a modification of the four link model of the seated person by Goossens and Snidjers (1995). There have been no other developments of this model to the author's knowledge. The model was developed to predict internal axial loads for the body segments, and external forces acting on the feet (or behind the knees if the feet are unsupported), ITs, back, and head. The purpose of the model is: 1) to predict posture; 2) to predict load distributions; 3) to predict the motion paths of the support surfaces; 4) to augment interpretation of interface pressure variables; 5) to aid with interpretation of spinal loading and changes in stature; and 6) to assist with the interpretation of back sEMG activity in the different seated test postures. In addition, the model provides a theoretical foundation to compare related research and help explain discordance between published findings. The novel aspects of the model are 1) geometrical detail of the pelvis and spine from anatomical studies; 2) inclusion of algorithms predicting pelvic rotation; 3) prediction of ischial-seat contact; and 4) derivation of the

pelvic stabilising force. To the author's knowledge, no previous biomechanical model can accurately predict seated postures, seated load distributions, and support surface motion paths.

6.1.1 Postural accuracy

The findings from this research support hypothesis H2a that the model will predict the various seated recline postures with an accuracy of 95% or more. The average percent difference between modelled and measured support contact for the head across all postures is 1.2%. This is the primary index for postural accuracy. In addition, the model accuracy was assessed against published anthropometric data. Surprisingly, few quantitative anthropometric data are available on sitting postures. In the early 1980s, the National Highway Traffic Safety Administration sponsored a study at the University of Michigan Transportation Research Institute (UMTRI) to develop anthropometric criteria for a new generation of crash dummies. The project used standard anthropometry and stereophotogrammetry to create detailed specifications for small-female, midsize-male, and large-male body forms. These surface reference data have been applied, in physical and digital form, to a wide variety of applications including the development of new crash dummies, tools for vehicle design, and applications unrelated to vehicles (Haffner, *et al*., 2001). Comparison between the model and the anthropometric data collected at UMTRI (Robbins, 1983) resulted in an estimated 2.2% difference for the sitting height. Figure 20, Section 3.2.2, shows the model superimposed with the original side-view drawing of the mid-sized male. The original drawing has a skeletal rendering with some large inaccuracies, the most notable being the pelvis which is too high. Comparison between the skeletal rendering of the pelvis and the model pelvis highlights the inaccuracy with the rendered pelvis' position (Figure 20). The model and rendered pelvis are in agreement on the pelvis rotation angle for this driving seat posture.

For the upright sitting posture, the predicted distance from the back of the seat to the IT seat contact was 0.6% of the measured distance to the peak pressure. This level of accuracy reduced, however, when tilting the test-rig, as the measure peak pressure moved posteriorly (a 2.2% difference for the TIS 2 configuration and a 5.8% difference for TIS 3). It is the author's opinion that the predicted pelvic postures for these tilted configurations were accurate and that the posterior translation of the measured peak pressure reflects the posterior translation of the centre of mass of the upper body. The greatest differences between predicted and measured indices for the ITs were for the standard recline and TIS 1 configurations (18.4% and 16.8% differences respectively). For these postures, the seat to backrest angle changes so there is a corresponding change in the predicted position of the pelvis in the model. It is believed that the predicted position of the pelvis for these postures is accurate and that, as a result of the orientation of the pelvis relative to the seat, the peak pressures have moved away from the ITs. Figure 74 shows the upright and standard recline seating configurations with the predicted anatomical landmarks and the measured pressure indices. The locations for the pressure indices were derived from the three 50th percentile male subjects from the group that participated in this study. Here it can be seen that the measured peak pressure agrees almost perfectly with the modelled IT position for the upright configuration but not for the standard recline where the pelvis has rotated posteriorly. Figure 75 shows the seat pressure distributions from the same three 50th percentile males for the upright and standard recline seating configurations. The difference between the upright and standard recline pressure distributions are clear. The distance between the peak pressures are greater for the upright distributions, with the peak pressure zone orientated anteriorly towards the pubic symphasis (Moes, 2007), as indicated by the black lines. For the standard recline pressure distributions, the distance between peak pressures significantly reduced, indicating pelvis rotation with a posterior translation of the peak pressures. For this posture the pressure distributions suggest that load is being borne by the soft tissues between the ITs and the sacrum, such as the sacrotuberous ligaments and surrounding muscle. It is likely that, with further pelvic rotation, the peak pressures would merge as the load transfers to the sacrum (Figures 74 and 75).

Pressure and motion sensor indices are also reported for skin over the L3 vertebrae and the scapula. Neither of these indices are considered to be reliable. Skin movement over the L3 vertebrae and scapula were likely causes for variability in the data. In addition, the scapula is relatively large and therefore capable of transferring load to different positions on the backrest for different seated postures.

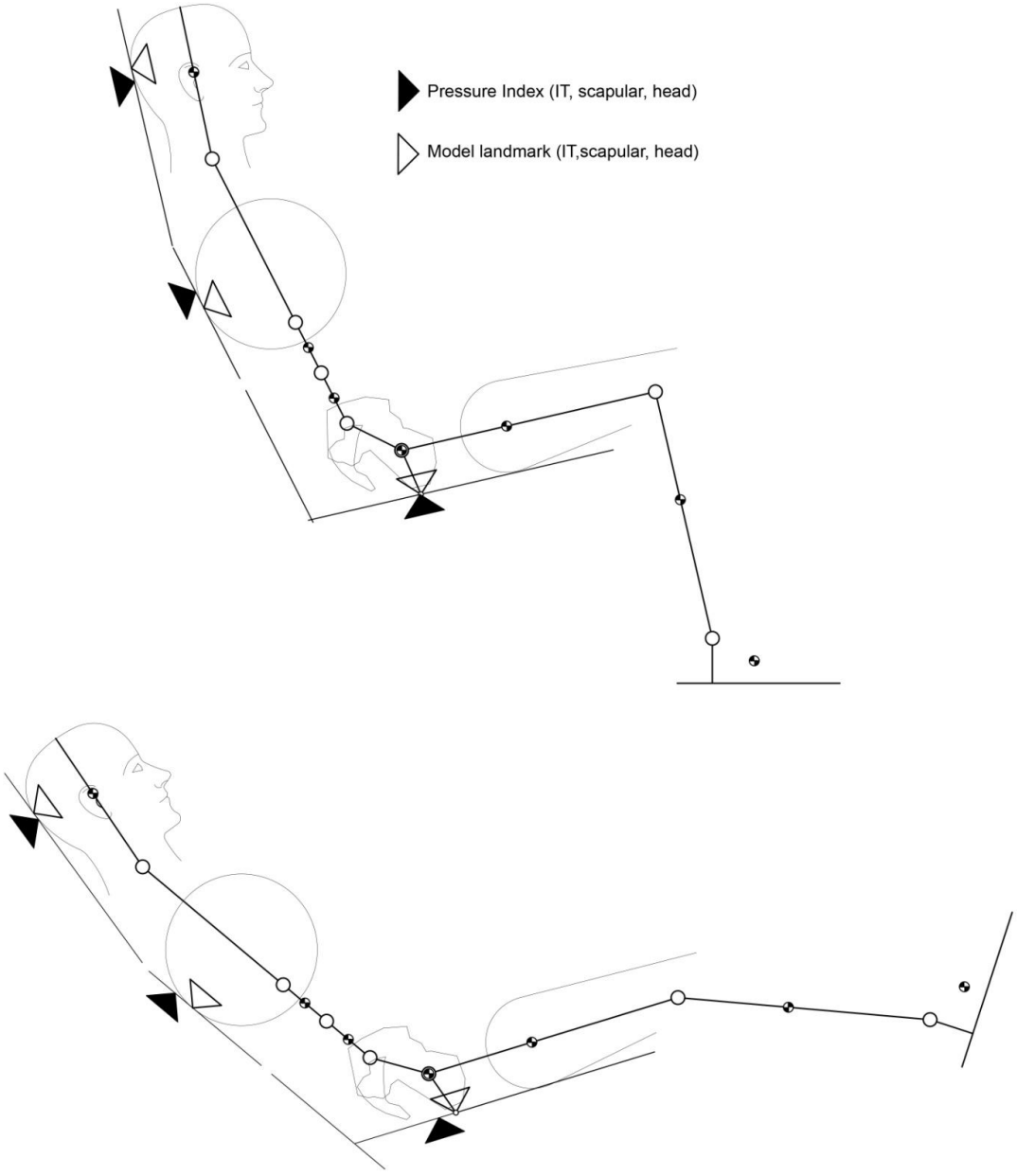

Figure 74 Upright (above) and Standard Recline (below) postures showing predicted and measured posture indices: head contact, scapula contact and IT contact

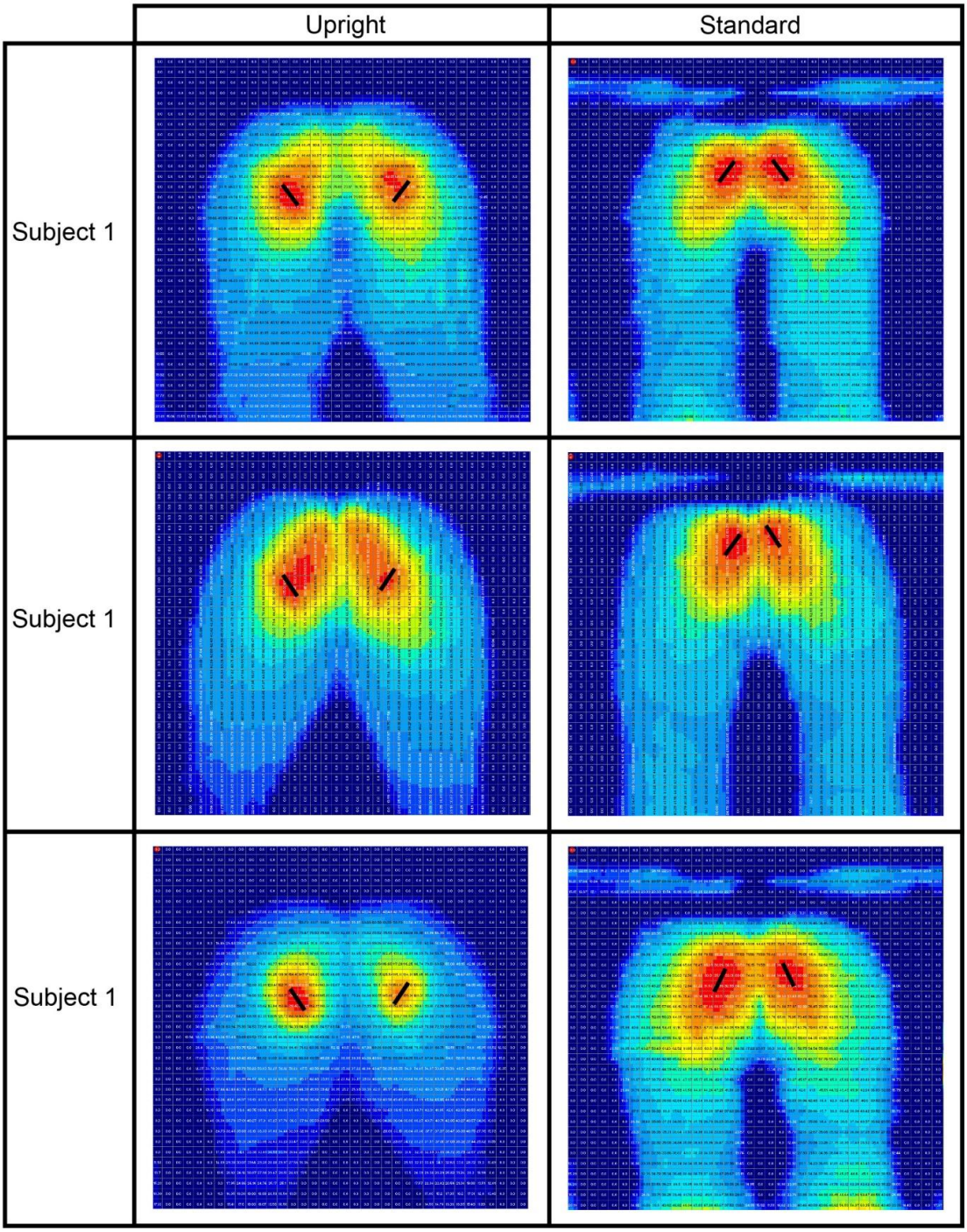

Figure 75 Seat pressure distributions for the Upright and Standard Recline postures for the three 50th percentile male subjects. The black lines indicate the position and orientation of the peak pressure zones

The displacement of the motion tracking sensors (modelled and measured) were used to verify the model's ability to predict the motion paths of the support surfaces, and test hypothesis H2b. Hypothesis H2b required that the model agrees with at least 95% of measured data. The percent

differences in Table 12 did not support the hypothesis, however, the 95% criteria may have been too severe. Although there were high standard deviations for the measured data, the overall trend supported the model predictions. For the standard recline posture, the difference in sensor displacement estimates were no greater than 7 mm. For the TIS 1 posture, where the model displacements were as high as 122 mm, the maximum difference between modelled and measured data was only 14 mm. The greatest difference between the modelled and measured data was for the TIS 2 and TIS 3 postures where it had been assumed that there was no displacement, and hence, the zero values for modelled data.

The motion paths of the model support surfaces are, therefore, assumed accurate. Figure 76 shows the backrest recline motion paths for 5th percentile woman, 50th percentile man and 95th percentile man. The movement of the backrest was defined by μ, d_9, and χ (Figure 77), which was derived in Equations 3, 5 and 6, respectively, in Section 3.1.3. This can be simplified, for example, Figure 78 shows the motion path of the backrest as defined by two points; the top of the backrest and the highest backrest joint, which rotate about the IT at a ratio of 18:17. If the backrest articulated, as with the TIS 1 seating configuration, then the backrest segments would rotate about the upper body linkage joints (Figure 79). For tilt-in-space, the model did not predict any relative movement of the support surfaces other than the whole system tilt, however, the experimental data does suggest some extension of the upper body. In all seating configurations, a leg rest should elevate about the knee joint.

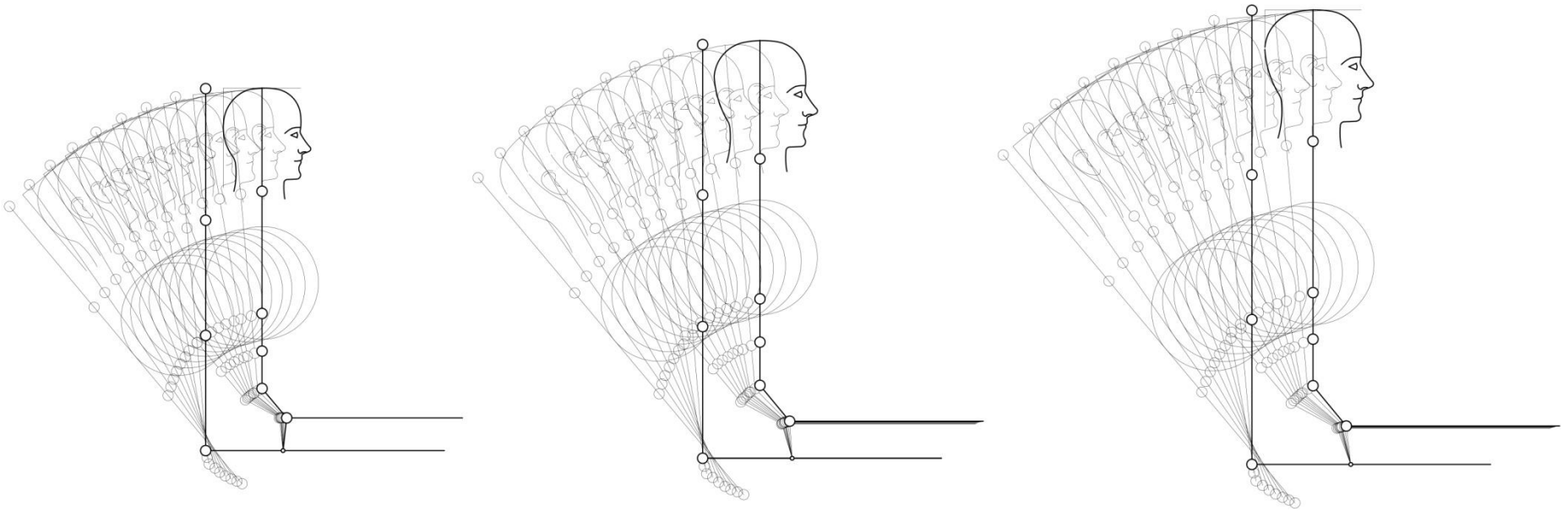

Figure 76 Motion paths for the backrest recline. Left; 5th percentile female model. Centre;50th percentile male model. Right; 95th percentile male model

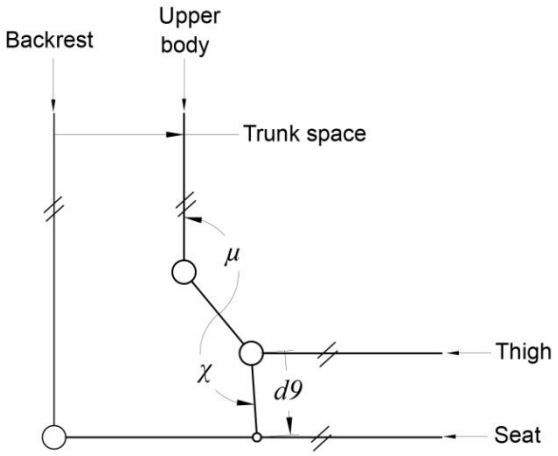

Figure 77 Controlling elements for the backrest recline

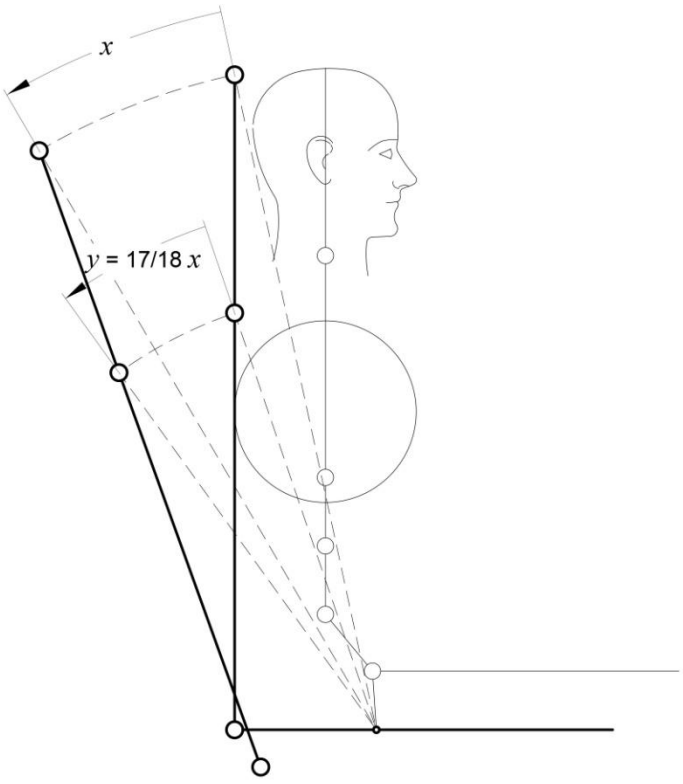

Figure 78 An example of how the backrest motion path can be simplified for the 50th percentile male model. Here, two points on the backrest rotate about the IT at a ratio of 18:17

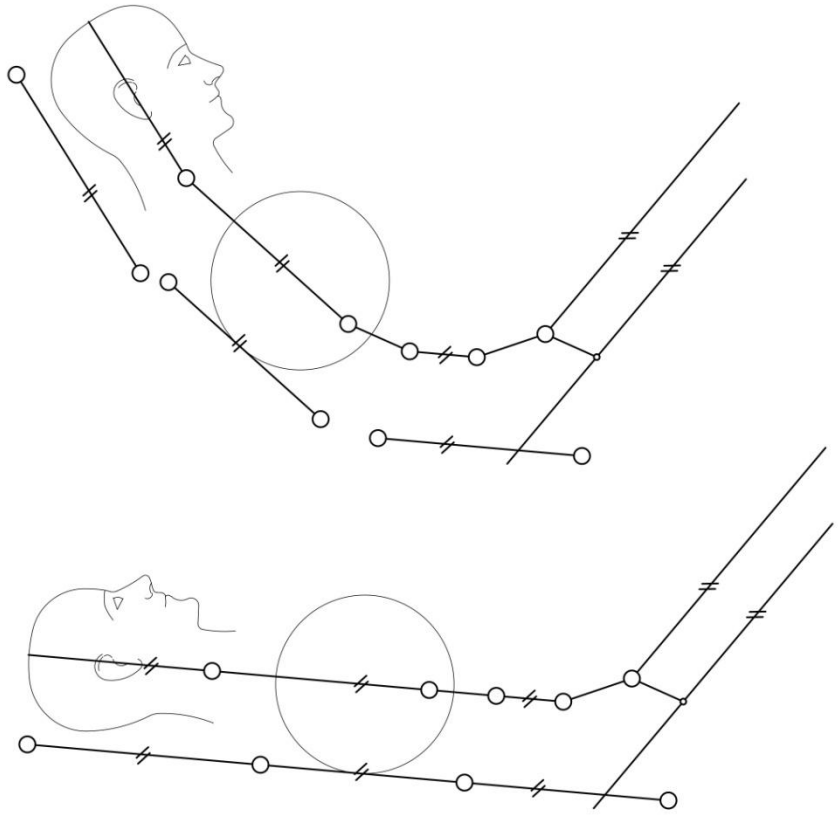

Figure 79 50th percentile model moving from TIS 3 to TIS 1 seating configurations showing the backrest articulation rotating about the model trunk and head linkage joints

6.1.2 Model validation

The findings from this research support the hypothesis H2d, stating that there is a significant relationship and a strong correlation between modelled and predicted force ($p < .001$, $r = 0.92$). Although highly correlated, a full scale error of 15% was found between the predicted and absolute data. To simplify the model and avoid the need for scaling to each individual subject, the model for 50th percentile man was normalised. When comparing the normalised model predictions to normalised measured data, the full scale error reduced to within 10%, which supports hypothesis H2c (FSE = 8%). Normalising also improved the correlation with experimental data slightly ($p < .001$, $r = 0.97$). A heterogeneous group of eight female (height range 1520 mm to 1810 mm) and seven male volunteers (1670 mm to 1860 mm), were used to

test the model predictions. Since no trends were found between root mean squares for gender and height, the model was assumed to be robust across body types.

6.1.3 Relationship between the model and the seated test postures

Significant relationships were found between the model and the experimental data on the test postures, which supports the hypotheses H3b, H4b, and H5b. Relationships were found for all interface pressure variables (peak and average pressure and contact area), height change, and all muscle groups, except for the left side of the multifidus and the iliocostalis. The R^2 values, which specify the amount of variance in the experimental data that is explained by the model, were typically low. The relationships between the model and the experimental data across test postures are discussed further in Section 6.2.

6.1.4 Model sensitivity and related publications

The model developed during this research was assessed against Goossens and Snidjers' model (1995) to test hypothesis H1b. Figure 23 shows the two models side by side to illustrate the modifications. Although the new model is based on standard body segment parameters, modifications have been made to incorporate an additional linkage connecting the hip to the IT (standard data do not include the ITs) and several linkages to provide some spinal mobility. The model also incorporates algorithms that control the position of the pelvis relative to the seated postures and the seat contact of the inferior ITs. The figures in Goossens and Snidjer's manuscript clearly show that the thigh linkage connects the ischial tuberosity to the knee joint. The paper also states that the thigh is parallel to the seat (both thigh and seat inclinations are denoted with β in the manuscript). This leads to large inaccuracies in predicting posture. Figure 23 shows the model in the neutral position and illustrates the thigh linkage, as level with the seat, which positions the knee incorrectly. The model does not include the head segment. In addition, there is no link force for the upper body.

Goossens and Snidjers modelled a relationship between posture and the position of the pelvic linkage based on Equation 36, by Stumbaum (1983) (Figure 23). The inclination of the pelvis was, therefore, a function of the backrest inclination to the ground and did not factor in the trunk to thigh angle, which is known to have the greatest influence on pelvic rotation (Keegan, 1953; Schoberth, 1969; Bashir, *et al*., 2006). Equation 36 may be appropriate for predicting the transference of force; however, it does not model the different seated postures well for the reasons described above.

The purpose of Goossens and Snidjers' model was to predict shear force at the IT only. Goossens and Snidjers derived formulas to determine the inclination of the seat, based on the inclination of the backrest, so that there would be no parallel force at the IT. Table 10 shows these seat inclination values for backrest inclinations ranging from 70° to 86° (Goossens & Snidjers, 1995), and the corresponding predictions for both Goossens and Snidjers' model and the model developed as part of this research. As expected, the parallel force predictions for the Goossens and Snidjers model are very low, which reflects their published results. High parallel forces where predicted from the new model, which reveals its sensitivity. The main reason for the differences between the two models is the position of the ITs. This can be seen by comparing the models in Figure 23. In Goossens and Snidjers' model, the ITs are located almost in line with the upper body, whereas in the new model they are located some distance in front.

To test the model sensitivity on IT position, different postures were simulated with varying pelvic rotations. Goossens and Snidjers' model of 50th percentile man was used for this because of the simple pelvic arrangement. Normal IT force ($F_{n,it}$), parallel IT force ($F_{p,it}$), normal force at the iliac crest ($F_{n,cr}$) and normal force at the thorax($F_{n,th}$) were predicted with no pelvic rotation (ITs directly beneath the upper body), a 5° anterior rotation, a 5° posterior rotation and a 25° posture rotation. These simulations were performed for the neutral posture and the neutral posture tilted 25°. Table 32 gives the results for the simulations and demonstrates that the model is robust against

the IT position in terms of normal force but sensitive in terms of parallel force. A 25° of posterior pelvic rotation in the neutral posture results in a 148 N increase in parallel force and a 184 N increase in parallel force when the whole system is tilted by 25°. This has a direct effect on the support to the iliac crest, as can be seen by the change of $F_{n,cr}$ values. There is negligible change in IT normal force and no effect on $F_{n,th}$.

Table 32 Model simulations to test model sensitivity to the position of the point of seat load transfer

Posture		IT Normal Force (N)	IT Parallel Force (N)	Iliac Crest Normal Force (N)	Thoracic Normal Force (N)
Neutral posture	No pelvic tilt	551	0	0	0
	5° anterior pelvic tilt	551	35	-35	0
	5° posterior pelvic tilt	551	-35	35	0
	25° posterior pelvic tilt	551	-148	148	0
Neutral posture tilted 25°	no pelvic tilt	543	61	48	124
	5° anterior pelvic tilt	543	97	15	124
	5° posterior pelvic tilt	543	25	80	124
	25° posterior pelvic tilt	540	-87	181	124

The model developed during this research has been shown to accurately predict posture, pelvic position and the location of peak pressure at the seat for the upright seating configuration. Experimental data simulating the Goossens and Snidjers model suggest, however, that the model is predicting parallel forces that may be too high. Elaboration of these findings showed the model is sensitive to the point of load transfer to the seat. Since the load transfer must be assumed to be the point of maximum pressure, and that this location has been successfully modelled for the upright posture, the parallel forces, predicted by the model, either do not exist or they are present but are resisted by the soft tissues surrounding the pelvis. Goossens and Snidjers used a force plate with strain gauges to measure the gross effect of posture on the entire seat, which may not detect local shearing in the soft tissues between the seat and the

pelvis. It has not been the objective of this study to assess shear, however, given its importance in pressure ulcer prevention, these issues are worth discussing.

In terms of predicting normal force, the model has shown a significant relationship with measured data and, therefore, has the potential to be a valuable tool for comparing and interpreting the related published literature. For example, two recent publications, with similar aims, have arrived at different conclusions. The first is by Sprigle, *et al*., (2010) who used pressure mats to measure force at the seat and backrest for varying degrees of tilt-in-space, back recline, and stand assist features in wheelchairs, using a specially constructed test-rig. The second is by Giesbrecht, *et al*., (2011) who used pressure mats to measure interface pressures for incremental degrees of tilt-in-space. Both studies arrived at relationships, one for force reduction and one for pressure reduction, with changing tilt angles. Sprigle, *et al*., concluded that a linear relationship exists, and Giesbrecht, *et al*., concluded that there is a quadratic relationship.

The model that was developed for this study was configured to the test postures described in the two publications and incorporating the mean stature and weight of the subjects who participated in the studies. Simulations were then carried out at various increments of tilt-in-space to determine the relationship of seat force and tilt angle. The results for the simulation of Giesdrechts', *et al*., postures were in agreement showing a quadratic relationship (R^2 = 0.99) (Figure 80). Figure 81 shows the results of the simulations of Sprigle's, *et al*., postures for tilt-in-space and recline. For recline, a linear relationship exists (R^2 = 0.98). For tilt-in-space, the model supports Sprigle's, *et al*., conclusions with a linear relationship (R^2 = 0.94), however, the true relationship is better described as a quadratic (R^2 = 0.99). Linear relationships were found between the change of predicted force and backrest angle. To conclude, based on the model predictions, a linear relationship exists between force on the backrest and the inclination of the backrest for both tilt-in-space and back recline, and for the seat for back recline. However, for the

seat, the relationship is better described with a quadratic equation. The model developed for this study has helped to explain an existing conflict in previously published research.

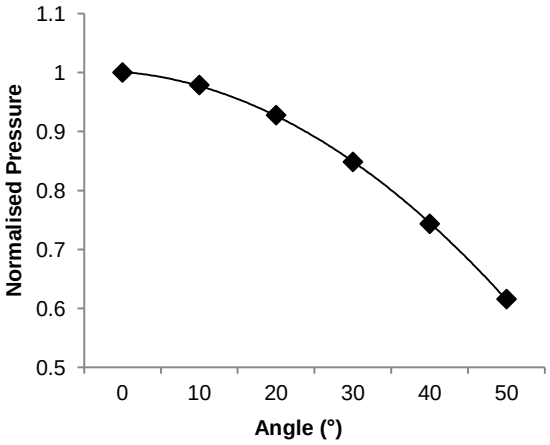

Figure 80 Model predictions for normalised pressure for the tilt-in-space postures described by Giesbrecht, *et al*., (2011). The tilt angle is measured from the horizontal to the seat. A quadratic curve is fitted to the predicted data

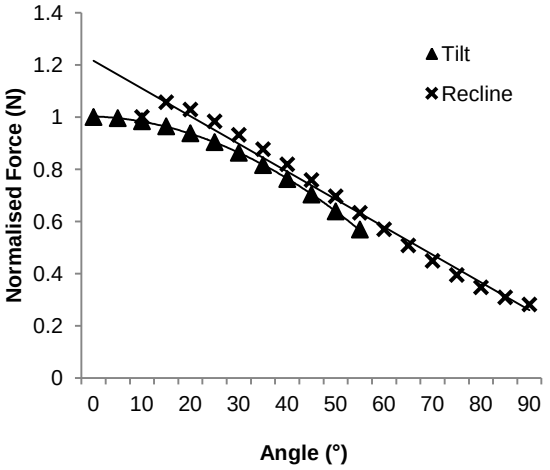

Figure 81 Model prediction of normalised seat force for the tilt-in-space and recline postures described by Sprigle, *et al*., (2010). The angle change for the tilt-in-space posture is measured from the horizontal to the seat and the angle change for the recline posture is measured from the vertical to the backrest. A quadratic curve is fitted to the predicted tilt-in-space data and a linear regression line is fitted to the predicted recline data

6.2 Interpretation of the seated test postures

This section discusses the experimental findings across the seated test postures. Reference is made to the biomechanical model to aid in interpretation. The section is concluded with consideration as to how the findings and concepts developed during this research could impact on current applications and future research.

6.2.1 Interface pressure

Significant differences in interface pressure were found between all postures, which support hypothesis H3a. Orientation of the upper body had the most significant effect on peak pressures, with a 65% decrease for the TIS 3 posture ($p < .001$), followed by the TIS 1 posture at 43% ($p < .001$). No difference in peak pressure index was found between the standard recline and TIS 2 postures, which was expected since they had similar upper body inclinations. Peak pressure index of these postures reduced by 40% ($p < .001$). Figures 56-60 gave the model predictions and the measured interface pressures for the test postures of this research. Peak pressure index values showed more sensitivity to posture change than the total seat force predictions. The relationship was significant ($p < .001$), so hypothesis H3b is supported.

A significant relationship exists between seat force predictions and average pressure, however, unlike peak pressure index, average pressure was more robust to the effects of posture than force predictions. In general, the order of differences was the same as for peak pressure index. There was a significant relationship between predicted force and measured seat contact area for the test postures, however, it could be seen that the contact area for the upright and standard recline postures was lower than predicted force (Figure 58). The explanation for this is the different methods employed for supporting the lower legs. For upright, the feet were supported on the ground. Using a wheelchair, Peters (1999) showed an 11% increase in IT pressure when the feet where supported by footplates compared to no support. Peters explained that this is

because there is less seat contact area when the feet were supported, and hence, higher pressure. It was logical, therefore, that there was less contact area for upright which was reflected in the measured contact area data but not the predicted force. For the standard recline posture, it was also logical that the use of the separate footstool may have lifted the thighs and consequently reduced the thigh contact area. For the TIS 1, TIS 2 and TIS 3 postures the feet were unsupported but the lower legs were supported by a leg rest integral to the test-rig. The knees were flexed at approximately the same angle for these three postures. The difference in seat contact area for the tilt-in-space postures could be explained by the difference in seat loading, which was supported by these results.

Significant relationships were found between the backrest force predictions and the backrest average pressure ($p < .001$) and contact area ($p < .001$). As with the seat, the model force predictions show more sensitivity to posture change than average pressure. For the pressure testing, the TIS 1 posture was measured twice. Once with the backrest articulated before the subject entered the test-rig (TIS 1) and once after the subject had been tilted (TIS 1a). The design of the backrest articulation was relatively unsophisticated, achieved with pivots located at the intersections of the three back segments (head, thoracic and lumbar support). It was therefore expected that the supports would not move in synchronisation with the subject and that this would affect the interface pressure distributions. When comparing TIS1a to TIS 1, the peak pressure index increased ($p < .001$), seat average pressure increased ($p < .001$) and seat contact area increased ($p < .001$). No statistical difference was found between the TIS 1 and TIS 1a for either the average pressure or contact area at the back. The increase in both seat pressures and contact area indicate that the subjects were being compressed when articulating the backrest after tilting, which confirmed that the motion paths of the backrest supports where independent of the movement of the subjects as they flexed their upper body. This was not detected in the backrest pressure distribution due to the relatively high load already in this region of the test-rig.

Sprigle, *et al*., (2010) measured seat and backrest forces using pressure mats. They found that, for a tilt angle of 55°, seat loading reduced by 48%. Using the biomechanical model configured to simulate Sprigle, *et al*.'s test conditions, a 43% reduction in seat force was found. Sprigle, *et al*., also evaluated a backrest only recline system, and found a 61% reduction in seat load when the backrest reached the horizontal (90° back from vertical). The model predicted a 72% force decrease for the same posture. The feet were supported for these simulations.

The same model simulations where performed with the feet unsupported. Figure 82 shows the results, which were in better agreement with Sprigle, *et al*. At the terminal positions, the model predicted a 46% reduction in seat load for the tilt-in-space posture and a 57% reduction for the backrest recline.

Although Sprigle, *et al*., collected data from only six able-bodied subjects (two men, four women), these findings gave further verification to the biomechanical model. This comparison also demonstrated the effect of support to the feet. When the biomechanical model simulated conditions with feet supported, there was only one seat force below the ITs. When the feet were unsupported, the model simulated the lower legs sliding with a second seat force behind the knees. Figure 82 shows that the standard recline posture was more sensitive to foot support than the tilt-in-space posture. This was because the model predicted posterior pelvic rotation for the standard recline but not for tilt-in-space (the seat and backrest angle does not change). So for postures with supported feet, where the only contribution to total seat force was at the ITs, the orientation of the pelvis had a greater influence. These data show that posterior rotation of the pelvis reduced normal force predictions.

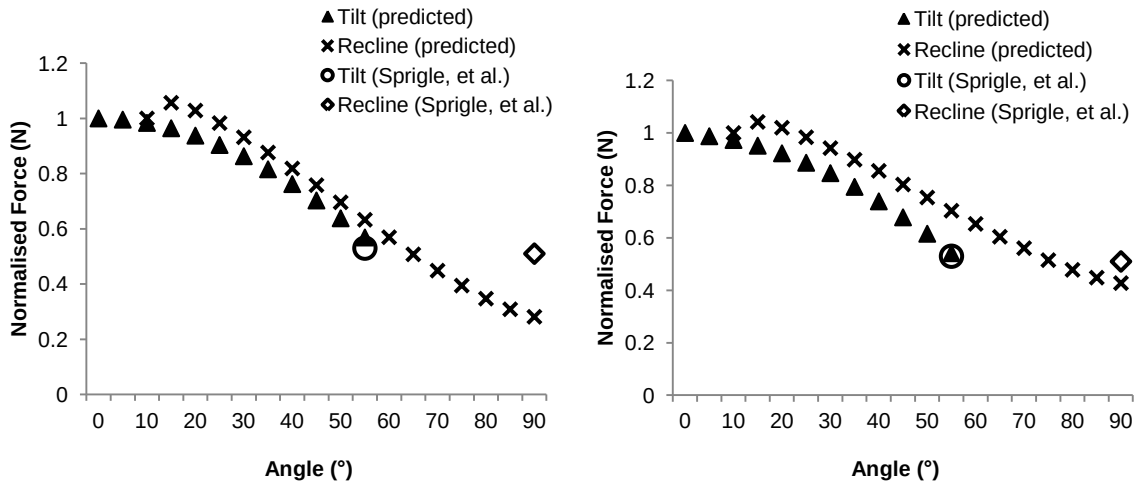

Figure 82 Model predictions of normalised force and measured normalised force (from Sprigle, *et al*., 2010) at terminal positions for tilt-in-space and backrest recline systems, with feet supported (Left) and feet unsupported (right)

Giesbrecht, *et al*., collected interface pressure data from ten tetraplegic and eight paraplegic individuals for increments of tilt-in-space. Their data are shown in Figure 83 along with the model seat force predictions for the same postures. Force predictions were related to the paraplegic data ($p < .001$, $R^2 = 0.97$) and tetraplegic data ($p < .001$, $R^2 = 0.99$). The rate of pressure reduction was greater than force reduction and greater for the tetraplegic subjects than the paraplegic subjects. Based on these data, peak interface pressure was likely to be more sensitive to posture change than the total force predictions.

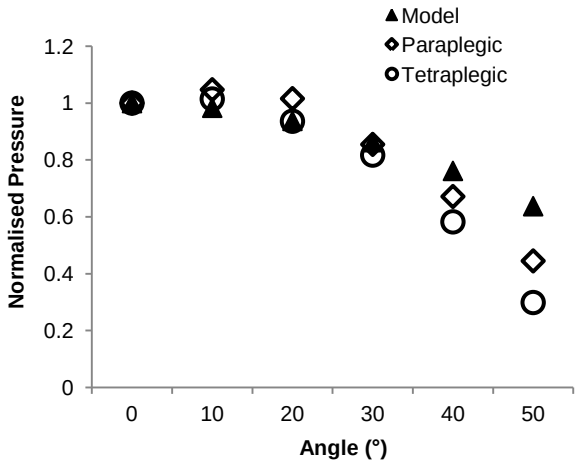

Figure 83 Model predictions of normalised force and measured normalised peak pressure index (from Giesbrecht, *et al*., 2011) at incremental positions for tilt-in-space

Interface pressure distributions are important in seating design, and have been described as the biomechanical correlation to comfort (Gross, *et al*., 1994). Various techniques have been employed to improve pressure distributions such as the selection of cushioning materials and contouring. Posture was also considered important. The application of the biomechanical model to the interpretation of experimental interface pressure collected during this research, and from previously published research, has highlighted some effects from supporting the feet and the lower legs. For example, it is possible that the IT interface pressures could be lower for the standard recline posture by supporting the lower legs in a similar way to the tilt-in-space postures where the knees are flexed allowing the thighs to drop fully onto the seat. This could increase contact area and lower interface pressure, since pressure is load per unit area. The biomechanical model has also shown that the orientation of the pelvis had an effect on IT force. Earlier, in Section 6.1.4, the orientation of the pelvis was shown to be important for the model, as high parallel forces were associated with pelvis rotation. It was postulated that, based on the biomechanical model, anterior pelvic rotation positioned the point of load transfer to the seat beneath the ITs. This in turn increased the normal force and decrease the parallel force which maybe important for reducing shear in the soft tissues, an important risk factor in pressure ulcer formation (Guttmann, 1976). The most significant effect on interface pressure was the TIS 3 posture. A quadratic relationship between tilt angle and pressure reductions was predicted which

corroborated previous research (Giesbrecht, *et al*., 2011). The TIS 1 posture was also effective at off loading the seat, however, the pressure distributions showed that the motion paths were interrelated with force and not synchronised with the body as it flexed. The standard recline posture also demonstrated significant reductions in seat pressures. The model predicted a linear relationship between the backrest recline angle and force reduction which agree with the study of Sprigle, *et al*. (2010).

Summary

Data collected during this study showed that the method of support to the lower legs and feet affected seat interface pressure. The model predicted that the orientation of the pelvis also affected interface pressure. The contribution of pelvic orientation to total force was greater when the lower legs or feet were supported in a way that lifts the knees. The standard recline posture was effective in reducing force, but a feature of this was a posterior translation of the point of load transfer away from the IT and towards the sacrum which might have increased shear. A quadratic relationship was confirmed between tilt angle and change in total seat force, whereas, there was linear relationship for backrest only recline. Comparison of the TIS 1 and TIS 1a postures demonstrated the support surface motion paths were inter-related with force and that they were not synchronised in the test-rig.

6.2.2 Stadiometry

Results from this investigation showed that stature increased for all sitting postures, in the following ascending order; upright and standard (similar mean values), TIS 1, TIS 2, lying and TIS 3. Significant differences were found between the upright and standard recline postures, and lying and the TIS 3 postures (Table 19), which supports hypothesis H4a.

Model predictions for spinal loading showed similar values for the standard recline and TIS 2 postures, which reflected the inclination of the upper body. The stadiometry results, however, indicated that the spine was recovering less in the standard posture than the TIS 2 posture. One possible explanation was differences in spinal curvature. Theoretically, the larger seat to backrest angle should have resulted in a larger hip angle which would have reduced lumbar flexion (Keegan, 1953; Bashir, *et al*., 2006). Differences in spinal curvature, specifically differences in the relative angular position of the vertebral endplates, influence load transmission and intradiscal pressure (Nachemson, 1960). Adams and Hutton (1986) showed, using cadaveric experiments, differences in diffusion rates between flexed and extended spinal motion segments. There were no differences measured in lumbar curvature, however, between the standard recline posture and TIS 2 which would otherwise support this. Another explanation could be higher back muscle activity for the standard reline posture which could have contributed to spinal loading, however, neither model predictions nor measured sEMG activity supported this explanation.

These findings are potentially important for seating ergonomic theory. The rate of spinal recovery for the standard recline and the upright postures were similar as they share similar mean values. However, when considering the statistical differences between these postures and TIS 3 and lying, the standard recline posture exhibited the least recovery. There are many chairs available that recline to this posture, which some manufacturers claim has stress relieving characteristics. Results from this study suggested that the standard recline posture would not improve spinal recovery when compared to chairs that do not recline.

Lying was included in this investigation. For this posture subjects lay supine on a treadmill with their legs extended. This phenomenon was not modelled, but if one considers only inclination of the upper body, then it follows that lying supine and the TIS 3 posture should result in similar rates of recovery. This was not the case and, although not statistically significant, the means indicated greater recovery for the TIS 3 posture than lying. Lying was also included in the sEMG

study, and for the multifidus muscle group significantly higher activity on both sides were recorded for lying than the TIS 3 posture (left: $p < .001$; right: $p < .01$). It was likely that, because the legs were extended, the lumbar spine would have been extended with no support from the flat surface of the treadmill. The combination of the weight of the trunk and the absence of support to the lumbar spine may have resulted in the multifidus muscles being recruited to act as a splint. The possibility of the paraspinal muscles splinting unstable areas of the spine had been previously proposed (Nouwen & Bush, 1984; Dolce & Raczynski, 1985). For the TIS 3 posture the hips were flexed, which was likely to have flattened the lumbar spine, increased support, reduced load and promoted recovery. In addition to other biomechanical factors, the transfer from the test posture to the stadiometer could have influenced the results. For all seated postures, the transfer from the test-rig to the stadiometer was consistent. For lying supine, volunteers lay on a tread mill which resulted in a different transfer movement to standing from the test-rig. Haslegrave, *et al*., (1989) found that stature could change very rapidly after a transfer from the load condition.

Of all the postures tested, the TIS 3 posture caused the maximum spinal recovery, with significant differences when compared to the upright and standard recline postures. These findings were supported by the biomechanical model. If one accepts that unloading the spine has the potential to relieve pressure on the sacroiliac joints, the zygapophysial joints, the intervertebral discs and the spinal nerve or its roots resulting from disc prolapse, then it is plausible that the TIS 3 posture could have the potential to relieve lower back pain whilst a person is reclined in this position. Pseudo-medical backcare chairs are currently on the market that offer this position (for example, the Backsaver™ Recliner, Backsaver Products Co., California, USA). Although beyond the scope of this thesis, the evaluation of patients with low back pain using a modification of this protocol would be a logical step towards understanding how these different seating postures could affect spinal loading, and pain.

Model predictions for the tilt-in-space postures were in approximate agreement with the stadiometry data. There was no significant difference in spinal recovery between the TIS 2 and TIS 3 postures, however, the TIS 2 posture had the same limitation that the head was orientated too far back for general use. The use of a headrest to bring the head forwards could potentially address this, however, it may not be desirable if it causes excessive localised flexion of the C7/T1 area, which could become uncomfortable over time.

The TIS 1 posture was conceived to deliver a tilt-in-space posture with good head position where flexion is shared across the entire spine. The interface pressure data have shown that the motion paths of the test-rig supports were not synchronised with the body. Support surfaces that follow the correct motion paths of the body are likely to result in a better fit and less compression of the subject between the back and seat, and this could improve spinal recovery for the TIS 1 posture. It was anticipated that there would be less load on the lumbar spine for this posture when compared to the TIS 2 posture, because this region is more horizontal. The results from the model showed the opposite trend with more loading for the lower lumbar segment. The model assumed no parallel force from the supports for the upper body so additional load that may be supported by the backrest was transferred to and passed down the linkages, resulting in higher link forces. It was necessary to assume no parallel forces from the upper body supports for the model to be statically determinant. This assumption renders the model inconclusive in terms of differentiating loading between the spinal segments, and is a limitation of this study.

Although the statistics showed no effect for the TIS 1 and TIS 2 postures, there appeared to be a trend, i.e. stature increased as tilt-in-space increased. In order to determine if this experiment had an appropriate sample size, a *post hoc* power analysis was performed using PASS software. The test implemented a power analysis for a *t*-test model. The difference between means and standard deviations were obtained from the standard recline and TIS 1 postures (Table 20). The mean difference was 0.687 and the standard deviation of this differences was 1.471. To achieve

a power greater than .8 for an alpha level of 0.05 required a sample size of 36. This basic paired *t*-test power analysis makes the point that given the variability of the stadiometry data, a lower effect size resulted, which suggests a larger sample size would be prudent. Because the p-value was not less than 0.0033 (including the Bonferroni correction) between the standard recline and TIS 1 postures, a significant difference was not demonstrated, however, since the power was low (i.e. < .8), it cannot be stated that definitely no difference exists. Results from the *post hoc* power analysis indicate that, if the stadiometry investigation was performed with a sample size of 36 test subjects, that the power would be adequate to detect an effect between the standard recline and TIS 1 postures. Based on these findings, there was no statistical significant difference for the TIS 1 and TIS 2 postures, as tested. *Post hoc* power analysis suggested that a larger sample size study employing stadiometry was warranted.

Significant inverse relationships were found between precise measurements of stature change, using the stadiometer, and the model predictions of axial loading of the lower lumbar spine (p < .01), upper lumbar spine (p < .05), thoracic spine (p < .05), and total spine (p < .01). Hypothesis H4b is therefore supported. Low R^2 values between modelled and measured data were obtained, which demonstrated that the model explained less than 10% of the variance in stadiometry data. The high variance exhibited in the stadiometry data (Figures 61-64) was a likely explanation which is a limitation of the technique (Van Dieën and Toussaint, 1993; Kanlayanaphotporn, *et al*., 2003)

Table 33 presents the data from this study and two others, where high coefficients of variation can be seen throughout. Van Dieën and Toussaint (1993) questioned the validity of stadiometry as a means of assessing various load conditions on the spine because of the high inter-subject variability. Kanlayanaphotporn, *et al*., (2003) recommended that subjects that differed in the presence of back pain, age, and gender should not be combined for statistical analysis of spinal creep and recovery. In the present study, no subjects had back disorders and a heterogeneous group of volunteers was selected. It is probable that data with lower variability and higher

statistical power would have been obtained from a more homogeneous group, but this would have compromised the extrinsic validity or generalisability of the study.

Table 33 Comparison of variance in the stadiometry data with previously published data

Study	Experimental treatment	Height change (mm)	Standard Deviation	Coefficient of Variation (%)
Tyrrell *et al.* 1985	2.5 kg rucksack	2.94	1.44	49
	10 kg rucksack	4.23	1.74	41
	10 kg barbell	3.9	1.71	44
	20 kg barbell	5.24	2.92	56
	30 kg barbell	7.37	3.99	54
	40 kg barbel	8.9	3.77	42
Althoff *et al*. 1992	Straight sitting without backrest	1.1	1	91
	Relaxed sitting without backrest	2	0.8	40
	Office chair with lumbar support	2.1	0.8	38
	Forward inclined seat with vertical backrest	2.3	1.3	57
	Forward inclined seat and forward inclined backrest	2.1	1.3	62
	Balans chair	2.5	1.6	64
	Balans chair with additional lumbar support	3.3	1.7	52
	Office chair with 30° inclined backrest and arm support	4.3	0.9	21
Present study	Upright	1.86	1.24	66
	Standard Recline	2.15	1.25	58
	TIS 1	2.78	1.57	56
	TIS 2	3.11	1.72	55
	TIS 3	4.22	1.5	35
	Lying	3.57	1.45	41

Other factors may have contributed to the high variance. It was observed during the investigation that subjects became fatigued before the end of the test session. Each subject was required to participate in the testing for 16 hours over two consecutive days, which was physically demanding for some. Eklund and Corlett (1984) reported that motivation, ability to concentrate, carefulness, and body awareness were factors that influenced the test results. The *a priori* power analysis for this investigation was based on data from Althoff, *et al*., (1992) who measured height change for various sitting postures, but on different days for each posture. This protocol may have improved the subject's concentration levels and proprioception during the measurements

which may explain why a sample of only nine subjects was calculated to detect the effect in their data. Althoff, *et al*., used a heterogeneous group of subjects.

The possibility of heel pad compression may have influenced the data. Foreman and Linge (1989) showed that heel pad tissue can compress between 0.8 and 8.9 mm. In the present study the heels were uncompressed during the test postures and compressed during measurements which may have contributed to the variance.

Although there are limitations with the stadiometry method, it has been used extensively in ergonomic research, and several studies have demonstrated good reliability (Rodacki, *et al*., 2001; Kanlayanaphotporn, *et al*., 2003; Healey, *et al*., 2005; Pennell, *et al*., 2012).

Summary

The standard recline posture showed no improvement over the upright position, which is potentially important for seating ergonomic theory. Spinal recovery from load in supine lying was inhibited when the lumbar spine was not supported. The TIS 1 posture might have been affected by incorrect seating motion paths. With correct motion paths, more recovery may occur based on the degree of tilt. Model predictions for this posture were inconclusive due to the absence of parallel forces in the backrest. The TIS 3 posture showed significant increases in height as measured by stadiometry and, therefore, may have applications for individuals with low back pain to reduce spinal load and pain experienced by these patients. A future study of the low back pain population is warranted.

6.2.3 sEMG

Significant differences were found between seating postures for all muscle groups ($p < .001$) and hence hypothesis H5a is supported. It was hypothesised that the myoelectric activity would change with respect to backrest inclination based upon the understanding that the paraspinal muscles support the spine, as informed by previous research (Andersson, *et al*., 1974[a-f]). Although changes in myoelectric activity were recorded with different backrest inclinations, the recruitment patterns could not be simply explained by load magnitude.

In general, the trend has been for muscle activity to reduce as the inclination of the upper body orientates to the horizontal and was, therefore, associated with changes in spinal load. One exception was lying, where muscle activity was recorded to be higher than the TIS 3 posture. Another observation was that the standard recline and TIS 1 postures exhibited relatively low muscle activity compared to TIS 2 (Figures 68-71). The model predicted similar values for the standard recline and TIS 2 postures for $F_{n,l}$, $F_{n,th}$ and $F_{n,sh}$, which reflected the inclination of the upper body (Figures 66 and 67), but very different values for F_{net} (Figure 65). For this model force, high values were predicted for upright, TIS 2 and TIS 3, but negligible force for the standard recline and TIS 1. F_{net} was a net force modelled to represent the sum of pelvic stabilising forces arising mostly from tension in the posterior spinal ligaments (Section 3.1.5). Tension was assumed when the ligaments resist pelvic rotation caused by the large passive forces that arise from the posterior thigh and gluteal muscles when the hip flexes (Keegan, 1953; Schoberth, 1969; Bashir, *et al*., 2006). In the context of relaxed sitting in chairs with backrest, pelvic rotation is resisted by fixation of the upper body. The model predicts larger angles between the lower part of the spine and pelvis for the standard recline and TIS 1 postures and hence less tension in the posterior spinal ligaments, which explains the values for F_{net}.

From observation of the trend in the force F_{net}, and the trend in the muscle activity, one could postulate that there is a link which would implicate lower than expected sEMG activity for the standard recline and the TIS 1 postures. The alternative is to consider that there is higher than expected sEMG activity for the TIS 2 posture and that this may not be related to load or the biomechanical model. Heart rate was monitored during this study as a quality control for the sEMG. It was found to be significantly higher for the TIS 2 posture than all other reclined postures (Figure 72) so it is possible that ECG could have elevated the sEMG data for the TIS 2 posture. This was not the case, as evident in the sEMG data for the iliocostalis left side (Figure 69), where ECG contamination was most apparent pre-filtering (Figure 35).

One other study was identified which investigated the effects of tilt-in-space on muscle activity (Nwaobi, 1986). This study investigated individuals with cerebral palsy whose distribution, type and intensity of muscle tone were classified as having spastic diplegia, with mild to moderated involvement. Two seating positions were investigated: an upright position and a 30° tilt-in-space position (similar to the TIS 2 position in the present investigation). Although the paper states that electrodes were located on the iliocostalis lumborum, it did not explicitly state where they were placed. EMG values taken at this region were significantly higher for the 30° tilt position than upright (Nwaobi, 1986). This was in agreement with the results from the current investigation for the TIS 2 posture. In order to understand why there was relatively high myoelectric activity for this posture; consideration is now given as to how tilt-in-space might affect sensory-motor control, and possible psychophysiological stress.

The sensory motor control system depends on input from various sensory stimuli. Haptic cues from cutaneous receptors at the skin surface, vision, the sense organs of the labyrinth and proprioception are all important components of the sensory-motor control system which tend to work in a concordant manner (Matthews,1988; Howard & Childerson, 1994). A possible

explanation for why the TIS 2 posture generated high muscle activity and increased heart rate is that these sensory systems may have been discordant.

The TIS 2 posture can be characterised as half way between an upright posture and a full tilt-in-space posture (where the upper body is almost horizontal). This 'half way' position might result in an ambiguity of contact forces at the seat and backrest, with neither positive pressure from the seat or backrest providing the necessary somatosensory information of body orientation in space. With the full tilt-in-space position (TIS 3) it is likely that more pressure will be perceived from the backrest. Myoelectric activity and heart rate were significantly less for the TIS 3 posture than the TIS 2 posture.

Head displacement may be an important consideration. For the TIS 1 posture, the backrest articulated to maintain a relatively functional head position. The myoelectric activity and heart rate for this posture was significantly less than the TIS 2 posture. Head displacement would have the greatest effect on sensory information pertaining to vision and the labyrinth.

The subjects in this study were instructed to keep their arms rested on their bodies for the tilt-in-space postures. Since there was no other difference in seat configuration other than tilt angle, the relative position of body parts would have been very similar to a normal upright sitting position. With no apparent change in muscular proprioception for the tilt-in-space posture, the concept of sensory discordance associated with these postures is strengthened. It would be interesting in further research to repeat the measurements with the volunteers having their hands placed on the armrests which are fixed relative to the ground. In several other studies it was shown that fingertip contact to a rigid surface helped to stabilise and control human posture, and reduce EMG activity (Jeka & Lachner, 1994; Holden, *et al*., 1994; Jeka & Lackner, 1995; Lackner & DiZio, 2000). Based on these findings, hand contact on armrests that are fixed relative to the

ground for the tilt-in-space postures may play an important role in postural control and position sense.

Significant relationships were found between model force and sEMG activity, for the multifidus right side ($p < .05$), longissimus both sides ($p < .001$), T8 left ($p < .001$) and T4 left ($p < .01$), which support hypothesis H5b. Although significant, the relationships were weak, with the model explaining between 16% and 29% of the variance in the experimental data, depending on the muscle group (Table 27).

Summary

sEMG activity generally reduced as the upper body orientated toward the horizontal, which favoured the TIS 1 and TIS 3 postures. Lumbar sEMG activity in supine lying was increased, which was probably to splint the unsupported lumbar spine. Low sEMG activity may be present in postures with larger pelvic-lumbar angles (TIS 1 and standard recline) due to reduced tension between these two structures as inferred by the model. There was high sEMG and heart rate for TIS 2, possibly due to discordance of the sensory-motor control system. Articulation of the backrest significantly reduced sEMG and heart rate for tilted postures, possibly because of the improved head orientation.

6.2.4 Spinal curvature

The biomechanical model was developed to predict posture and load distributions internally along the segment axis and externally between the model and support surfaces. The model was not developed to predict lumbar and thoracic curvature, since this would require representation of each motion segment. However, data were collected on the back profiles of the same cohort of subjects across the same seated test postures to build a comprehensive set of biomechanical

data. The Flock of Birds motion capture system was used because in addition to spinal curvature, data were required on the test-rig and the relative position of the sensors to the supports which were used for building the model, to verify postural accuracy and determine the motion paths of the supports. Previous studies showed that the Flock of Birds motion capture system is a reliable and valid method for obtaining kinematic data (Umberger, *et al*., 1999; Koerhuis, *et al*., 2003). The initial tests undertaken as part of this investigation were to confirm reliability within the current test conditions. Results presented in Table 23 and 11 demonstrate that there is good repeatability for lumbar curvature with coefficients of variation ranging between 4-9%. Measurements of thoracic curvature were found to be less repeatable with coefficients of variation ranging between 0-25%. Tests were also carried out to validate the Flock of Birds data using the Flexicurve technique. This was only done for maximum extension and flexion for lumbar curvature. The Flock of Birds data was in good agreement with the Flexicurve profiles for maximum flexion with root mean square errors (RMS) of 2° and 3°. However, the Flock of Birds data was found to overestimate lumbar curvature for maximum extension with RMS errors of 36° and 43°. This was probably due to a combination of skin motion artefact between the sensors and underlying bony landmarks, as well as movement between neighbouring sensors and cables. The maximum extension posture, therefore, was not included in subsequent testing. The study by Dolan, *et al*. (1988) suggested that sitting postures flex the spine when compared to standing. Therefore, for the present experiment, measurements were made at varying degrees of flexed postures relative to standing, with standing representing zero flexion for normalisation.

A significant difference was found for % lumbar ($p < .001$) and % thoracic flexion ($p < .001$) which supports hypothesis H6. The TIS 1 posture resulted in significantly more flexion than all postures, as expected (Figure 73). The upright posture was found to exhibit the least flexion compared with all other sitting postures, which was statistically significantly when compared to TIS 1, TIS 2 and TIS 3 postures. The TIS 2 and TIS 3 postures were both found to have approximately the same lumbar curvature, which was probably the maximum flexion allowed by the backrest. For these postures, more of the upper body weight may have been transferred to the backrest which would

have had the effect of pressing the spine into the backrest shape hence discriminating these postures from upright. There was no significant difference in mean lumbar flexion for the standard recline posture and upright posture. It was expected that there would be less flexion for the standard recline posture because of the larger trunk to thigh angle. A possible explanation could be the legs being supported by a footstool where the knees were extended. This could have created extra tension on the hamstrings and stretched the posterior thigh muscles which might have rotated the pelvis further backwards. Without support from the backrest to the pelvis and lower lumbar spine this could have flexed the spine.

All of the sitting postures, except for unsupported sitting, exhibited less thoracic flexion than the TIS 1 posture (Figure 73). This suggested that all of the sitting postures had the effect of flattening the thoracic spine. This was probably due to the head and shoulder girdle being fully supported on a flat plane. As more weight was transferred to the backrest, the thoracic spine became flatter, with the exception of the TIS 1 posture where the backrest was not straight.

All of the sitting postures measured exhibited lumbar flexion. Adams, *et al*., (2006) argued that flexed postures offer several advantages over lordotic postures providing that the flexion is moderate. Flexed postures have been shown to reduce the compressive loading acting on the zygapophysial joints, and orientate the articular surfaces so they are parallel to each other resulting in low and evenly distributed contact stresses (Adams & Hutton, 1980). Lordotic postures increase compressive loading on the zygapophysial joints (Adams & Hutton, 1980), and concentrate stresses in the inferior margins of the articular surfaces and on the tips of the inferior processes (Dunlop, *et al*., 1984; Shirazi-Adl, 1991). Pynt, *et al*., (2008), on the other hand, argue against flexed postures, explaining that they narrow the disc due to creep loading, which increases loading on the zygapophysial joints (Yang & King, 1984). For people who have back pain which originates in the zygapophysial joints, a tilt-in-space posture that flexes the spine

could be beneficial since it may relieve load on the zygapophysial joints with less risk of narrowing the disc space than upright sitting.

Flexed postures may also help aid intervertebral disc nutrition. It is known that the supply of metabolites to cells within the intervertebral disc is barely adequate for normal requirements (Maroudas, *et al*., 1975; Urban, *et al*., 1977; Stairmand, *et al*., 1991) and impaired metabolite transport is associated with disc degeneration (Nachemson, *et al*., 1970; Holm & Nachemson, 1982,). One of the transport mechanisms for nutrients into the disc is diffusion. The amount of metabolites that can diffuse into the disc is dependent on the distance to the nearest blood vessel on the disc's surface or in the vertebral body. Compared to erect standing, flexed postures stretch the posterior anulus by 60%, and compress the anterior anulus by 35% (Adams & Hutton, 1982; Pearcy & Tibrewal, 1984). There is a corresponding thinning of the posterior anulus and a thickening of the anterior anulus. Flexion therefore reduces the diffusion path length into the posterior anulus. This has been shown in cadaveric experiments (Adams & Hutton, 1986), and in measurements of diffusion into living discs (Urban, *et al*., 1977).

In addition to enhancing diffusion, the stretched posterior anulus has an increased surface area resulting in a greater flux of metabolites being 'funnelled' into the inner posterior anulus (Adams & Hutton, 1986). Flexion will cause the opposite effect in the anterior anulus (Adams & Hutton, 1986) but this is the last region of the disc to show degenerative changes (Adams, *et al*., 2006). Pynt, *et al*., (2008) refer to these studies arguing against flexed postures because they exhibit more creep loading, due to a higher rate of expulsion of fluid from the discs when compare to lordotic postures. For the tilt-in-space postures, greater rates of spinal recovery have been shown which was probably due to osmotic swelling of the discs. In these positions, flexed discs would appear to be advantageous since disc nutrition would appear to be improved. However, for upright sitting possible fluid expulsion from the discs due to flexion must be considered.

Flexed postures can also effect spinal nerve root compression. Studies into cadaveric spines have shown that nerve root compression is 15% for flexed postures and 33% for lordotic postures (Inufusa, *et al*., 1996). Based on this, flexed postures could be beneficial for people with spinal stenosis. Spinal stenosis is a medical condition in which the spinal canal narrows and compresses the spinal cord and nerves. This is usually due to the common occurrence of spinal degeneration that occurs with aging. It can also sometimes be caused by spinal disc herniation, osteoporosis or a tumour (Adams, *et al*., 2006). Although flexion would reduce the effects of nerve root compression, it would increase any effects of nerve root tension, especially if the nerve root were tethered to underlying structures by scar tissue (Adams, *et al*., 2006).

It is likely that a high degree of flexion could stretch the back muscles. Muscles can generate substantial passive tension in their non-contractile tissues, and this passive tension increases considerably as the muscle is stretched (Purslow, 1989). Flexed postures also stretch the posterior intervertebral ligaments. The combined effect of tension from stretched muscles and intervertebral ligaments are likely to increase the compressive force acting on the intervertebral discs, which could happen in both upright and reclined positions.

Excessive flexion could also stretch the intervertebral ligaments, which is damaging to the spine (Adams, *et al*., 2006). Ligaments contribute to proprioception and kinesthesia due to the presence of afferents (receptor neurons) (Solomonow, 2004). They play an important role in spinal reflexes, which serve to stabilise and protect the spine. When ligaments are stretched and held over time the tension-relaxation phenomenon is observed (Solomonow, 2004). As time passes, tension in the ligaments decrease while the length remains the same. As ligaments develop creep, and the tension-relaxation phenomenon occurs, the length or tension sensory thresholds of the various afferents are shifted significantly in the range of motion and with loads experienced by the ligament through the same range of motion (Eversull, *et al*., 2001; Solomonow *et al*., 2001). This results in altered kinesthetic and proprioception, leading to

inaccuracies of movement and dysfunctional reflexive activation of muscles (Solomonow, 2004). Data obtained from normal volunteers showed that, during maximum static flexion, spasms developed in the erector spinae musculature, and, after the period of maximally flexed posture, a significant modification of muscle activity, primarily hyperactivity, was observed (Solomonow, *et al*., 2003). Excessive flexion has been demonstrated in this study for the TIS 1 posture. Based on the work by Solomonow, this could stretch the viscoelastic spinal structures and predispose the spine to damage.

Taken as a whole, moderate flexion appears to be preferable for static postures (Adams, *et al*., 2006). All of the sitting postures measured in the present investigation exhibited moderate lumbar flexion, with the exception of the TIS 1 posture. The data suggest that the lumbar spine was maximally flexed for the TIS 1 posture. Too much flexion is worse than too little because prolonged lumbar flexion severely compromises the ability of the back muscles to protect the lumbar spine, as described above.

Summary

All sitting postures resulted in flexion compared to the standing shape of the spine. Load transfer to the backrest for the TIS 2 posture resulted in the lumbar spine adopting the shape of the backrest and this did not increase with further tilt. Load transfer to the backrest for all sitting postures resulted in the thoracic spine adopting the shape of the backrest and this was different for all postures. There appeared to be more lumbar flexion with the standard recline than the upright posture, which was probably a result of the use of the footstool, tight hamstrings and a lack of support to the lower lumbar and posterior superior iliac spines.

6.3 Future research and application

The remaining of this discussion considers future research for the biomechanical model and the concepts developed during this study, in the context of various current applications of reclined seating postures. These are backcare chairs, specialist seating for elderly in long term care, specialist seating for patients with neuromotor deficits, wheelchairs and long haul flight economy airline seating.

6.3.1 The biomechanical model

Further development work could be carried out to optimise the model developed during this study. It was assumed that the seat contact of the ITs would be the peak point of load transfer to the seat; however, this was not the case for all postures. There was a posterior translation of the point of load transfer for tilt-in-space where the pelvis to seat angle did not change. This was, presumably, because of a posterior translation of the centre of mass of the upper body. The most significant shift in the point of load transfer was for the TIS 1 posture and the standard recline posture, where the pelvis rotated posteriorly. For these postures, the point of load transfer approached the sacrum. The model could be optimised to accommodate this mechanism. Although the model predictions of normal force correlated well with measured data, the seat parallel forces were higher than Goossens and Snidjers (1995). Further research could be carried out to understand why these parallel forces have not been measured experimentally in previous research, if they really do exist, and if so what is responsible for balancing the forces.

The LifeMod and Anybody software offer greater biomechanical functionality than the model developed for this study, however, they are not necessarily sensitive to human geometry and no publications have been identified that describe the level of detail on the pelvis; its orientation, its relative position to the supports, the position of the ITs and their contact with the seat, the position of the point of load transfer to the seat, and the support surface motion paths. Other than

Goossens and Snidjers (1995), no other biomechanical modelling studies have been identified that analyse reclined seating. These are the novel aspects of the model developed for this study. After optimisation, the next logical step would be to investigate the cross over potential with anthropometric digital humans and musculoskeletal modelling software packages.

6.3.2 Backcare chairs

Pseudo-medical chairs, sold as therapeutic seating for alleviation of low back pain, offer tilt-in-space positions similar to the TIS 3 seated test posture. The results from the stadiometry investigation have shown significant spinal recovery for this posture compared to the upright and standard recline postures, and therefore, could be tested in future research with individuals having low back pain to investigate the potential for pain relief.

Tilt-in-space at terminal positions may unload the spine enough to introduce greater flexion which could unload the zygapophysial joints, aid intervertebral disc nutrition and increase fluid flow into the discs. Flexion can also relieve spinal nerve root compression which could be particularly important for people with spinal stenosis. Pain associated with intervertebral disc pressure relates to fissures that reach the innervated posterior annulus fibrosis (Vanharanta, *et al*., 1987; Moneta, *et al*, 1994). It is plausible that tilted positions that flex the discs redistribute the stress peaks away from the innervated posterior portion of the disc to the nucleus pulposus and anterior margins, and reduce pain (Adams, *et al*., 1996). The TIS 1 posture was conceived for this study to flex the spine in the terminal tilt position. The results of this study for spinal curvature confirm that the motion paths of the support surfaces do not follow the human body, and have resulted in too much flexion. Caution is needed as too much flexion can compromise spinal reflexes and lead to injury. A development of the TIS 1 postures, or intermediate postures, with the correct motion paths that are predicted by the biomechanical model would make an interesting subject for future research with back pain sufferers to understand potential mechanisms of pain alleviation.

6.3.3 Specialist seating for care of the elderly

In the UK, specialist recliner chairs are available that offer additional functionality for the needs of frail elderly people who cannot tolerate conventional seating, such as mobility, adjustability for correct sizing, positioning supports, pressure relieving cushioning and cover materials, and waterproof materials. The main features of these chairs tend to be the positions they can recline to, and many offer tilt-in-space. This study extended previous findings for the importance of foot support on IT pressures (Peters, 1999) to the role of the leg rest. A next logical step for future research would be to systematically evaluate the effects of different methods of supporting the feet and legs on IT pressure for reclined postures. An analysis of how pelvic position and the point of load transfer to the seat relates to the lower legs support is also warranted.

The TIS 1 concept, or derivative, could potentially be found comfortable by elderly people, since the prevalence of kyphosis increases with age (Milne & Lauder, 1974). A kyphosed spine would be accommodated by the articulating backrest, with the individual likely to be more supported in recline positions.

6.3.4 Specialist seating for patients with neuromotor deficits

Nwaobi's (1986) research into the effect of tilt-in-space on the tonic muscle activity of patients with cerebral palsy demonstrated significant increases in back extensor and hip adductor muscles. Nwaobi explained that it is probable because the increased extensor tone is a direct result of the tonic labyrinthine reflex stimulated by the position of the head in the reclined position. Nwaobi explains that the increased tonic activity in the reclined position is a reaction to the loss of the horizontal relationship with the environment, including eye contact, and there is a tendency to struggle against gravity in this position which consequently increases muscle tone. When there is asymmetric muscle tone, prolonged sitting in tilted/reclined postures may accelerate the onset and progression of scoliosis (Nwaobi, 1986). The findings from this study suggested that the TIS 1 posture significantly reduced muscle activity in healthy individuals,

probably because of the improved head position. Evaluation of the TIS 1 posture involving patients with cerebral palsy could be a logical extension of the work by Nwaobi to enhance the understanding of neuromotor responses to tilt-in-space postures.

6.3.5 Wheelchairs

Weight shifts, or pressure reliefs, are strategies employed in preventing pressure ulcers for people with spinal cord injuries. When individuals are not physically able to lift, forward lean, or side-to-side weight shift, variable positioning wheelchairs might be recommended. To the author's knowledge, this study is the first to use a validated biomechanical model to predict the relationship between varying angles of tilt-in-space and recline on seat force, which correlates well with empirical evidence from previous studies (Sprigle, *et al*., 2010; Giesbrecht, *et al*., 2011). The next logical extension of the model would be to determine how normal and parallel forces for these postures are affected by the pelvic position relative to the supports and the point of load transfer to the seat. The relationship between normal force and shear as the pelvis rotates posteriorly may be of particular significance to the prevention of pressure ulcers.

6.3.6 Airline seating

A review of studies on airline seating revealed only one investigation of reclined posture (Souza, 2010). The conventional reclined seat (backrest only) and a tilt-in-space ('joint reclining mechanism' described by Souza) were compared using interface pressure mapping and subjective ratings. The reclined angle was 8° and the tilt angles were 8° and 16°. The results of Souza's investigation favoured tilt over recline. This study highlights the opportunity for alternative reclined systems in economy airline seating. The TIS 1 concept, where the backrest is segmented and articulates as a function of seat tilt, could be explored for this application. The aim and potential benefit would be to maximise seat tilt and lower lumbar segment inclination within the tight space envelop of economy airline cabins.

The stadiometry data indicate that the standard recline posture offered no improvement to spinal loading over chairs that do not recline, and tilt-in-space aided recovery. In the study by Souza (2010), respondents reported a greater feeling of stability with the tilt-in-space prototype airline seat compared to the conventional reclining seat. Creep loading of the intervertebral discs maybe particularly important in long haul flight where people are in fixed postures, often sleeping, and at the end of their journey are almost immediately carrying heavy luggage. Tilt-in-space postures may therefore offer a better alternative to conventional reclined seating on the basis of disc creep loading and, hence, warrants further investigation. Positional MRI, as used by Bashir, *et al*., (2006) in their study of seating, would be a useful tool in evaluating both posture and creep loading of the intervertebral discs.

7 Conclusions

A two-dimensional biomechanical model was developed, validated and applied to the evaluation of reclined seating postures. A comprehensive set of biomechanical data was collected from fifteen gender and age diverse subjects to examine the foundational principles for reclined seating ergonomics. The model was developed to predict posture, the internal axial loads of the body segments, and the external forces that interface with each seating posture at the feet (or behind the knees if feet are unsupported), the ITs, various landmarks on the back, and the head. The purpose of the model is to predict body posture, load distributions, and the motion paths of the support surfaces, while assisting with the interpretation of *in vivo* experimentally measured pressure distributions, stature change, and sEMG activity in a spectrum of seated postures. The novel aspects of the model include 1) geometrical of the pelvis and spine from anatomical studies; 2) new algorithms predicting pelvic rotation; 3) new algorithms predicting the ischial-seat contact; and 4) derivation of a pelvic stabilising force.

Measured data agreed with 98.8% of modelled data for head contact location, averaged across all postures. For the upright posture, the measured data agreed with 99.4% of the model prediction for IT contact location. For the standard recline and TIS 1 postures, posterior pelvic rotation resulted in a translation of the point of load transfer to the seat away from the ITs toward the sacrum. There was a significant relationship and a strong correlation between modelled data and predicted force ($p < .001$, $r = 0.92$). Simplifying the model to the 50^{th} percentile male and normalising force predictions did not alter the significance of its relationship to normalised measured force ($p < .001$), the correlation was improved ($r = 0.97$) and the full scale error was improved to 8%. No trends were found between root mean square errors from the normalised data for gender and height, showing the simplified model was robust across body types.

The model was found to be sensitive to the point of load transfer at the seat with respect to IT parallel force but robust in terms of IT normal force. There was an inverse relationship between IT parallel force and normal force for varying pelvic rotations. Model predictions for IT parallel force were significantly higher than Goossens and Snidjers' model and force plate data, although the accuracy has not been assessed as part of this study. A quadratic relationship was found between the seat force and tilt-in-space angle, a linear relationship was found between backrest force and tilt-in-space, and linear relationship was found for both the seat and backrest forces for backrest only recline. These findings have explained several conflicts between the conclusions of previous studies.

Significant differences were found between the seated test postures in all of the experimental data. The analysis of interface pressure distributions confirmed that the motion paths of the support surface were not synchronised with the body as it flexed. This is likely to have affected spinal loading and spinal curvature for the TIS 1 seated test posture. A limitation with the biomechanical model was the absence of parallel force on the backrest which may have affected the spinal link force predictions, particularly for the TIS 1 seated test posture where the three backrest segments were articulated to varying inclinations. Analysis of the interface pressure distributions confirmed previous research findings for the role of foot support on IT pressures, and extended the theory to the role of lower leg support in reclined postures. Measurements of changes in stature suggested that the standard recline posture had no effect on spinal loading compared to chairs that do not recline. Although spinal loading is not the only factor contributing to stress relief in recliner chairs, this is potentially important to seating ergonomic theory. There appeared to be a positive effect on spinal loading from tilt-in-space postures with significance for the TIS 3 posture. High variance in the stadiometry data limited the power of this experiment so there might have been effects that were not statistically demonstrated. Both sEMG data and stadiometry data suggested that lying supine on a flat surface loaded the lumbar spine and recruited the lumbar muscles to act a splint. The biomechanical model predicted tension between the pelvis and lower lumbar spine for the seated test postures, however, this was reduced when

opening the seat to backrest angle, as with the standard recline and the TIS 1 postures. This was reflected in the sEMG patterns. Relative high sEMG activity for the TIS 2 posture was not explained by the model, but may be related to discordance of the sensory motor control system. Articulating the backrest, as with the TIS 1 posture, significantly reduced muscle activity presumably because of improve head orientation. All sitting postures flexed the spine compared to standing. Overall, the shape of the backrest determined the shape of the spine in reclined seating postures, with the additional influence of pelvic rotation for the standard recline posture resulting from extended legs and tension in the hamstrings.

This research is unique in creating a framework around reclined seating postures and, through this, bridges previously disparate areas of seating research. The biomechanical model, experimental results, and theories developed from this research have potential implications in research, and design, for applications including backcare chairs, seating for long-term care and patients with neuromotor deficits, wheelchairs and airline seating. Furthermore, this study exists at the interface of anthropometric and biomechanical modelling, and therefore may have cross over potential to the digital humans, where their integration with biomechanical models is at the cutting edge of the field.

References

Abdel-Malek, K., Yang, J., Marler, T., Beck, S., Mathai, A., Zhou, X., Patrick, A., & Arora, J. 2006, "Toward a new generation of human models", *International Journal of Human Factors Modeling and Simulation*, vol. 1, no. 1, pp. 2-39.

Adams, M. A, Bogduk, N., Burton, K., & Patricia, D. 2006, *The Biomechanics of Back Pain*, Second edition, Elsevier, London.

Adams, M. A. & Hutton, W. C. 1980, "The effect of posture on the role of the apophysial joints in resisting intervertebral compressive forces", *British Journal of Joint and Bone Surgery*, vol. 62, pp. 358-362.

Adams, M. A. & Hutton, W. C. 1982, "Prolapsed intervertebral disc. A hyperflexion injury. 1981 Volvo Award in basic science", *Spine*, vol. 7, pp. 184-191.

Adams, M. A. & Hutton, W. C. 1983, "The effect of posture on the fluid content of lumbar intervertebral discs", *Spine*, vol. 8, pp. 665-671.

Adams, M. A. & Hutton, W. C. 1986, "The effect of posture on diffusion into lumbar intervertebral discs", *Journal of Anatomy*, vol. 147, pp. 121-134.

Adams, M. A., McNally, D. S., Dolan, P. 1996, "'Stress distributions inside intervertebral discs. The effects of age and degeneration", *The Journal of Bone and Joint Surgery, British Volume*, vol. 78, no. 6, pp. 965-72.

Aissaoui, R. 2001, "Analysis of sliding and pressure distribution during a repositioning of persons in a simulator chair", *IEEE Transactions on neural systems and rehabilitation engineering*, vol. 9, no. 2, pp. 215-224.

Åkerblom, B. 1948, *Standing and Sitting Posture.* A.-B. Nordiska Bokhandeln, Stockholm.

Althoff, I., Brinckmann, P., Frobin, W., Sandover, J., & Burton, K. 1992, "An improved method of stature measurement for quantitative determination of spinal loading", *Spine*, vol. 17, no. 6, pp. 682-693.

Anderson, J. H. D. & Sweetman, B. J. 1975, "A combined flexirule/hydrogoniometer for measurement of lumbar spine and its sagittal movement", *Rheumatology and Rehabilitation*, vol. 14, pp. 173-179.

Andersson, B. & Örtengren, R. 1974[a], "Myoelectric back muscle activity during sitting", *Scandinavian Journal of Rehabilitation Medicine*, Suppl. 3, pp. 73-90.

Andersson, B., Jonsson, B., & Örtengren, R. 1974[b], "Myoelectric activity in individual lumbar erector spinae muscles in sitting. A study with surface and wire electrodes", *Scandinavian Journal of Rehabilitation Medicine*, Suppl. 3, pp. 91-108.

Andersson, B., Örtengren, R., Nachemson, A., & Elfström, G. 1974[c], "Lumbar disc pressure and myoelectric back muscle activity during sitting. I. *Studies on an experimental chair*", *Scandinavian Journal of Rehabilitation Medicine*, vol. 6, pp. 104-114.

Andersson, B. & Örtengren, R. 1974[d], "Lumbar disc pressure and myoelectric back muscle activity during sitting. II. *Studies on an office chair*", *Scandinavian Journal of Rehabilitation Medicine*, vol. 6, pp. 115-121.

Andersson, B. & Örtengren, R. 1974[e], "Lumbar disc pressure and myoelectric back muscle activity during sitting. III. *Studies on a wheelchair*", *Scandinavian Journal of Rehabilitation Medicine*, vol. 6, pp. 122-127.

Andersson, B., Örtengren, R., Nachemson, A., & Elfström, G. 1974[f], "Lumbar disc pressure and myoelectric back muscle activity during sitting. IV. *Studies on a car driver's seat*", *Scandinavian Journal of Rehabilitation Medicine*, vol. 6, pp. 128-133.

Andersson, B., Örtengren, R., Nachemson, A., Elfström, G., & Broman, H. 1975, "The sitting posture: an electromyographic and discometric study", *Orthopedic Clinics of North America*, vol. 6, no. 1, pp. 105-120.

Andersson, B. J. G., Murphy, R. W., Örtengren, R., & Nachemson, A. 1979, "The influence of backrest inclination and lumbar support on lumbar lordosis", *Spine*, vol. 4, pp. 52-58.

Ascension Technology Inc. 1999, *Motion Star Wired Manual*.

Baratta, R. V., Solomonow, M., Zhou, B. H., & Zhu, M. 1998, "Methods to reduce the variability of EMG power spectrum estimates", *Journal of Electromyography and Kinesiology*, vol. 8, pp. 279-285.

Bashir, W., Torio, T., Smith, F., Takahashi, K., & Pope, M. The way you sit will never be the same! Alterations of the lumbosacral curvature and intervertebral disc morphology in normal subjects in variable sitting positions using whole-body positional MRI. RSNA Conference 2006.

Belytschko, T. & Privitser, E. 1978, Refinement and validation of a three-dimensional head-spine model. Aerospace Medical Research Laboratory, Aerospace Medical Division, Air Forec Systems Command, Wright-Patterson Air Force Base (OH). Publication No. AMRL-TR-78-7.

Bendix, T. & Biering-Sørensen, F. 1983, "Posture of the trunk when sitting on forward inclining seats", *Scandinavian Journal of Rehabilitation Medicine*, vol. 15, pp. 197-203.

Bendix, T., Jessen, F., & Krohn, L. 1988, "Biomechanics of forward-reaching movements while sitting on fixed forward- or backward-inclining or tiltable seats", *Spine*, vol. 13, no. 2, pp. 193-196.

Berrington de González, A. & Darby, S. 2004, "Risk of cancer from diagnostic X-rays: estimates for the UK and 14 other countries", *The Lancet*, vol. 363, no. 31, pp. 345-351.

Beynon, C. & Reilly, T. 2001, "Spinal shrinkage during a seated break and standing break during simulated nursing tasks", *Applied Ergonomics*, vol. 32, pp. 617-622.

Bishu, R., Hallbeck, S., Riley, M., & Stentz, T. 1991, "Seating comfort and its relationship to spinal profile: a pilot study", *International Journal of Industrial Ergonomics*, vol. 8, pp. 89-101.

Blanchonette, P. 2010, "Jack human modelling tool: a review", Air Operations Division, DSTO Defence Science and Technology Organisation, Australian Government Department of Defence, Australia.

Bogduk, N. 1997, *Clinical Anatomy of the Lumbar Spine*, Third edition, Churchill Livingstone, Edinburgh.

Bonney, R. A. 1988, "Some effects on the spine from driving", *Clinical Biomechanics*, vol. 3, pp. 236-240.

Bonney, R. A. & Corlett, E. N. 2002, "Head posture and loading of the cervical spine", *Applied Ergonomics*, vol. 33, pp. 415-417.

Botsford, D. J., Esses, S. I., & Ogilvie-Harris, D. J. 1994, "*In vivo* diurnal variation in intervertebral disc volume and morphology", *Spine*, vol. 19, pp. 935-940.

Broberg, K. B. 1993, "Slow deformation of intervertebral discs", *Journal of Biomechanics*, vol. 26, pp. 501-512.

Burns, S. P. & Betz, K. L. 1999, "Seating pressures with conventional and dynamic wheelchair cushions in tetraplegia", *Archives of Physical Medicine and Rehabilitation*, vol. 80, pp. 566-571.

Burton, A. K. & Tillotson, M. K. 1994, "Estimation of spinal loads in overhead work", *Ergonomics*, vol. 37, no. 8, pp. 1311-1321.

Burton, A. K. 1986, "Regional lumbar sagittal mobility; measurement by flexicurves", *Clinical Biomechanics*, vol. 1, pp. 20-26.

Chaffin, D. B. 2005, "Improving digital human modelling for proactive ergonomics in design", *Ergonomics*, vol. 48, no. 15, pp. 478-491.

Claus, A. P., Hides, J. A., Moseley, G. L., & Hodges, P. W. 2009, "Is 'ideal' sitting posture real? Measurement of spinal curves in four sitting postures", Manual Therapy, vol. 14, no. 4, pp. 404-408.

Cohen, J. 1988, "Statistical power analysis for the behavioural sciences," 2nd edn, Academic Press, New York.

Cohen, J. 1992, "A power primer", *Psychological Bulletin*, vol. 112, no. 1, pp. 155-159.

Colombini, D. & Occhipinti, E. 1986, "Biomechanical, Electromyography and Radiological Study of Seated Postures," in *The Ergonomics of Working Postures: Models, Methods and Cases*, E. N. Corlett, J. Wilson, & I. Manenica, eds., Taylor & Francis, London, pp. 331-344.

Corlett, E. N. & Eklund, J. A. E. 1986, "Change of stature as an indication of load on the spine," in *The Ergonomics of Working Postures: Models, Methods and Cases*, E. N. Corlett, J. Wilson, & I. Manenica, eds., Taylor and Francis, London, pp. 232-242.

Crawford, N. R., Yamaguchi, G. T., & Dickman, C. A. 1999, "A new technique for determining 3-D joint angles: the tilt/twist method", *Clinical Biomechanics*, vol. 14, pp. 153-165.

De Carvalho, D. E. & Callaghan, J. P. 2012, "Influence of automobile seat lumbar support prominence on spine and pelvic postures: A radiological investigation", Applied Ergonomics, vol. 43, no. 5, pp. 876-82.

Dempster, W. T. 1955, "Space requirements of the seated posture operator: geometrical, kinematic and mechanical aspects of the body with special reference to the limbs." *WADC Tech. Note*. Write Patterson Air Force Base, OH, pp. 55-159.

De Pukey, P. 1935, "The physiological oscillation of the length of the body", *Acta Orthopaedica Scandinavica*, vol. 6, p. 338.

De Vries, H. 1965, "Muscle tonus in postural muscles", *American Journal of Physical Medicine*, vol. 44, no. 6, pp. 275-291.

Diesing, P., Hochman, D., & Boenick, U. "Numerical accuracy of pressure mapping systems - a comparative evaluation", European Pressure Ulcer Advisory Panel, ed.

Dolan, P., Adams, M. A., & Hutton, W. C. 1988, "Commonly adopted postures and their effect on the lumbar spine", *Spine*, vol. 13, no. 2, pp. 197-201.

Dolan, P. & Adams, M. A. 1993, "Influence of lumbar and hip mobility on the bending stresses acting on the lumbar spine", *Clinical Biomechanics*, vol. 8, pp. 185-192.

Dolce, J. & Raczynski, J. 1985, "Neuromuscular activity and electromyography in painful backs: psychological and biomechanical models in assessment and treatment", *Psychological Bulletin*, vol. 97, no. 3, pp. 502-520.

Duffy, V. G. (Ed) 2008, *Research for applied ergonomics and human factors engineering*, CRC Press, Taylor and Francis Group, Boca Raton, Florida.

Dunk, N. M., Kedgley, A. E., Jenkyn, T. R., & Callaghan, J. P. 2012, "Evidence of a pelvis-driven flexion pattern: are the joints of the lower lumbar spine fully flexed in seated postures? ", Clinical Biomechanics, vol. 24, no. 2, pp. 164-168.

Dunlop, R. B., Adams, M. A., & Hutton, W. C. 1984, "Disc space narrowing and the lumbar facet joints", *British Journal of Joint and Bone Surgery*, vol. 66, pp. 706-710.

Eklund, J. A. E. & Corlett, E. N. 1984, "Shrinkage as a measure of the effect of load on the spine", *Spine*, vol. 9, no. 2, pp. 189-194.

Eklund, J. A. E. & Corlett, E. N. 1986, "Experimental and biomechanical analysis of seating," in *The Ergonomics of Working Postures: Models, Methods and Cases*, E. N. Corlett, J. Wilson, & I. Manenica, eds., Taylor & Francis, London, pp. 331-344.

Eversull, E., Solomonow, M., Zhou, B. H., Baratta, R. V., & Zhu, M. 2001, "Neuromuscular neutral zones sensitivity to lumbar displacement rate", *Clinical Biomechanics*, vol. 16, pp. 102-113.

Field, A. 2005, *Discovering statistics using SPSS*, 2nd edn, SAGE Publications, London.

Fisher, R. A. 1925, "Statistical methods, experimental design, and scientific inference," Oxford University Press, Oxford.

Foreman, T. K. & Linge, K. 1989, "The importance of heel compression in the assessment of diurnal stature variation", *Applied Ergonomics*, vol. 20, pp. 299-300.

Fountain, F., Minear, W., & Allison, R. 1966, "Function of longus colli and longissimus cervicis muscles in man", *Archives of Physical Medicine and Rehabilitation*, vol. 47, no. 10, pp. 665-669.

Frey, J. K. & Tecklin, J. S. 1986, "Comparison of lumbar curves when sitting on the Westnofa Balans® Multi-Chair, when sitting on a conventional chair, and standing", *Physical Therapy*, vol. 66, no. 9, pp. 1365-1369.

Frigo, C., Carabalona, R., Dalla Mura, M., & Negrini, S. 2003, "The upper body segmental movements during walking by young females", *Clinical Biomechanics*, vol. 18, pp. 419-425.

Frisina, W. & Lehneis, R. H. 1970, "Pressure mapping: a preliminary report", *Journal of Biomechanics*, vol. 3, no. 5, p. 526.

Fritz, M. 2000, "Simulating the response of a standing operator to vibration stress by means of a biomechanical model", *Journal of Biomechanics*, vol. 33, pp. 795-802

Fryer, J. C. J., Quon, J. A., & Smith, F. W. 2010, " Magnetic resonance imaging and stadiometric assessment of the lumbar discs after sitting and chair-care decompression exercise: a pilot study", The Spine Journal, vo. 10, no. 4, pp. 297-305.

Giesbrecht, E. M., Ethans, K. D., & StaleyGiesbrecht, D. 2011, "Measuring the effect of incremental angles of wheelchair tilt on interface pressure among individuals with spinal cord injury", Spinal Cord, vol. 49, no. 7, pp. 827-31.

Gilsdorf, P., Patterson, R., Fisher, S., & Appel, N. 1990, "Sitting forces and wheelchair mechanics", *Journal of Rehabilitation Research and Development*, vol. 27, no. 3, pp. 239-246.

Golinski, W. Z., & Gentle, R. 2002, "Whiplash injury assessment – A biomechanical FE model approach", *SAE Digital Human Modeling Conference*, Munich. VDI-Berichte Nr. 1675, pp. 431-443.

Goossens, R. H. M. & Snijders, C. J. 1995, "Design criteria for the reduction of shear forces in beds and seats", *Journal of Biomechanics*, vol. 28, no. 2, 225-230.

Gross, C. M., Goonetilleke, R. S., Menon, K. K., Banaag, J. C. N., & Nair, C. M. 1994, "The biomechanical assessment and prediction of seat comfort," in *Hard Facts About Soft Machines: Ergonomics of Seating*, R. Lueder & K. Noro, eds., Taylor and Francis, London, pp. 231-253.

Guttmann, L. 1976, "The prevention and treatment of pressure sores", in *Bedsore Biomechanics*, Kenedi, R. M., Cowden, J. M., & Scales, J. T., eds., Macmillan, London, pp. 153-159.

Hadley, T. J. & Haslegrave, C. M. 2000, "Drivers spinal responses to the effects of sitting posture," in *Contemporary Ergonomics 2000*, S. Robertson, M. Hanson, & P. McCabe, eds., Taylor & Francis, London, pp. 401-405.

Hart, D. L. & Rose, S. J. 1986, "Reliability of a noninvasive method for measuring the lumbar curve", *Journal of Orthopaedic and Sports Physical Therapy*, vol. 8, no. 4, pp. 180-184.

Harrison, D. D., Harrison, S. O., Croft, A. C., Harrison, D. E., & Troyanovich, S. J. 1999, "Sitting biomechanics Part I: Review of the literature", *Journal of Manipulative and Physiological Therapeutics*, vol. 22, no. 9, pp. 594-609.

Härtel, T., Hildebrand, F., & Knoll, K. 2006, "Methods of simulation and manipulation for the evaluation of figure skating jumps", in *The Engineering of Sport 6,* E.F. Moritz & S. Haake, eds, Volume 2, Developments for Disciplines, Springer Science+Business Media, New York, pp. 179-184.

Healey, E. L., Fowler, N. E., Burden, A. M., & McEwan, I. M. 2005, "The influence of different unloading positions upon stature recovery and paraspinal muscle activity", *Clinical Biomechanics*, vol. 20, pp. 365-371.

Hedberg, K., Alexander, L. A., Cooper, K., Hancock, E., Ross, J., Smith, F. W. 2012, "Low back pain: An assessment using positional MRI and MDT", Manual Therapy, electronic publication ahead of print.

Henderson, J. L., Price, S. H., Brandstater, M. E., & Mandac, B. R. 1994, "Efficacy of three measures to relieve pressure in seated persons with spinal cord injury", *Archives of Physical Medicine and Rehabilitation*, vol. 75, pp. 535-539.

Hermens, H., Freriks, B., Merletti, R., Stegeman, D., Blok, J., Rau, G., Disselhorst-Klug, C., & Hägg, G. 1999, *European Recommendations for Surface Electromyography* Roessingh Research and Development b. v.

Hirsch, C., Ingelmark, B., & Miller, M. 1963, "The anatomical basis for low back pain. Studies on the pressure of sensory nerve endings in ligamentous, capsular and intervertebral disc structures in the human lumbar spine", *Acta Othopeadica Scadinavica*, vol. 33, pp. 1-17.

Hobson, D. A. 1992, "Comparative effects of posture on pressure and shear at the body-seat interface", *Journal of Rehabilitation Research and Development*, vol. 29, no. 4, pp. 21-31.

Holden, M., Ventura, J., & Lackner, J. 1994, "Stabilization of posture by precision contact of the index finger", *Journal of Vestibular Research*, vol. 4, pp. 285-301.

Holm, S. & Nachemson, A. 1982, "Nutritional changes in the canine intervertebral disc after spinal fusion", *Clinical Orthopaedics*, vol. 169, pp. 243-258.

Howard, I. & Childerson, L. 1994, "The contribution of motion, the visual frame, and visual polarity of sensations of body tilt", *Perception*, vol. 23, pp. 753-762.

International Organisation for Standardisation 2001, *Wheelchair seating. Part 2: Test methods for devices intended to manage tissue integrity and cushions.* Geneva, Switzerland.

Inufusa, A., An, H. S., Lin, T. H., *et al*. 1996, "Anatomic changes of the spinal canal and intervertebral foramen associated with flexion-extension movement", *Spine*, vol. 21, pp. 2412-2420.

Israel, M. 1959, "A quantitative method of estimating flexion and extension of the spine - a preliminary report", *Military Medicine*, vol. 124, no. 3, pp. 181-186.

Jafrey, T. & Haslegrave, C. M. 1992, "The development of a precision seated stadiometer for measuring the effects of vibration on the human spine," in *Contemporary Ergonomics 1992: Ergonomics for Industry*, E. J. Lovesey, ed., Taylor & Francis, London, pp. 79-84.

Jeka, J. & Lackner, J. 1994, "Fingertip contact influences human postural control", *Experimental Brain Research*, vol. 100, pp. 495-502.

Jeka, J. & Lackner, J. 1995, "The role of haptic cues from rough and slippery surfaces in human postural control", *Experimental Brain Research*, vol. 103, pp. 267-276.

Kanlayanaphotporn, R., Trott, P., Williams, M., & Fulton, I. 2003, "Effects of chronic low back pain, age and gender on vertical spinal creep", *Ergonomics*, vol. 46, no. 6, pp. 561-573.

Karadimas, E. J., Siddiqui, M., Smith, F. W., Wardlaw, D. 2006, "Positional MRI changes in supine versus sitting postures in patients with degenerative lumbar spine", Journal of Spinal Disorders and Techniques, vol. 19, no. 7, pp. 495-500.

Keegan, J. J. 1953, "Alterations of the lumbar curve related to posture and seating", *Journal of Bone and Joint Surgery*, vol. 35, pp. 589-603.

Keppler, V. 2003, "Biomechanische de modellbildung aur simulation zweier mensch-maschinen-schnitt-stellen", Dissertation an der Universität Tübingen.

Knutsson, B., Lindh, K., & Telhag, H. 1966, "Sitting - an electromyographic and mechanical study", *Acta Orthopaedica Scandinavica*, vol. 37, pp. 415-428.

Koerhuis, C. L., Winters, J. C., van der Helm, F. C. T., & Hof, A. L. 2003, "Neck mobility measurement by means of the 'Flock of Birds' electromagnetic tracking system", *Clinical Biomechanics*, vol. 18, pp. 14-18.

Kraemer, W. J., Kolditz, D., & Gowin, R. 1985, "Water and electrolyte content of human intervertebral discs under variable load", *Spine*, vol. 10, pp. 69-71.

Krag, M. H., Cohen, M. C., Haugh, L. D., *et al*. 1990, "Body height change during upright and recumbent posture", *Spine*, vol. 15, pp. 202-207.

Lackner, J. & DiZio, P. 2000, "Human orientation and movement control in weightless and artificial gravity environments", *Experimental Brain Research*, vol. 130, pp. 2-26.

Lehner, S. & Wallrapp, O. 1999, "3D-simulation of the human knee-joint", in *Proceedings of the 10th Conference of European Society of Biomechanics* (G. V. d. Perre, ed), Leuven.

Leivseth, G. & Drerup, B. 1997, "Spinal shrinkage during work in a sitting posture compared to work in a standing posture", *Clinical Biomechanics*, vol. 12, no. 7/8, pp. 409-418.

Lewis, S. E. & Fowler, N. E. 2009, "Changes in intervertebral disk dimensions after a loading task and the relationship with stature change measurements", Archives of Physical Medicine and Rehabilitation, vol. 90, no. 10, pp. 1795-9.

Lewis, S. E. & Fowler, N. E. 2010, "Evaluation of the loading response of intervertebral discs using measurements of stature change and magnetic resonance", Journal of Bone & Joint Surgery, British volume, vol. 92-B, no. SUPP I 233.

Linden, O., Greenway, R. M., & Piazza, J. M. 1965, "Pressure distribution on the surface of the human body, evaluation in lying and sitting positions using a bed of springs and nails", *Archives of Physical Medicine and Rehabilitation*, vol. 46, pp. 378-385.

Link, C., Nicholson, G., Shaddeau, S., Birch, R., & Gossman, R. 1990, "Lumbar curvature in standing and sitting in two types of chairs: relationship of hamstring and hip flexor muscle length", *Physical Therapy*, vol. 70, no. 10, pp. 611-618.

Magnusson, M., Almvist, M., & Lindström, I. 1990, "Measurement of time dependent height loss during sitting", *Clinical Biomechanics*, vol. 5, pp. 137-142.

Magnusson, M., Hansson, T., & Pope, M. 1994, "The effect of seat back inclination on spine height changes", *Applied Ergonomics*, vol. 25, no. 5, pp. 294-298.

Maroudas, A., Stockwell, R. A., Nachemson, A., *et al*. 1975, "Factors involved in the nutrition of the human lumbar intervertebral disc: cellularity and diffusion of glucose *in vitro*", *Journal of Anatomy*, vol. 120, pp. 113-130.

Marras, W. S. & Davis, K. G. 2001, "A non-MVC EMG normalization technique for the trunk musculature: Part 1. Method development", *Journal of Electromyography and Kinesiology*, vol. 11, pp. 1-9.

Matthews, P. 1988, "Proprioceptors and their contribution to somatosensory mapping: complex messages require complex processing", *Canadian Journal of Physiology and Pharmacology*, vol. 66, pp. 430-438.

McMillian, D. W., Garbutt, G., & Adams, M. A. 1996, "Effect of sustained loading on the water content of intervertebral discs: implications for disc metabolism", *Annals of the Rheumatic Diseases*, vol. 55, pp. 880-887.

Meister, D. (1999). The History of Human Factors and Ergonomics. Mahwah, N.J.: Lawrence Erlbaum Associates.

Meskers, C. G. M., Vermeulen, H. M., de Groot, J. H., van der Helm, F. C. T., & Rozing, P. M. 1998, "3D shoulder position measurements using a six-degree-of-freedom electromagnetic tracking device", *Clinical Biomechanics*, vol. 13, pp. 280-292.

Michel, D. P. & Helander, M. G. 1994, "Effects of two types of chairs on stature change and comfort for individuals with healthy and herniated discs", *Ergonomics*, vol. 37, no. 7, pp. 1231-1244.

Milne, J. S., Lauder, I. J., 1974, "Age effects in kyphosis and lordosis in adults", *Annals of Human Biology*, vol. 1, no. 3, pp. 327-337.

Mirka, G. A. 1991, "The quantification of EMG normalization error", *Ergonomics*, vol. 34, no. 3, pp. 343-352.

Moes, N. C. C. M. 2007, "Variation in sitting pressure distribution and location of the points of maximum pressure with rotation of the pelvis, gender and body characteristics", *Ergonomics*, vol. 50, no. 4, pp. 536-561.

Moneta, G. B., Videman, T., Kaivanto, K., *et al*. 1994, "Reported pain during lumbar discography as a function of anular ruptures and disc degeneration. A re-analysis of 833 discograms", *Spine*, vol. 17, pp. 1968-1974.

Mooney, V., *et al*. 1971, "Comparison of pressure distribution qualities in seat cushions", *Bulletin of Prosthetics Research*, vol. Spring.

Mootanah, R. & Bader, D. 2006, "Pressure sensors in biomedical engineering," in *Wiley's encyclopaedia of biomedical engineering*, John Wiley and Sons, New York.

Morin, F. & Portnoy, H. 1956, "Electromyographic study of postural muscles in various positions and movements", *The American Journal of Physiology*, vol. 186, no. 1, pp. 122-126.

Mølhave, A. 1958, *A Biostatic Investigation,* Munksgaard.

Nachemson, A. 1960, "Lumbar intradiscal pressure", *Acta Orthopaedica Scandinavica,* Supplement 43, pp. 1-93.

Nachemson, A. & Morris, J. M. 1964, "*In vivo* measurements of intradiscal pressure", *The Journal of Bone and Joint Surgery*, vol. 46-A, no. 5, pp. 1077-1092.

Nachemson, A. 1966, "Electromyographic studies on the vertebral portion of the psoas muscle", *Acta Orthopaedica Scandinavica* , vol. 37, no. 2, pp. 177-190.

Nachemson, A., Lewin, T., Maroudas, A., *et al*. 1970, "*In vitro* diffusion of dye through the end-plates and the anulus fibrosus of human lumbar inter-vertebral discs", *Acta Orthopaedica Scandinavica*, vol. 41, pp. 589-607.

Newell, P. H., Thornburgh, J. D., & Fleming, W. C. 1970, "The management of pressure and other external factors in the prevention of ischemic ulcers", *Transactions of the ASME. Journal of Basic Engineering*, Sept.

Nouwen, A. & Bush, C. 1984, "The relationship between paraspinal EMG and chronic low back pain", *Pain*, vol. 20, pp. 109-123.

Nwaobi, O. 1986, "Effects of body orientation in space on tonic muscle activity of patients with cerebral palsy", *Developmental Medicine and Child Neurology*, vol. 28, pp. 41-44.

Paul, G. & Lee, W. C. 2011, "Interfacing Jack and anybody: towards anthropometric musculoskeletal digital human modeling", in *1st International Symposium on Digital Human Modelling*, 14-16 June 2011, Université Claude Bernard, Lyon.

Pearcy, M. J. & Tibrewal, S. B. 1984, "Lumbar intervertebral disc and ligament deformations measured *in vivo*", *Clinical Orthopaedics* pp. 281-286.

Pearcy, M. J., Gill, J. M., Hindle, R. J., & Johnson, G. R. 1987, "Measurement of human back movements in three dimensions by opto-electronic devices", *Clinical Biomechanics*, vol. 2, pp. 199-204.

Pearcy, M. J., Gill, J. M., Whittle, M. W., & Johnson, G. R. 1987, "Dynamic back movement measured using a three-dimensional television system", *Journal of Biomechanics*, vol. 20, no. 10, pp. 943-949.

Pearcy, M. J. & Hindle, R. J. 1989, "New method for the non-invasive three-dimensional measurement of human back movement", *Clinical Biomechanics*, vol. 4, pp. 73-70.

Pellow, T. R. 1999, "A comparison of interface pressure readings to wheelchair cushions and positioning: a pilot study", *Canadian Journal of Occupational Therapy*, vol. 66, no. 3, pp. 140-149.

Pennell, P. N., Owens, S. C., Brismee, J. M., Dedrick, G. S., James, C. R., & Sizer, P.S. 2012, "Inter-tester and intra-tester reliability of a clinically based spinal height measurement protocol", The Journal of Spine, vol. 1, no. 2, electronic publication.

Peters, E. S., 1999, *A Comparison of Thermography, Interface Pressure and Transcutaneous Oxygen Measurements in Assessing Pressure Sore Risk in Wheelchair Users*, M.Phil thesis, Bournemouth University.

Pheasant, S. 1986, *Bodyspace: Anthropometry, Ergonomics and the Design of Work*, 1st edn, Taylor and Francis, London.

Pheasant, S. & Haslegrave, C. M. 2006, *Bodyspace: Anthropometry, Ergonomics and the Design of Work*, 3rd edn, Taylor and Francis, London.

Pipkin, L. & Sprigle, S. 2008, "Effect of model design, cushion construction, and interface pressure mats on interface pressure and immersion", *Journal of Rehabilitation Research and Development*, vol. 45, no. 6, pp. 875-882.

Pope, M. & Klingenstierna, U. 1986, "Height changes due to autotraction", *Clinical Biomechanics*, vol. 1, pp. 191-195.

Purslow, P. P. 1989, "Strain-induced reorientation of an intramuscular connective tissue network: implications for passive muscle elasticity", *Journal of Biomechanics*, vol. 22, pp. 21-31.

Pynt, J., Mackey, M., & Higgs, J. 2008, "Kyphosed seated postures: extending concepts of postural health beyond the office", *Journal of Occupational Rehabilitation*, vol. 18, pp. 35-45.

Reinecke, S., Coleman, K., & Pope, M. 1994, "Measurement of lumbar and pelvic motion during sitting," in *Hard Facts about Soft Machines: the Ergonomics of Seating*, R. Lueder & K. Noro, eds., Taylor & Francis, London, pp. 193-204.

Reynolds, H. M. 1978, "The inertial properties of the body and its segments", in *NASA, Anthropometric Source Book Volume 1: Anthropometry for Designers*, (NASA defense publication No. 1024, chapter IV), Webb Associates, Ohio.

Reynolds, H. M., Snow, C. C., & Young, J. W. 1982, *Spatial Geometry of the Human Pelvis*, (Technical report FAA-AM-82-9), National Technical Information Service, Virginia.

Robbins, D. H. 1983, *Anthropometric Specification for Mid-sized Male Dummy, Volume 1*, US Department of Transport, (Technical report UMTRI-83-53-2) U.S. Department of Transport, Washington, D.C.

Rodacki, C. L. N., Fowler, N. E., Rodacki, A. L. F., & Birch, K. 2001, "Repeatability of measurement in determining stature in sitting and standing postures", *Ergonomics*, vol. 44, no. 12, pp. 1076-1085.

Schoberth, H. 1969 "Die Wirbelsäule von Schulkindern - Orthopädische Forderungen an Schulsitze", in *Sitting Posture*, E. Grandjean, ed., Taylor and Francis, London, pp. 98-111.

Schwarzer, A. C., Aprill, C. N., & Bogduk, N. 1995, "The sacroiliac joint in chronic low back pain", *Spine*, vol. 20, no. 1, pp. 31-37.

Serber, H. 1994, "The Study of Lumbar Motion in Seating", in *Hard Facts about Soft Machines: The Ergonomics of Seating*, R. Lueder & K. Noro, eds., (pp. 98–111), Taylor and Francis, London.

Shan, X., Zhang, Y., Zhang, T., Chen, Z., & Wei, Y. 2012, "Flexion relaxation of erector spinae response to spinal shrinkage", Journal of Electromyography and Kinesiology, vol. 22, pp. 370-375.

Shields, R. K. & Cook, T. M. 1988, "Effect of seat angle and lumbar support on seated buttock pressure", *Physical Therapy*, vol. 68, no. 11, pp. 1682-1686.

Shirazi-Adl, A. 1991, "Finite-element evaluation of contact loads on facets of an L2-L3 lumbar segment in complex loads", *Spine*, vol. 16, pp. 533-541.

Snyder, R. G., Chaffin, D. B., & Schutz, R. K. 1972, *Link System of the Human Torso*, (Technical report No. HSRI-71-112), National Technical Information Service, Virginia.

Solomonow, M. 2004, "Ligaments: a source of work-related musculoskeletal disorders", *Journal of Electromyography and Kinesiology*, vol. 14, pp. 49-60.

Solomonow, M. 2006, "Sensory – Motor control of ligaments and associated neuromuscular disorders", *Journal of Electromyography and Kinesiology*, vol. 16, pp. 549-567.

Solomonow, M., Baratta, R. V., Banks, A., Freudenberger, C., & Zhou, B. H. 2003, "Flexion-relaxation response to static lumbar flexion in males and females", *Clinical Biomechanics*, vol. 18, pp. 273-279.

Solomonow, M., Baratta, R. V., Zhou, B. H., Burger, E., Zieske, A., & Gedalia, A. 2003, "Muscular dysfunction elicited by creep of lumbar viscoelastic tissue", *Journal of Electromyography and Kinesiology*, vol. 13, pp. 381-396.

Solomonow, M., Eversull, E., Zhou, B. H., Baratta, R. V., & Zhu, M. 2001, "Neuromuscular neutral zones associated with viscoelastic hysteresis during cyclic lumbar flexion", *Spine*, vol. 26, p. E314-E324.

Souza, A. 2010, "Pressure distribution analysis on aircraft seats using a joint reclining mechanism," *SAE Technical Paper* 2010-36-0210, doi:10.4271/2010-36-0210.

Spijkerman, D. C. M., Terburg, M., Goossens, R. H. M., & Stijnen, T. 1995, "Effects of inflation pressure and posture on the body-seat interface pressure of spinal cord injured patients seated on an air-filled wheelchair cushion", *Journal of Rehabilitation Sciences*, vol. 8, no. 1, pp. 8-12.

Sprigle, S., Dunlop, M. S., & Press, L. 2003, "Reliability of bench tests of interface pressure", *Assistive Technology*, vol. 15, pp. 49-57.

Sprigle, S., Maurer, C., & Sorenblum, S. E. 2010, "Load redistribution in variable position wheelchairs in people with spinal cord injury", The Journal of Spinal Cord Medicine, vol. 33, no. 1, pp. 58-64.

Sprigle, S. & Sonenblum, S. 2011, "Assessing evidence supporting redistribution of pressure for pressure ulcer prevention": a review, *Journal of Rehabilitation Research and Development*, vol. 48, no. 3, pp. 203-213.

Stairmand, J. W., Holm, S., & Urban, J. P. 1991, "Factors influencing oxygen concentration gradients in the intervertebral disc. A theoretical analysis", *Spine*, vol. 16, pp. 444-449.

Steen, B. 1966, "The function of certain neck muscles in different positions of the head with and without loading on the cervical spine", *Acta morphologica Neerlando-Scandinavica*, vol. 6, no. 3, pp. 301-310.

Stumbaum, F., 1983, *Experimentelle Untersuchung and Methematische Simulation der Sitzhaltung auf Arbeitsstühlen*, Ph.D thesis, Institut für Arbeitsphysiologie, Technischen Universität München.

Sullivan, A. & McGill, S. M. 1990, "Changes in spine length during and after seated whole-body vibration", *Spine*, vol. 15, no. 12, pp. 1257-1250.

Swain, I. D. & Bader, D. L. 2002, "The measurement of interface pressure and its role in soft tissue breakdown", *Journal of Tissue Viability*, vol. 12, no. 4, pp. 132-146.

Swinkels, A. & Dolan, P. 1998, "Regional assessment of joint position sense in the spine", *Spine*, vol. 23, no. 5, pp. 590-597.

Tilley, A. R., Henry Dreyfuss Associates, 2002, *The Measure of Man and Woman: Human Factors in Design*, revised edn., John Wiley & Sons, New York.

Tyrrell, A. R., Reilly, T., & Troup, J. D. 1985, "Circadian variation in stature and the effects of spinal loading", *Spine*, vol. 10, pp. 161-164.

Umberger, B. R., Nawoczenski, D. A., & Baumhauer, J. F. 1999, "Reliability and validity of first metatarsophalangeal joint orientation measured with an electromagnetic tracking device", *Clinical Biomechanics*, vol. 14, no. 1, pp. 74-76.

Urban, J. P., Holm, S., Maroudas, A., *et al*. 1977, "Nutrition of the intervertebral disc. An *in vivo* study of solute transport", *Clinical Orthopaedics* pp. 101-114.

Vaisbuch, N., Meyer, S., & Weiss, P. L. 2000, "Effect of seated posture on interface pressure in children who are able-bodied and who have myelomeningocele", *Disability and Rehabiliation*, vol. 22, no. 17, pp. 749-755.

van Deursen, D. L., Goossens, R. H. M., Evers, J. J. M., van der Helm, F. C. T., & van Deursen, L. L. J. M. 2000, "Length of the spine while sitting on a new concept for an office chair", *Applied Ergonomics*, vol. 31, pp. 95-98.

van Dieën, J. H. & Toussaint, H. M. 1993, "Spinal shrinkage as a parameter of functional load", *Spine*, vol. 18, no. 11, pp. 1504-1514.

van Dieën, J. H., Creemers, M., Draisma, I., & Toussaint, H. M. 1994, "Repetitive lifting and spinal shrinkage, effects of age and lifting technique", *Clinical Biomechanics*, vol. 9, no. 6, pp. 367-374.

van Dieën, J. H., de Looze, M. P., & Hermans, H. 2001, "Effects of dynamic office chairs on trunk kinematics, trunk extensor EMG and spinal shrinkage", *Ergonomics*, vol. 44, no. 7, pp. 739-750.

Vanharanta, H., Sachs, B. L., Spivey, M. A., *et al*. 1987, "The relationship of pain provocation to lumbar disc deterioration as seen by CT/discography", *Spine*, vol. 12, pp. 295-298.

Verver, M. M. & Van Hoof, J. 2002, "Vibration analysis with MADYMO human models", *SAE Digital Human Modeling Conference*, Munich, VDI-Berichte Nr. 1675, pp. 447-455.

Wilke, H., Neef, P., Caimi, M., Hoogland, T., & Claes, L. E. 1999, "New *In Vivo* measurements of pressures in the intervertebral disc in daily life", *Spine*, vol. 24, no. 8, pp. 755-762.

Winter, D. A. 1979, *Biomechanics of Human Movement*, John Wiley & Sons, New York.

Wu, C., Miyamoto, H., & Noro, K. 1998, "Research on pelvic angle variation when using a pelvic support", *Ergonomics*, vol. 41, no. 3, pp. 317-327.

XSENSOR Technology Corporation, Sensor specification datasheet [PDF]. Retrieved October 30, 2012 from http://www.xsensor.com/media/upload/xsensor-spec-X3-PX100-36-36-02.pdf.

Yang, K. H. & King, A. I. 1984, "Mechanism of facet load transmission as a hypothesis for low-back pain", *Spine*, vol. 9, pp. 557-565.

Yang, J. F. & Winter, D. A. 1983, "Electromyography reliability in maximal and submaximal isometric contractions", *Archives of Physical Medicine and Rehabilitation*, vol. 64, pp. 417-420.

Zacharkow, D. 1884, *Wheelchair Posture and Pressure Sores*, Charles C Thomas Publisher, Springfield, Illinois.

Appendix A

A-1 **Information sheet and consent form**

Information sheet

Help us to understand the effects that different sitting postures have on our bodies

We would like to invite you to take part in our research. This information sheet contains all information about our research into sitting postures. Please take time to read through this sheet and feel free to ask us any questions.

What are the different sitting postures?

We are looking at the kind of sitting postures people assume when they relax in a recliner chair at home. The postures will range between upright and fully reclined. Some postures are good for watching television, chatting or reading a book and others are suited to having a snooze. The tests are planned to look at 5 sitting postures and (so we can compare results) lying down.

How will the different postures be measured?

Before measuring the different sitting postures the subjects will need to be measured. This will be done by the senior lecturer of the department at the university. Measurements will be taken of body parts such as hip breadth and leg length. Skin fold measurements will need to be taken (pinching the skin behind the shoulder blades and taking a measurement), and also weight will be taken.

The only part of the body that will need to be accessed in the study is the back so subjects will be asked to wear a loose T-shirt that can be rolled up at the back. All information will be strictly confidential. The study needs to be done on a group of people that best represents the population which the test result will be relevant to. Therefore the measurements are needed to validate the study.

We have designed and built a highly adjustable chair called a test-rig which will achieve all of the postures we want to study.

We plan to measure 5 things in each posture:

Changes in people's height

Many people are already aware that they are taller in the morning than in the afternoon. The reason for this is that the sponge like discs between the vertebrae in the spine get squashed. With very accurate measurements it is possible to get an understanding of the condition of the spine by measuring how squashed the discs are. For example, if a person is carrying a heavy bag the spine is likely to shrink because of the extra loading. In the same sense if a person lies down it is likely that the spine will increase in height because there is less loading. Therefore we can understand more about the effects of different postures by measuring changes in the height of the spine.

The measurement has to be very accurate though because the changes are quite small. A special piece of equipment has been made for the job called a stadiometer. This is all

about controlling posture so that the same posture can be repeated again and again. Some of the ways in which the stadiometer controls posture is to tilt the body back 10°, weigh the distribution under the feet, align the spine and align the head.

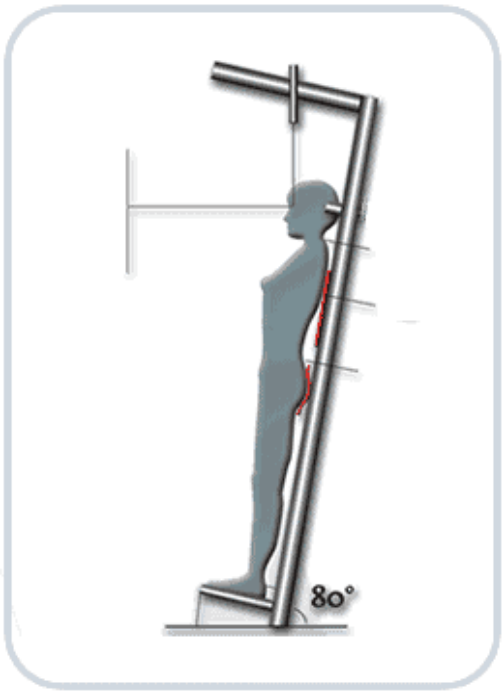

Stadiometer

Changes in seat and backrest pressure
Special flexible mats will be placed on the seat cushion and back cushion. The mats have sensors in them which send signals to a computer that displays the pressure distribution. An example is shown below. Here the red shows the highest pressure.

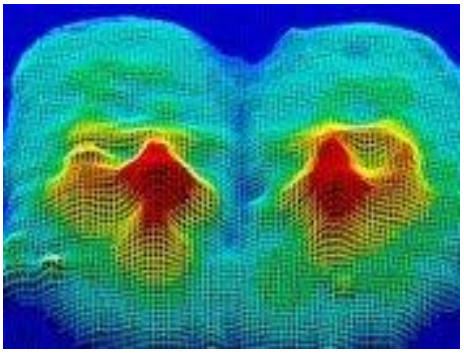
Pressure mapping

Changes in muscle activity
Even when sitting relaxed or lying down our muscles are at work. This can be measured by putting electrodes over the muscles of interest. In sitting this tends to be the back muscles. The electrodes are about the size of a 5p coin and taped in position with anti-allergic tape. In order to ensure that they can be placed in the same place on different days a mark will be made with a permanent marker. The subject will be asked to wear a loose T-shirt so that it can be rolled up at the back so the electrodes can be placed. The process is called Surface Electromyography (SMEG). The sensors do not give any sensation to the subject; they simply pick up the natural electric signals which come from the muscles.

Changes in the shape of the spine
For this special equipment will be used that records motion. An example is given below of how the equipment has been used to look at the swing of a golfer when striking the ball.

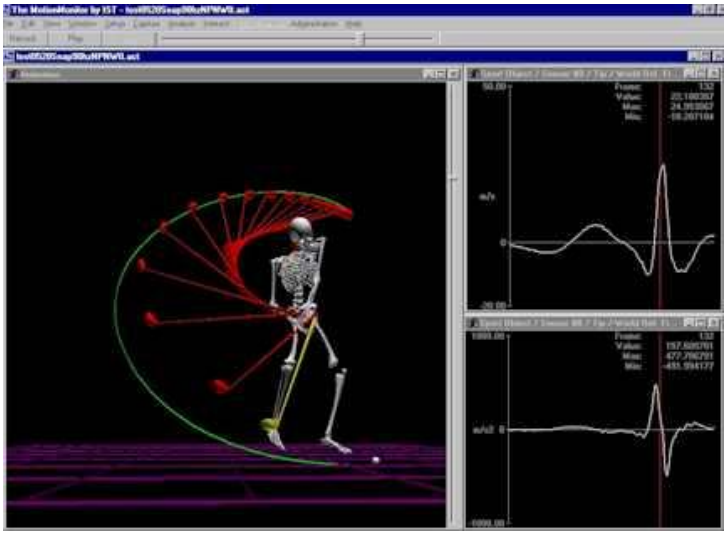

Motion tracking

The equipment consists of:

- 8 small sensors that have a similar size as a 2p coin. These are place on the skin over the spine with anti-allergic tape.
- Special magnetic equipment that measures the position of the sensors. This device will be placed approximately 1 meter away from the subject.
- A computer and software to record, calculate, and display accurate positions of the sensors as shown above.

Is the process painful?
Not at all!

Is there any health risk involved?
The measurement methods described have been used in many studies. The most recent technology used in the testing is the motion tracking and this system has been used for over 15 years in many hospitals around the world. The level of current and magnetic field used in this study are so small that they will not affect the subject.

Is the subject insured if he/she is injured during the study?
It is very unlikely that an accident should happen during the study. However, if an accident happens, the subject is injured and it is the fault of the researcher, then the subject will automatically be covered by insurance. If an accident happens, the subject is hurt and it is not because of negligence on the part of the researcher, then the subject will not be covered by insurance.

How confidential is the subject information?
Only the researcher and research supervisor will have access to the subject's information, which will be kept strictly confidential.

Who will cover the travel costs?
Transportation will be arranged for the subjects so no cost will be incurred.

What if the potential subject refuses to participate in the study?

Nothing. If the potential subject is a person who might be involved in the University or collaborating company, there will be no pressure whatsoever from the researcher. People will be treated with dignity, courtesy and respect. You can decline participation in this study if you do not feel comfortable with it and you will not have to give any reason for your decision.

Does the subject have to reply immediately whether he/she will participate in the study?

No. You are encouraged to take you time to think about it. You are welcome to contact the researcher for more information before making your mind up.

Any further questions?

Please do not hesitate to contact the researcher for more information.

Consent Form

Kirton Healthcare Group Limited,
23 Rockwood Way, Haverhill, Suffolk CB9 8PB

Title of Project: The investigation into effects of relaxing sitting postures

Name of Researcher: David Wickett

	Please initial box
1. I confirm that I have read and understand the information sheets for the above study and have had the opportunity to ask questions	
2. I understand that my participation is voluntary and that I am free to withdraw at any time, without giving any reason, without my medical care or legal rights being affected.	
3. I agree to take part in the above study	

Name of participant		Signature		Date	

Appendix B

B-1 **Assessment of filtering settings for sEMG data**

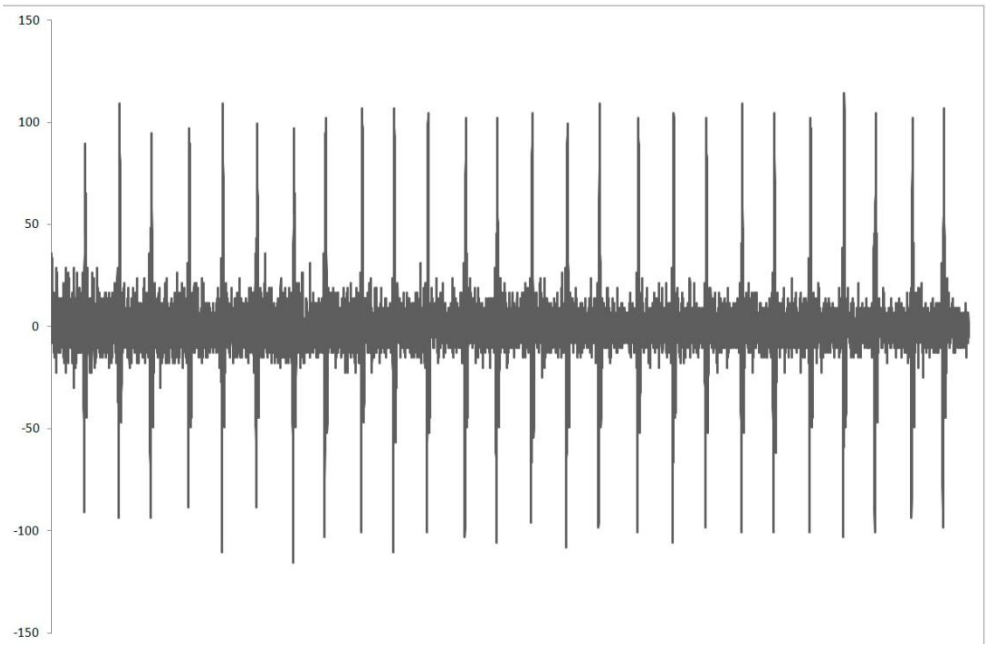

Figure B-1-1 T8 raw sEMG data

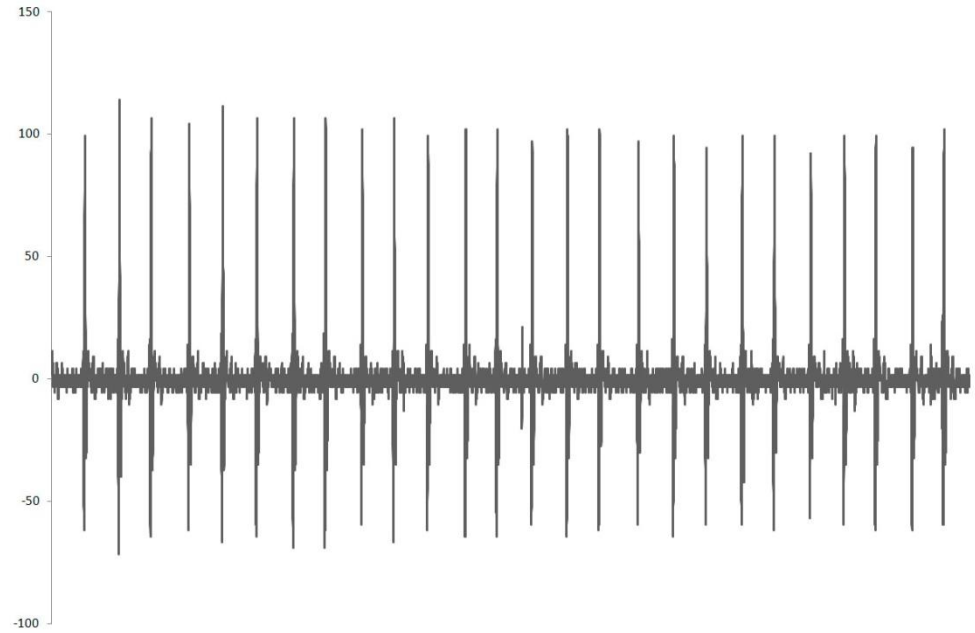

Figure B-1-2 Iliocostalis left raw sEMG data

Figure B-1-3 T8 raw data high-pass filtered at 10 Hz

Figure B-1-4 Iliocostalis left raw data high-pass filtered at 10 Hz

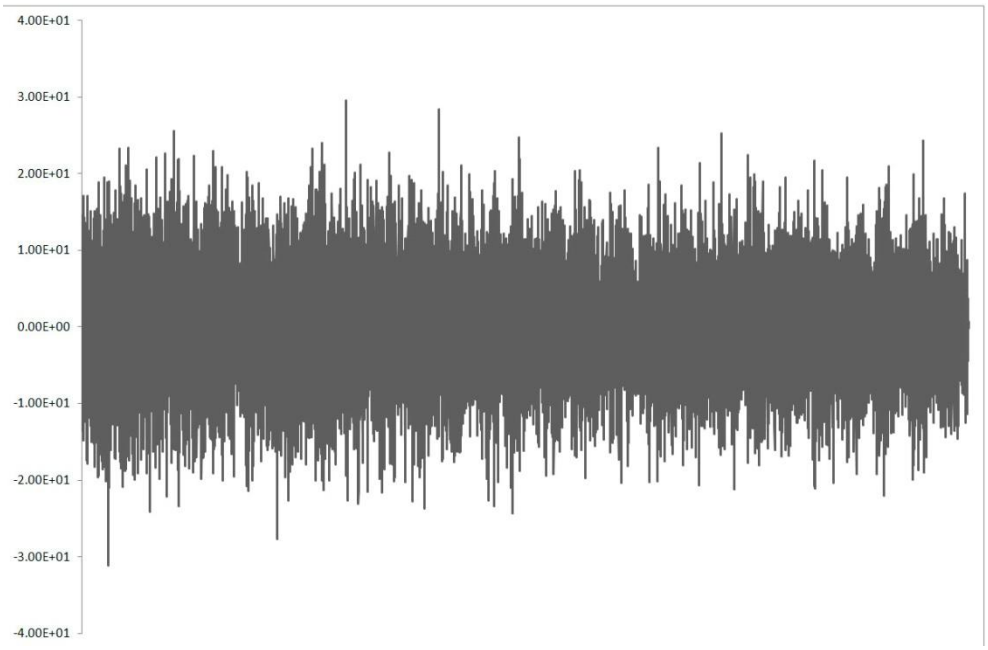

Figure B-1-5 T8 raw data high-pass filtered at 20 Hz

Figure B-1-6 Iliocostalis left raw data high-pass filtered at 20 Hz

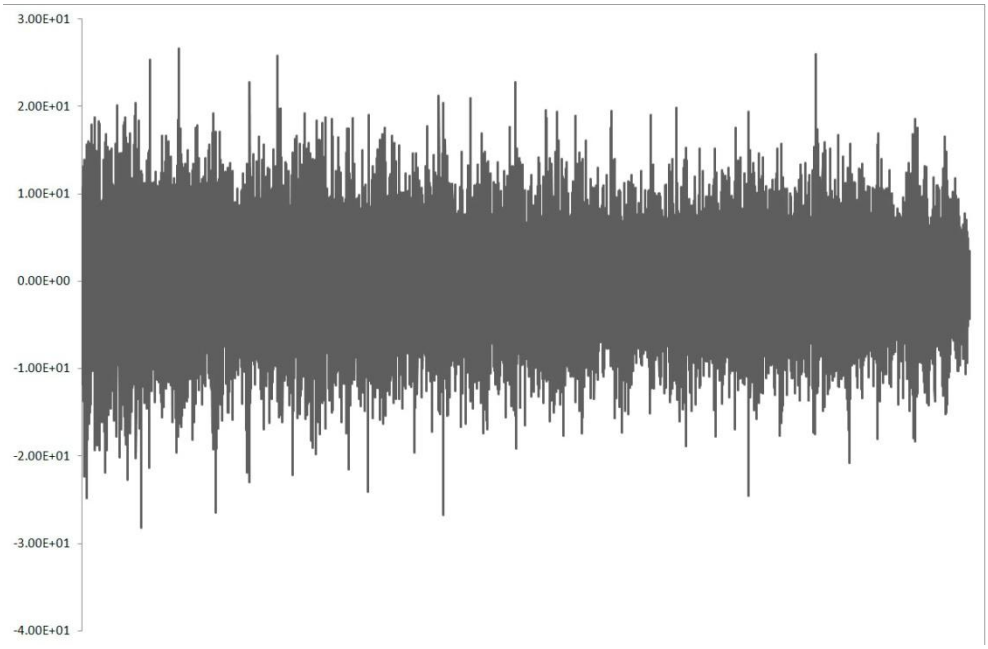

Figure B-1-7 T8 raw data high-pass filtered at 30 Hz

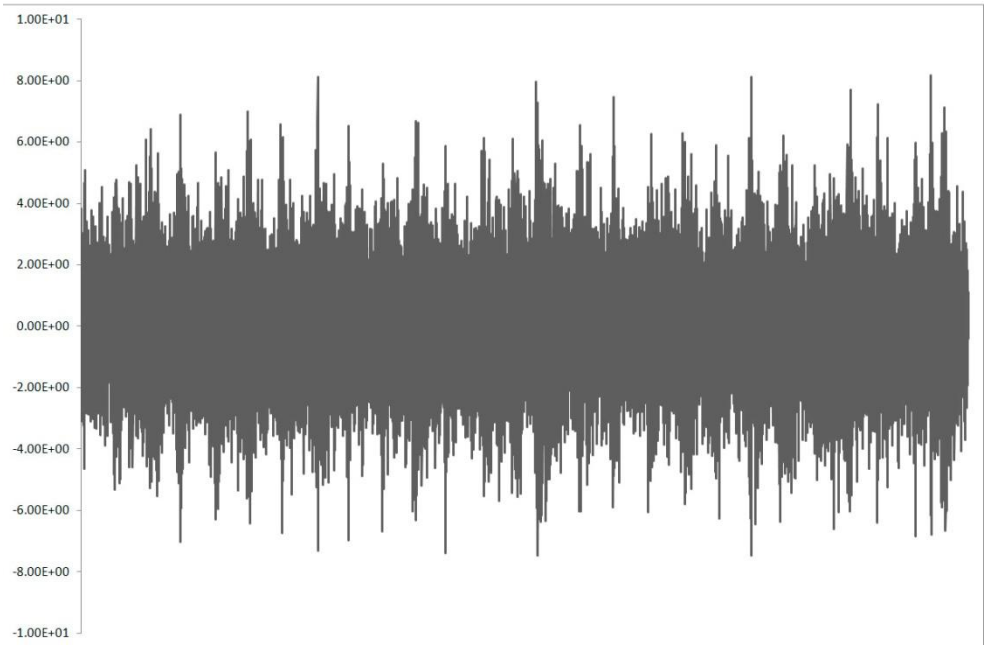

Figure B-1-8 Iliocostalis left raw data high-pass filtered at 30 Hz

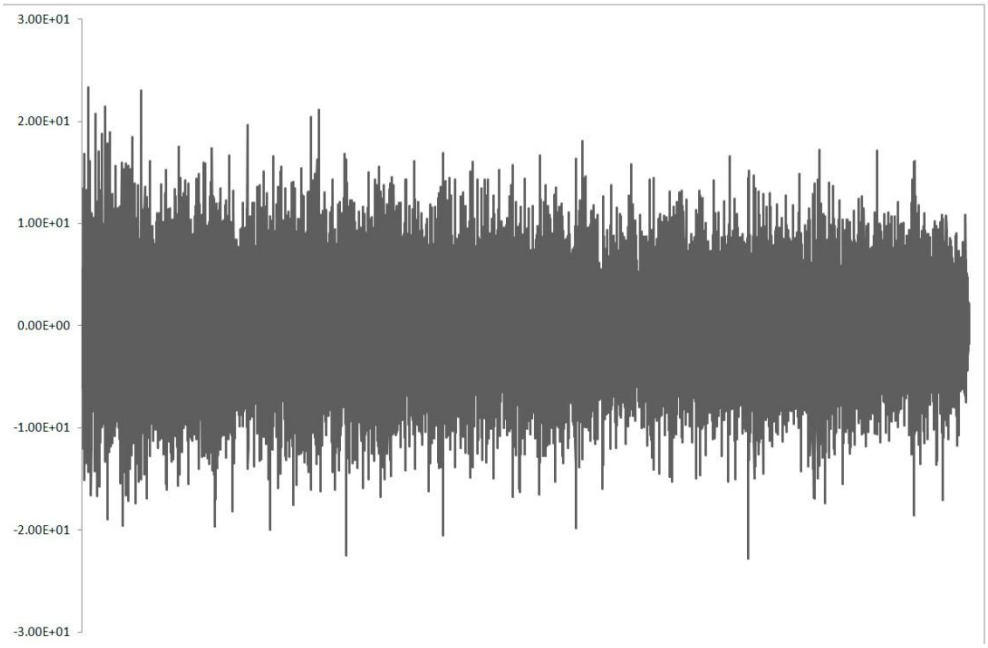

Figure B-1-9 T8 raw data high-pass filtered at 50 Hz

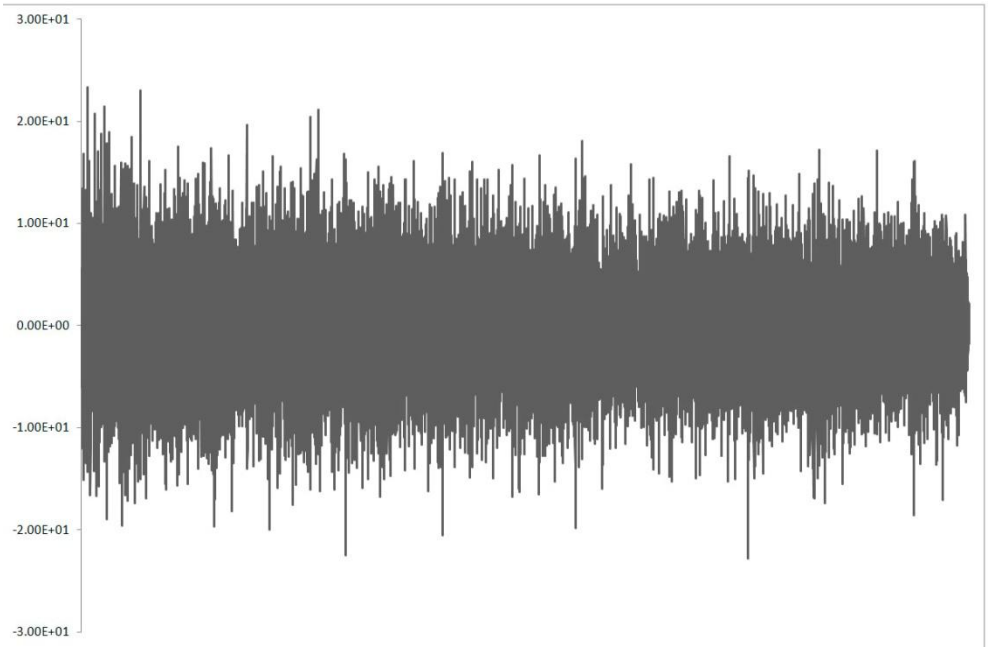

Figure B-1-10 Iliocostalis left raw data high-pass filtered at 50 Hz

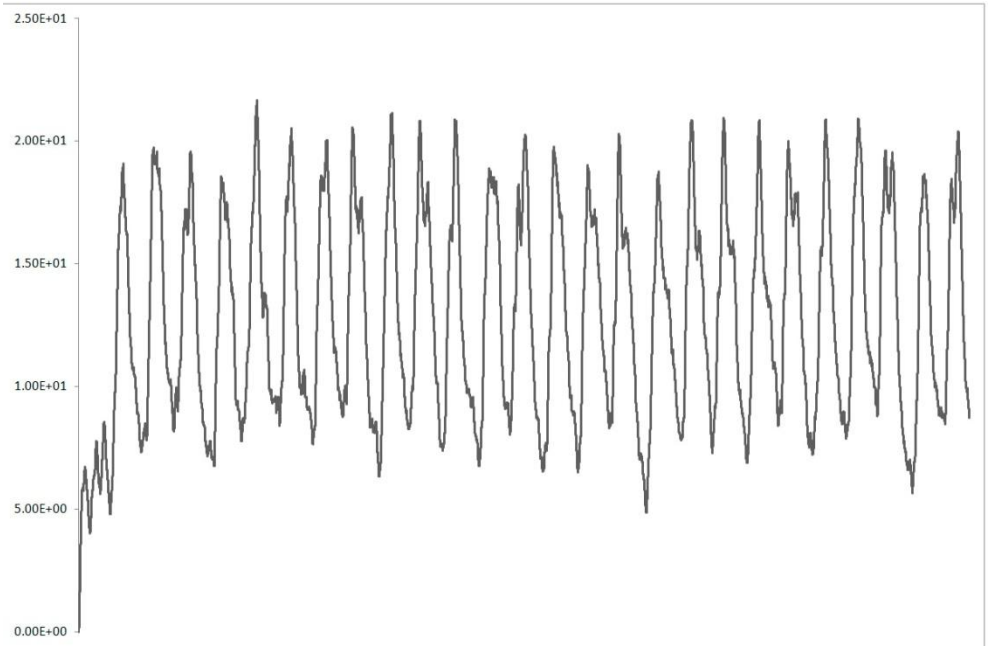

Figure B-1-11 T8 linear envelope: high-pass filter cut-off frequency 10 Hz, linear envelope time-constant 50 ms

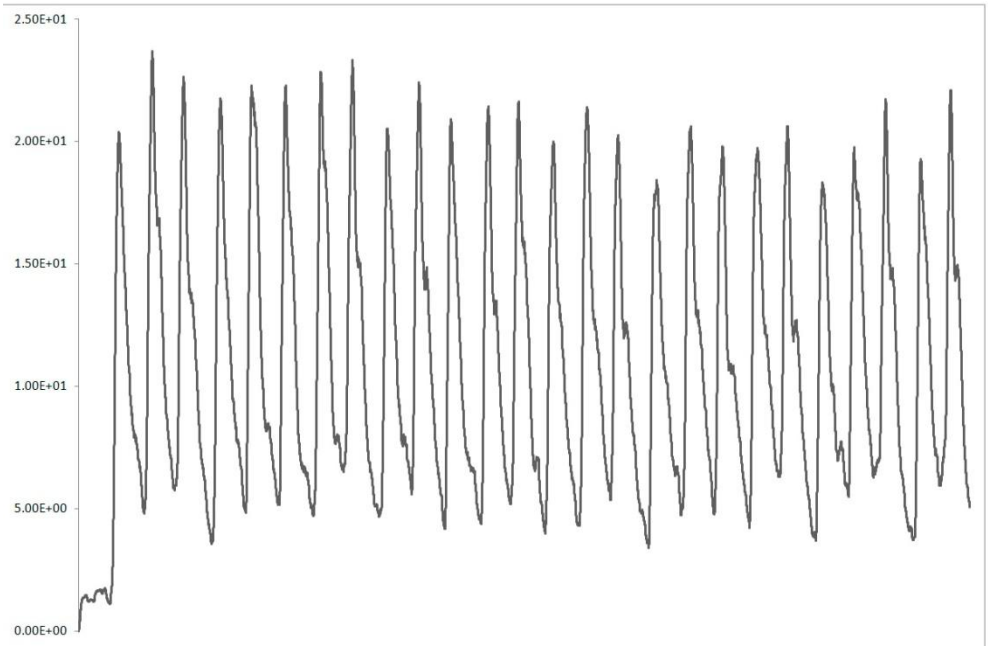

Figure B-1-12 Iliocostalis left linear envelope: high-pass filter cut-off frequency 10 Hz, linear envelope time-constant 50 ms

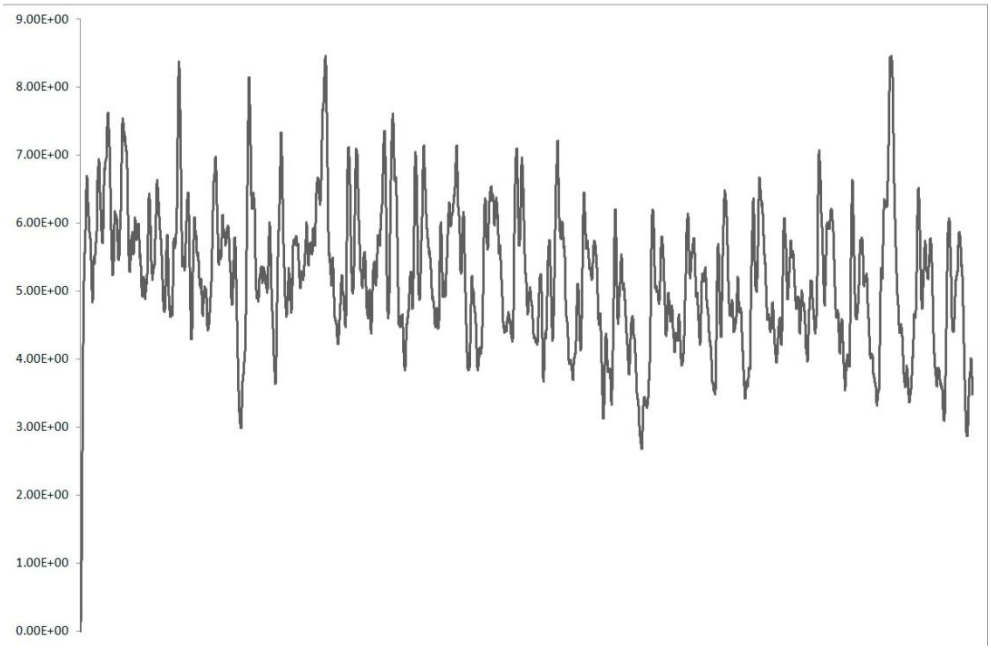

Figure B-1-13 T8 linear envelope: high-pass filter cut-off frequency 20 Hz, linear envelope time-constant 50 ms

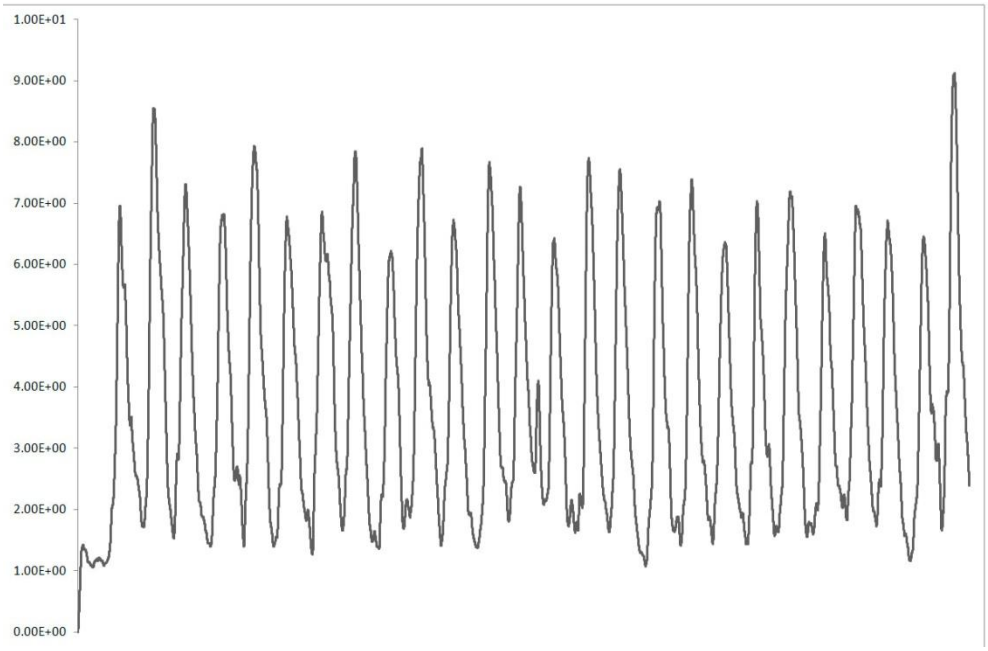

Figure B-1-14 Iliocostalis left linear envelope: high-pass filter cut-off frequency 20 Hz, linear envelope time-constant 50 ms

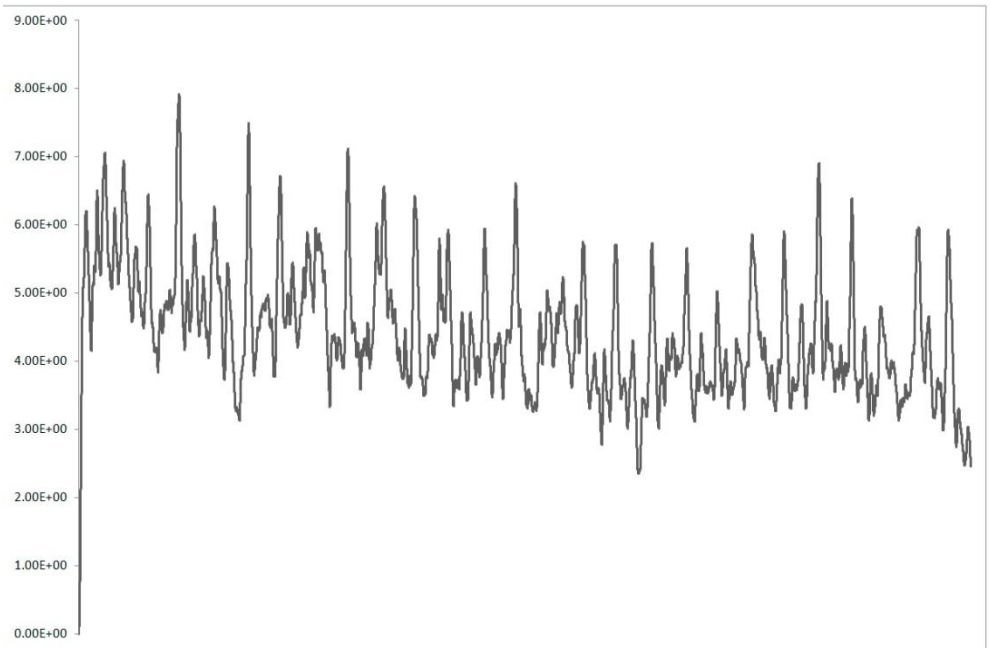

Figure B-1-15 T8 linear envelope: high-pass filter cut-off frequency 30 Hz, linear envelope time-constant 50 ms

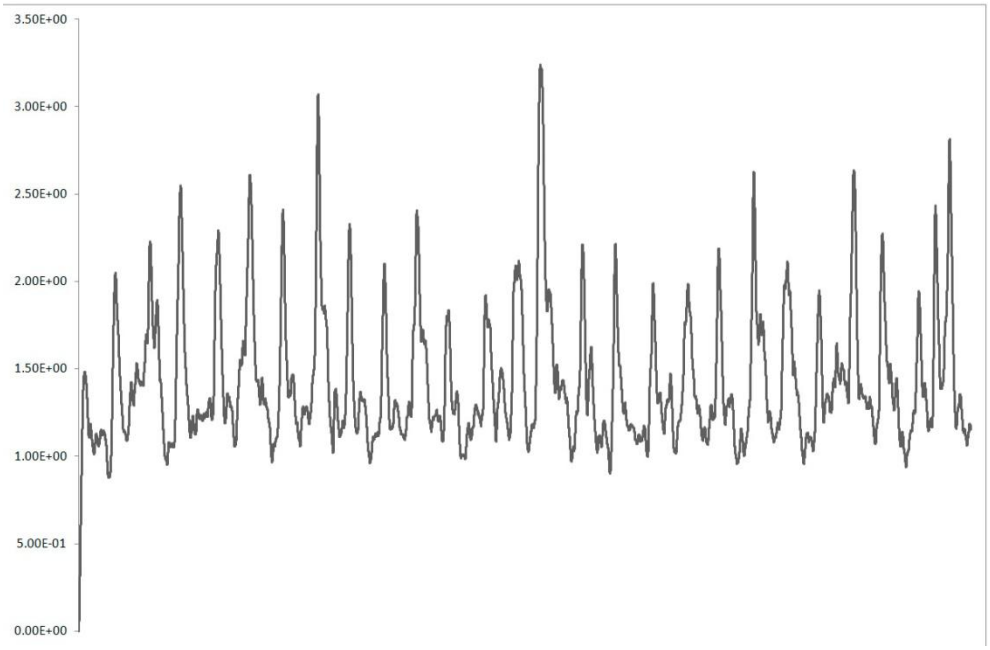

Figure B-1-16 Iliocostalis left linear envelope: high-pass filter cut-off frequency 30 Hz, linear envelope time-constant 50 ms

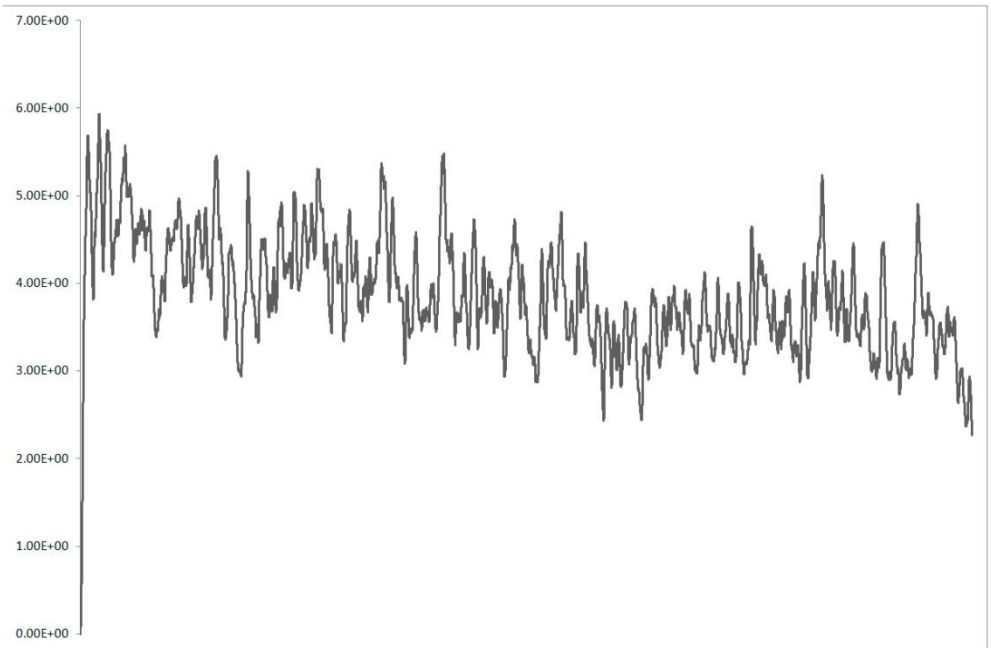

Figure B-1-17 T8 linear envelope: high-pass filter cut-off frequency 50 Hz, linear envelope time-constant 50 ms

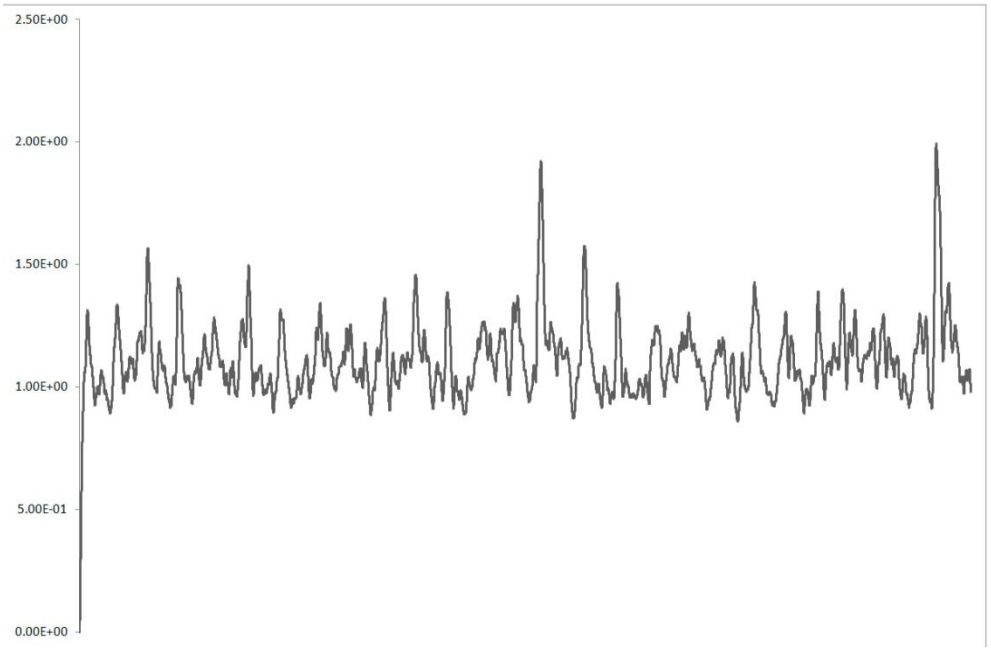

Figure B-1-18 Iliocostalis left linear envelope: high-pass filter cut-off frequency 50 Hz, linear envelope time-constant 50 ms

Appendix C

C-1 Pressure mapping data (giving mean, standard deviation and the coefficient of variation)

Table C-1-1 Seat Contact Area Threshold data (values = mean contact area over all frames for each recording session)

Subject	Upright	Standard	TIS 1	TIS 1a	Half tilt	Full tilt
1	1103	1010	1031	1119	1097	913
2	1140	1167	1116	1156	1195	960
3	1082	1076	1095	1116	1116	1005
4	1106	1397	1416	1476	1469	1218
5	1226	1187	1182	1290	1302	1147
6	1198	1098	1202	1239	1160	1008
7	1189	1156	1261	1377	1334	1165
8	1252	1235	1311	1290	1327	1166
9	1389	1360	1390	1439	1437	1308
10	1279	1181	1287	1410	1339	1127
11	1237	1218	1223	1281	1268	1076
12	1237	1184	1194	1247	1268	1165
13	1034	1090	1097	1153	1148	958
14	1334	1255	1179	1135	1295	942
15	1234	1095	1140	1195	1237	1000
Average	1203	1181	1208	1262	1266	1077
SD	96	104	110	119	110	117
COV (%)	8	9	9	9	9	11

Table C-1-2 Back Contact Area Threshold data (values = mean contact area over all frames for each recording session)

Subject	Upright	Standard	TIS 1	TIS 1a	Half tilt	Full tilt
1	761	948	1445	1390	860	1100
2	881	1204	1484	1537	961	1248
3	711	789	984	1073	602	994
4	953	1026	1663	1621	1010	1455
5	763	924	1437	1468	1006	1294
6	702	858	1235	1335	1105	1195
7	840	960	1566	1487	1056	1311
8	869	1100	1624	1461	1189	1374
9	1108	1463	1887	1856	1352	1577
10	1071	1277	1697	1758	1161	1466
11	806	994	1340	1316	756	1123
12	831	1002	1542	1371	1010	1297
13	568	921	1221	1197	810	1060
14	674	882	1471	1418	960	1261
15	877	990	1435	1426	995	1166
Average	828	1022	1469	1448	989	1261
SD	144	175	219	198	184	162
COV (%)	17	17	15	14	19	13

Table C-1-3 Seat Average Pressure data (values = mean average pressures over all frames for each recording session)

Subject	Upright	Standard	TIS 1	TIS 1a	Half tilt	Full tilt
1	52	43	39	45	48	37
2	49	43	39	43	43	33
3	46	41	43	45	43	34
4	55	42	39	43	44	33
5	51	47	43	47	47	38
6	50	42	41	42	41	30
7	55	45	43	48	46	36
8	53	45	41	43	46	37
9	50	42	49	51	50	40
10	51	44	41	47	43	32
11	53	41	43	47	44	35
12	50	45	41	44	46	37
13	48	37	39	44	44	33
14	47	37	35	43	39	28
15	49	42	40	44	44	33
Average	51	43	41	45	45	34
SD	3	3	3	3	3	3
COV (%)	5	7	7	6	6	9

Table C-1-4 Back Average Pressure data (values = mean average pressures over all frames for each recording session)

Subject	Upright	Standard	TIS 1	TIS 1a	Half tilt	Full tilt
1	28	31	32	32	33	37
2	29	28	33	32	30	34
3	27	29	31	32	33	35
4	28	30	32	33	33	36
5	27	30	33	33	30	36
6	28	30	36	36	33	37
7	26	31	30	33	30	36
8	27	29	33	30	32	37
9	28	34	32	35	34	40
10	30	33	35	38	33	37
11	28	32	31	34	30	35
12	27	29	31	33	30	35
13	30	31	32	32	30	35
14	26	28	32	33	29	34
15	28	31	32	34	32	37
Average	28	30	32	33	31	36
SD	1	2	1	2	2	1
COV (%)	4	6	4	6	5	4

Table C-1-5 Peak Pressure Index data (values = mean PPI values over all frames for each recording session)

Subject	Upright	Standard	TIS 1	TIS 1a	Half tilt	Full tilt
1	184	91	72	116	121	68
2	128	75	68	74	79	46
3	83	84	86	81	66	46
4	180	83	81	102	80	52
5	120	93	80	82	74	47
6	93	81	72	93	76	42
7	195	102	81	120	94	49
8	100	89	85	92	74	53
9	154	88	92	116	98	59
10	113	98	100	135	65	43
11	127	68	65	71	73	43
12	95	99	66	66	71	49
13	219	69	80	100	111	52
14	171	71	89	135	87	49
15	129	95	74	97	72	42
Average	139	86	79	99	83	49
SD	42	11	10	22	17	7
COV (%)	30	13	13	22	20	14

C-2 Exploration of the pressure mapping data (examples of histograms for skewed data)

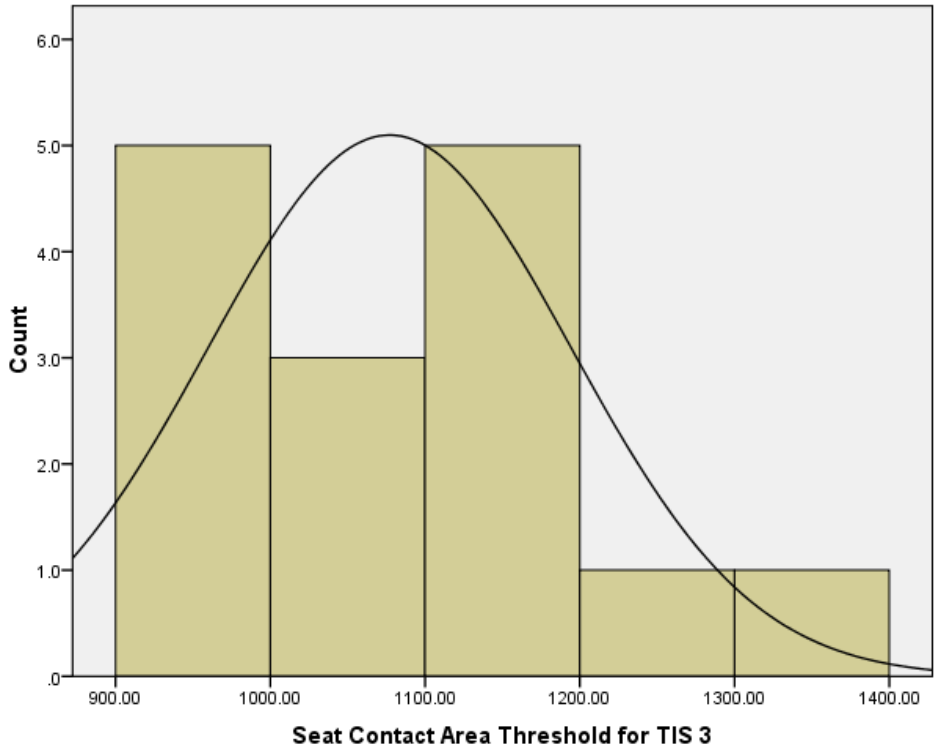

Figure C-2-1 Histogram for Seat Contact Area Threshold data for the TIS 3 posture

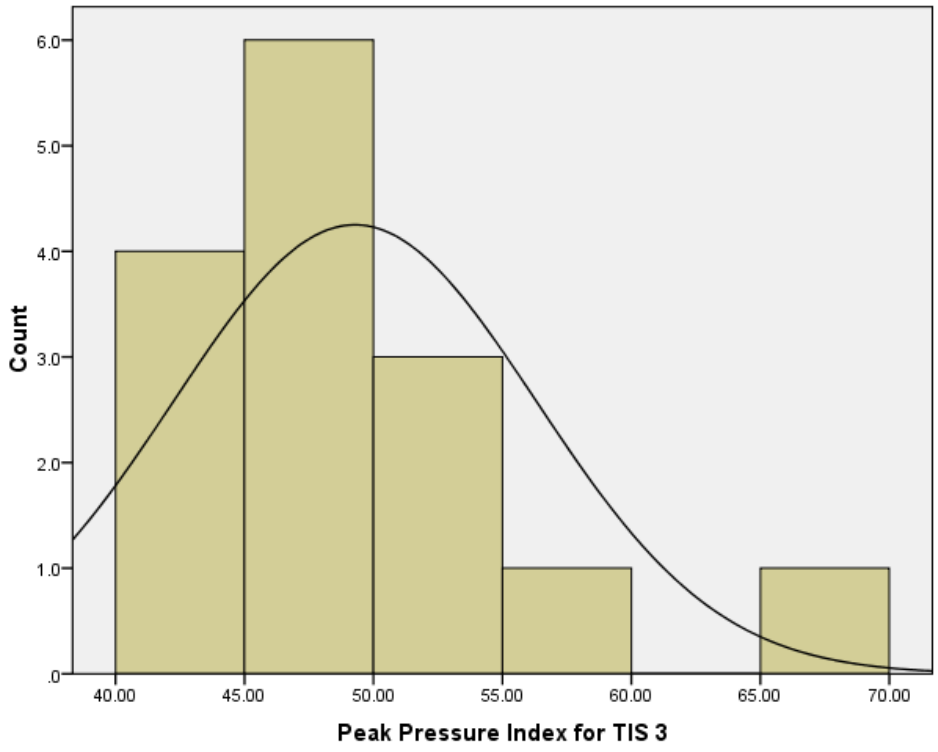

Figure C-2-2 Histogram for Peak Pressure Index data for the TIS 3 posture

C-3 Test results for normality of distributions and homogeneity of variance

SCAT = Seat Contact Area Threshold

BCAT = Back Contact Area Threshold

SA = Seat Average Pressure

BA = Back Average Pressure

PPI = Peak Pressure Index

Table C-3-1 Results for tests for normality of distribution for all pressure parameters (*.200 is the lower bound of the true significance)

		Kolmogorov-Smirnova			Shapiro-Wilk		
	Posture	Statistic	df	Sig.	Statistic	df	Sig.
SCAT	Upright	.128	15	.200*	.973	15	.905
	Standard	.142	15	.200*	.952	15	.549
	TIS 1a	.144	15	.200*	.924	15	.218
	TIS 1	.124	15	.200*	.966	15	.803
	TIS 2	.121	15	.200*	.964	15	.758
	TIS 3	.188	15	.159	.937	15	.344
BCAT	Upright	.157	15	.200*	.970	15	.852
	Standard	.226	15	.038	.891	15	.069
	TIS 1a	.154	15	.200*	.967	15	.806
	TIS 1	.173	15	.200*	.976	15	.932
	TIS 2	.170	15	.200*	.976	15	.937
	TIS 3	.112	15	.200*	.983	15	.984
SA	Upright	.105	15	.200*	.959	15	.682
	Standard	.143	15	.200*	.944	15	.436
	TIS 1a	.161	15	.200*	.924	15	.221
	TIS 1	.152	15	.200*	.933	15	.302
	TIS 2	.125	15	.200*	.983	15	.987
	TIS 3	.105	15	.200*	.984	15	.990
BA	Upright	.115	15	.200*	.955	15	.604
	Standard	.089	15	.200*	.977	15	.949
	TIS 1a	.156	15	.200*	.946	15	.465
	TIS 1	.191	15	.144	.902	15	.103
	TIS 2	.252	15	.011	.859	15	.024
	TIS 3	.135	15	.200*	.946	15	.466
PPI	Upright	.199	15	.115	.939	15	.369
	Standard	.110	15	.200*	.945	15	.449
	TIS 1a	.116	15	.200*	.952	15	.551
	TIS 1	.136	15	.200*	.964	15	.757
	TIS 2	.242	15	.018	.858	15	.023
	TIS 3	.186	15	.171	.864	15	.028

Table C-3-2 Results for tests for homogeneity of variance for all pressure parameters

		Levene Statistic	df1	df2	Sig.
SCAT	Based on Mean	.431	5	84	.826
	Based on Median	.413	5	84	.838
	Based on Median and with adjusted df	.413	5	82.208	.838
	Based on trimmed mean	.424	5	84	.831
BCAT	Based on Mean	.290	5	84	.917
	Based on Median	.294	5	84	.915
	Based on Median and with adjusted df	.294	5	76.336	.915
	Based on trimmed mean	.293	5	84	.916
SA	Based on Mean	.183	5	84	.968
	Based on Median	.188	5	84	.966
	Based on Median and with	.188	5	80.343	.966
	Based on trimmed mean	.185	5	84	.968
BA	Based on Mean	1.316	5	84	.265
	Based on Median	.924	5	84	.470
	Based on Median and with adjusted df	.924	5	72.214	.470
	Based on trimmed mean	1.297	5	84	.273
PPI	Based on Mean	15.173	5	84	.000
	Based on Median	8.610	5	84	.000
	Based on Median and with adjusted df	8.610	5	32.914	.000
	Based on trimmed mean	14.302	5	84	.000

Table C-3-3 Normality test results on transformed data (*.200 is the lower bound of the true significance)

		Kolmogorov-Smirnova			Shapiro-Wilk		
	Posture	Statistic	df	Sig.	Statistic	df	Sig.
BCAT_square_root	Upright	.143	15	.200*	.977	15	.946
	Standard	.210	15	.074	.915	15	.162
	TIS 1a	.142	15	.200*	.971	15	.876
	TIS 1	.188	15	.161	.963	15	.750
	TIS 2	.189	15	.155	.965	15	.781
	TIS 3	.102	15	.200*	.986	15	.995
BCAT_log	Upright	.132	15	.200*	.978	15	.958
	Standard	.194	15	.133	.936	15	.339
	TIS 1a	.131	15	.200*	.971	15	.872
	TIS 1	.203	15	.095	.945	15	.447
	TIS 2	.208	15	.079	.945	15	.448
	TIS 3	.092	15	.200*	.987	15	.997
BA_square_root	Upright	.113	15	.200*	.956	15	.618
	Standard	.088	15	.200*	.980	15	.972
	TIS 1a	.151	15	.200*	.951	15	.547
	TIS 1	.187	15	.166	.908	15	.127
	TIS 2	.250	15	.013	.861	15	.025
	TIS 3	.133	15	.200*	.950	15	.523
BA_log	Upright	.112	15	.200*	.956	15	.629
	Standard	.088	15	.200*	.983	15	.985
	TIS 1a	.146	15	.200*	.956	15	.626
	TIS 1	.183	15	.189	.914	15	.155
	TIS 2	.247	15	.014	.862	15	.026
	TIS 3	.130	15	.200*	.953	15	.577
PPI_square_root	Upright	.174	15	.200*	.950	15	.526
	Standard	.120	15	.200*	.939	15	.369
	TIS 1a	.122	15	.200*	.958	15	.662
	TIS 1	.148	15	.200*	.966	15	.796
	TIS 2	.229	15	.033	.879	15	.046
	TIS 3	.172	15	.200*	.886	15	.058
PPI_log	Upright	.148	15	.200*	.956	15	.621
	Standard	.130	15	.200*	.932	15	.289
	TIS 1a	.126	15	.200*	.961	15	.701
	TIS 1	.160	15	.200*	.966	15	.803
	TIS 2	.215	15	.062	.898	15	.087
	TIS 3	.158	15	.200*	.905	15	.113

Table C-3-4 Homogeneity of variance tests results on transformed data

		Levene Statistic	df1	df2	Sig.
BCAT_square_root	Based on Mean	.101	5	84	.992
	Based on Median	.085	5	84	.994
	Based on Median and with adjusted df	.085	5	78.056	.994
	Based on trimmed mean	.094	5	84	.993
BCAT_log	Based on Mean	.407	5	84	.843
	Based on Median	.312	5	84	.904
	Based on Median and with adjusted df	.312	5	73.22	.904
	Based on trimmed mean	.375	5	84	.865
BA_square_root	Based on Mean	1.342	5	84	.255
	Based on Median	.948	5	84	.455
	Based on Median and with adjusted df	.948	5	72.713	.456
	Based on trimmed mean	1.33	5	84	.260
BA_log	Based on Mean	1.426	5	84	.223
	Based on Median	1.015	5	84	.414
	Based on Median and with adjusted df	1.015	5	73.058	.415
	Based on trimmed mean	1.419	5	84	.226
PPI_square_root	Based on Mean	9.522	5	84	.000
	Based on Median	6.273	5	84	.000
	Based on Median and with adjusted df	6.273	5	45.92	.000
	Based on trimmed mean	9.165	5	84	.000
PPI_log	Based on Mean	4.901	5	84	.001
	Based on Median	3.632	5	84	.005
	Based on Median and with adjusted df	3.632	5	61.832	.006
	Based on trimmed mean	4.785	5	84	.001

D-1 Box plots and histograms for the stadiometry data

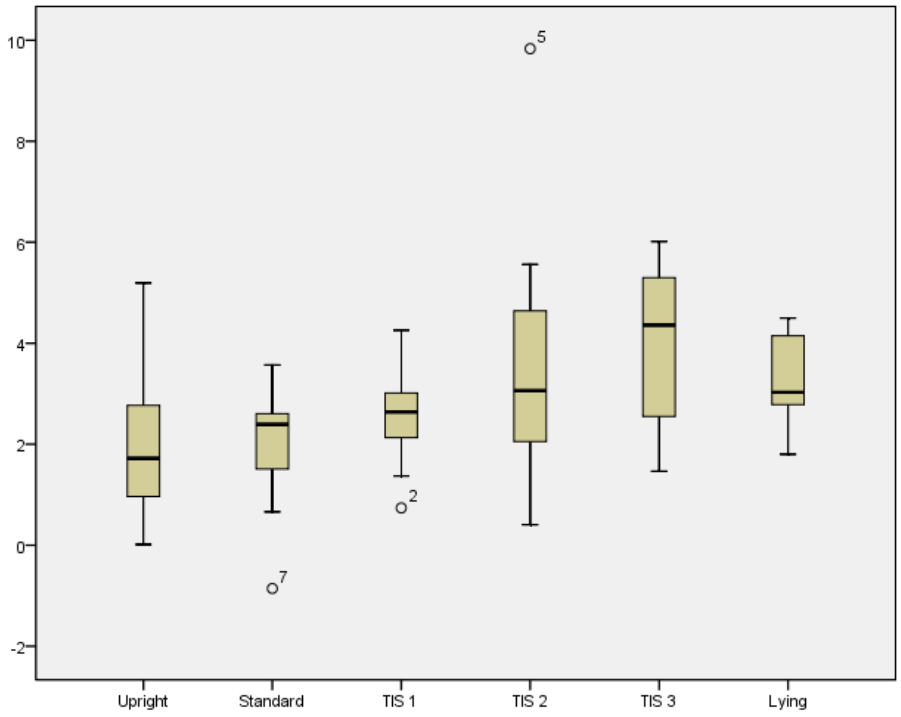

Figure D-1-1 Box plot for the stadiometry data (case 5 identified as an outlier)

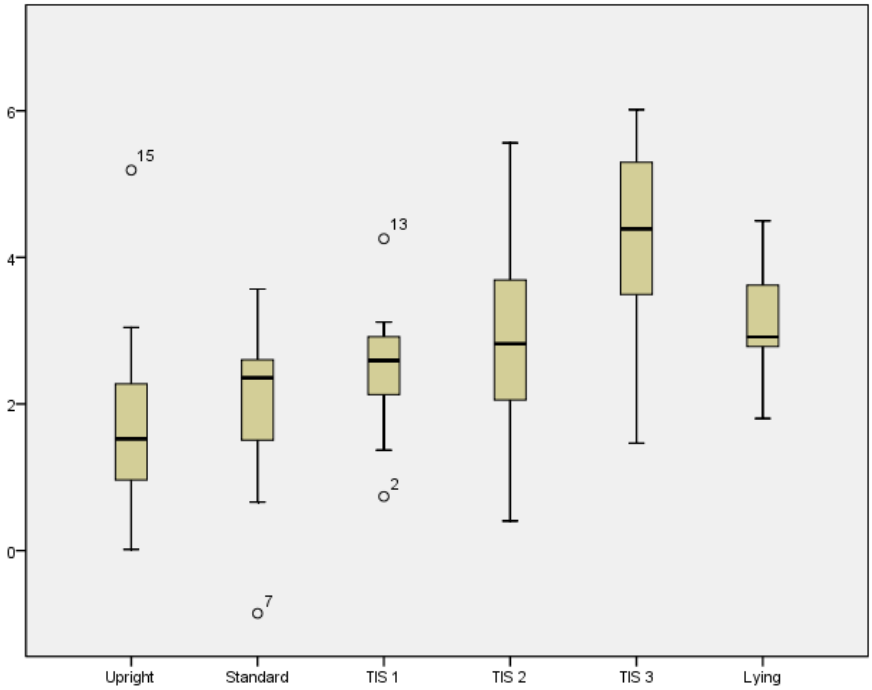

Figure D-1-2 Box plot for the stadiometry data with case 5 removed

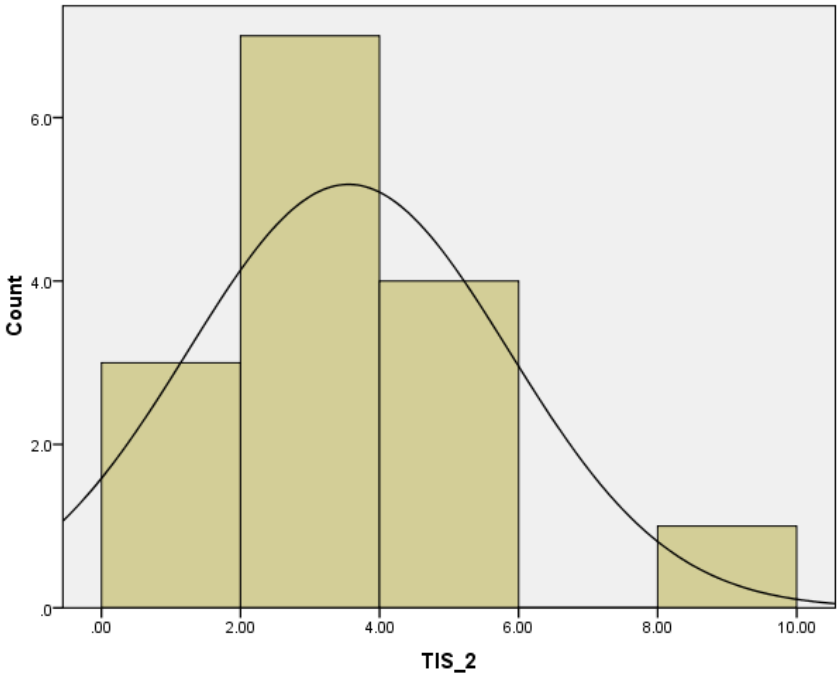

Figure D-1-3 Histogram of the stadiometry data for the TIS 2 posture (before the outliers were removed)

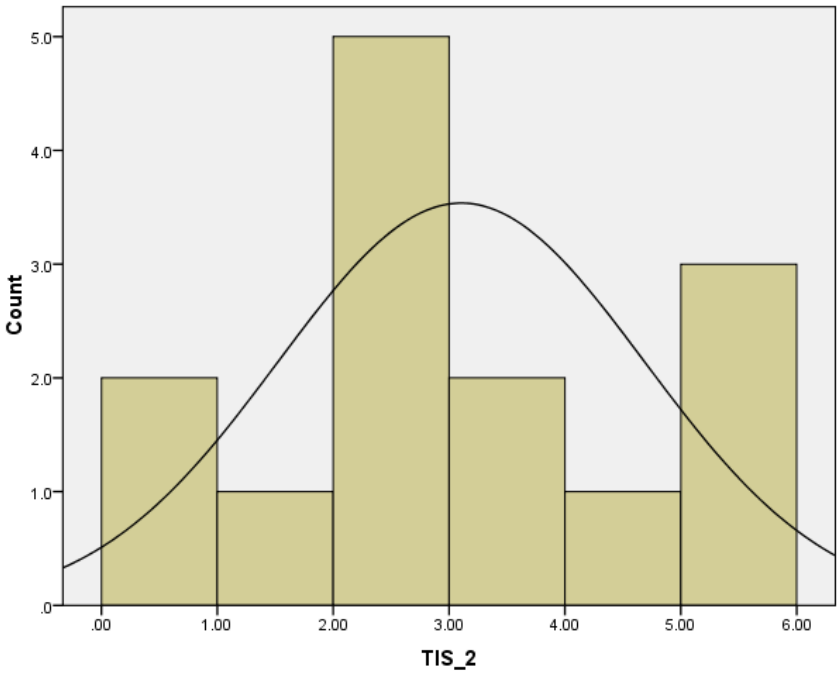

Figure D-1-4 Histogram for the TIS 2 posture after the outliers were removed

D-2 Test results for normality of distribution and homogeneity of variance (including transformations)

Table D-2-1 Results for the tests of normality of distribution for the stadiometry data (*.200 is the lower bound of the true significance)

		Kolmogorov-Smirnova			Shapiro-Wilk		
	Posture	Statistic	df	Sig.	Statistic	df	Sig.
Change in stature	Upright	.098	14	.200*	.965	14	.805
	Standard	.214	14	.082	.870	14	.042
	TIS 1	.247	13	.029	.897	13	.120
	TIS 2	.157	14	.200*	.939	14	.408
	TIS 3	.177	15	.200*	.955	15	.602
	Lying	.203	14	.121	.927	14	.279

Table D-2-2 Results for the test of homogeneity of variance for the stadiometry data

		Levene Statistic	df1	df2	Sig.
Change in stature	Based on Mean	.471	5	78	.797
	Based on Median	.470	5	78	.797
	Based on Median and with adjusted df	.470	5	75.895	.797
	Based on trimmed mean	.495	5	78	.779

Table D-2-3 Results for the tests of normality for the square root transformed data (*.200 is the lower bound of the true significance)

		Kolmogorov-Smirnova			Shapiro-Wilk		
	Posture	Statistic	df	Sig.	Statistic	df	Sig.
Change in stature	Upright	.127	14	.200*	.973	14	.917
square_root	Standard	.272	14	.006	.737	14	.001
	TIS 1	.216	13	.100	.940	13	.455
	TIS 2	.193	14	.164	.935	14	.358
	TIS 3	.205	15	.090	.937	15	.352
	Lying	.187	14	.198	.949	14	.553

Table D-2-4 Results for the tests of normality for the log transformed data (*.200 is the lower bound of the true significance)

		Kolmogorov-Smirnova			Shapiro-Wilk		
	Posture	Statistic	df	Sig.	Statistic	df	Sig.
Change in stature	Upright	.172	14	.200*	.945	14	.492
log	Standard	.334	14	.000	.557	14	.000
	TIS 1	.190	13	.200*	.950	13	.599
	TIS 2	.237	14	.032	.904	14	.129
	TIS 3	.231	15	.030	.912	15	.147
	Lying	.169	14	.200*	.962	14	.751

D-3 Results from the *post hoc* power analysis

Table D-3-1 Results from the *post hoc* power analysis

Power size	N	Alpha	Beta	Mean 0	Mean 1	SD	Effect size
0.18123	5	0.05	0.81877	0	-0.7	1.5	0.467
0.20818	6	0.05	0.79182	0	-0.7	1.5	0.467
0.2351	7	0.05	0.7649	0	-0.7	1.5	0.467
0.26189	8	0.05	0.73811	0	-0.7	1.5	0.467
0.28847	9	0.05	0.71153	0	-0.7	1.5	0.467
0.31476	10	0.05	0.68524	0	-0.7	1.5	0.467
0.34071	11	0.05	0.65929	0	-0.7	1.5	0.467
0.36624	12	0.05	0.63376	0	-0.7	1.5	0.467
0.39132	13	0.05	0.60868	0	-0.7	1.5	0.467
0.4159	14	0.05	0.5841	0	-0.7	1.5	0.467
0.43994	15	0.05	0.56006	0	-0.7	1.5	0.467
0.4634	16	0.05	0.5366	0	-0.7	1.5	0.467
0.48628	17	0.05	0.51372	0	-0.7	1.5	0.467
0.50853	18	0.05	0.49147	0	-0.7	1.5	0.467
0.53015	19	0.05	0.46985	0	-0.7	1.5	0.467
0.55113	20	0.05	0.44887	0	-0.7	1.5	0.467
0.57146	21	0.05	0.42854	0	-0.7	1.5	0.467
0.59112	22	0.05	0.40888	0	-0.7	1.5	0.467
0.61013	23	0.05	0.38987	0	-0.7	1.5	0.467
0.62847	24	0.05	0.37153	0	-0.7	1.5	0.467
0.64616	25	0.05	0.35384	0	-0.7	1.5	0.467
0.6632	26	0.05	0.3368	0	-0.7	1.5	0.467
0.6796	27	0.05	0.3204	0	-0.7	1.5	0.467
0.69536	28	0.05	0.30464	0	-0.7	1.5	0.467
0.7105	29	0.05	0.2895	0	-0.7	1.5	0.467
0.72502	30	0.05	0.27498	0	-0.7	1.5	0.467
0.73895	31	0.05	0.26105	0	-0.7	1.5	0.467
0.75229	32	0.05	0.24771	0	-0.7	1.5	0.467
0.76506	33	0.05	0.23494	0	-0.7	1.5	0.467
0.77727	34	0.05	0.22273	0	-0.7	1.5	0.467
0.78894	35	0.05	0.21106	0	-0.7	1.5	0.467
0.80009	36	0.05	0.19991	0	-0.7	1.5	0.467
0.81073	37	0.05	0.18927	0	-0.7	1.5	0.467
0.82088	38	0.05	0.17912	0	-0.7	1.5	0.467
0.83055	39	0.05	0.16945	0	-0.7	1.5	0.467
0.83977	40	0.05	0.16023	0	-0.7	1.5	0.467

Appendix E

E-1 sEMG linear envelop data normalised to the standing posture, mean and standard deviation

Table E-1-1 Mean linear envelope data normalised to standing for the multifidus left side

Subject	Upright	Upright ps	Standard	Standard ps	TIS 1	TIS 1 ps	TIS 2	TIS 2 ps	TIS 3	TIS 3 ps	Lying
1	26%	35%	11%	11%	2%	2%	8%	3%	2%	2%	2%
2	28%	47%	28%	21%	19%	19%	21%	23%	17%	17%	19%
3	28%	28%	25%	26%	22%	21%	40%	30%	26%	22%	34%
4	27%	26%	23%	23%	22%	23%	25%	28%	21%	21%	40%
5	41%	36%	28%	28%	26%	24%	33%	30%	24%	24%	24%
6	20%	23%	24%	20%	18%	19%	21%	27%	16%	18%	19%
7	66%	83%	68%	72%	47%	50%	64%	58%	41%	43%	84%
8	38%	35%	34%	33%	32%	33%	34%	33%	30%	29%	31%
9	58%	58%	0%	12%	13%	8%	55%	91%	9%	8%	10%
10	29%	30%	27%	28%	26%	29%	27%	32%	24%	29%	28%
11	87%	108%	84%	83%	73%	81%	75%	84%	63%	82%	81%
Mean	41%	46%	32%	33%	27%	28%	37%	40%	25%	27%	34%
SD	21%	27%	24%	23%	19%	21%	20%	27%	16%	21%	26%

Table E-1-2 Mean linear envelope data normalised to standing for the multifidus right side

Subject	Upright	Upright ps	Standard	Standard ps	TIS 1	TIS 1 ps	TIS 2	TIS 2 ps	TIS 3	TIS 3 ps	Lying
1	41%	46%	64%	34%	8%	8%	53%	9%	8%	8%	8%
2	38%	28%	21%	21%	20%	18%	22%	21%	17%	17%	21%
3	58%	50%	47%	46%	41%	39%	52%	49%	40%	43%	50%
4	114%	72%	29%	38%	30%	31%	86%	63%	27%	31%	77%
5	63%	63%	44%	51%	52%	49%	63%	50%	54%	44%	51%
6	24%	26%	25%	23%	14%	15%	31%	46%	16%	16%	20%
7	23%	26%	25%	23%	19%	19%	26%	21%	19%	17%	28%
8	57%	41%	40%	40%	38%	40%	41%	37%	35%	34%	38%
9	15%	46%	4%	33%	3%	3%	41%	11%	3%	3%	4%
10	89%	63%	49%	54%	51%	56%	44%	52%	38%	53%	55%
11	74%	72%	72%	75%	58%	63%	72%	73%	60%	Outlier	64%
Mean	54%	48%	38%	40%	30%	31%	48%	39%	29%	27%	38%
SD	30%	17%	20%	16%	19%	20%	20%	21%	18%	17%	24%

Table E-1-3 Mean linear envelope data normalised to standing for the iliocostalis left side

Subject	Upright	Upright ps	Standard	Standard ps	TIS 1	TIS 1 ps	TIS 2	TIS 2 ps	TIS 3	TIS 3 ps	Lying
1	63%	73%	63%	63%	56%	51%	48%	50%	40%	42%	40%
2	70%	105%	74%	77%	60%	66%	53%	88%	44%	64%	58%
3	46%	51%	53%	53%	41%	46%	50%	54%	40%	43%	38%
4	78%	89%	83%	75%	82%	97%	74%	92%	77%	88%	65%
5	66%	74%	66%	74%	53%	56%	56%	72%	50%	57%	56%
6	75%	92%	75%	94%	84%	84%	74%	87%	62%	75%	75%
7	83%	86%	81%	80%	87%	79%	76%	87%	62%	79%	106%
8	90%	102%	103%	94%	97%	98%	90%	94%	86%	91%	87%
9	71%	92%	29%	88%	62%	85%	68%	83%	73%	59%	54%
10	68%	94%	61%	73%	48%	51%	59%	61%	47%	49%	48%
11	73%	92%	68%	73%	54%	59%	76%	85%	47%	47%	50%
Mean	71%	86%	69%	77%	66%	70%	66%	77%	57%	63%	62%
SD	11%	15%	19%	12%	18%	19%	13%	16%	16%	18%	21%

Table E-1-4 Mean linear envelope data normalised to standing for the iliocostalis right side

Subject	Upright	Upright ps	Standard	Standard ps	TIS 1	TIS 1 ps	TIS 2	TIS 2 ps	TIS 3	TIS 3 ps	Lying
1	45%	49%	62%	47%	34%	34%	67%	34%	26%	29%	28%
2	51%	46%	38%	37%	34%	35%	35%	38%	33%	35%	39%
3	86%	80%	84%	74%	64%	73%	83%	84%	70%	65%	73%
4	111%	88%	57%	55%	61%	61%	95%	66%	54%	57%	55%
5	68%	78%	70%	77%	79%	76%	79%	85%	80%	82%	89%
6	74%	81%	79%	76%	82%	81%	72%	79%	68%	77%	84%
7	83%	103%	106%	103%	80%	89%	84%	88%	67%	71%	96%
8	87%	90%	88%	89%	90%	88%	83%	79%	76%	74%	96%
9	50%	54%	35%	51%	39%	44%	53%	48%	37%	41%	41%
10	92%	92%	77%	75%	70%	70%	74%	77%	70%	72%	82%
11	53%	57%	47%	50%	45%	48%	63%	55%	44%	45%	42%
Mean	73%	74%	67%	67%	62%	64%	72%	67%	57%	59%	66%
SD	21%	20%	22%	20%	21%	20%	17%	20%	19%	19%	25%

Table E-1-5 Mean linear envelope data normalised to standing for the longissimus left side

Subject	Upright	Upright ps	Standard	Standard ps	TIS 1	TIS 1 ps	TIS 2	TIS 2 ps	TIS 3	TIS 3 ps	Lying
1	120%	156%	82%	70%	34%	35%	79%	77%	28%	29%	28%
2	56%	105%	66%	22%	14%	15%	18%	29%	12%	13%	17%
3	188%	179%	91%	126%	21%	21%	293%	210%	83%	94%	61%
4	69%	45%	25%	23%	21%	22%	48%	59%	20%	21%	31%
5	110%	149%	60%	55%	46%	47%	80%	62%	41%	42%	57%
6	79%	104%	123%	45%	22%	22%	58%	98%	26%	19%	46%
7	139%	312%	148%	179%	59%	70%	108%	137%	41%	52%	162%
8	99%	81%	48%	44%	39%	40%	64%	49%	40%	36%	43%
9	168%	238%	26%	40%	38%	26%	128%	177%	56%	30%	27%
10	177%	148%	104%	75%	76%	39%	198%	49%	42%	40%	50%
11	105%	333%	94%	106%	78%	75%	103%	93%	67%	66%	71%
Mean	119%	168%	79%	71%	41%	37%	107%	94%	42%	40%	54%
SD	44%	92%	39%	48%	22%	20%	78%	58%	21%	24%	39%

Table E-1-6 Mean linear envelope data normalised to standing for the longissimus right side

Subject	Upright	Upright ps	Standard	Standard ps	TIS 1	TIS 1 ps	TIS 2	TIS 2 ps	TIS 3	TIS 3 ps	Lying
1	189%	133%	193%	54%	13%	12%	107%	50%	12%	12%	12%
2	53%	39%	27%	13%	9%	9%	25%	24%	11%	9%	11%
3	108%	85%	74%	69%	25%	26%	83%	65%	29%	26%	33%
4	93%	67%	17%	15%	10%	10%	87%	49%	9%	9%	10%
5	97%	86%	40%	33%	31%	29%	40%	39%	32%	30%	32%
6	91%	134%	101%	69%	20%	21%	79%	115%	23%	21%	70%
7	29%	71%	38%	28%	22%	22%	58%	23%	18%	18%	33%
8	148%	101%	61%	48%	46%	46%	92%	55%	46%	45%	49%
9	81%	76%	13%	34%	15%	16%	83%	39%	17%	16%	15%
10	313%	241%	67%	44%	31%	31%	71%	47%	33%	32%	42%
11	98%	105%	71%	79%	66%	72%	84%	77%	63%	68%	70%
Mean	118%	103%	64%	44%	26%	27%	74%	53%	27%	26%	34%
SD	77%	54%	51%	22%	17%	18%	24%	26%	17%	18%	22%

Table E-1-7 Mean linear envelope data normalised to standing for the T8 left muscle

Subject	Upright	Upright ps	Standard	Standard ps	TIS 1	TIS 1 ps	TIS 2	TIS 2 ps	TIS 3	TIS 3 ps	Lying
1	177%	130%	73%	102%	66%	56%	107%	140%	49%	56%	63%
2	126%	123%	97%	31%	24%	21%	86%	76%	36%	25%	26%
3	144%	165%	105%	128%	15%	13%	127%	125%	56%	46%	80%
4	93%	99%	61%	64%	38%	47%	101%	82%	34%	23%	117%
5	153%	170%	106%	44%	40%	42%	172%	128%	51%	48%	51%
6	100%	99%	129%	31%	26%	28%	92%	104%	39%	23%	39%
7	107%	160%	100%	115%	59%	60%	117%	121%	67%	54%	163%
8	106%	105%	100%	85%	81%	85%	112%	94%	87%	84%	81%
9	253%	207%	26%	145%	111%	152%	194%	167%	439%	266%	68%
10	33%	35%	27%	14%	6%	4%	32%	11%	12%	4%	7%
11	219%	376%	62%	70%	79%	77%	82%	78%	82%	86%	229%
Mean	137%	152%	81%	75%	49%	53%	111%	103%	87%	65%	84%
SD	62%	87%	34%	44%	32%	42%	44%	42%	119%	71%	64%

Table E-1-8 Mean linear envelope data normalised to standing for the T4 left muscle

Subject	Upright	Upright ps	Standard	Standard ps	TIS 1	TIS 1 ps	TIS 2	TIS 2 ps	TIS 3	TIS 3 ps	Lying
1	94%	75%	40%	43%	50%	36%	64%	54%	32%	34%	48%
2	68%	62%	52%	28%	17%	14%	59%	50%	22%	17%	23%
3	93%	110%	77%	86%	37%	26%	93%	96%	23%	26%	38%
4	63%	76%	51%	44%	40%	48%	78%	51%	37%	27%	85%
5	115%	120%	68%	33%	32%	32%	109%	87%	34%	31%	27%
6	96%	87%	98%	28%	33%	31%	96%	74%	46%	33%	30%
7	58%	57%	49%	42%	26%	29%	60%	54%	25%	25%	68%
8	85%	84%	71%	72%	92%	93%	75%	70%	80%	78%	65%
9	115%	105%	55%	68%	64%	58%	86%	76%	117%	77%	61%
10	18%	21%	23%	13%	12%	4%	20%	9%	11%	7%	9%
11	272%	274%	53%	54%	54%	52%	84%	60%	60%	60%	65%
Mean	98%	97%	58%	46%	42%	39%	75%	62%	44%	38%	47%
SD	64%	65%	20%	22%	23%	24%	24%	23%	31%	24%	23%

E-2 Histograms and box plots of the sEMG data

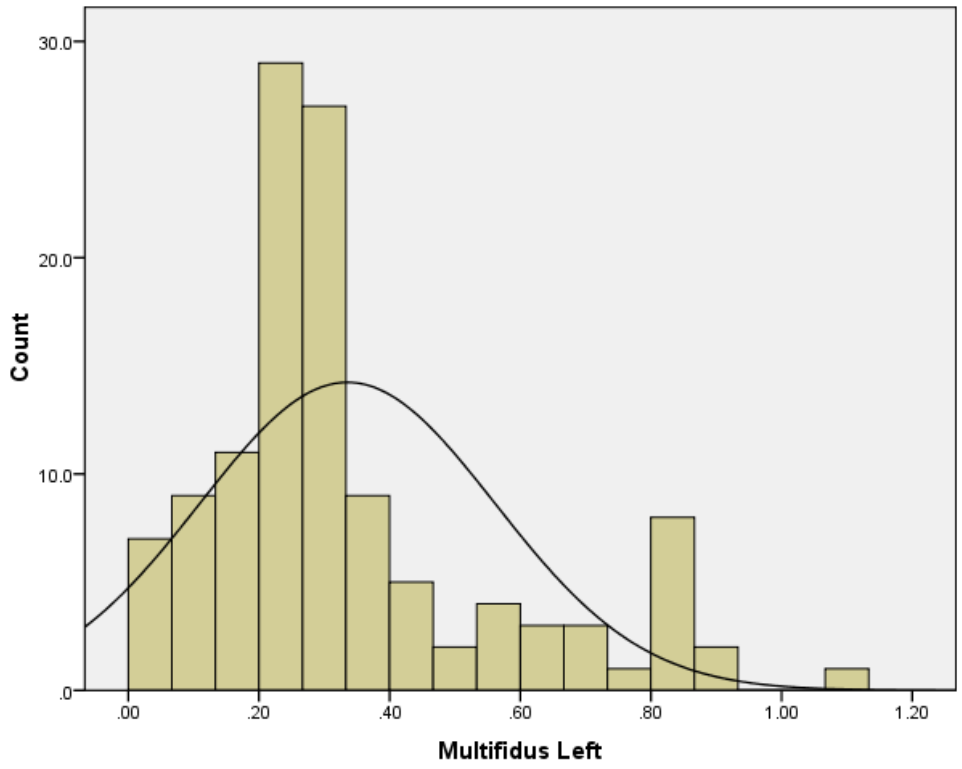

Figure E-2-1 Histogram of the mean linear envelope data normalised to the standing posture for the multifidus left side

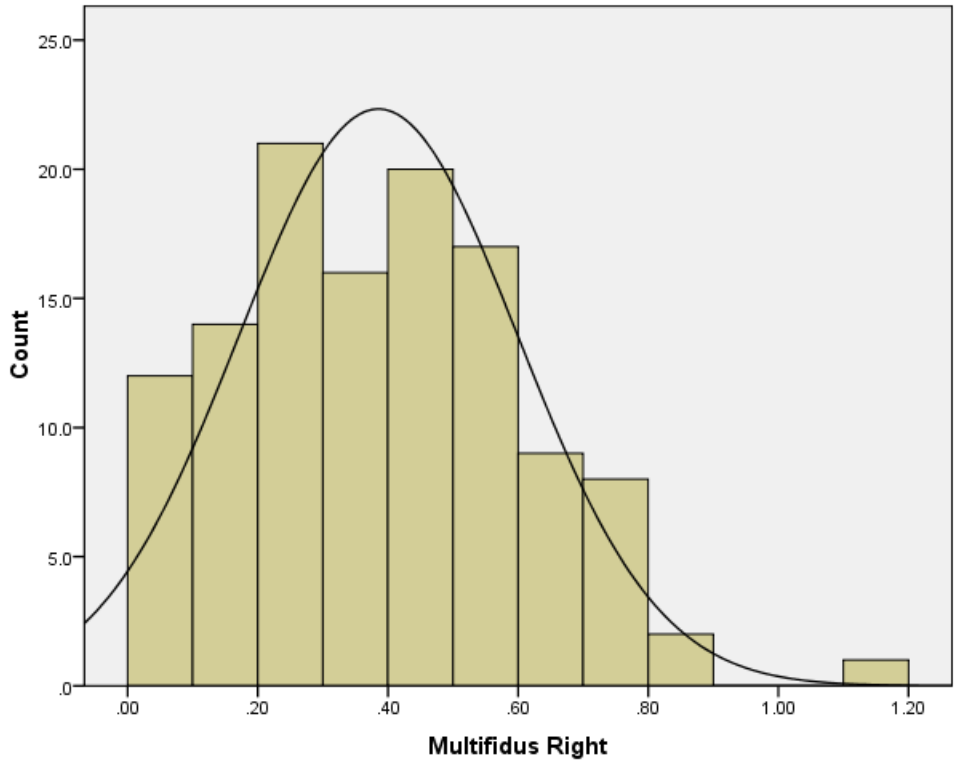

Figure E-2-2 Histogram of the mean linear envelope data normalised to the standing posture for the multifidus right side

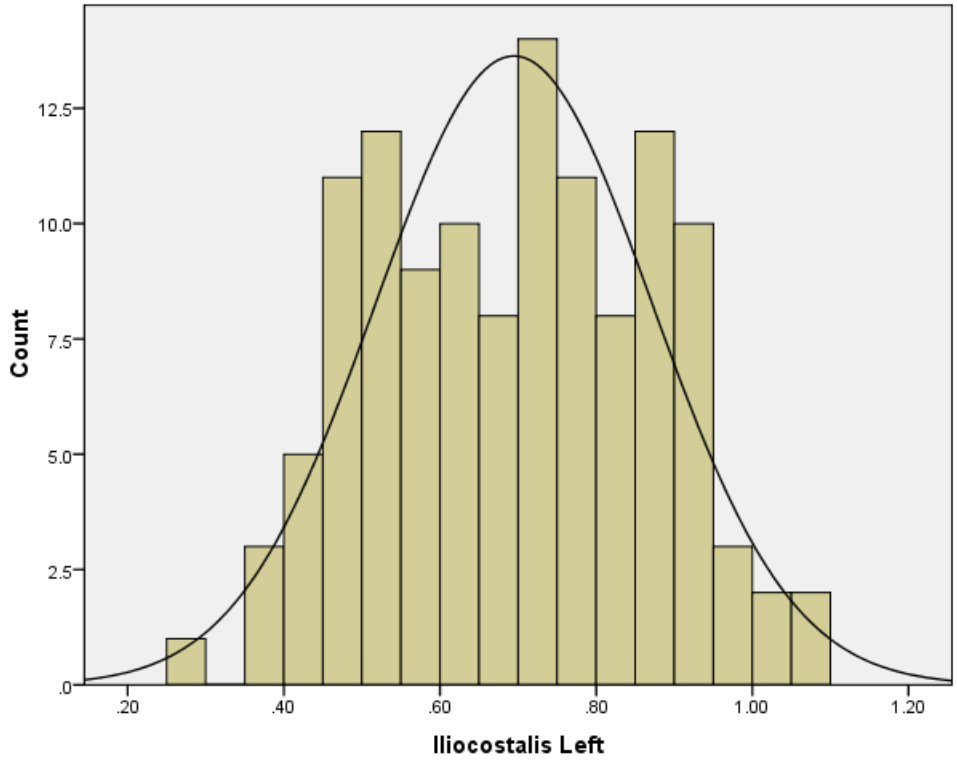

Figure E-2-3 Histogram of the mean linear envelope data normalised to the standing posture for the iliocostalis left side

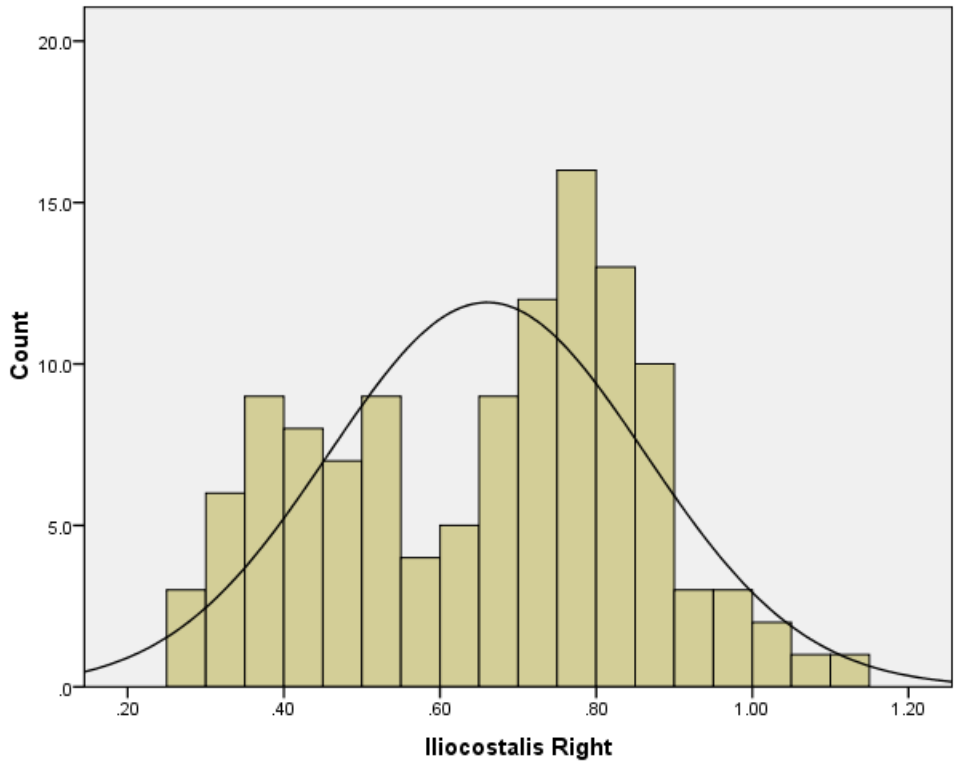

Figure E-2-4 Histogram of the mean linear envelope data normalised to the standing posture for the iliocostalis right side

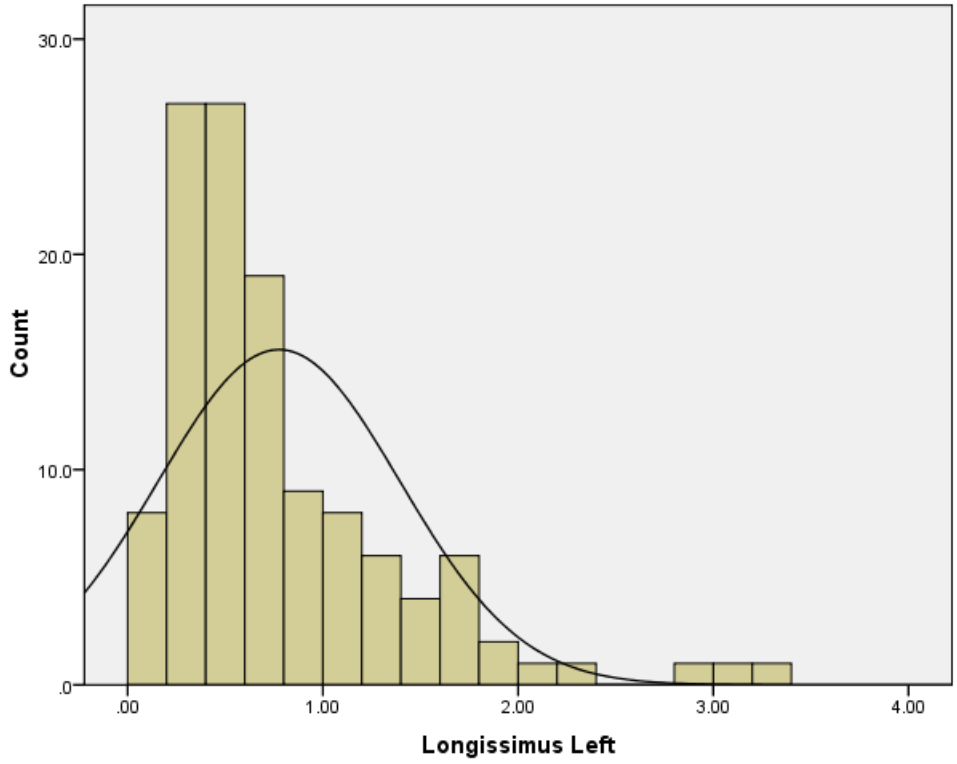

Figure E-2-5 Histogram of the mean linear envelope data normalised to the standing posture for the longissimus left side

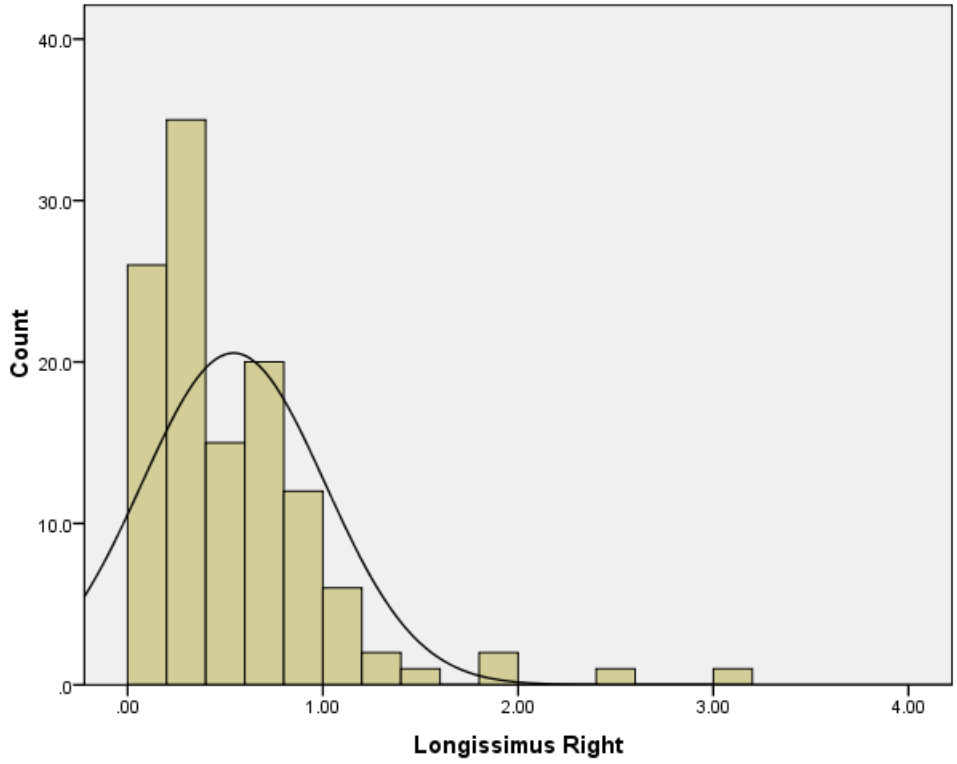

Figure E-2-6 Histogram of the mean linear envelope data normalised to the standing posture for the longissimus right side

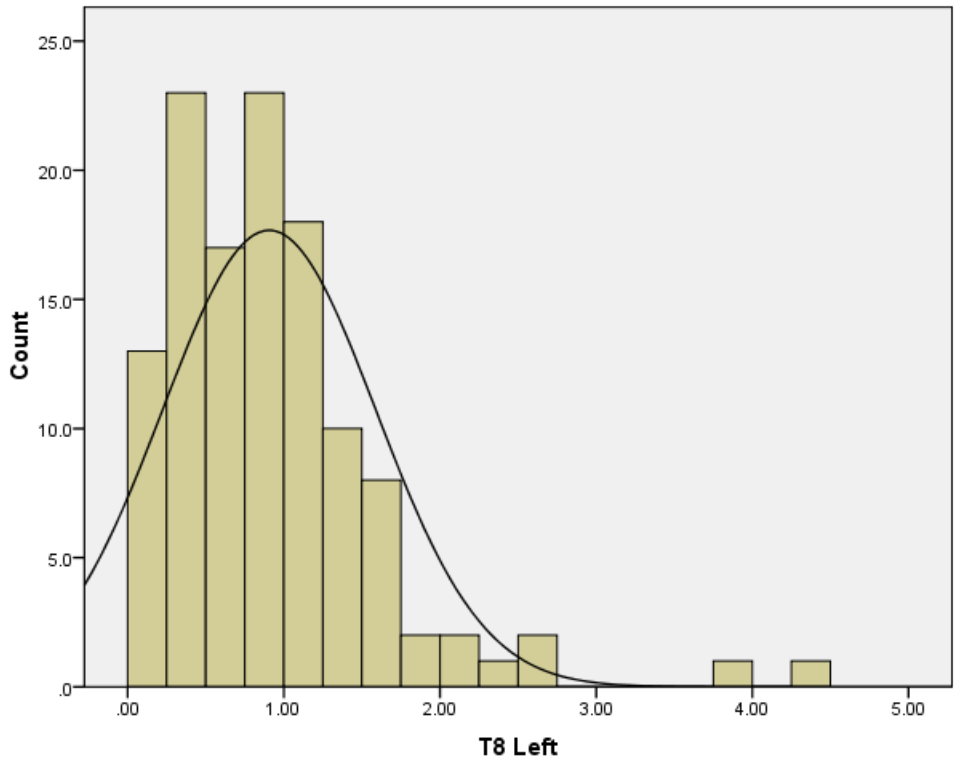

Figure E-2-7 Histogram of the mean linear envelope data normalised to the standing posture for the T8 left muscle

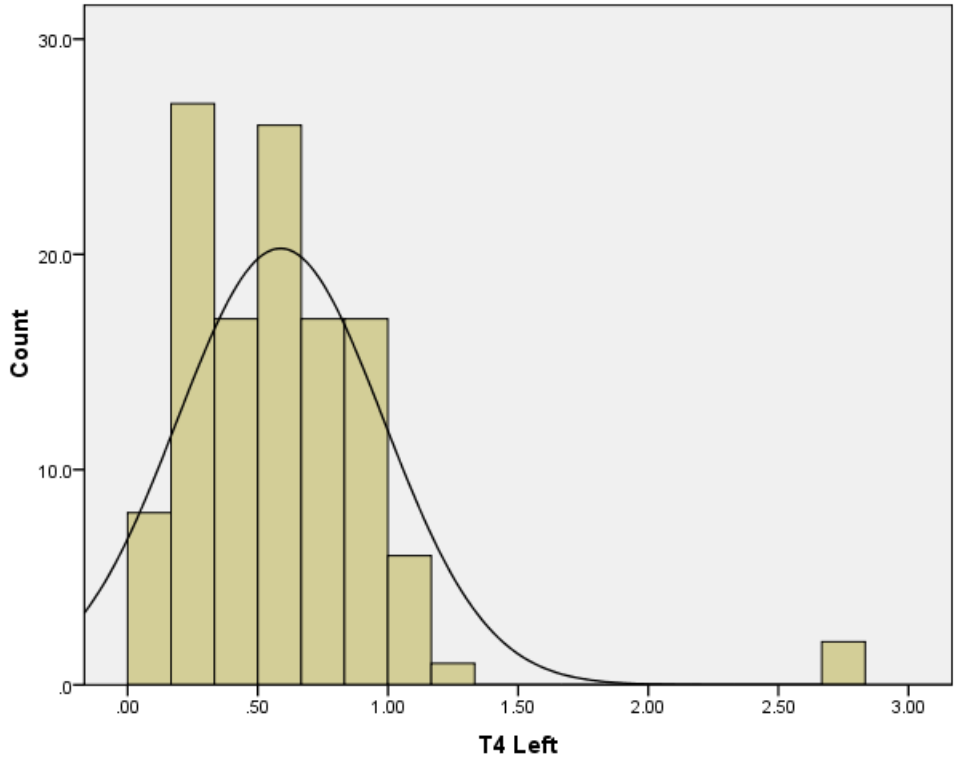

Figure E-2-8 Histogram of the mean linear envelope data normalised to the standing posture for the T4 left muscle

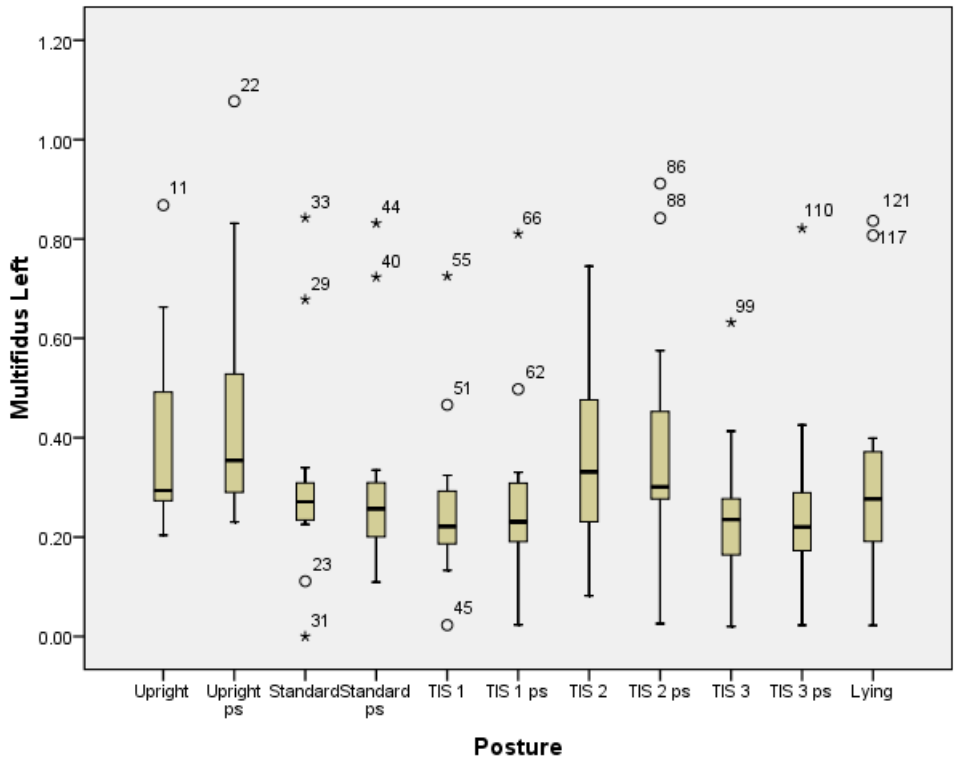

Figure E-2-9 Box plot for the multifidus left data

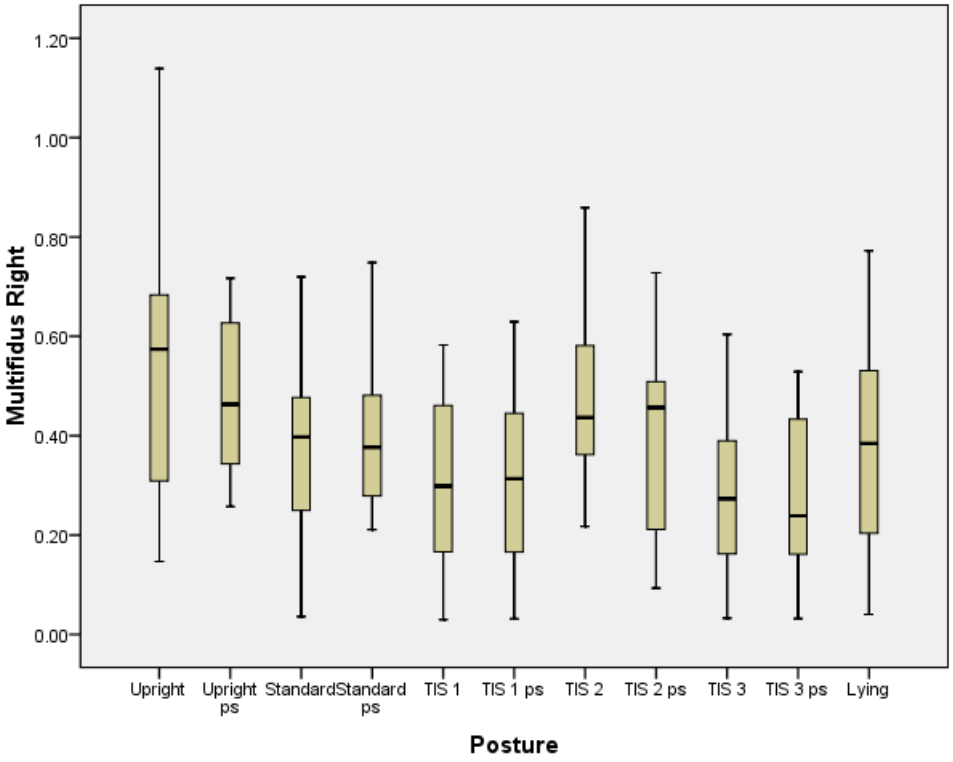

Figure E-2-10 Box plot for the multifidus right data

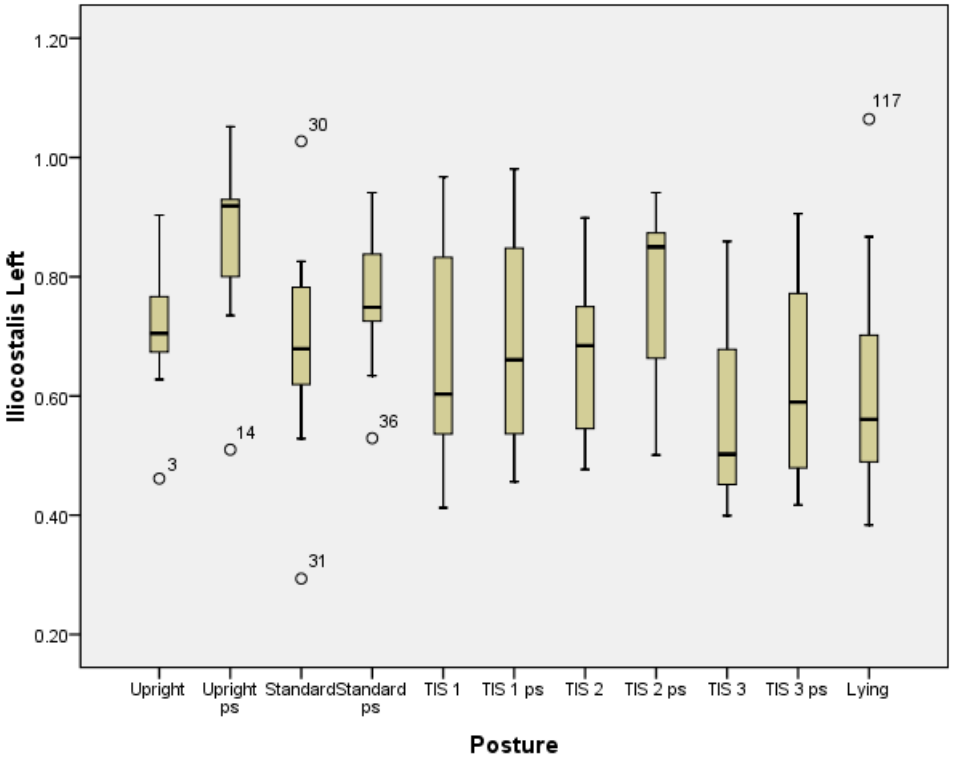

Figure E-2-11 Box plot for the iliocostalis left data

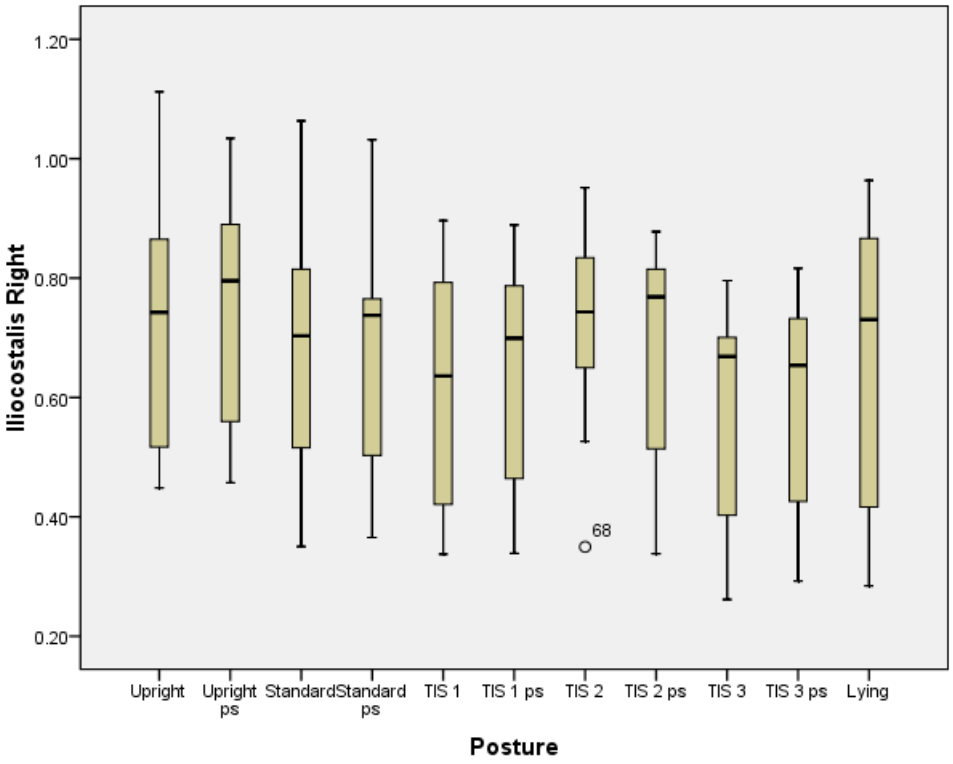

Figure E-2-12 Box plot for the iliocostalis right data

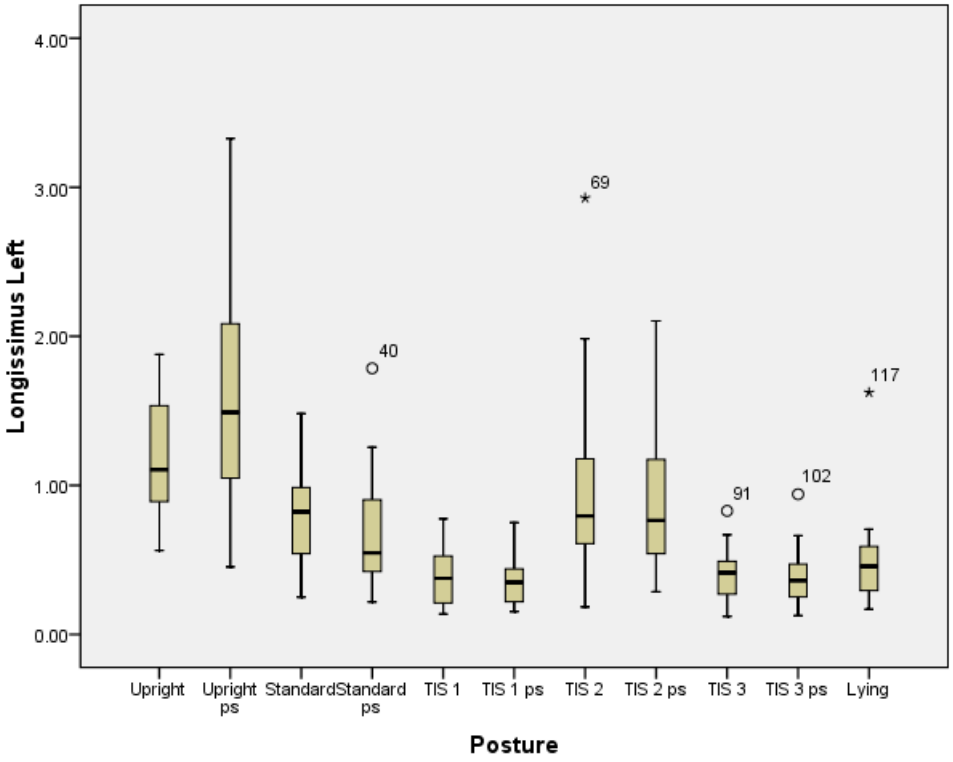

Figure E-2-13 Box plot for the longissimus left data

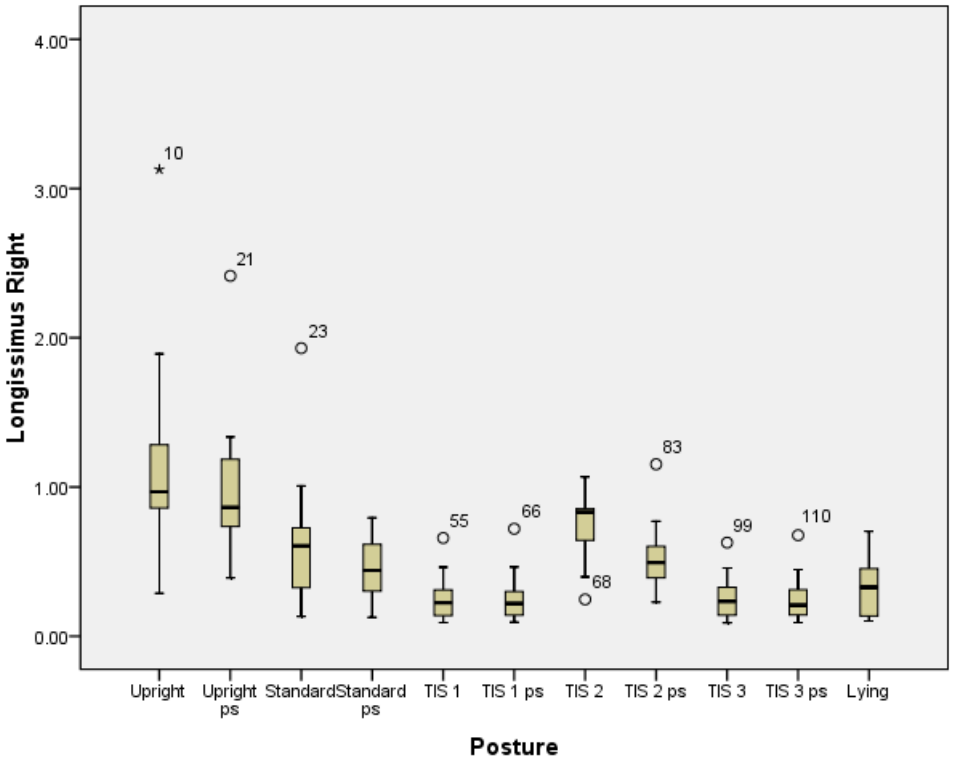

Figure E-2-14 Box plot for the longissimus right data

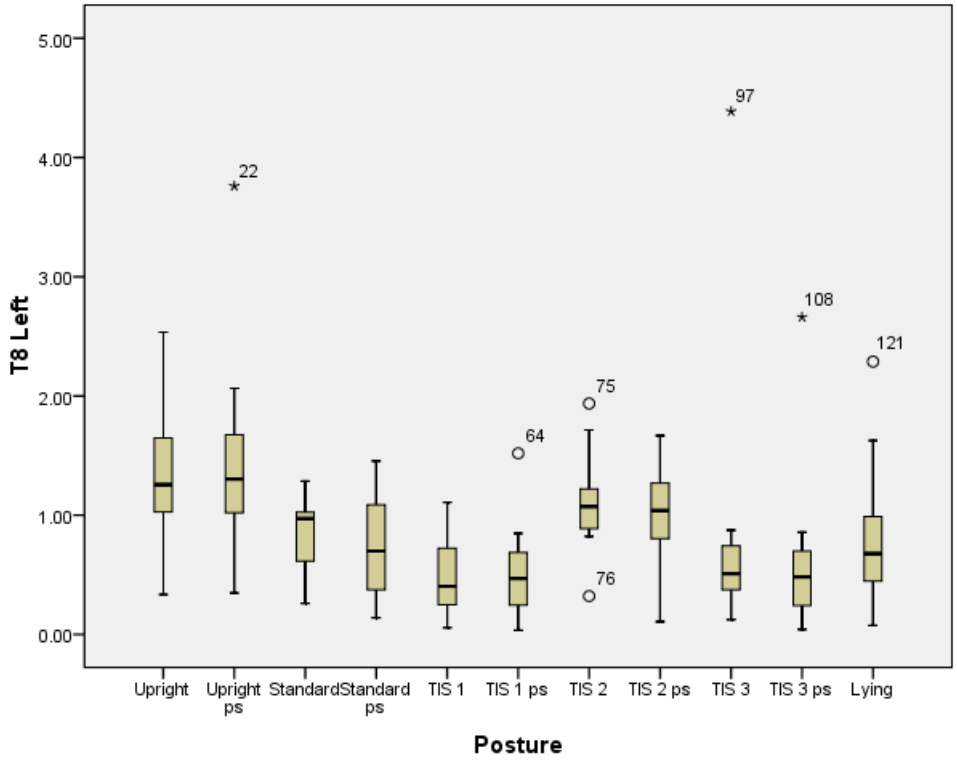

Figure E-2-15 Box plot for the T8 left data

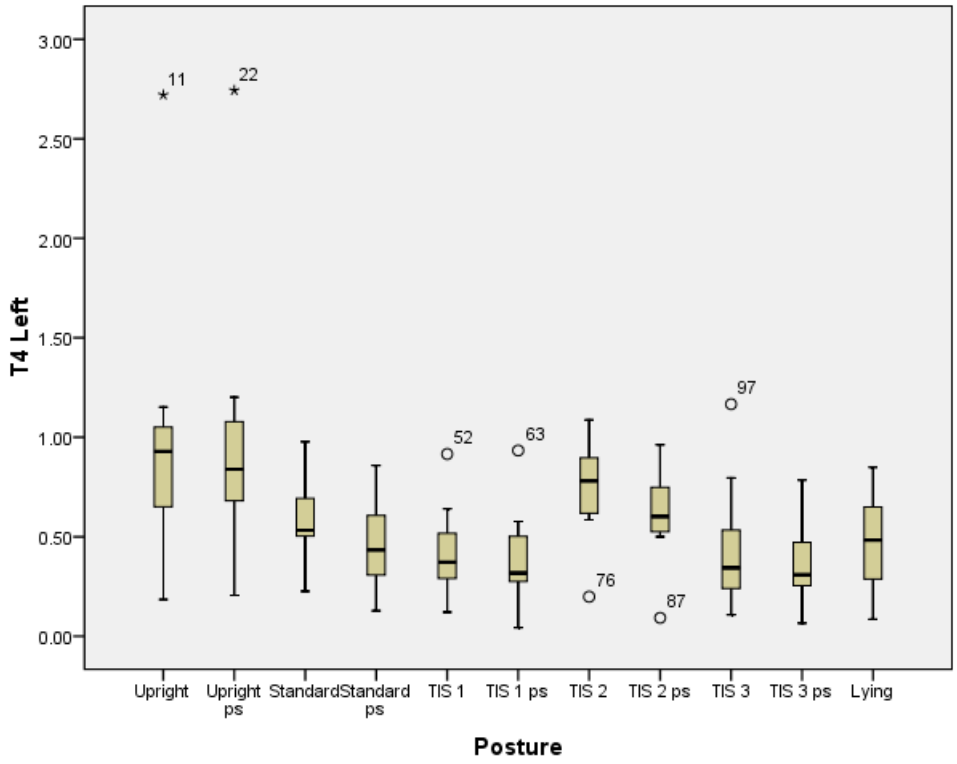

Figure E-2-16 Box plot for the T4 left data

Test results for normality of distributions and homogeneity of variance

Table E-3-1 Results for the tests for normality of distribution (sEMG) (*.200 is the lower bound of the true significance)

		Kolmogorov-Smirnova			Shapiro-Wilk		
	Posture	Statistic	df	Sig.	Statistic	df	Sig.
Multifidus Left	Upright	.252	11	.049	.827	11	.022
	Upright ps	.281	11	.015	.802	11	.010
	Standard	.295	11	.008	.837	11	.029
	Standard ps	.302	11	.006	.768	11	.004
	TIS 1	.252	11	.049	.866	11	.068
	TIS 1 ps	.228	11	.115	.851	11	.044
	TIS 2	.195	11	.200*	.937	11	.487
	TIS 2 ps	.330	11	.001	.839	11	.030
	TIS 3	.209	11	.193	.912	11	.261
	TIS 3 ps	.150	10	.200*	.974	10	.923
	Lying	.226	11	.121	.852	11	.046
Multifidus Right	Upright	.123	11	.200*	.955	11	.711
	Upright ps	.159	11	.200*	.909	11	.240
	Standard	.122	11	.200*	.977	11	.944
	Standard ps	.126	11	.200*	.927	11	.380
	TIS 1	.170	11	.200*	.942	11	.546
	TIS 1 ps	.182	11	.200*	.950	11	.650
	TIS 2	.139	11	.200*	.962	11	.796
	TIS 2 ps	.168	11	.200*	.940	11	.518
	TIS 3	.165	11	.200*	.957	11	.733
	TIS 3 ps	.222	10	.175	.939	10	.540
	Lying	.150	11	.200*	.961	11	.788
Iliocostalis Left	Upright	.149	11	.200*	.956	11	.724
	Upright ps	.222	11	.137	.883	11	.113
	Standard	.160	11	.200*	.962	11	.795
	Standard ps	.187	11	.200*	.944	11	.573
	TIS 1	.222	11	.136	.913	11	.267
	TIS 1 ps	.180	11	.200*	.909	11	.234
	TIS 2	.177	11	.200*	.929	11	.405
	TIS 2 ps	.280	11	.016	.848	11	.040
	TIS 3	.211	11	.184	.898	11	.177
	TIS 3 ps	.128	10	.200*	.933	10	.478
	Lying	.208	11	.198	.906	11	.217
Iliocostalis Right	Upright	.186	11	.200*	.934	11	.458
	Upright ps	.219	11	.147	.915	11	.279
	Standard	.121	11	.200*	.969	11	.881
	Standard ps	.182	11	.200*	.947	11	.611
	TIS 1	.165	11	.200*	.906	11	.216
	TIS 1 ps	.166	11	.200*	.914	11	.273

Table E-3-1 continued

		Kolmogorov-Smirnova			Shapiro-Wilk		
	Posture	Statistic	df	Sig.	Statistic	df	Sig.
Iliocostalis Right	TIS 2	.152	11	.200*	.932	11	.428
	TIS 2 ps	.245	11	.063	.876	11	.092
	TIS 3	.250	11	.052	.901	11	.188
	TIS 3 ps	.207	10	.200*	.883	10	.142
	Lying	.195	11	.200*	.887	11	.129
Longissimus Left	Upright	.137	11	.200*	.948	11	.621
	Upright ps	.190	11	.200*	.922	11	.333
	Standard	.096	11	.200*	.970	11	.887
	Standard ps	.199	11	.200*	.882	11	.109
	TIS 1	.166	11	.200*	.903	11	.202
	TIS 1 ps	.169	11	.200*	.882	11	.109
	TIS 2	.223	11	.133	.855	11	.049
	TIS 2 ps	.203	11	.200*	.891	11	.142
	TIS 3	.213	11	.175	.952	11	.669
	TIS 3 ps	.218	10	.194	.845	10	.050
	Lying	.245	11	.065	.742	11	.002
Longissimus Right	Upright	.278	11	.018	.825	11	.020
	Upright ps	.219	11	.145	.832	11	.025
	Standard	.235	11	.092	.830	11	.023
	Standard ps	.143	11	.200*	.954	11	.696
	TIS 1	.209	11	.194	.872	11	.082
	TIS 1 ps	.239	11	.078	.836	11	.028
	TIS 2	.229	11	.111	.904	11	.209
	TIS 2 ps	.198	11	.200*	.888	11	.133
	TIS 3	.159	11	.200*	.902	11	.196
	TIS 3 ps	.136	10	.200*	.934	10	.492
	Lying	.172	11	.200*	.887	11	.129
T8 Left	Upright	.147	11	.200*	.961	11	.787
	Upright ps	.237	11	.086	.842	11	.034
	Standard	.236	11	.086	.906	11	.220
	Standard ps	.130	11	.200*	.957	11	.729
	TIS 1	.156	11	.200*	.958	11	.749
	TIS 1 ps	.159	11	.200*	.906	11	.219
	TIS 2	.176	11	.200*	.944	11	.563
	TIS 2 ps	.171	11	.200*	.949	11	.628
	TIS 3	.406	11	.000	.522	11	.000
	TIS 3 ps	.335	10	.002	.650	10	.000
	Lying	.248	11	.058	.895	11	.160
T4 Left	Upright	.302	11	.006	.764	11	.003
	Upright ps	.271	11	.023	.763	11	.003
	Standard	.198	11	.200*	.962	11	.799
	Standard ps	.178	11	.200*	.966	11	.845
	TIS 1	.160	11	.200*	.940	11	.525
	TIS 1 ps	.182	11	.200*	.929	11	.403
	TIS 2	.158	11	.200*	.935	11	.462
	TIS 2 ps	.213	11	.177	.926	11	.371
	TIS 3	.231	11	.104	.857	11	.053
	TIS 3 ps	.320	10	.005	.811	10	.020
	Lying	.178	11	.200*	.959	11	.756

Table E-3-2 Results for the test for homogeneity of variance (sEMG)

		Levene Statistic	df1	df2	Sig.
Multifidus Left	Based on Mean	.760	10	109	.667
	Based on Median	.298	10	109	.980
	Based on Median and with adjusted df	.298	10	90.865	.980
	Based on trimmed mean	.668	10	109	.752
Multifidus Right	Based on Mean	.925	10	109	.513
	Based on Median	.796	10	109	.633
	Based on Median and with adjusted df	.796	10	85.351	.633
	Based on trimmed mean	.951	10	109	.491
Iliocostalis Left	Based on Mean	1.127	10	109	.349
	Based on Median	.648	10	109	.770
	Based on Median and with adjusted df	.648	10	92.681	.769
	Based on trimmed mean	1.057	10	109	.402
Iliocostalis Right	Based on Mean	.667	10	109	.752
	Based on Median	.396	10	109	.946
	Based on Median and with adjusted df	.396	10	104.155	.946
	Based on trimmed mean	.680	10	109	.741
Longissimus Left	Based on Mean	3.768	10	109	.000
	Based on Median	2.434	10	109	.012
	Based on Median and with adjusted df	2.434	10	51.123	.019
	Based on trimmed mean	3.505	10	109	.000
Longissimus Right	Based on Mean	3.251	10	109	.001
	Based on Median	1.881	10	109	.055
	Based on Median and with adjusted df	1.881	10	34.978	.082
	Based on trimmed mean	2.746	10	109	.005
T8 Left	Based on Mean	.851	10	109	.581
	Based on Median	.438	10	109	.925
	Based on Median and with adjusted df	.438	10	40.556	.919
	Based on trimmed mean	.598	10	109	.812
T4 Left	Based on Mean	1.351	10	109	.213
	Based on Median	.996	10	109	.451
	Based on Median and with adjusted df	.996	10	39.56	.463
	Based on trimmed mean	1.124	10	109	.351

Appendix F

F-1 Tests results for normality of distribution and homogeneity of variance

Table F-1-1 Results for the tests for normality of distribution (spinal curvature) (*.200 is the lower bound of the true significance)

		Kolmogorov-Smirnova			Shapiro-Wilk		
	Posture	Statistic	df	Sig.	Statistic	df	Sig.
% Lumbar Flexion	Upright	.168	14	.200*	.906	14	.138
	Upright PS	.095	14	.200*	.982	14	.986
	Unsupported sitting	.250	11	.053	.782	11	.005
	Standard	.112	10	.200*	.992	10	.998
	Standard PS	.217	14	.072	.921	14	.226
	TIS 1	.290	14	.002	.585	14	.000
	TIS 1 PS	.116	14	.200*	.981	14	.981
	TIS 1a	.173	8	.200*	.942	8	.635
	TIS 2	.365	12	.000	.641	12	.000
	TIS 2 PS	.203	14	.124	.849	14	.021
	TIS 3	.320	14	.000	.583	14	.000
	TIS 3 PS	.125	14	.200*	.969	14	.857
% Thoracic Flexion	Upright	.300	14	.001	.724	14	.001
	Upright PS	.308	14	.001	.692	14	.000
	Unsupported sitting	.343	11	.001	.610	11	.000
	Standard	.290	10	.017	.803	10	.016
	Standard PS	.322	14	.000	.675	14	.000
	TIS 1	.374	14	.000	.680	14	.000
	TIS 1 PS	.196	14	.149	.899	14	.108
	TIS 1a	.412	8	.000	.629	8	.000
	TIS 2	.361	12	.000	.717	12	.001
	TIS 2 PS	.265	14	.008	.705	14	.000
	TIS 3	.325	14	.000	.696	14	.000
	TIS 3 PS	.328	14	.000	.744	14	.001

Table F-1-2 Results for the test for homogeneity of variance (spinal curvature)

		Levene Statistic	df1	df2	Sig.
% Lumbar Flexion	Based on Mean	.931	11	141	.513
	Based on Median	.799	11	141	.641
	Based on Median and with adjusted df	.799	11	78.778	.640
	Based on trimmed mean	.864	11	141	.577
% Thoracic Flexion	Based on Mean	.536	11	141	.876
	Based on Median	.275	11	141	.989
	Based on Median and with adjusted df	.275	11	117.753	.989
	Based on trimmed mean	.355	11	141	.971

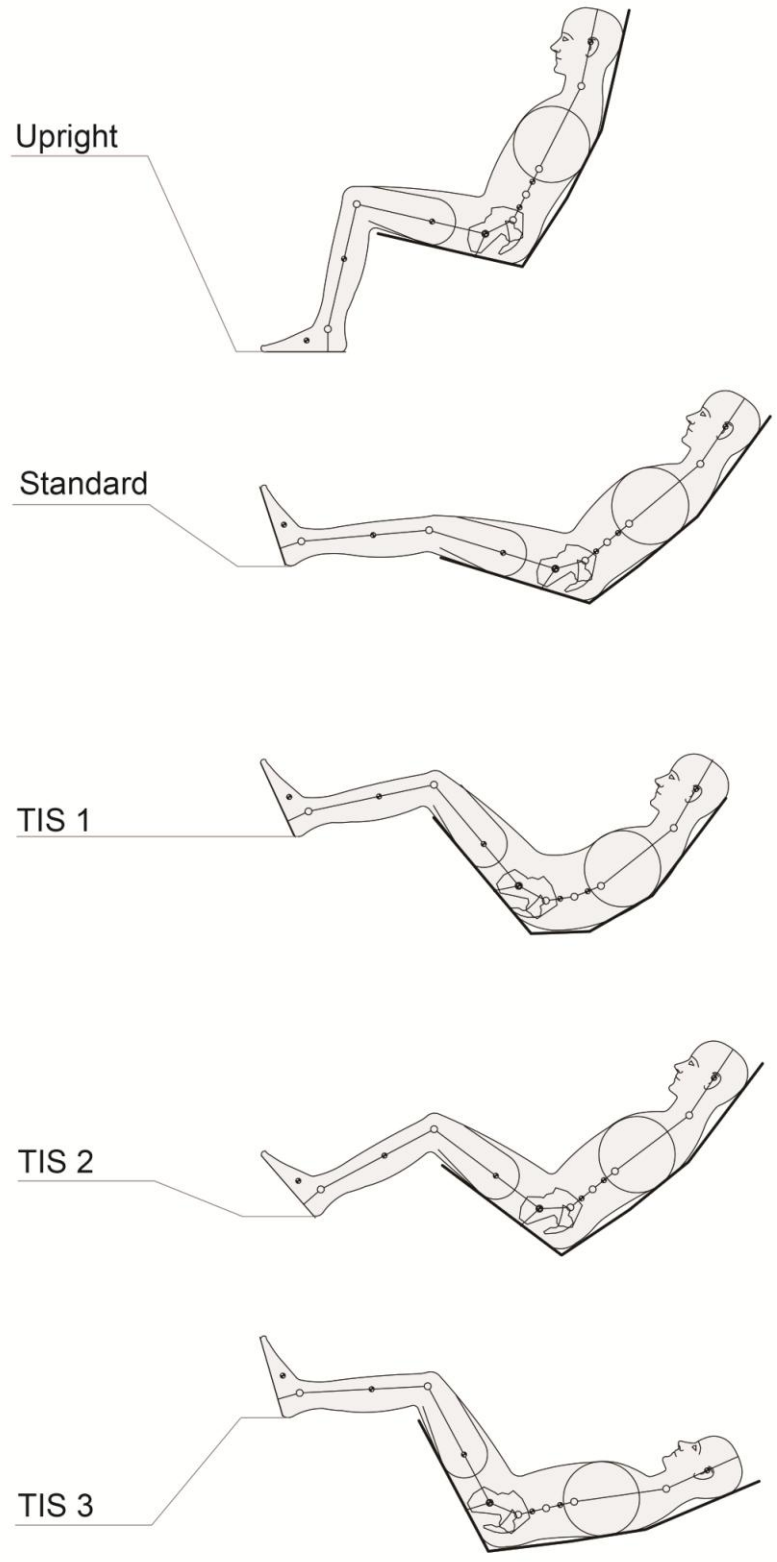

Seated Test Postures